Semi-rigid behaviour of plane timber structures

By

Steve Ka Fai Man B.Eng

Thesis submitted to City University for the degree of Doctor of Philosophy

School of Engineering and Mathematical Sciences

City University, London

February 2004

THESIS CONTAINS

VIDEO CD ✓ DVD TAPE CASSETTE

Table of Contents

List of Figures iv

List of Tables vii

Acknowledgements viii

Declaration ix

Abstract x

Notations xi

Chapter 1 Introduction 13
- 1.1 Background 14
- 1.2 Connections in structures 16
- 1.3 Semi-rigid behaviour of connections 16
- 1.4 Type of connectors 18
- 1.5 Metal plate connected joints 20
- 1.6 Objectives 24
- 1.7 Scope and layout of the thesis 25

Chapter 2 Literature review 27
- 2.1 Semi-rigid behaviour 27
- 2.2 Metal plate connector 29
- 2.3 Fictitious member 34
- 2.4 Combined loads 37
- 2.5 Timber models 41
- 2.6 Literature summary 46
- 2.7 Parameters for investigation 50

Chapter 3 Experimental work 53
- 3.1 Introduction 53
- 3.2 Truss design 54
- 3.3 Instrumentation 57
- 3.4 Close range photogrammetry 58
- 3.5 Test data interpretation 71
  - 3.5.1 Semi-rigid moment rotation deformation 73
  - 3.5.2 Semi-rigid axial deformation 82
  - 3.5.3 Semi-rigid shear deformation 84
- 3.6 Loading arrangement 99
  - 3.6.1 Crown joint test 107
  - 3.6.2 Heel joint test 114
  - 3.6.3 Top chord joint test 119
  - 3.6.4 Bottom chord joint test 123
  - 3.6.5 Full-scale truss tests 126
- 3.7 Test procedure 138

Chapter 4 Semi-rigid plane frame analysis 140
- 4.1 Introduction 140
- 4.2 Assumptions 141
- 4.3 Rigid jointed frame analysis 142
- 4.4 Semi-rigid joint rotational stiffness 145
- 4.5 Semi-rigid joint axial stiffness 154
- 4.6 Semi-rigid joint shear stiffness 158
- 4.7 Stability functions 167
- 4.8 Non-linear connection behaviour 169
- 4.9 Computational procedure 171

Chapter 5	**Finite element analysis**	**174**
5.1	Introduction	174
5.2	Assumptions	175
5.3	Finite element model	176
Chapter 6	**Results & Discussion**	**192**
6.1	Laboratory experimental test	192
6.2	Crown joint test	193
6.3	Heel joint test	199
6.4	Top chord Joint test	205
6.5	Bottom chord joint test	211
6.6	Joint test summary	216
6.7	Full-scale truss test	219
6.8	Semi-rigid plane frame analysis	225
6.9	Finite element	233
Chapter 7	**Conclusion**	**242**
7.1	General	242
7.2	Joint tests	242
7.3	Truss tests	243
7.4	STRUSS and finite element model	245
7.5	Summary	247
7.6	Future work	247
References		**249**
Bibliography		**253**
Appendix A1	**Truss design**	**254**
Appendix A2	**Punched metal plate certificate**	**275**
Appendix A3	**Loading arrangement**	**280**
Appendix B1	**2-D non-linear semi-rigid analysis**	**287**
Appendix B2	**Finite element**	**306**
Appendix C1	**Test results**	**310**
Appendix C2	**Close range photogrammetry**	**320**
Appendix C3	**Pinned and rigid analysis**	**323**

List of Figures

Fig. 1.4.1 – Shanked nails 18

Fig. 1.4.2 – Connectors 19

Fig. 1.5.1 – Nail Plate 21

Fig. 2.1.1 – Results of analysis and experiments 28

Fig. 2.2.1 – Experimental and model results 30

Fig. 2.4.1 – Testing apparatus 38

Fig. 2.5.1 – Partial loading of timber specimen 43

Fig. 2.5.2 – Plan view of loaded timber specimen 43

Fig. 2.5.3 – Sketch of model 45

Fig. 3.2.1 – Assembling the nail plate 55

Fig. 3.2.2 – Queen Truss 56

Fig. 3.4.1 – Camera Geometry 61

Fig. 3.4.2 – Effect of light rays due to the lens 62

Fig. 3.4.3 – Measuring targets 66

Fig. 3.4.4 – Targets on a connection 68

Fig. 3.5.1 – Inverted Crown Joint 72

Fig. 3.5.1.1 – Rotation analysis 74

Fig. 3.5.1.2 – Local co-ordinate axis 75

Fig. 3.5.1.3 – Semi-rigid moment rotation analysis 76

Fig. 3.5.1.4 – Offset distance constant throughout test 78

Fig. 3.5.1.5 – Plate Analysis 79

Fig. 3.5.1.6 – Plate distortion 80

Fig. 3.5.2.1 – Semi-rigid axial displacements 83

Fig. 3.5.3.1 – Semi-rigid shear displacements 85

Fig. 3.5.3.2 – Break down of semi-rigid shear displacements 86

Fig. 3.5.3.3 – Step by step semi-rigid shear displacement analysis 88

Fig. 3.5.3.4 – Inverted Crown Joint 93

Fig. 3.5.3.5 – Heel Joint 94

Fig. 3.5.3.6 – Top Chord Joint 95

Fig. 3.5.3.7 – Bottom chord joint 96

Fig. 3.6.1 – Force components of the truss 101

Fig. 3.6.2 – Crown Joint dimensions 102

Fig. 3.6.3 – Heel Joint dimensions 103

Fig. 3.6.4 – Top chord joint dimensions 104

Fig. 3.6.5 – Bottom chord joint dimensions 105

Fig. 3.6.1.1 – Crown Joint test 108

Fig. 3.6.1.2 – Axial load system 111

Fig. 3.6.1.3 – Axial load system with moment rotation 112

Fig. 3.6.2.1 – Heel Joint test 116

Fig. 3.6.2.2 – Inverted axial loading system 117

Fig. 3.6.2.3 – Moment loading system 118

Fig. 3.6.3.1 – Top chord joint test 121
Fig. 3.6.3.2 – Compression load to the top chord 122
Fig. 3.6.4.1 – Bottom chord joint test 125
Fig. 3.6.5.1 – Truss load combinations 127
Fig. 3.6.5.2 – Loading of the truss 128
Fig. 3.6.5.3 – Assembling the truss 130
Fig. 3.6.5.4 – Test-set-up for symmetrical loading 131
Fig. 3.6.5.5 – Truss loading system 134
Fig. 3.6.5.6 – Support at the heel joint 135
Fig. 3.6.5.7 – Test-setup for symmetrical loading 137
Fig. 4.3.1 – Rigid jointed member 143
Fig. 4.4.1 – Semi-rigid joint rotational stiffness 145
Fig. 4.4.2 – Rotationally semi-rigid jointed member 147
Fig. 4.4.3 – Internal shear/reaction 148
Fig. 4.4.4 – Member load force diagram 149
Fig. 4.4.5 – Matrix components of a rotationally semi-rigid joint member 152
Fig. 4.5.1 – 2 D.O.F Semi-rigid joint representation 154
Fig. 4.5.2 – Axial spring and member displacements 154
Fig. 4.5.3 – Matrix components of an axial and rotational semi-rigid joint member 157
Fig. 4.6.1 – System of rotational, axial and shear semi-rigidity 158
Fig. 4.6.2 – Displacement system of shear semi-rigidity 158
Fig. 4.6.3 – Matrix components of 3-DOF semi-rigid joint member 163
Fig. 4.6.4 – Semi-rigid joint model 166
Fig. 4.8.1 – Foschi Power function 169
Fig. 4.9.1 – STRUSS program flow chart 172
Fig. 5.3.1 – Stress state of body 177
Fig. 5.3.2 – Nail plate interaction shell idealisation 180
Fig. 5.3.3 – Bilinear kinematic model 183
Fig. 5.3.4 – Von mises failure surface 183
Fig. 5.3.5 – Kinematic hardening 184
Fig. 5.3.6 – Crown joint finite element model 187
Fig. 5.3.7 – Heel joint finite element model 188
Fig. 5.3.8 – Top chord joint Finite element model 189
Fig. 5.3.9 – Bottom chord joint Finite element model 190
Fig. 6.2.1 – Tensile axial load failure 194
Fig. 6.2.2 – Effect of bending moments on axial stiffness for Crown Joint 195
Fig. 6.2.3 – Bending moment load failure 197
Fig. 6.2.4 – Effect of axial loads on rotation stiffness for Crown Joints 198
Fig. 6.3.1 – Typical plate failure for HJTM series test 199
Fig. 6.3.2 – Effect of bending moments on Axial stiffness for Heel Joints 201
Fig. 6.3.3 – Failure mechanism for HJTA series test 202
Fig. 6.3.4 – Effect of axial loads on rotation stiffness for Heel Joints 204

Fig. 6.4.1 – Failed test specimen from TCJTM5 206
Fig. 6.4.2 – Effect of bending moment on axial stiffness for Top chord Joints 207
Fig. 6.4.3 – TCJTA2 connection failure 208
Fig. 6.4.4 – Effect of axial loads on rotation stiffness for Top chord Joints 210
Fig. 6.5.1 – Typical failure of BCJTM test series 211
Fig. 6.5.2 – Nail and plate deformation of BCJTM series 212
Fig. 6.5.3 – Effect of bending moment on axial stiffness of Bottom chord joints 213
Fig. 6.5.4 – Effect of axial loads on rotation stiffness for Bottom chord joints 215
Fig. 6.7.1 – Failure mode for support at the bottom chord 220
Fig. 6.7.2 – Failure mode for support at the rafter for test FST3 220
Fig. 6.7.3 – Failed heel joint for two different support points 221
Fig. 6.7.4 – Results of the Symmetrical full scale truss test 222
Fig. 6.7.5 – Results of the Unsymmetrical full scale truss test 223
Fig. 6.7.6 – Overall truss results 224
Fig. 6.8.1 – Load and Boundary conditions 225
Fig. 6.8.2 – STRUSS compared to symmetrical test results 227
Fig. 6.8.3 – Load conditions in joint and truss tests 228
Fig. 6.8.4 – Modelling eccentricity in STRUSS 229
Fig. 6.8.5 – Joint and Truss test 229
Fig. 6.8.6 – STRUSS compared to unsymmetrical test results 232
Fig. 6.9.1 – FE model compared to symmetrical truss load experimental results 234
Fig. 6.9.2 – FE model compared to unsymmetrical truss load experimental results 235
Fig. 6.9.3 – Stress analysis of heel joint in X direction 236
Fig. 6.9.4 – Stress analysis of heel joint in Y direction 237
Fig. 6.9.5 – Deflection for symmetrical finite element analysis 240
Fig. 6.9.6 – Deflection for unsymmetrical finite element analysis 241

List of Tables

Table 5.3.1 – Contact element parameters 186

Table 6.2.1 – CJTM series test programme 193

Table 6.2.2 – CJTA series test programme 196

Table 6.3.1 – HJTM series test programme 199

Table 6.3.2 – HJTA series test programme 202

Table 6.4.1 – TCJTM series test programme 205

Table 6.4.2 – TCJTA series test programme 208

Table 6.5.1 – BCJTM series test programme 211

Table 6.5.2 – BCJTA series test programme 214

Table 6.6.1 – Summary of joint test results 218

Table 6.7.1 – Full scale truss test programme 219

Table 6.8.1 – Foschi parameters for truss joints 226

Table 6.9.1 – Finite element joint strengths 223

Acknowledgements

This research was carried out under the supervision and guidance of Professor Kuldeep Singh Virdi for whom the author is deeply grateful for his encouragement and tireless support and advice throughout the course of this research. Financial support from the EPSRC in the form of a studentship is gratefully acknowledged.

The experimental work formed a significant part for the research and was only made possible with the collaboration with a number of personnel both in and out of City University. The author would like to thank Mr. Tony Jones, Mr. Ahmed Saeed and Mr. Jim Rose who gave their support and advice towards the tests. In particular, a deep sense of gratitude is paid to Mr. Jim. Hooker for his motivation and efforts, which gave a ray of light in the darkest of times. A special thank you is extended to Dr. Stuart Robson and Dr. Neil Woodhouse of University College London, Geomatics Department for so generously lending the photogrammetry equipment for long periods and giving their quick response to hardware and software problems.

Thanks are expressed to the Carpentars Company for providing financial support during the final year. The generosity of Alpine Automation is acknowledged for supplying the nail plates and providing design data. In particular, thanks are extended towards Mr John Peek for taking time out to visit City University.

Finally, the author would like to thank two close friends, Mr Wing-Tsong To and Mr Tony Shergill for their all round support and in particular software and hardware problems encountered during the research. Support in printing from Mr Phuok Gia Pham is greatly appreciated. A heartfelt gratitude is paid towards my parents and friends for their support and encouragement, in particular Miss Angela Ko for being there through thick and thin.

Declaration

I declare that the work contained within this thesis is all of my own work except where explicit reference is given. I also hereby give consent to the library for this thesis, in whole or in part, to be copied without the need to seek permission from the author.

Signed: 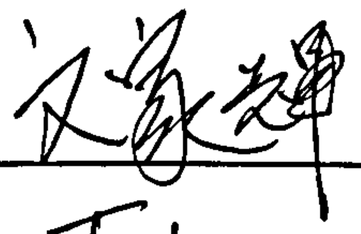 Steve Ka Fai Man.

Date: Feb 2004

Abstract

It is common practice in the analysis of structural frames, to either assume that the joints are pinned or rigid. In fact the real behaviour of a joint is neither pinned nor rigid, and lies somewhere between the pinned and rigid assumption. This is referred to as the semi-rigid behaviour. Semi-rigidity not only refers to the rotational behaviour of the joint as commonly studied, but also in axial and shear actions. The moment distribution between pinned and rigid analysis differs substantially and therefore a more accurate method of modelling the semi-rigid joint is necessary to predict the overall structure response. The level of semi-rigid behaviour varies in different joints due to the material, construction and type of connector. The degree of semi-rigidity can be determined through physical tests. The type of joint for this study is the Metal Plate Connector (MPC) for timber trusses, a chosen connector used in residential trusses.

An extensive test program was carried out in this study. Four different types of joints of a Queen truss were tested. In addition, the effect of combined loads on the joint characteristics was investigated. The loading arrangement in the tests allowed independent control of the bending moment and axial load. A novel approach is adopted to measure displacement, using high-resolution digital photogrammetry and specially developed software. The data produced gave details of timber movement in cartesian co-ordinates and measurement of plate deformation. From these tests, semi-rigid bending moment and axial stiffness values were determined for use in the theoretical study. An attempt to measure shear stiffness is also presented. Further tests were carried out on full-scale trusses under two different load conditions.

The theoretical work comprises two approaches to truss modelling. The first is an automated structural analysis program, which accounts for non-linear semi-rigid joint characteristics derived from the joint tests using the Foschi power function. The effects of stability and geometrical non-linearity are also implemented into the analysis. The second approach calculates truss response using Finite elements where 2-D planar elements were used to calculate the response of the truss. Parameters for the connection strength are derived from the joint tests.

Moment stiffness and axial stiffness values of the connections were determined. Combined load tests showed that there is indeed a measurable effect on joint stiffness and capacity due to combined loads, some of which actually contribute to the stiffness, but also some which are detrimental. There is good correlation between the truss test results and the FE model using semi-rigid joints. However, results of the simpler non-linear frame analysis did not compare so well, but nevertheless exhibited fundamental characteristics of the truss.

Notations

2-D Semi-rigid frame analysis properties

E	Member modulus of Elasticity
A	Member cross sectional area
I	Member second moment area
l	Beam length
r_i, r_j	Rotational spring fixity at node i and j
λ_i, λ_j	Rotational spring stiffness
r_{ai}, r_{aj}	Axial spring stiffness at node i and j
r_{si}, r_{sj}	Stiffness of shear spring at node i and j
$\vartheta_{mi}, \vartheta_{mi}$	Member rotational displacement at node I and j
ϑ_{ri}	Spring rotational displacement
u_{mi}, u_{mj}	Horizontal member displacement at node i and j
u_{si}, u_{sj}	Axial spring displacement at node i
v_{mi}, v_{mj}	Vertical member displacement at node i and j
v_{si}, v_{sj}	Shear spring displacement
ϑ	Total rotational displacement
v_j, v_i	Total vertical displacement at node i and j
u_i, u_j	Total horizontal displacement at node i and j
ϕ	Inclined angle of member
δ_{mem}	Local displacement of member
δ_{con}	Local displacement of rotational spring and member
δ	Local displacement of the axial spring, rotational spring and member
Δ_t	Total relative displacement
Δ_s	Spring relative displacement
Δ_m	Member relative displacement
$R', \alpha, \beta, \varepsilon, \gamma, \lambda$	Arbitrary symbols to simplify derivation
S_i, S_j	Internal shear force at node i and j
M_i, M_j	Internal moments at node i and j
P_i, P_j	Member axial force at node i and j
M_i^F, M_j^F	Fixed end moments at node i and j

Matrix notations

$[\bar{f}]$	Member loads in local form
$[f]$	Nodal loads in local form
$[F]$	Nodal loads in global form
$[S]$	Member stiffness matrix
$[T]$	Transformation matrix
$[U]$	Displacement in global form
$[u]$	Displacement in local form
$[C]_R$	Connection matrix with rotational spring function

$[C]_{RA}$	Connection matrix with rotational, and axial spring function
$[C]_{RAS}$	Connection matrix with rotational, axial, and shear spring function

Stability function properties

P_E	Euler load
s, c, ρ, α	Stability parameters
K, K_0, K_1	Foschi parameters

Finite element analysis properties

$E_{//}$, $E_{\perp}$	Modulus parallel and perpendicular to the grain respectively
E, E_T	Elastic modulus/Initial elastic and Tangent modulus respectively
$\sigma_{//}, \sigma_{\perp}$	Stress parallel and perpendicular to the grain respectively
σ_y	Yield stress
α	Stress at angle to the grain

Test data interpretation properties

x_{m2}, y_{m2}	X, Y Co-ordinate of member at time 2
x_{p1}, y_{p1}	X, Y Co-ordinate of plate at time 1
ϑ_{m2-1}	Member rotational displacement at time 2 relative to 1
ϑ_{p2-1}	Plate rotational displacement at time 2 relative to 1
ϑ_{m2}	Member rotation due to moments at time 2
ϑ_{p2}	Plate rotation due to moments at time 2
ϑ_2	Semi-rigid moment rotation at time 2
O	Offset distance
a_{m2}, a_{m1}	Mean axial member y co-ordinate at time 2 and 1
a_{p2}, a_{p1}	Mean axial plate y co-ordinate at time 2 and 1
a_{m2-1}	Axial member displacement at time 2 relative to 1
a_{p2-1}	Plate member displacement at time 2 relative to 1
a_2	Axial semi-rigid displacement at time 2
x_{m11}, y_{m11}	Member X, Y co-ordinate due to axial displacement
x_{m12}, y_{m12}	Member X, Y co-ordinate due to rotation
x_{m13}, y_{m13}	Member X, Y co-ordinate due to shear
x_{p11}, y_{p11}	Plate X, Y co-ordinate due to axial displacement
x_{p12}, y_{p12}	Plate X, Y co-ordinate due to rotation
x_{p13}, y_{p13}	Plate X, Y co-ordinate due to rotation
X_a, Y_a	X, Y displacement of target “a” due to rotation
R_a	Radius of rotation for target “a”
s_{m2}	Member shear displacement at time 2
s_{p2}	Plate shear displacement at time 2

Chapter 1

Introduction

Structural timber is heavily used in many countries such as Canada, Sweden, UK, Denmark, Finland, U.S.A and others. Although steel and concrete have been the dominant materials for construction, there is a demand for timber as it is very practical and economical in construction and at the same time its aesthetics are a bonus. The use of timber is further encouraged because of the environmentally conscious society we live in today. Timber is considered to be a far "Greener" material for construction as it contributes to our environment through many aspects. Trees absorb Carbon Dioxide, an ozone damaging gas source, so when trees are planted for more building materials a contribution to the environment is already made during the process. Of course, there will be other contributions such as the wild life surrounding the tree. When timber is felled it requires energy to cut, transport and construct to form the structure. Steel and concrete, which are significantly heavier materials, require far more energy and heavy machinery to transport and construct. Timber is a much more practical material to work with and as a result reduces the cost of construction significantly. With contributions to the environment and construction economy, timber becomes an attractive option.

1.1 Background

Timber strength parameters are affected by its surroundings and extra care must be exercised when storing and using it. Generally, a higher moisture content reduces the stiffness of the timber as voids in the timber are replaced by water. This effect varies linearly with 85% strength, at 10% moisture to 35% strength, at 30% moisture, after which further moisture increase has little effect on strength[45]. Furthermore, the effect of moisture in timber is not uniform for all strength properties. The compression strength parallel to the grain is more sensitive to moisture content than tension strength parallel to the grain. The effect of moisture content also varies in different timber species. The cause of the timber sensitivity to moisture is due to the micro structure in the timber as voids are replaced by water. This underlines the importance of considering the surroundings where the timber is being used. Moisture content can vary within the timber which affects the size of structural members. This is because increased moisture in the fibres forces the material to swell whilst reduced moisture enables it to shrink and poses problems when fitting joints as the swelling of the member can induce stresses if the fitting is tight. Swelling and shrinkage occurs perpendicular and parallel to the grain. However, the rate of shrinkage/swelling is not uniform and is much greater parallel to the grain, 10-20 times in fact, thereby introducing the problem of splitting fibres because of differential stresses induced during movement caused by shrinkage and expansion. The problem can be overcome by gradually introducing timber to a new moisture content environment such that the rate of movement is minimal. This is necessary especially when timber is used in a different environment than that from where it was produced. A period of 1-4 weeks of conditioning is usually required for the timber to adjust to its surroundings.

Timber is an anisotropic material, i.e. its properties are different in different directions. Its strength parallel to the grain is much greater than that perpendicular to the grain. Tension strength properties parallel to the grain are approximately 40 times greater than perpendicular to the grain. In addition, behaviour is dependent on load characteristics. The strength value of timber under long term loading is approximately 60% of the value if it were loaded short term. The density of timber is also contributory to the strength as coarse timber contains less solid material. This in effect reduces the strength of the material.

There are many species of timber. This inevitably means different timber species possess different strength characteristics. Furthermore, because timber relies on its surroundings for growth, the strength from the same species is also variable. The strength characteristics are further complicated through different cuttings from the same tree. Every cutting of timber needs to be graded individually because each cutting is derived from a different part of the tree cross section and at different angles.

With all these points to consider when using timber there are other typical features, which have not been addressed, such as knots, checks, shakes, slope of grain, and decay. These are some of the factors, which can have an effect on the strength of the timber. However, it is not the intention of this thesis to discuss the aspects of timber in anymore detail but to acknowledge and take note when using timber and examining failed specimen.

1.2 Connections in structures

On the commercial aspect of this subject, the joint is probably one of the most expensive part of the structure in terms of material and labour. On the structural side it is also the most important part of the structure. A joint provides a junction for forces to travel from one member to another. In its simplest form, tensile forces can be transferred from one member to another involving no change of angle. On the other hand, a complex joint can involve large forces with many members connected at different angles.

With the advancement in computer technology, it is now possible to conduct complex analyses, involving different behavioural aspects of structural response. Years ago this was either a major task in itself or unfeasible. As a result, many aspects of material and joint behaviour can be included in a computer generated model down to the smallest detail.

1.3 Semi-rigid behaviour of connections

It has now been well established that the conventional method of structural analysis assuming either pinned or rigid joints does not reflect the true behaviour of several types of structures. In reality, the joint is neither pinned nor rigid. The pinned assumption assumes that there is no moment resistance from the connection, thus in trusses the forces travel down the centroidal axis of the members and the forces meet each other at the intersection of the axis of the joint, thus eccentricity is eliminated. The rigid analysis assumes that the stiffness of the joint is large and infinite, thus, it stays fully rigid under any load. In reality, there is a finite strength of the joint which will deteriorate under increasing load. The two assumptions are extremities of joint behaviour. In

reality, joint behaviour lies somewhere between pinned and rigid behaviour, the term used in literature is semi-rigid. Semi-rigidity is variable and depends on the material and construction of the joint. The assumption of a pinned joint leads to over designing and therefore increases cost and waste of material on a structure. It has been commonly adopted because of its simplicity in analysis.

Although the concept of the semi-rigid connection has long been recognised as a more accurate approach to the real behaviour, it has yet to be widely accepted by engineers. This is due to the extra computational work involving more data required for the design. The joint behaviour data is usually lacking. The design for semi-rigid behaviour can be achieved by simplifying the process of designing for semi-rigid joints. This can be helped by employing user friendly computer programs to allow the user to carry out joint designs with semi-rigidity in mind via simple computing methods. Indeed this is the aim of the thesis

1.4 Type of connectors

There are many types of mechanical fasteners used in timber structures. Within the connection, stresses are transferred from one member to another. The strength of the connection depends on how efficiently it has been prepared. The selection for the type of connection depends on factors such as site conditions, whether prefabrication is required, and costs.

Connectors range from a simple nail to the more complex nail plate. Some connectors require timber surface preparation. Nails are simple connectors and provide easy construction of the joint. However, there are different types of nails. For example, annular ringer shanked nails are designed to give extra lateral strength against withdrawal, which may arise due to vibrations. When the nail is hammered into the timber the shank acquires a bite into the timber thus resisting lateral movement (Fig. 1.4.1).

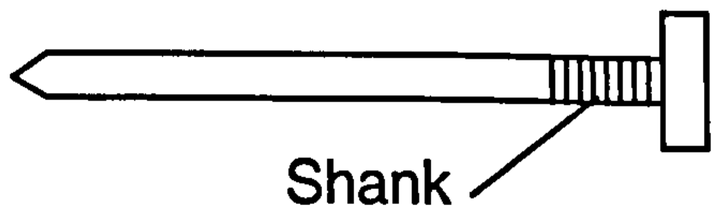

Fig. 1.4.1 – Shanked nails

Nails can also be fired into timber by the use of a nail gun, which gives good fit and precision and speeds up construction. Another type of connector which requires the use of a gun is the staple. Staples are used for lighter loads such as securing light cladding such as plaster-boards onto timber members. Glued joints are frequently nailed to allow the glue to cure for a tight fit. Screws are also used and are particularly popular in DIY furniture where the option of dismantling the joint is possible. Because of the thread in the screw, there is also resistance to withdrawal. Bolts are frequently used in timber connections. The strength of the connection lies in the bolt bearing against the timber therefore little advantage is gained by using high strength bolts. Large washers

are usually used under the head and nut to distribute lateral loading and preserve timber crushing thereby increasing strength. More complex connections such as the split ring are used to extend members for large span timber structure. Grooves with a hole at the centre are cut into two members to allow the ring to be sandwiched between them. The connection is completed once tightened with a nut and bolt. Galvanised tooth plate connectors are also popular and allow prefabricated structures to be delivered on site. More complex connectors such as beam hangers allow joists to be connected at perpendicular to each other. Fig. 1.4.2 below shows just some of the examples of connectors mentioned.

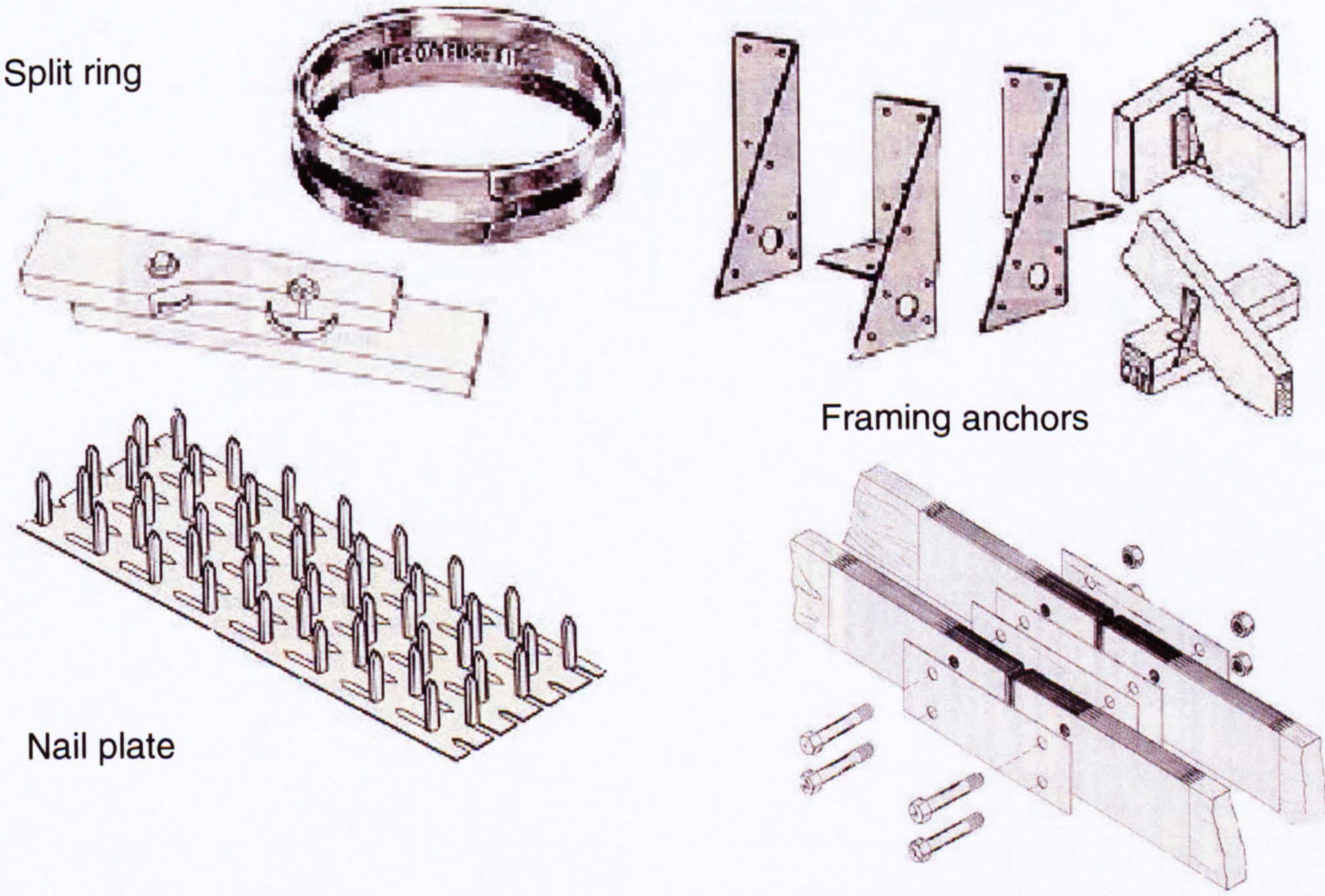

Fig. 1.4.2 – Connectors[49, 50]

1.5 Metal plate connected joints

Through the literature review, much technical information had been revealed on Metal plate connected (MPC) joint design. Much of these aspects of MPC joint design will not be considered in depth. To do so would have been beyond the scope of this thesis. However, these aspects are acknowledged as tests carried out in this project (mentioned later) will exhibit some of the characteristics and need to be recognised to understand the failure modes. Some of the more notable points are discussed here.

Nail plate

The nail plate originated from the USA in the late 1950's. The design was developed from hand nailed steel plate. Punch metal plates proved to be easy to fabricate and were cheap to manufacture. Furthermore, the connector also made it convenient to pre-fabricate trusses before delivery. These factors drove down the cost of construction thus the connector became popular in timber construction. The popularity of the connector demanded efficient timber connections. The design of the connector has been developed over the years to carry loads effectively. Some of the factors considered in the development are the result of much research and are discussed in this section.

The overall strength of an MPC connection depends on the angle at which the load is applied to the plate and the angle of the load to the grain. As shown below the direction of the nails runs perpendicular to the length of the plate.

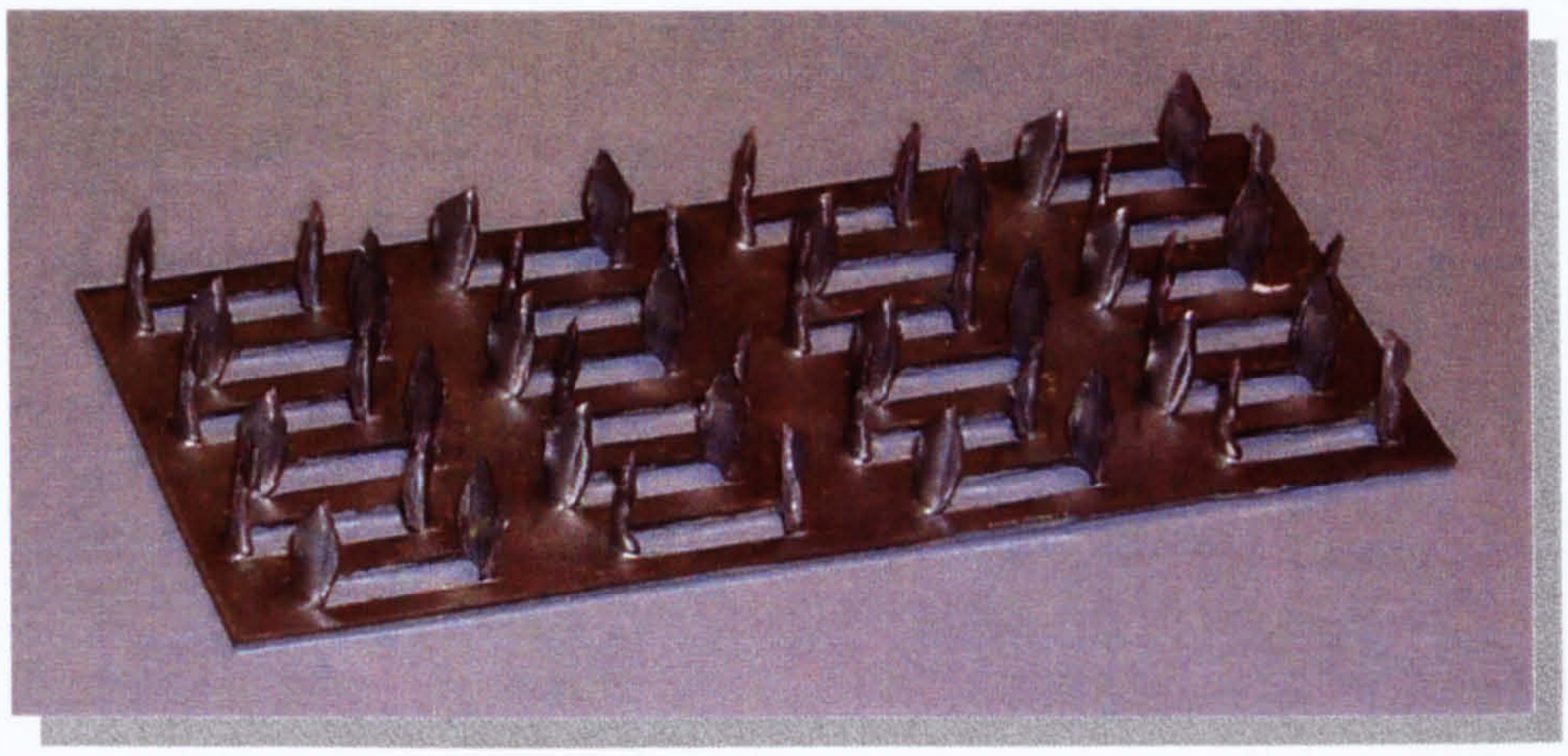

Fig. 1.5.1 – Nail Plate

In general the connection performs best when the nail is perpendicular to the grain, with the load parallel to the grain. The strengths of various orientations are detailed in Appendix A2. In the table, the angle at which the load is applied to the grain has a greater effect on connection strength which suggests that the timber is the critical component of the joint. Indeed this aspect of MPC design has also been investigated as mentioned in the literature review. The two particular joints investigated were T joints and tension splice joints. The results of this paper agree with Alpine's certificate.

Another aspect of nail design is the location/pattern of how nails are distributed on the plate. It can be postulated that if plates are designed in a way such that there is a high number of nails per unit area, i.e. high nail density, it can lead to premature failure. The nature of the failure maybe shredding of the timber because of the number of nails already punched in the timber, they effectively destroy the foundation for the nail to react on. At the other end of the scale is the minimal nails spread over a large area. This would again cause premature failure, however, this time the mode of failure maybe the failure of the nails by bending or pull-out. What has been described is an example of the two extremes of nail design. The discussion points out the requirement to design the plate such that there is a good balance of nail spacing to distribute

forces efficiently and therefore prolong joint failure. There should be sufficient cover of timber for each nail to provide a strong foundation. A common practice in achieving the above is to stagger the nails so they are not too close but provide a good distribution of force from nail to timber. Staggered nails give the plate extra rigidity as stresses are distributed to the plate more evenly.

The design of the nail itself is also a subject for discussion. Inadequate material at the root of the nail will give a weak bending stiffness and cause the nail to bend, since the bending moment is greatest at this point. Nails are made by punching the plate and pulling out the metal which is then twisted to form the nail. The twist in the nail gives the nail extra stiffness and increases bending stiffness at the base and along its length. Whilst the twist increases the bending capacity the shape of the nail allows sufficient contact between the face of the nail and the timber. The tapered design of some nails is also notable. The reason for this is that less material is required at the tip of the nail because bending and shear moment are minimum there. This is also necessary for the joining of the connection where the plate is compressed into the timber. A tapered nail would sink into the timber quite easily without weakening or distorting the nail.

Gap of abutting members

Gaps have an effect on connections in compression. The gap in the joint allows compression forces to transfer from one member through the plate to the adjacent member. This system places extra stress on the plate. Where possible, gaps should be avoided and the members should be in contact. Hence, connections with members touching will most certainly sustain higher compression forces. So why are the gaps used? The answer is, that gaps are

provided because of the automated process of constructing the truss. Typically trusses are rolled onto some sort of manufacturing line and are restrained. Plates are positioned and compressed in, either by a roller or flat press. During this process there can be no guarantee that the timber will be absolutely still. Hence, gaps may or may not occur. Consequently, design codes are conservative and assume gaps do occur. The effect makes no difference for connections in tension.

1.6 Objectives

The objectives of the thesis are:

- Determine experimentally the shear, axial and rotational stiffness of all connections from a selected truss and determine whether there is any interaction between axial loading and rotational stiffness, and bending moments on axial stiffness.
- Conduct full-scale test on the selected truss to provide data for overall truss analysis.
- Develop a 2-D beam element structural analysis program using test data to deal with the effects of non-linear semi-rigid connection analysis.
- Develop 2-D finite element model to view stress regime in the plate and other areas of the truss.
- Compare all models with each other and with full-scale truss test and draw conclusions.

How the objectives were determined is discussed in detail in section 2.7

1.7 Scope and layout of the thesis

Chapter 2 gives a review of literature, selected for their relevance to the project. It is not aimed to be an exhaustive review of literature on timber connections. The Chapter concludes with a discussion of how the project objectives were established

Chapter 3 describes the experimental side of this thesis. The preparations and the design of the truss for this research are presented along with all the instrumentation involved. The general theory and the necessary hardware and software involved in the digital measurement system are also presented. This is followed by a description of how the data is interpreted to produce semi-rigid rotational, axial and shear connection properties from the joint tests. The loading arrangement for 4 combined loading tests and one full scale truss test is demonstrated with illustrations, then ending the chapter with the test procedure.

In Chapter 4 the theory used to analyse trusses with semi-rigid joints is presented. Equations for non-linear semi-rigid effects are derived from the slope deflection method. The assumptions of the analysis are outlined. The computational procedures used for the automated solution are presented next. For the finite element analysis, the FE software ANSYS is used for 2-D modeling and analysis is presented in Chapter 5. Facilities to model non-linear material behaviour are also detailed.

The results of the experimental tests are presented in Chapter 6 where joint failures are postulated. Results of the analysis mentioned in Chapters 4 and 5 are also presented. A comparison is made between the methods of analysis and the truss test results. Finally, the theoretical and experimental results are

discussed in Chapter 6 followed by the conclusion in Chapter 7. Recommendations for further work are presented in Section 7.6.

Chapter 2

Literature review

The literature review concentrates on the Metal plate Connection as this is the connection of interest. More general text on timber strength properties will not be mentioned here but those of which have been referred to are listed in the bibliography. The literature mentioned herein were either used to develop ideas in this thesis or of some direct relevance.

2.1 Semi-rigid behaviour

These papers provide a light introduction to semi-rigid analysis. Semi-rigid joint behaviour has been recognised for some time now. Using a matrix method, Monforton and Wu[1] explicitly derived the semi-rigid joint equations by using the conjugate beam method. The semi-rigidity of the joint was introduced by modifying the fixed end forces and the element stiffness matrix. Lei and Grierson[2] derived similar equations but used the slope deflection equations. Both these papers present the semi-rigid connection as a rotational spring. The rotational spring is simply a concept used to visualise stiffness of a connection and represents no physical dimension.

Sasaki and Takemura[3] extend the joint semi-rigidity concept to axial and shear components. Joint tests were conducted to investigate the effects of different orientations of plate axis to loads in tension, and moment. Load-deflection curves similar to that of Foschi[12] were fit to the results of these tests. A stiffness matrix program with rigid joints was used where the functions were implemented into the analysis, and calculated non-linear semi-rigid truss displacements. Four different types of full-scale parallel chord trusses, namely

the Howe, Pratt, Warren 1 & 2 truss were tested. The load deflection analysis of the program agreed well with experimental results, but not always when the truss reached near its capacity. Computed truss member axial strains were in good agreement with the tests. From the analysis they found that increasing the joint stiffness is more effective than increasing the member Young's Modulus for overall truss stiffness. The results are presented in graph form and are reproduced in Fig. 2.1.1 below. It shows the comparison of the physical test and analytical results for the mid span deflection of the trusses mentioned.

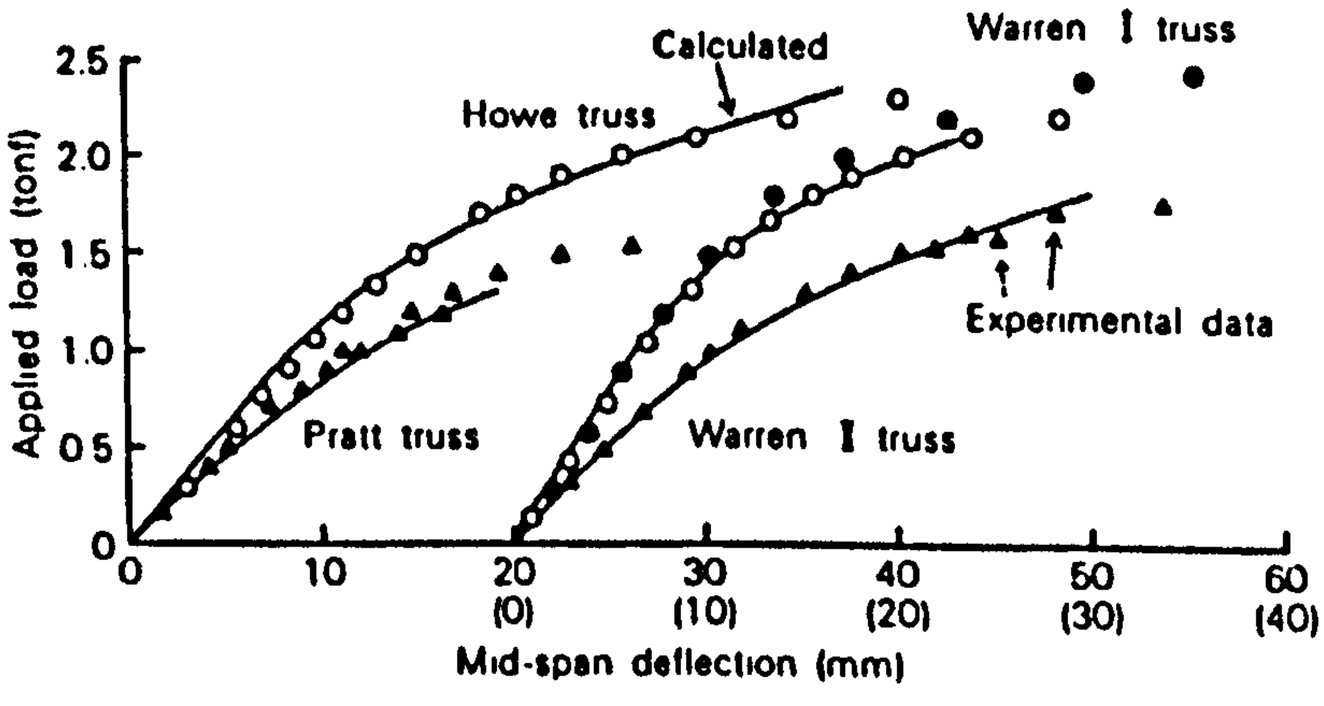

Fig. 2.1.1 – Results of analysis and experiments

Gupta, Gebremedhin and Cooke[4] applied experimental joint test data[51] to a semi-rigid truss program. A 'fink' truss was the subject for the analysis. Three model variants under loading were analysed. This comprised of a pinned, rigid and semi-rigid joint model. A comparison of the displacements at the bottom chord joint, tension splice joint and heel joint was made between them as presented in Table 2.1.1.

Displacement	Method of Analysis		
	PP	RR	SR
Web at the bottom chord joint (Y-displacement, mm)	6.64	6.42	6.94
Tension splice joint (Max. Y-displacement of truss, mm)	15.78	8.35	10.39
Heel joint (Rotation, rad)	0.001307	0.01115	0.01195

Table 2.1.1 – Comparison of predicted joint displacements

The calculated forces at the top and bottom chord member were also made and are presented below.

		Top Chord			Bottom Chord		
Force	End	SR	RR	PP	SR	RR	PP
Axial (N)	i-end	11583	11677	11726	-11178	-11276	-11339
	j-end	-12482	-12575	-12629	11178	11277	11339
Shear (N)	i-end	1259	1299	1335	294	297	311
	j-end	903	867	827	538	535	520
Moment (Nm)	i-end	493	567	584	-82	-69	0
	j-end	-82	-69	0	-270	-268	296

Table 2.1.1 – Comparison of predicted joint displacements

They concluded that the semi-rigid analysis was more accurate than the pinned and rigid analysis. Thus, the predicted response depended on the assumption for joint behaviour. This highlights the importance of accurately defining the behaviour of the connection.

2.2 Metal plate connector

More advanced and complex methods of understanding the root of semi-rigid behaviour for metal plate connected joints have been proposed with varying degrees of success. Vatovec, Miller and Gupta[5] developed a metal-plate-connected joint model using commercially available Finite element analysis software, ANSYS. They incorporated the material properties, and three components, teeth-to-grain-to-direction of force orientation, wood-to-wood interaction, and gaps between the abutting members. This was represented by three springs simulating the behaviour of the three components. Good agreement of the displacements was achieved between experimental tests and analysis results. A plots of the results are reproduced in Fig. 2.2.1 below.

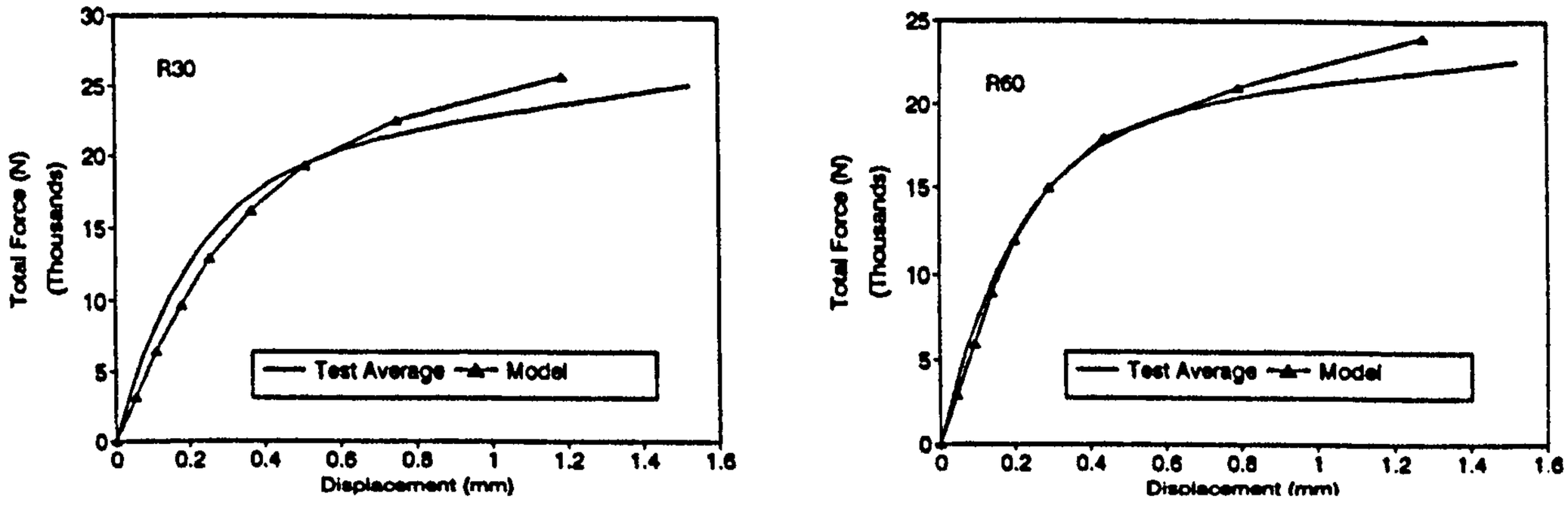

(a) (b)

Fig. 2.2.1 – Experimental and model results

The plots shows the experimental and modelled response of a joint with a plate-to-grain orientation of 30° and 60° for plots (a) and (b) respectively. The analysis was developed further in a paper by Vatovec *et al*[6], where the ANSYS joint models were used to investigate the overall scissor truss response in a 3-D model. In addition to this, a 2-D model was investigated for pinned, rigid and semi-rigid mode. For the semi-rigid analysis, the value of joint semi-rigidity was obtained from existing joint test results. The deflections of the models were compared with experimental test results and were shown to be within 10% at the centre span of the truss. However, member force and moment predictions were not so good. The bending moment prediction of the 3-D model at the heel joint was shown to be significantly higher than the 2-D models. In general, between the 2-D and 3-D models, there are larger discrepancies in the prediction of bending moments than axial forces. This demonstrated the potential of employing a 2-D or 3-D model for the analysis of trusses and the importance of defining a joint model for accurate force predictions in the truss.

Crovella and Gebremedhin[7] conducted laboratory connection tests and proposed two analytical approaches to predict joint stiffness. The first was a finite element method where the action of the nail and timber was modelled.

From the analysis, elongation, tensile stresses and strains were predicted throughout the plate and timber. The second approach was to model the nail and timber system as an elastic foundation. The idea was to treat the nail as a cantilever like a cantilever beam, but supported by an elastic foundation which is the wood. The wood and steel plate are given moduli of elasticity determined experimentally. The other end of the nail attached to the base of the plate can be modelled as a joint with some stiffness. Two conditions were tried, pinned and rigid. It was further found that the finite element predictions of stiffness values were conservative and that the properties by the elastic foundation method was more comparable to the experimental results. It further concluded that for the elastic foundation method, the assumption that the base of the nail is free to translate but rotationally fixed is more realistic than the pinned assumption.

The use of this elastic foundation model was extended by Gebremedhin and Crovella[8]. They attempted to analyse the load distribution along the length of the plate through modelling the action of single tooth of a metal plate connector. Forces per nail were evaluated to give total force and deformation in the plate, thus the total stiffness of the joint could be determined. To validate the model 12 tension splice plates were tested. Beams were classified into 3 groups, short, long and medium. The length of the beam plays a factor in the two possible types of failure. The first is the withdrawal effect of the nail where the nail pulls out of the timber. The second, is due to the elastic foundation where the timber fails through timber crushing by the nail. An error analysis was used to quantify potential errors that can be induced due to the uncertainty of parameters. From these results they concluded that the foundation modulus

introduced the largest error in the model. Analysis was carried out using the model and different load distribution patterns and failure modes mentioned above were noted.

Groom and Polensek[9] developed a model of the mechanism between the nail and timber of the MPC joint. The model was adapted from the Kuenzi[15] model of beam-on-elastic-foundation concept. The objective of the paper was to develop a method of predicting the mechanism of force transfer between wood and truss plate. Kuenzi's model was modified to account for the inelastic behaviour of the tooth and wood foundation due to bearing pressures. It also accounts for the location of the tooth and changing of moment of inertia along the tooth length. The model requires grain and teeth orientations, plate geometry and the properties of timber and wood. It was then compared to joint tests where good agreement was found for joint slip. The Beam-on-elastic foundation model is a general model and can be applied to any bar like timber connection that is bedded in wood such as nails and bolts.

Cramer et al[10] presented a model for combined bending and axial loading of a wood splice joint. A model was built through 2-D plane stress finite elements. The basis of the model is to consider individual stiffness contributions of the wood, wood-tooth interaction and the plate. The timber is treated as a solid, linear continuum possessing orthotropic properties and the plate as non-linear with isotropic properties. The wood-tooth interaction is modelled through non-linear elastic spring elements possessing two degrees of freedom. These springs account for friction/bearing between wood and steel tooth, and the out-of-plane bending of the tooth due to withdrawal effects. The properties of the

spring are evaluated from actual test data and is represented by Foschi's[12] exponential function. Results of the model showed a different proportion of deformation for the three components: wood, plate, and wood-tooth for different size plates and members. This indicates different contributions of stiffness from the three components. In general, on a per-tooth basis, it was concluded that smaller size plates exhibited a uniform load distribution whilst larger plates did not, contrary to design assumptions. However, it does indicate that the model may not be as accurate for larger plates as it is for smaller plates. Later Cramer, Shrestha and Mtenga[11] presented a Metal plate connected model in an attempt to predict truss member forces. The proposed model accounts for joint eccentricities and non-linear semi-rigid joint behaviour. One rotational and two translational springs were modelled at the centroid of each plate-timber contact area in a connection. The springs having no dimension and were lumped and connected to the member through a rigid link. Input was simplified by automated means. The spring and rigid link were calibrated from experimental tests where geometry and tooth characteristics were obtained. Typically cross-section sizes, boundary conditions and strength properties etc. are required for the model. Several existing models are compared to the new one presented. The result of this comparison concluded that existing models do not predict member forces as accurately as the proposed method.

Beineke and Sudarth[13] stressed the need for sophisticated mathematical techniques to model punched metal plate connectors. They used Demarkles[14] equation, which is analogous to an adhesive layer and is used to predict mechanical joint response under axial loads. The theoretical model essentially predicts joint slip at a given load. 35 tension splice joints were tested with 3" by

4", 6", 8", 10", and 12" long plates. However, data collected from these tests did not compare well with those from the analytical approach. Subsequently, an alternative simple method involving an empirical system where the plate is essentially replaced by one solid member and calibrated with test data from the shortest and longest plates. Thus, the parameters required for joints with plates between these two boundaries can be extrapolated to obtain joint stiffness values.

2.3 Fictitious members

Lau[16] used a software called PPSA 2[17] (Purdue Plane Structural Analysis), which is a plane frame structural analysis program where members are assumed to be linearly elastic. Pinned, rigid and semi-rigid joint models are possible with fictitious members. These imaginary members and nodes are inserted at the connection model joint response. Force displacement results from shear and heel joint tests was used to calibrate fictitious member properties and implemented into PPSA 2 to simulate overall truss behaviour. A fictitious member is an imaginary member placed in between nodes which can simulate joint rigidity and eccentricity. The modulus of elasticity of the fictitious member is varied until it matches the force displacement results of the joint experimental test. This calibrated member can then be placed in the truss model to represent that particular member to predict overall truss semi-rigid response. Another program developed for the same purpose is the Canadian program called SAT[18] (Structural Analysis of Trusses). SAT treats the frame as linear elastic and the joints non-linear using the exponential Foschi[12] function derived from test data. The variables of the function are varied until a good fit is achieved with the joint test force displacement plots. To verify these models a

total of 12 shear joints were tested, 3 different types of plate orientation repeated 4 times. For the heel joints 4 different orientations were repeated 5 times. There was generally good agreement with SAT's predictions of joint stiffness and forces. However, the predictions for heel joint tests were not so good. Finally the heel joint tests were simulated by PPSA 2 where the value of the modulus of elasticity for the fictitious member was calibrated to fit the experimental data.

Another example of the use of the fictitious member method was presented by Poutanen[19]. He discussed ways of modelling eccentric loads in a truss using fictitious members where imaginary nodes and members are inserted into 2 dimensional truss analysis to model eccentric loads. He argues how the position of the nodes can affect the stress levels in the connected timber. This relates to where the centroid or reference point of the joint is designated. This can be at the centre of the plate itself or where all the centre lines of the members meet. There are two methods, one is called the edge method and the other the centre line method. The edge method is based on the fact that the centre of the joint is located at the chord edge, whereas the centre line method is where the centre lines of the members meet. It was found that the stress distributions in the members were significantly different for the two analyses due to different eccentricities. However, a new analysis has been developed which can be applied to several joint configurations. The model accounts for eccentricity in the plate, timber and the contact between abutting members. Experimental tests designed to measure eccentricity were performed. The results of the analysis agree with the experimental tests.

The use of PPSA2 was described again by King and Wheat[20]. Four different analogue models were tried with. The first model assumed that the top and

bottom chords were rigidly connected to other members. Web members connected to the chord were assumed pinned. The second model was similar to the first, but the modulus of elasticity values of the web members were reduced to account for joint slippage. Reduction factors were 1/4, 1/5, and 1/6. The model with the best fit the truss test results was chosen for a comparison. The third model incorporated the fictitious member joint model to account for contact area. The model was similar to analogue models 1 and 2 except that the web was again rigidly connected but incorporated fictitious members to account for the connection end eccentricity. Finally model 4 was similar to 3 but the specific gravities of the timber and gaps of the connection were accounted for by reducing the stiffness. Timber contains moisture and voids. The specific gravity is a measure of how much solid substance is actually in the timber. The member contributes to the joint stiffness and therefore a reduction in timber material can also reduce the stiffness of the connection. The results concluded that for most cases all 4 models yielded similar member forces suggesting member forces are influenced by the truss configuration and geometry rather than the stiffness of the joint. However, significant differences were found in the bending moment for each model. This suggests that bending moment is sensitive to the stiffness of the joint. Results for model 4 were similar to those for model 3. This suggests that the effect of plate/wood gaps and member specific gravity on overall truss behaviour are small. Finally a comparison of the models were made with full-scale parallel chord truss tests, nine parallel chord trusses were designed and tested, 3 replications of 3 designs. It was found that model 1 underestimated the truss deflections. It explains that additional deflections from the truss are due to slippage at the joints. Model 2 compared better to experimental results due to the reduction in the modulus of elasticity to

account for slippage. The deflection predicted for model 3 and 4 are very similar. This suggests that the specific gravity and plate wood gaps did not significantly affect the truss deflections. Both models predicted truss displacements better than model 2.

Another example with the use of fictitious members to demonstrate semi-rigid connection was presented in Riley, Gebremedhin and White[21]. The fictitious members were sized using joint test results. Once the sizes of the fictitious members were determined they were then rigidly connected to the appropriate member of the truss. The fictitious member analysis of a fink truss is compared to the pinned, rigid, and semi-rigid analysis of the same truss. The semi-rigid analysis employs the Truss Plate institute (TPI) specification for truss analysis through the matrix method where fixed end forces and element stiffness matrix are modified to account for semi-rigid connection behaviour. The matrix method is also reported in Monforton and Wu[1], Lei and Grierson[2] and Sasaki and Takemura[3]. The results show that displacement and maximum bending moment of the truss in the fictitious member method lies between the pinned and rigid analysis, and less than the semi-rigid analysis. It is also closest to the semi-rigid analysis. The pinned and rigid analyses exhibited the largest and smallest deflection respectively. In general, results indicate that semi-rigidity is somewhere between the extremes of pinned and rigid assumption, but closer to the latter.

2.4 Combined loads

Papers mentioned so far always at some point require experimental results to verify and calibrate theory and methods to predict structural response.

Gupta and Gebremedhin[22] *et al* carried out tests using a specially developed apparatus that could contain all manner of joints to determine the axial and rotational joint stiffness as shown in Fig.2.4.1.

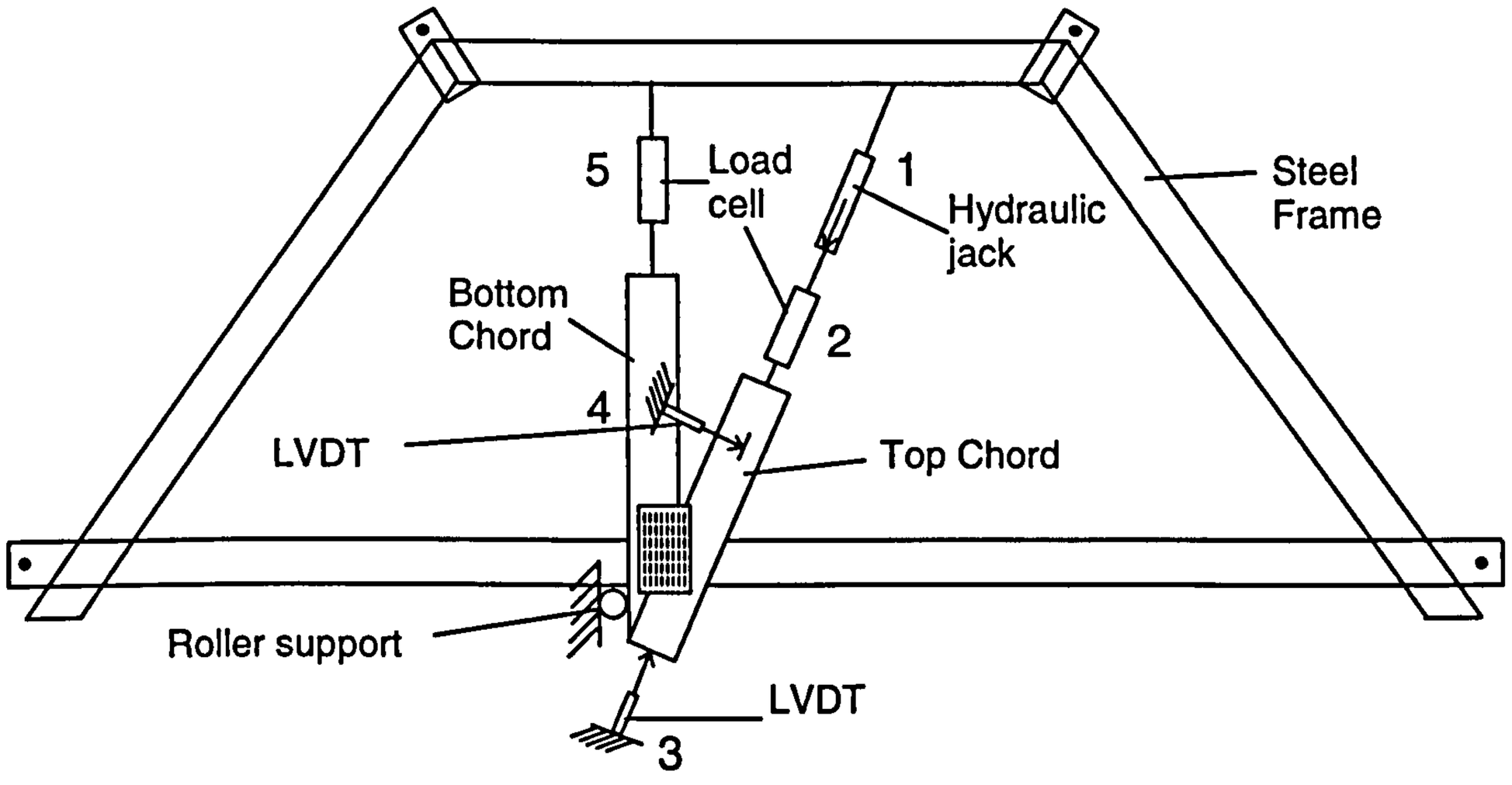

Fig. 2.4.1 – Testing apparatus

As illustrated in the diagram, at 1, load is applied directly by a hydraulic jack to the top chord member. At 2, a load cell is placed in between the jack and the top chord to measure axial loads. The corresponding displacement for the applied load is measured via an LVDT at 3. Some redundancy is introduced where a load cell and displacement transducer is located at 5 and 4 respectively. The connection is supported by a roller on the bottom chord. Whilst the hydraulic jack is manually operated the LVDTs record displacement via a computer. The versatility of introducing other connections can be easily implemented.

A tension splice, bottom chord and heel joint of a fink truss were tested. The apparatus was further used in Vatovec, Gupta and Miller[23] . Five joints were tested this time. Again, the main object of the work was to evaluate strength,

stiffness and the failure mode of the joints. The loads in the members connecting to the joint were determined by running a finite element model in ANSYS assuming rigid joint conditions. These loads were then applied to joint tests to determine axial and rotational stiffness. Different failure modes were reported for different joints where joints behaved in a non-linear fashion. The results of the joint tests were then used in the preliminary model. The model compared well with full scale truss experimental results produced by the plate manufacturer, Alpine automation.

Moment loading in a joint occurs when the direct axial forces at the joint transmitted from the members do not pass through the centroid of the joint due to joint dimensions. In addition, direct axial loads rarely travel through the centre of the member. This combination inevitably creates eccentric loads and in-turn induces bending moments at the connection. Thus pure axial loads can never exist in a truss system. The effects of eccentricity have been identified in trusses, and tests designed to investigate the effects of eccentrically loaded joints have been reported. A paper presented by Wolfe[24] reported on combined loading tests. Pure axial tension, bending and combined loading were applied to tension splice joints. Direct axial loads were applied eccentrically at different distances from the connection centre thus varying the moment load. He concluded that there is a clear indication of interaction between tension and bending and that the behaviour is non-linear. The results of the tests showed that as the eccentricity increased the axial stiffness capacity decreased. However, the decrease in rotational stiffness with the increase in axial loading was much less significant. This implies that a bending moment has a detrimental effect on the axial stiffness. A tension and bending interaction

equation was derived to represent the results. A paper presented by Gupta[25] investigates this interaction behaviour and reports of similar results. He also concluded that there is a clear indication of interaction between tension and bending and that the behaviour is non-linear.

Another example of combined/eccentric loading is presented by Massé and Salinas[26]. They adopted an approach to predicting deflection in a truss. Again axial load was applied eccentrically to tension splice joints to achieve combined loads. The conclusion was that the axial force poses a significant effect on rotational stiffness of the joint. The effect of moment loading on axial stiffness is thus measured as a function of eccentricity. Joint rotational stiffness decreases as axial force increases. There clearly is interaction between the two strength parameters. However, the joints tested were not metal plate connected joints, but multi-laminated nailed joints. Nevertheless, it was shown that combined loads in truss joints are significant factors regardless of joint type.

O'Regan, Woeste and Lewis[27] present a design procedure to determine the allowable design capacity of the steel net-section of a tension splice joint. Three models were developed to determine the ultimate strength of the net-section of the joint subjected to tension and bending and then compared to tests. The models were adaptions of three of Noguchi's[28] models. The most accurate model assumed linear stress distribution in the timber. The entire steel plate was assumed to have reached a maximum equal to the ultimate tensile stress. The design procedure was based on this model and then compared to alternative design methods and was shown to be more suitable.

2.5 Timber models

The prediction of timber structure response must be accompanied by a knowledge of the material that has been used. With the increasing demand of non-destructive testing for timber strength, the definition of timber strength from elastic and beyond have been a focus of study with varying methods.

Hasbe and Usuki[30] provide a failure criterion for wood. The criterion is derived from Tsai and Wu[29] for isotropic materials and is a general theory for anisotropic materials. It is simplified to an orthotropic problem and includes the effects of compression, tension along the grain and shear forces perpendicular to the grain only, i.e. plane stress conditions. Timber tests were conducted and values substituted into the failure model.

The Tsai criterion appeared again in a paper presented by Bouchair and Vergne[31]. It is used as part of a model to predict the behaviour of a bolted joint. The criterion is again reduced to that of a 2-D orthotropic material as timber is frequently idealised. The difference in tension and compression strength in the timber is taken into account. The criterion is used as part of a finite element analysis to predict the non-linear response of a bolted joint. The model provides a good comparison with experimental results produced by other authors.

An alternative approach to evaluating timber strength is presented by Goodman and Bodig[32]. A sinusoidal function to predict timber strength was developed in conjunction with the Hankinson's formula. The Hankinsons[33] formula is used to predict timber strength loaded at an angle to the grain, where the ring angle is constant, i.e. it is a 2-D model. A tree grows a layer of timber annually and the result of this is annular rings in a timber section. To simplify analysis, it is

assumed that the strength of the annular ring loaded at any angle is constant, i.e. the ring angle is constant. The new proposed sinusoidal model is 3-D and allows variation of the ring angle as well. Compression tests were conducted for specimens with varying grain angles and ring angles. The axial load was applied parallel to the longitudinal axis of the specimen. The model is considered to be conservative but compared well with experimental data. The same authors later attempted to predict timber elastic parameters as presented in Bodig and Goodman[34]. They present a non-destructive method to predict various elastic parameters for some species of timber. Power type regression curves were developed for 12 elastic parameters of 18 softwood species. An exponential relationship was used to fit a regression curve to match the experimental data from timber tests. The density of the timber is used as the basis of the predictions because good correlation was found between density and modulus of elasticity. This technique is claimed to be reasonably accurate in the absence of test data. Thus the strength of the timber can be found through density.

Pellicane, Bodig and Mrema[35] presented a Finite element analysis to model loading perpendicular to grain. Results of the model showed that a complex stress regime exists within the timber even when a uniformly distributed load is applied. The paper reports the effect on timber with regards to the loading area and the size of the specimen. Tests conducted showed that the specimens, which were loaded through a plate partially covering the specimen gives higher strength than a plate covering the entire specimen. This is the so called "edge effect". Fig. 2.5.1 illustrates the load system.

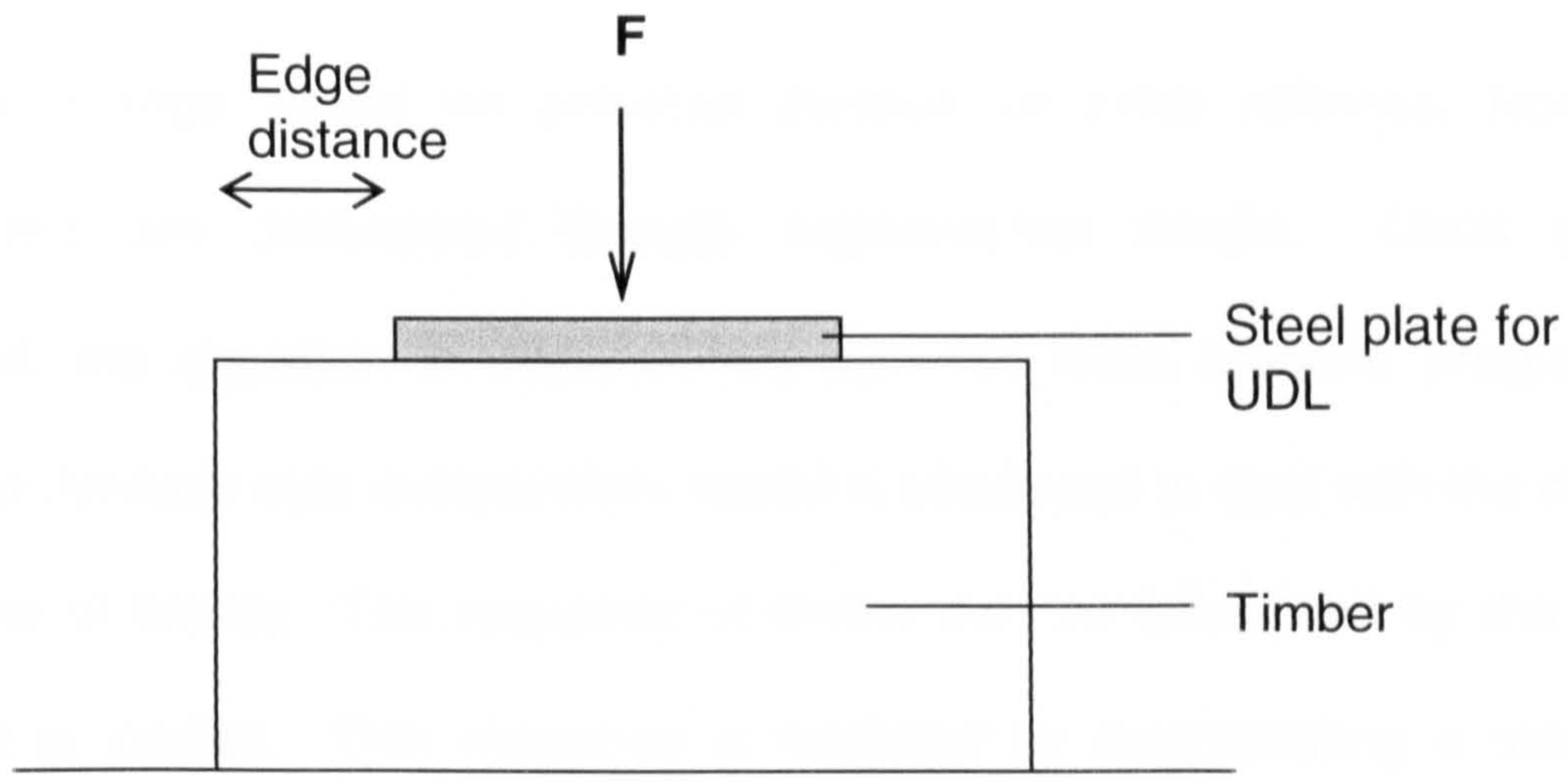

Fig. 2.5.1 – Partial loading of timber specimen

Using data from the finite element model, an empirical equation was developed to compute maximum stress concentration as a function of loading, specimen geometry and material properties. They concluded that transverse compression capacity of the wood increases with increasing total edge to surface area ratio of the plate. The formulae could be used to improve design codes. As illustrated in Fig. 2.5.2, the edge distance is indicated as a bold line, i.e. the circumference of the timber.

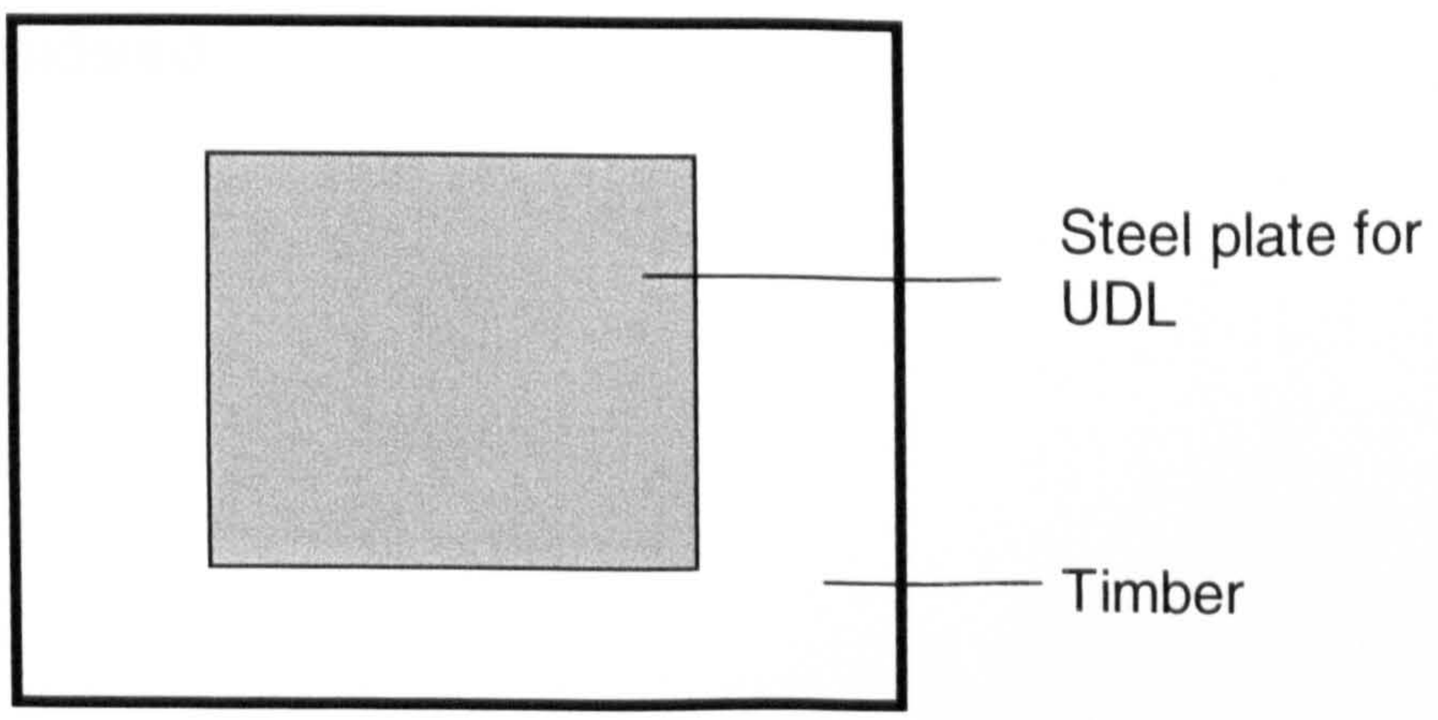

Fig. 2.5.2 – Plan view of loaded timber specimen

Tabiei and Wu[36] developed 3-D constitutive equations for wood materials and implemented the model into the finite element code program DYNA3D. An incremental and iterative procedure is used to calculate stresses. The constitutive material matrix for stress strain relationship is determined

experimentally. User defined non-linear parameters are used to control the stiffness change based on previous iteration or initial stiffness. Non-linear parameters are determined through experimental results. Once a fit is obtained, the equation is implemented into the finite element program. A modified Johnson rate independent model is employed to deal with the dynamic response of timber. The response of timber can be influenced by the rate at which it is loaded. This response is captured by incorporating a strain rate function into the model. The model was validated by test results from other researchers. Good agreement was found between the model and test results.

Mallory *et al*[37] developed a three dimensional constitutive model for timber for use in a bolted connection loaded parallel to the grain using the finite element program, ABAQUS. A tri-linear compression stress-strain relationship and tri-linear shear stiffness degradation for the timber model was used where the bolt was treated as elastic-perfectly plastic. Fig. 2.5.3 below illustrates the model. The symmetry of the load system has been taken advantage of where only half the model is considered.

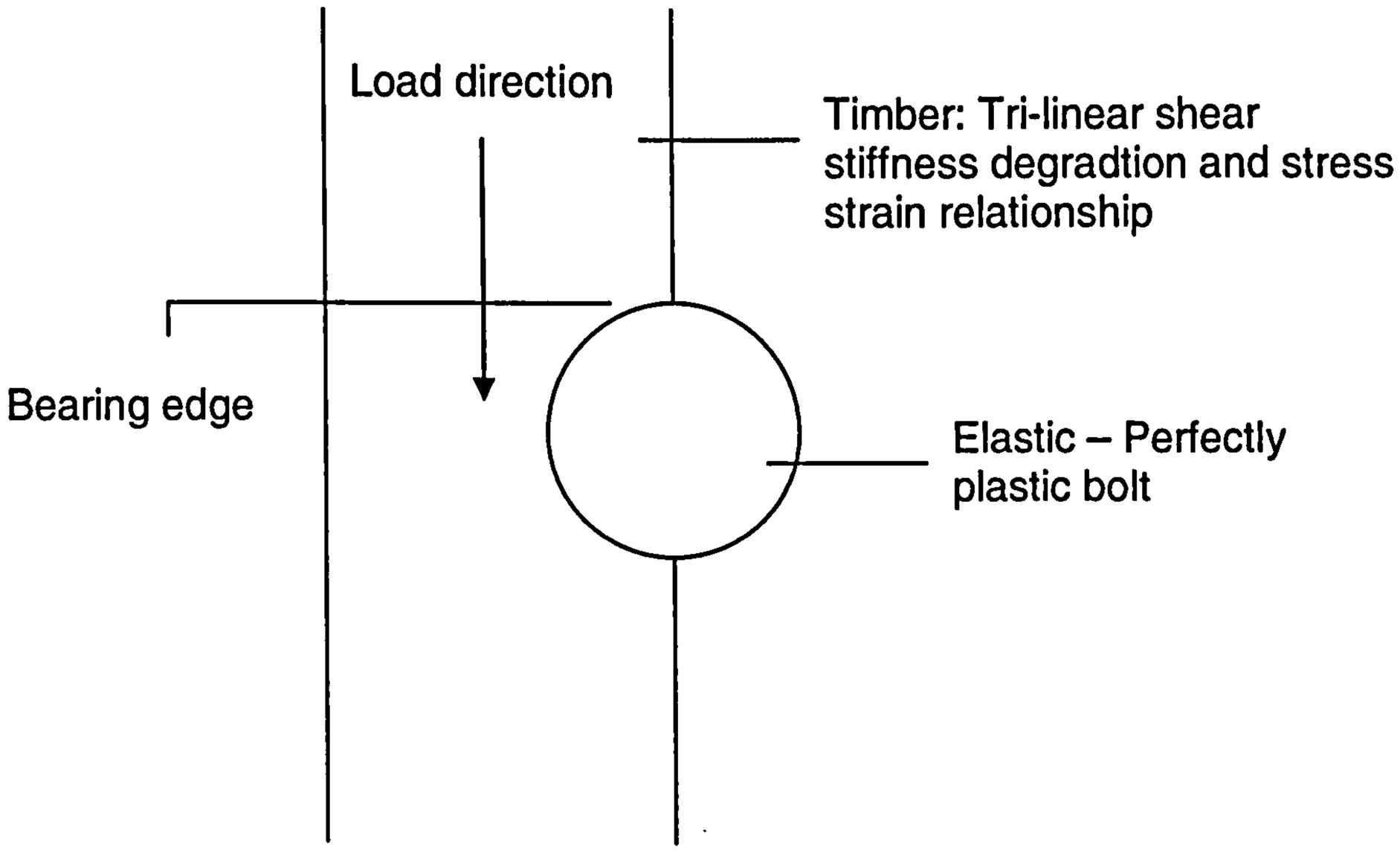

Fig. 2.5.3 – Sketch of model

The material values are input to a finite element model with contact elements. Force displacement results of the model were compared to experimental results. The model was found to be adequate up to a displacement of 0.8mm. In general the models predicted a slightly stiffer force-displacement curve than the experimental tests. A possible explanation for this difference could be due to ignoring the degradation of the tension strength perpendicular to the grain in the model. A more complex model is required for higher load and other wood grain orientations.

2.6 Literature summary

The metal plate connected joint was first originated from the US in the early 1950's. Since then its popularity has spread across the world in roof trusses. The achievement of its popularity in timber joints is due to the price in producing these plates and practicality in constructing the joint. However, such advantage doesn't come at a cheap price in terms of complexity. The nature of the connection lends itself to extremely complicated stress regimes under load. This is coupled by the already complex and less predictable anisotropic strength of timber. All in all, it is a very difficult task to understand and ultimately predict the response of these connections.

Much research, both experimental and theoretical has already been conducted in metal plate connected joints. The literature reveals what has generally been done and leaves room for more research.

The semi-rigid approach is widely accepted and several solutions with various levels of complexity have been reviewed. The stiffness matrix method utilises imaginary springs for 2-D analysis to account for the semi-rigid joint behaviour. The use of Foschi's exponential function is notable, as it has been widely used by many authors to model non-linear semi-rigid behaviour. Another useful tool is the use of fictitious members to describe the behaviour of the semi-rigid joint. Although these methods do account for plate deformation and joint slip they do not, however, provide data for stress analysis. The use of commercially available finite element packages such as ABAQUS and ANSYS can produce models at very fine levels, such as modeling the mechanism between the nail and timber and provide a detailed analysis of the stress regime in the connection. However, these methods usually demand time and much data to bear fruit and usually require more powerful processors. The importance of

computer programs as part of the advance in timber structural engineering is evident from PPSA 2 and SAT, the two pieces of software developed to model semi-rigid timber trusses. It is widely agreed that the connection behaviour is fundamental to the prediction of truss behaviour, which makes this process of the analysis more important. Simple analysis can provide accurate but not detailed results and has limited application. On the other hand, detailed analysis can provide accurate detailed data but requires much data and computer power, although power is not a problem due to the advances in computer technology. Therefore, a balance must be struck between the two in the time available for practical analysis.

Timber as a material has been a subject of study well before the Metal plate connected joint. Theories and equations have been drawn to predict the complex strength properties of timber. Formulas have been derived empirically in conjunction with test results. Curve fitting techniques and statistical techniques have also been employed. On the numerical level, the Tsai strength criterion has been used to represent behaviour of timber beyond elasticity. Although timber is an anisotropic material, it is frequently assumed to be orthotropic for simplicity.

All of the theoretical methods mentioned above required experimental data as part of the solution or verification and calibration at some point. Therefore test data are an essential part of research. Simple connection tests have been reported to determine joint properties, such as the axial and rotational stiffness. Results of these tests are used to verify proposed theoretical methods or curve fitting techniques to express the semi-rigid connection as an equation. In

particular combined load tests have been reported to investigate the effects of eccentric or combination loading. The verification and calibration of overall truss analysis must come from full scale truss tests. Whilst these tests are expensive and time consuming to prepare, a few researchers have used test results produced by commercial plate companies.

The Table below is a summary of the literature reviewed which involved laboratory tests conducted by their respective authors.

Author	Ref	Type of test	Type of structure	Loads applied	Joint Stiffness		Measured	
					Axial	Rotational	loads	Disp.
Sasaki and Takemura	3	Truss	Howe, Warren, Pratt	Point			*	*
Gupta *et al*	4	Joint	Heel, Tension splice and Web	Axial comp Ten	*	*		
Vatovec *et al*	5	Joint	Tension Splice, T joint	Axial Ten.and bending	*		*	*
Vatovec *et al*	6	Joint/Truss	Splice, Heel, Crown, Ridge, Tension splice, Scissor truss	Bending/ vertical loads	*	*		
Crovella and Gebremedhin	7	Joint	Tension Splice	Axial Ten.	*		*	
Gebremedhin and Crovella	8	Joint	Tension Splice	Axial Ten.	*		*	
Groom and Polensek	9	Joint	Tension Splice/T Joint	Axial Ten.			*	
Cramer *et al*	10	Joint	Tension Splice		*		*	
Foschi	12	Cube Bearing	Cube	Direct Comp			*	*
Beinke and Suddarth	13	Joint	tension Splice	Axial Ten.	*		*	*
Lau	16	Joint	Heel	Tensile/Shear/ comp.	*		*	*
Foschi	18a	Frame	Wood Diaphragm	Point				*
Foschi	18b	Joint	Crown	Point/Bending	*			*
Poutanen	19	Truss/Frame	Frame	Point				*
King and Wheat	20	Truss	Parallel Chord	UDL			*	*
Gupta *et al*	22	Joint	Tension splice/Heel/Web	Axial Ten./Comp.	*		*	*
Vatovec *et al*	23	Joint	Bottom chord splice/Heel/Crown/ Bottom chord ridge/Top chord	Axial Ten./Comp. and Bending	*	*	*	*
Wolfe	24	Joint	Tension splice	Axial Ten. And Bending	*	*	*	*
Gupta	25	Joint	Tension splice	Axial Ten. And Bending	*	*	*	*
Masse and Salinas	26	Joint	Multi laminated nailed	Axial Ten. And Bending	*	*	*	*
Noguchi	28	Joint	Tension splice	Bending		*	*	*

Table 2.6.1 – Summary of papers with structural testing

2.7 Parameters for the investigation

The review of literature above indicates interaction between axial forces and rotational stiffness, and bending moments and axial stiffness. Previous investigations were concerned with the tension splice joint and only in tensile axial loading. It is quite possible the same phenomenon exists in other connections in the truss and therefore it is of interest to extend the tests to other connection types and to determine whether similar results can be achieved.

It was therefore decided to conduct MPC joint tests to determine the strength of each connection in a particular truss. By the same token, the effects of combined loads on stiffness parameters of the joint were to be investigated. In the literature, the bending moment load is induced through eccentrically loaded axial forces. Thus, a ratio between eccentricity and axial load is pre-selected and the bending moment becomes a function of the axial loads. Results of these tests will be useful for truss analysis where loads are applied at the connections of the joint and eccentric loads are caused by axial loads. However, when loads are applied on the members of the truss, larger moment loads will be induced and therefore load ratios will change. Consequently, the connection can behave in a different manner for larger bending moments. Thus, the tests were to be conducted in such a way that the axial force and the end moment were to be applied independently.

It was anticipated that this approach will give a direct relationship for the strength of the connection between the axial and moment component of the applied load.

The basic definition of semi-rigid connection movement is the relative displacement between the connector and the member, and this includes the

deformation of the connector itself. Up until now the investigations have measured the overall semi-rigid deformation where only the displacement of the timber member was measured. However, existing data do not give details of semi-rigid contribution from the plate. A different approach has been employed in these tests to measure semi-rigid deformations where plate deformation was also to be measured. Data of plate deformation, which are currently not available, can be used for future development to verify theoretical plate analysis. Traditional joint test data do not provide this information and this type of data could become useful in the future for MPC design. In addition to this, the data produced will be interpreted in a more rigorous way, where semi-rigid rotational, as well as axial stiffness will be measured with an attempt in measuring shear stiffness. In summary, data describing the movement of the plate, member and the plate relative to the member will be reported, thus providing a more informative picture of metal plate connection behaviour. In addition to the joint tests, full truss tests will also be conducted to provide data for a comparison of the overall structural behaviour.

On the theoretical side, a 2-D beam element, structural analysis program was written. For this purpose FORTRAN programming language was selected. Joint test data was used in the analysis to account for non-linear semi-rigid joint and eccentric effects. Pinned and rigid analysis could also be performed by the same program for comparison. The second part of the theory involves more complex 2-D and finite element analysis of the truss to obtain a picture of the stress regime in the connection. Results of these models will be compared with each other and with the full scale tests in order to draw conclusions. The literature review presented some papers, which reported of some finite element

analysis work using commercially available finite element analysis package. Only brief details of methods used and material strengths are presented. Furthermore, there has been no mention of any non-linear behavioural aspects implemented into the models. Therefore it is proposed to use the test results to model non-linear connection response in a truss in a Finite element model. Results of these models will be compared with each other and with the full-scale tests in order to draw conclusions.

Chapter 3

Experimental work

3.1 Introduction

This chapter describes an extensive test programme on semi-rigid connections, some of the tests were aimed at determining connection properties. A Queen truss comprising 4 different types of joints were chosen for this research, In all experiments only the Metal Plate Connections were used. Different combined load cases were simulated for each connection. Some tests were repeated to investigate any variability in timber behaviour. Finally, 4 full-scale trusses were fabricated and tested to investigate overall truss response under simple loading schemes.

The objective of the connection tests was to determine the strength of each connection in the truss and at the same time, to investigate whether axial loads have an effect on rotational stiffness and moment loads on axial stiffness. The joint test data are directly used to calculate the overall truss response in a 2-D beam element program as described in section 4.9. The full-scale truss tests data were used to validate the proposed models.

It should be emphasised that the connection tests were not aimed at defining the behaviour of metal plate connections for all possible configurations. That approach is indeed taken by MPC manufacturers to provide relevant information to designers. The target here was to develop sufficient experimental data for a number of joint configurations, which could then be fed into the semi-rigid truss analysis, which was then, in turn, compared with test results for full-scale trusses.

3.2 Truss design

In the time available for a typical doctoral research project it would be difficult to test all connections comprising a truss if the truss were complex involving many different connections. As a result, the configuration of the truss chosen for this study has been singled down to the Queen truss as illustrated in Fig. 3.2.2

The span of the truss was dictated by the space available in the laboratory. A relatively short span of 6m was chosen so that the truss could be accommodated on the strong floor for full-scale testing. The cant of the truss is 34° with a height of 2.1m. Chord members and web members are $35\times97mm$ and $35\times72mm$ respectively. The connection type is the Punched Metal Plate Connection (PMPC) as this is a popular connector in truss rafter construction and has been described in many published papers. The design of the truss conforms to BS5268[38] part 2 and 3, details of which are given in Appendix A1. The softwood timber grade chosen for these tests is grade TR26. Nail plates were supplied by Alpine Automation for which a certificate for nail and plate strength, conforming to the "British Board of Agrement" was used to determine plate sizes for each connection and is reproduced in Appendix A2.

For design purposes, the principal dimensions of the truss were input to a semi-rigid joint 2-D rod element program coded in Fortran as detailed in section 4.9. The program was simulated in pin jointed mode to determine shear and axial forces in the members. In addition to this, the truss analysis calculation was performed on an automated truss computer program used by the plate supplier. Manual calculations of the plate sizes were found to agree with the manufacturers automated method. Connections were all assembled at the City

University Heavy Structures Laboratory. To fabricate the connection a template for each joint was formed. Members were cut to size then positioned and clamped onto the template. As shown below in Fig. 3.2.1 of the heel joint, the set piece is moved to a press consisting of an existing steel frame. A hydraulic jack bolted to the frame, is used to press the nail plate into the timber. A thick metal plate is placed on top of the nail plate to evenly distribute the pressure.

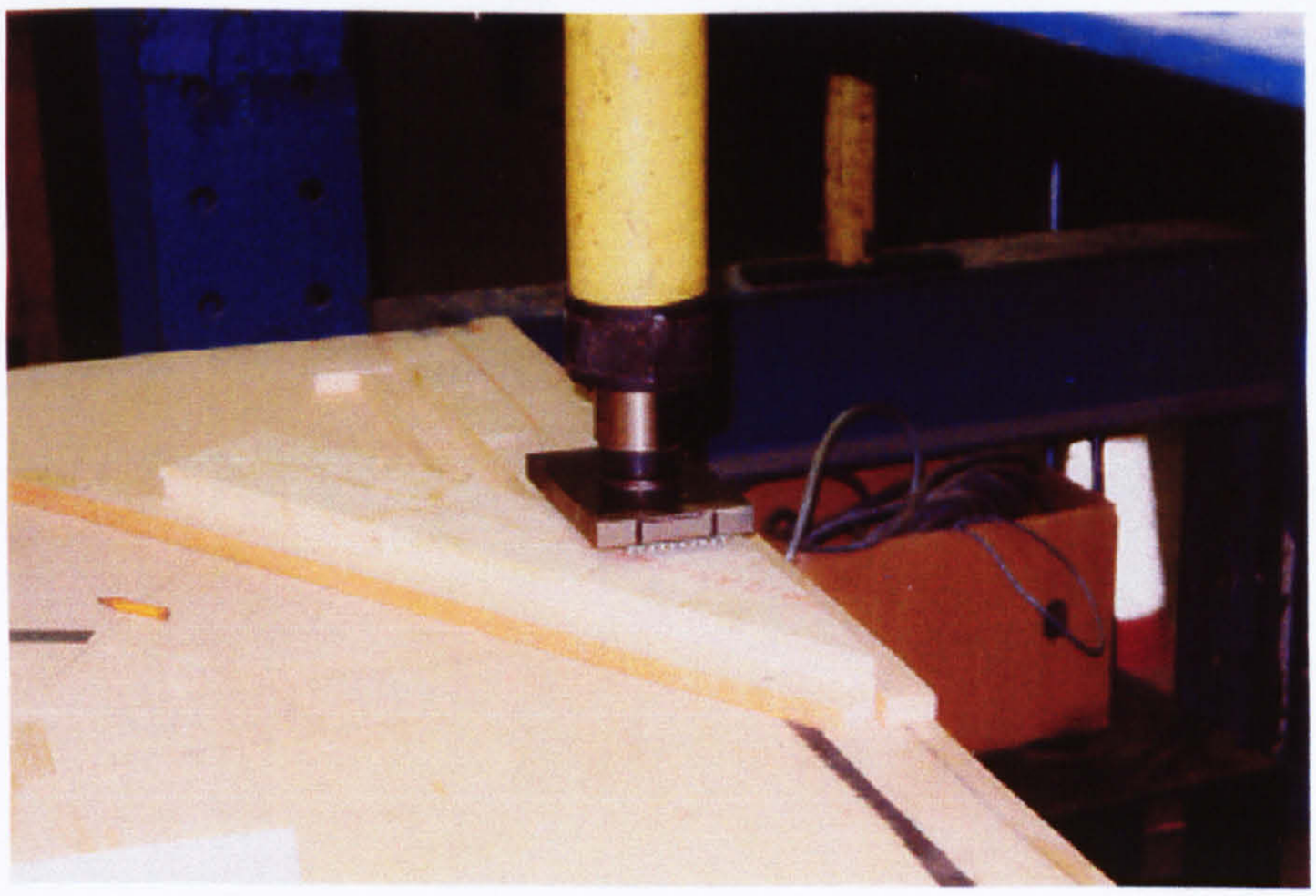

Fig. 3.2.1 – Assembling the nail plate

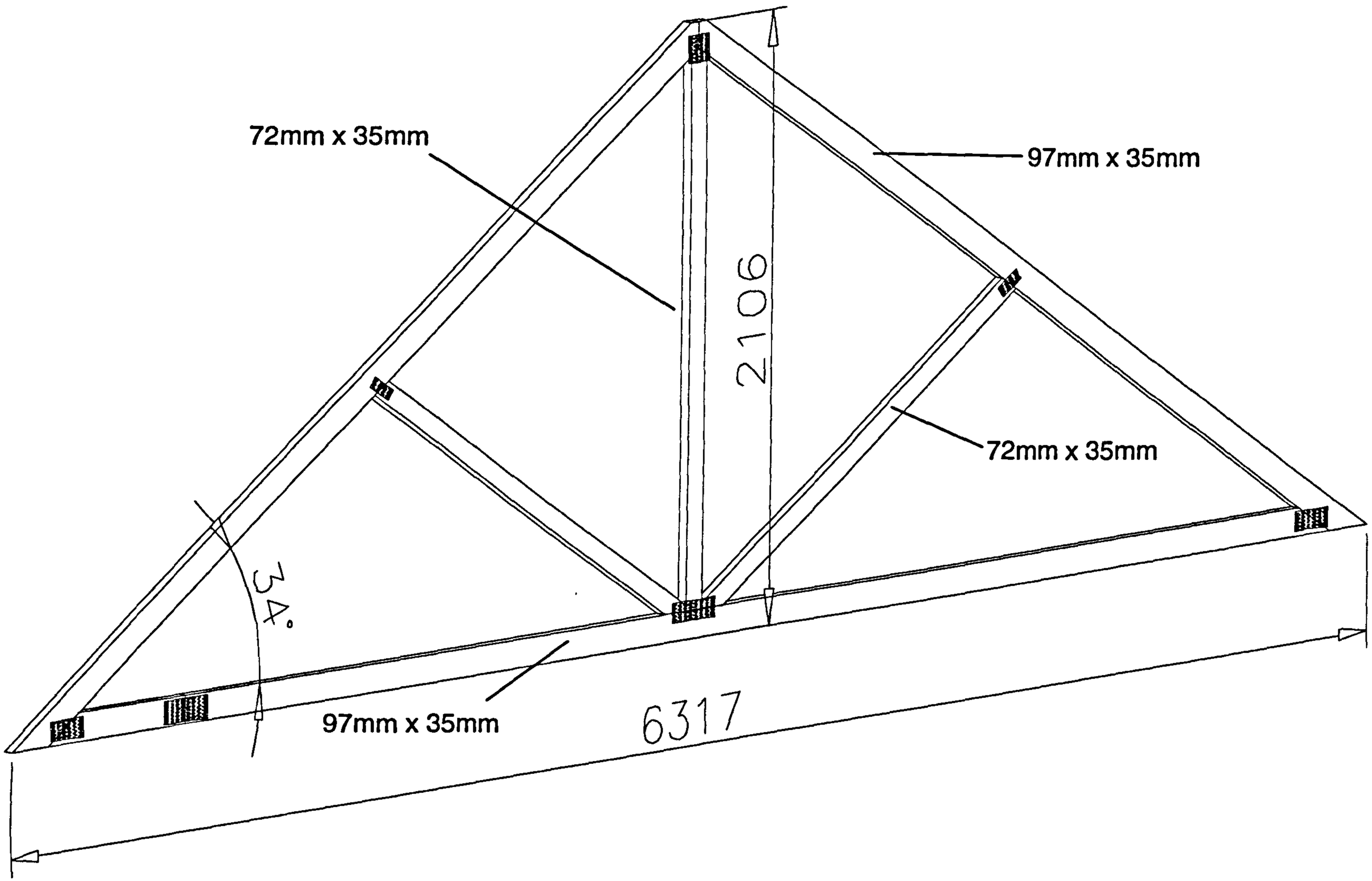

Fig. 3.2.2 - Queen Truss

3.3 Instrumentation

The load measuring equipment available in the laboratory were generally of high to very high capacity and thus were not suitable for timber tests. Compared to concrete and steel, timber possesses a much lower load capacity. Thus new load cells of capacity 25KN were purchased. Test designs were based around different types of load cells. This was done to determine which load cell would be most compatible with the loading arrangements. However, the newly purchased compression load cells were not ideal for measuring compression in inclined members due to the fittings supplied with the load cells, which were more suitable for vertical compression tests. Nevertheless, the cells and displacement transducer, used to measure displacement were wired and calibrated to a data logger controlled through a computer with data acquisition software. With the exception of the moment loading in the crown joint test as explained later, throughout the tests, all loads were applied through a ram and a manually operated jack with a pressure gauge connected in between. The gauge was used as a load indicator during the test.. Ultimately, for accuracy, load was measured through the load cells.

The biggest problem with these tests initially was in deciding how plate deformation could be measured. Conventional methods such as displacement transducers, would be very unsuitable because of physical limitations and the size of the transducer. Such attempt would be difficult and could be erroneous. One method could be to glue strain gauge rosettes on the plate and thus the vertical and horizontal strain could be determined between points. However, strain gauges have to be carefully stuck on the plate and the physical nature of the plates with holes does not lend itself to this. Furthermore, failures such as

pull out would be difficult to measure. It was conceded that this would almost be an impossible task if conventional displacement measuring techniques were to be used. Therefore, another technique was adopted as described in the next section

3.4 Close range photogrammetry

This section presents a novel approach to measuring displacement in timber structural tests. Imaging techniques provide no physical restrictions to the test and pose a significant advantage over conventional techniques. However, such techniques do not come without a price. Time, effort and patience spent to produce the results far exceed those required for conventional methods. In addition to this, the equipment is very specialist, expensive and requires training to operate the list of instruments and software.

The basis of this technique called close range photogrammetry uses cameras placed at some distance from the object to acquire images of movement. Thus, no physical restrictions are imposed with the only requirement of a clear line of sight between the object and the camera. Points to be measured are designated with a reflective circular target stuck on the object. Targets can vary in size and can be quite small hence, many may be stuck within a small area for a very detailed description of displacement. The requirement is that each target is visible on the image with some clear area around it. Cameras can be placed at an angle to the target and therefore some awkward points can still be measured. Displacement measurements are presented in 3D cartesian co-ordinates. This is an added bonus as it is rare that out of plane displacements are measured by conventional means. Once all the data have been collected,

targets can be visualised frame by frame in a 3D space model portraying timber and plate movement. The nature of this technique affords the advantage of having as many targets as required. This means very comprehensive data can be produced for the test. Concentration of targets at the nail plate can give unprecedented detailed analysis of deformation. Details of this technique are now presented.

Although the technique employed to measure structural movements is undoubtedly beneficial from the structural testing point of view, it is not the intention of this section to fully discuss the theory behind it. However, when such techniques are relatively new to structural testing, and more so for timber testing, the basic principle of such methods should be understood.

The theory mentioned herein can be found in Non-topographic photogrammetry[51] and Atkinson, K.B[52]. It was the Frenchman Laussedat in the middle 19th century who developed photogrammetric methods for mapping using aerial photographs. Since then, the method has been advanced by many individuals, where its application has spread from the most diverse disciplines from monitoring ground movement by geologists to life saving research for medical applications. It is no doubt that computer and technology have made a significant contribution to such diverse applications.

What follows is a brief description of the camera calibration and target measurement process which only gives a general idea of what is involved as far as this project was concerned.

Due to the novelty of the measurement system adopted, the description of the technique has been included in the main text rather than in the Appendix.

Imaging geometry and camera calibration

The basis of camera imaging geometry explains how images are taken. As the name suggests, the object plane is where the object is placed for the image to be taken (in front of the camera). As illustrated in Fig. 3.4.1, when an image is taken, a ray of light travels from object point, "A", and runs through perspective centre, "O" and then through to projection plane at "a".

Part of the requirements to measure points on an image is to know the internal geometry of the camera. This comprises the focal length of the lens and the dimensions of the image as illustrated in Fig. 3.4.1.

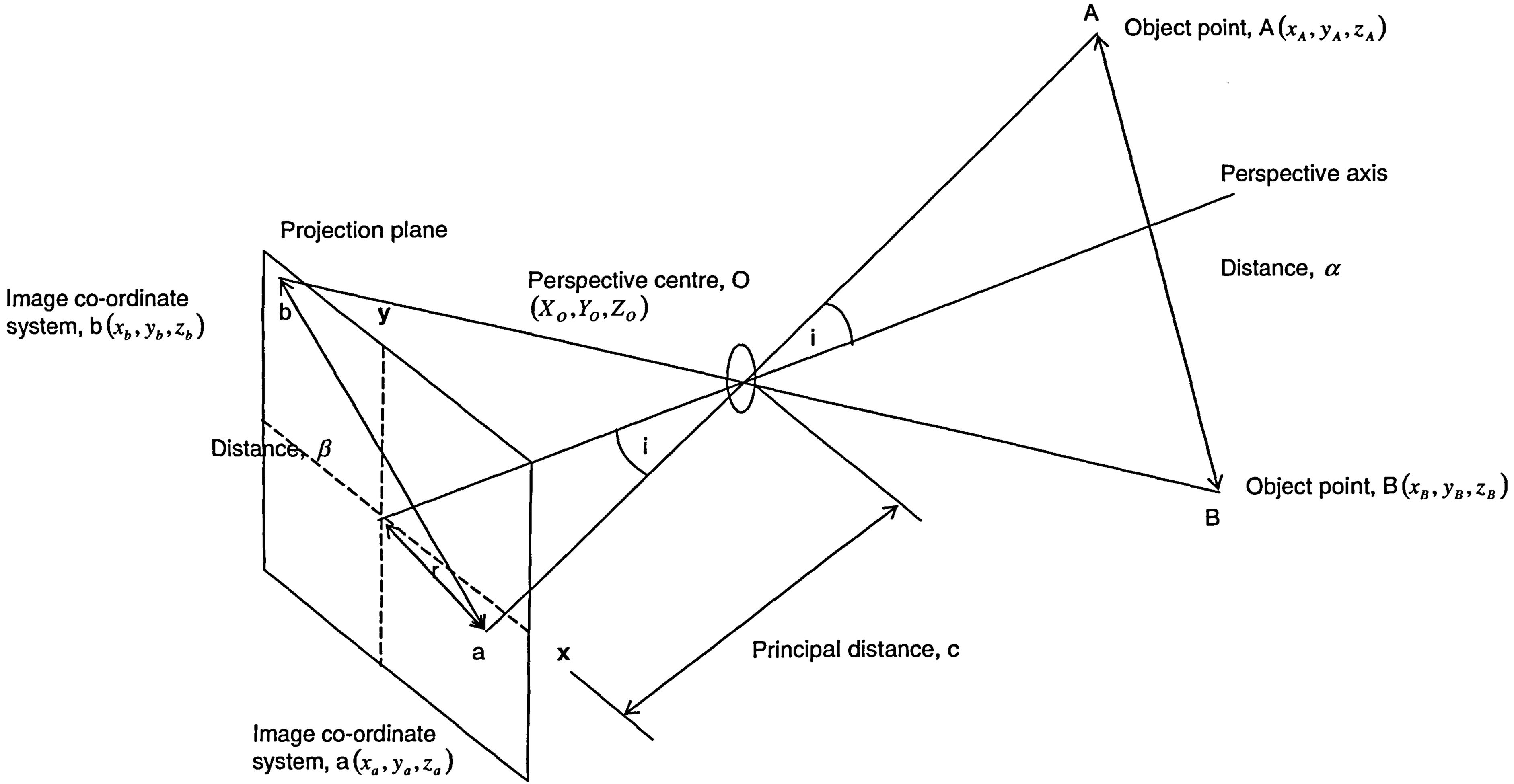

Fig. 3.4.1 – Camera Geometry[52]

In a real camera, the idea of a simple perspective centre requires further enhancement. A camera lens will not allow light to travel straight through as it would in the perspective case as illustrated in Fig. 3.4.1. In Fig. 3.4.2 light is refracted and distorted when it travels though a lens, which could be made up of two asymmetrical groups of lens elements. The way in which light is refracted within the lens is attributable to the material and shape of the lens.

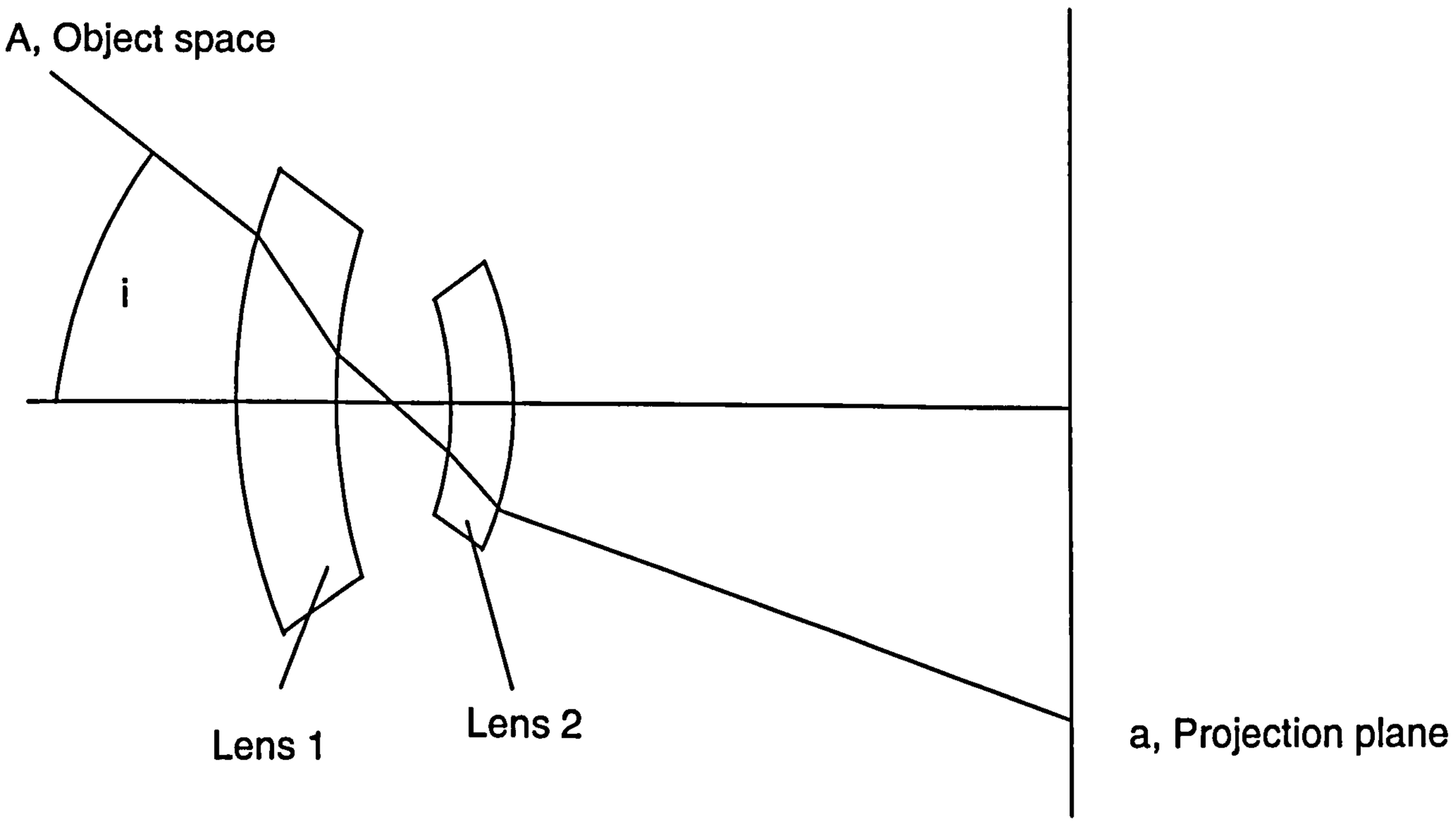

Fig. 3.4.2 – Effect of light rays due to the lens[52]

The most important part of taking images as far as the user is concerned is the focus. The camera lens must be focused before images are taken. As focus changes so will the perspective centre O, principal distance c, distance in Fig. 3.4.1 and Fig. 3.4.2. Hence, in order to obtain measurements at a given focus position, the O and c must be determined, which is the purpose of the camera calibration. Test areas can vary substantially in size, so the cameras will need to be positioned to cover most if not all of the area. This invariably means the camera focus will have to be adjusted for each set of experimental work, thus, with each different test a calibration is required. Ultimately, what the calibration

process determines is the difference between Fig. 3.4.1 and Fig. 3.4.2 and adjustments will be made to any image measurements by the calibration.

The parameters O and c are unknown at this stage although camera position and focus are mechanically set. There are several unknowns and a mathematical model needs to be drawn in order to determine them. Referring back to Fig. 3.4.1, we have known targets A and B. The distance between these control points can be physically measured with reasonable precision. Part of the computer model for calibration requires a set of such known distances. The derivation of the actual equation will not be detailed here as it is not the purpose of this thesis to discuss close range photogrammetric theory in depth. However, the theory can be found in the listed references[51&52]. There are several unknown fixed camera parameters. By including more targets, more distances can be measured, the accuracy of measurement can be improved. Thus, similar equations with different distances can be generated and the unknown parameters can be found by simultaneous equations. This process is called resection.

The accuracy and reliability of such a solution does not account for lens errors and is difficult to measure from a single resection. In order to quantify accuracy and reliability, resections from different camera positions at roughly the same distance are required to put into a least square estimation model and to further tune the parameters. This process is repeated for all cameras used for measurements. After all the cameras have been resected from several positions, a bundle adjustment is performed to adjust all measurements and parameters from all the cameras. From this, the quality of the calibration of

each camera can be measured and if satisfactory the calibration is complete. The quality of the calibration is measured by the sum of squares of the residual values of the measured co-ordinates. The distance of the camera from the targets during calibration must approximate the distance of the cameras during the actual test.

For convenience targets used for calibration can be fixed points around the test specimen. These points are called control points as they assist measurements in the next stage.

Target measurement

Now that the cameras have been calibrated, they are ready for measurement and must be placed in positions, which must not be moved during the course of the test. Once images are acquired they are ready for processing. Before any measurements are made the orientation of the cameras is established through another resection on the cameras. At this point the camera calibrations are fixed and only the photo orientations need to be established. The process by which 3D target data are computed is called intersection. The targets on the test specimen, i.e. object space are initially unknown. In photogrammetry, only targets common to a pair of images has to be measured. That is, at least 2 cameras must have a clear line of sight of any target for it to be measured. As illustrated in Fig. 3.4.3, target 'A' cartesian co-ordinates are measured through evaluating photo co-ordinates (x_1, y_1) and (x_2, y_2) using the camera calibrations, known distances between control targets and photo orientations. In the case of two images, there are 4 equations and 3 unknowns, (X_A, Y_A, Z_A), therefore a least square estimation is made. Target co-ordinates can be improved by capturing the same targets on another image, thus improving the quality of the

target co-ordinates. If more lines of sight are available the measurements made will be more precise and reliable.

The intersection is repeated for each target in the object space. Once all target co-ordinates are acquired a bundle adjustment involving iterative least square methods is made to simultaneously adjust all target co-ordinates in order to provide a homogenous data set. The set of images taken simultaneously at any one time is referred to as an epoch. Thus in Fig. 3.4.3 camera 1 and 2 acquire an image simultaneously, therefore in this case there are 2 images to an epoch. After the adjustments are made subsequent epochs can be measured through an automated system explained in the next paragraph.

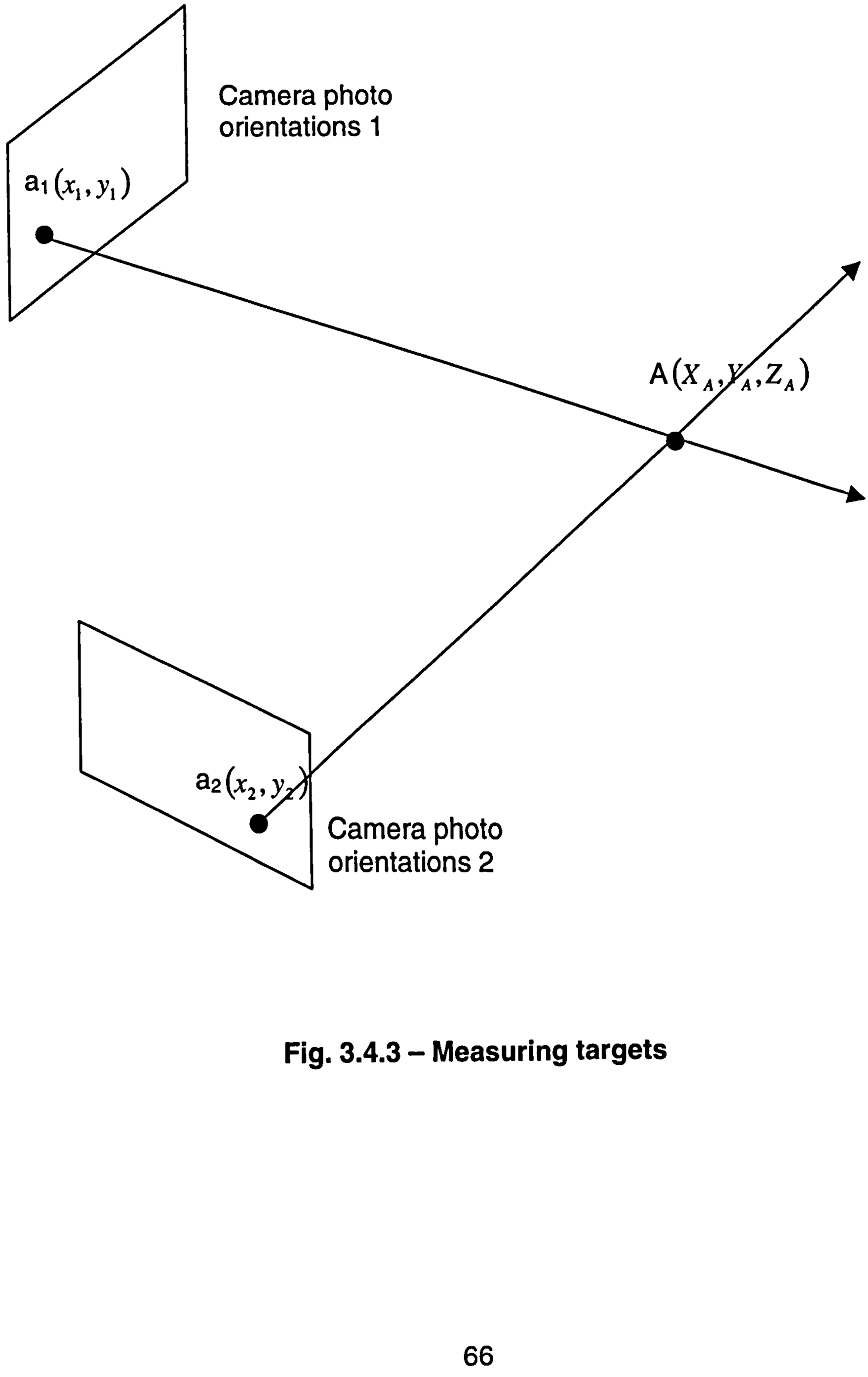

Fig. 3.4.3 – Measuring targets

Hardware and Software

The close range photogrammetric technique can use several cameras placed at some distance away from the object to acquire displacement. In this study 4 cameras are used. Each pair of camera is connected to a computer thus two computers were required. A frame grabber board is installed inside each computer which is the hardware necessary to transfer images from the camera to the computer. Computers are linked together via a network box, one being the master and the other slave. Software is developed specifically to acquire images on all 4 cameras simultaneously through control from the master machine. The calibration and target measurement stage is carried out using VMS (Vision Measuring System), a software developed initially at City University then at University College London (UCL). The Engvis software also developed at UCL is, for this study, primarily used to check for errors and provide a medium for producing data files for data interpretation. The data interpretation program developed by the author during the research uses curve fitting and data extrapolation techniques to measure movement behind the nail plate. The process behind this technique now follows.

Test preparation

The Vision Measuring System relies on reflective targets on an image to measure target co-ordinates. Also it helps target recognition during the automation process, which will be explained in more detail later. Therefore, it is imperative that these targets are clearly identified in the image. To facilitate this, the appearance of the target is enhanced by a combination of a dark background and the reflective material itself. During preparation, the timber joint was sprayed matt black before the special reflective material was stuck on.

Target spacing is important, as targets too close together would appear to impose on each other on the image. Neither of these targets would be recognised by the software used to measure them. So as a rule of thumb targets need to be small in areas where they are placed in close proximity. On the other hand, small targets too far from the camera are also difficult to pick and so the two contributory factors must be balanced. Target sizes can vary although it is preferable to adopt one size as this assists target recognition in VMS. Typically, the diameter of a target would be between 2-3mm. Preparations for each joint test were extremely painstaking and laborious. A total of 72 connections and 6 full size trusses were sprayed then precisely marked for targets to be stuck on. Below shows a failed specimen, which had been prepared before hand for a test.

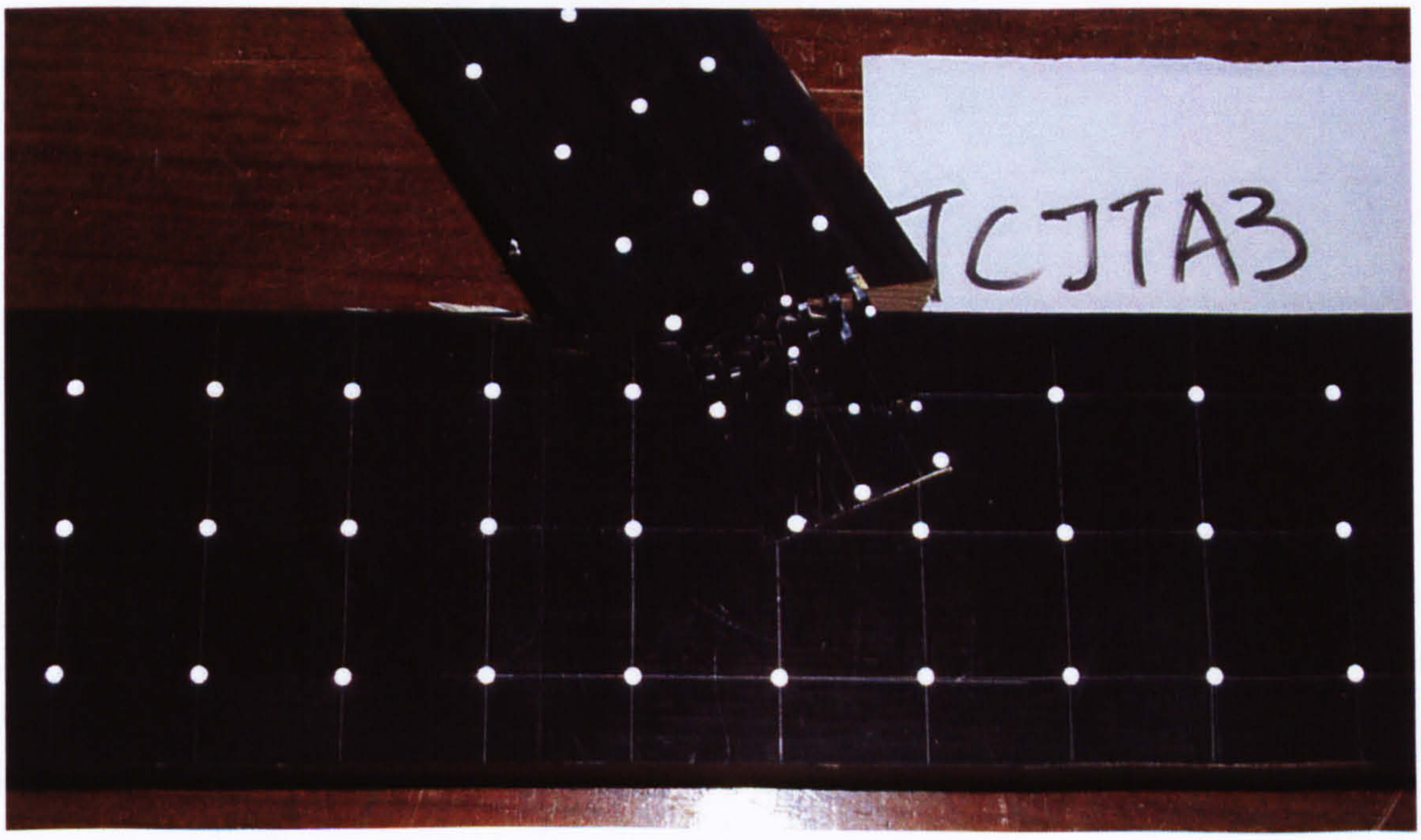

Fig. 3.4.4 – Targets on a connection

Targets were stuck on the columns and beams of the test frame at approximately 150mm intervals for the calibration. These were treated as targets for calibration and control targets for the VMS. The exact distances between the targets were measured precisely with a vernier calipar and tape.

The mean of the distance measured 3 times, was used as the measured distance. The distances would be used to assist the measurements in VMS. Components bolted to the frame were sprayed black with added targets for additional measurements to improve the quality of the data during the data processing. These targets were subject to alteration between tests, but control targets on the frame are used throughout the joint tests. For the calibration, each camera was focused for the testing distance. It was imperative that the focus adjustment remained the same during the entire course of tests otherwise this would change the calibration that was to made. Therefore, once the cameras were focused, the focus knob was fixed by strapping sticky tape round it. To calibrate the cameras, approximately 10 images for each camera were taken from various positions and orientations around the frame. The calibration distance of the camera from the frame is approximately the same as the testing distance.

Data Processing

The data processing task was again extremely laborious. Cameras are initially calibrated for each test set-up in VMS. Once done, the measuring can begin. After measuring the first epoch, subsequent epochs are measured through an automated system in VMS. The automated system basically uses a 3D co-ordinate tracking method to locate the co-ordinates of the targets for the next epoch. This is possible through storing individual target co-ordinates of the last 3 epochs then using a motion equation based algorithm to predict where the target may be in the next epoch. However, visual checks on all images were necessary after the automation, as targets would sometimes be misrepresented

by VMS. In addition to this, many other software problems were encountered because the software is still at its development stages.

Post processing

After completing measurements in VMS, EngVis is used to graphically display targets where errors become more obvious then manually ironed out. Afterwards, ASCII files are produced by EngVis where rows of target co-ordinates are saved in text format. A file is produced for every epoch each giving co-ordinates of the targets measured for that epoch. Thus a series of epochs will give target displacements of the test specimen. There are as much as 200 targets in one test and therefore 200 per file. Some tests contain over 50 epochs, therefore manual calculations would be extremely laborious and erroneous so automated means are sought. A program developed in Visual basic 5.0 was subsequently written solely for this purpose. The program was developed to extract co-ordinates from selected targets in the files epoch by epoch. The data is then processed using curve fitting and data extrapolation techniques, details of which are covered in the next section. To cross check the imaging data, displacement transducers were also used.

3.5 Test data interpretation

In this section the method of how the experimental data is interpreted from EngVis is discussed. It is only with the data generated that such a rigorous analysis of the joint can be made possible.

By definition, semi-rigidity allows relative movement between members of the connection. For the metal plate connected joint, this comprises the deformation of the nail plate, and the relative displacement between the plate and the member. This leads to the idea of treating one joint as many joints. An inverted Crown joint in Fig 3.5.1 is used to explain this idea. As illustrated, there are

three faces on the Crown joint. Each face/anchorage is connected to a member which we will refer to as a leg. Face 1 is connected to the web, and face 2 & 3 are connected to the top chords. For a face there is a leg. Each face is treated as a sub-joint where some degree of semi-rigidity exists. Circles on the joint represent reflective targets used in the tests. Displacements are measured from these targets, which contributes to the semi-rigid analysis. Semi-rigid behaviour has three components, axial, rotational and shear. It is important that the points at which semi-rigidity is to be measured is not biased so a fair representation of the connection in this respect is identified. Face 1 will be used to describe the analysis. From these targets, the moment, axial and shear semi-rigidity can be deduced. The determination of these 3 parameters will now be discussed separately.

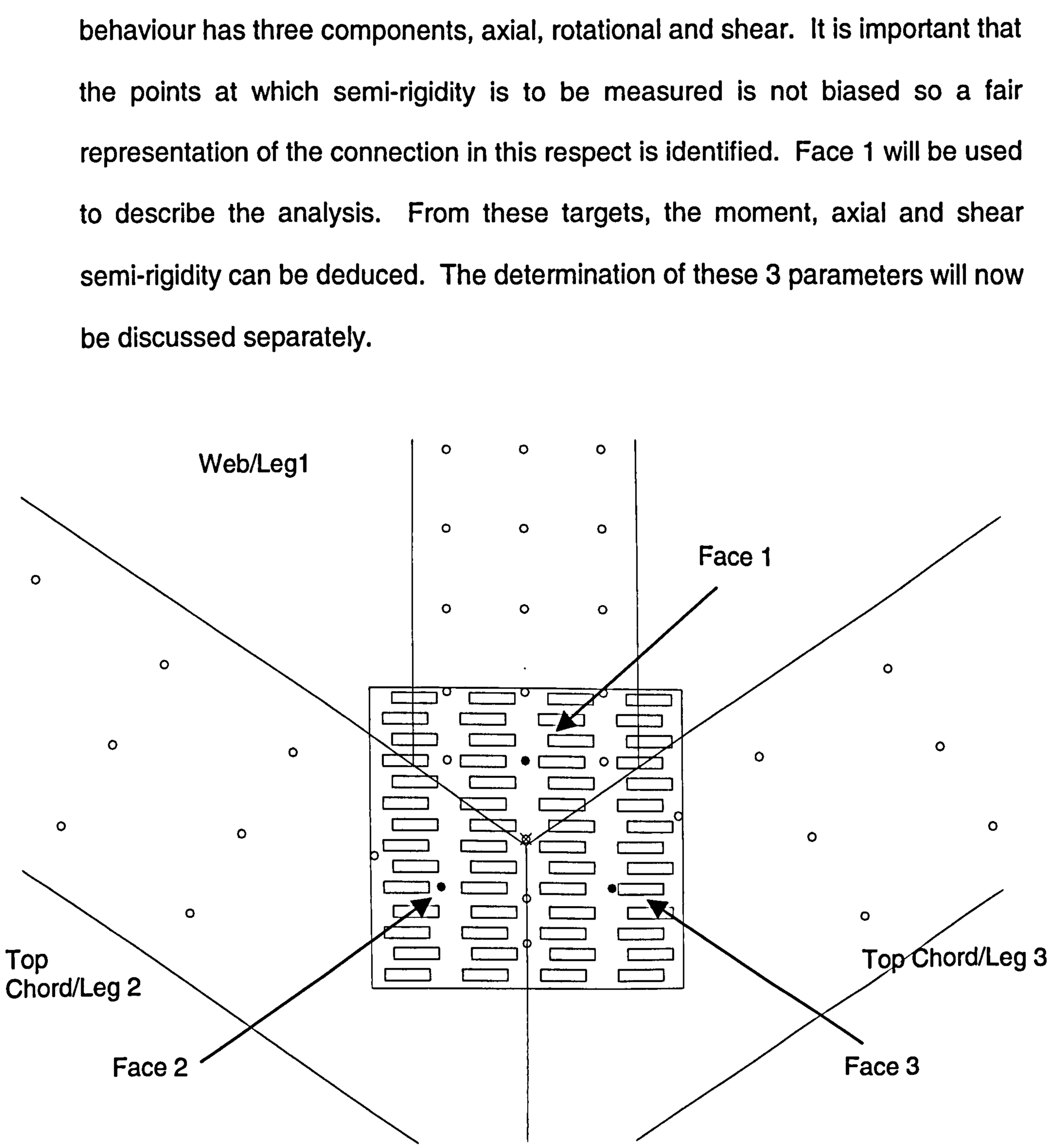

Fig. 3.5.1 - Inverted Crown Joint

3.5.1 Semi-rigid moment rotational deformation

The basis of the moment rotation characteristics determination is a least square regression curve of second order. This requires a set of co-ordinates to obtain the curve. Fig. 3.5.1.1 illustrates a series of targets on the web member and plate of the crown joint. The bending moment caused by loading at the top of the member is exaggerated to illustrate the point. Targets on the timber and plate follow the movement and thus outline the curve of the member under such load. The co-ordinates of these targets are determined from the Visual Measuring System (VMS) and Engineering Vision (EngVis) software as explained in section 3.4. From these co-ordinates least square regression curves can be drawn as represented by blue (dashed dot) and red (dashed) lines on the member and plate respectively. Once the blue curves are determined the curve can be extended down to the plate and the position of the timber extrapolated. In effect the position of the timber behind the plate has been determined. By differentiating the polynomial, the member rotation can also be deduced. A similar concept is applied to the plate except there is no need for extrapolation as all targets are visible. What follows is a detailed analysis of this proposed method.

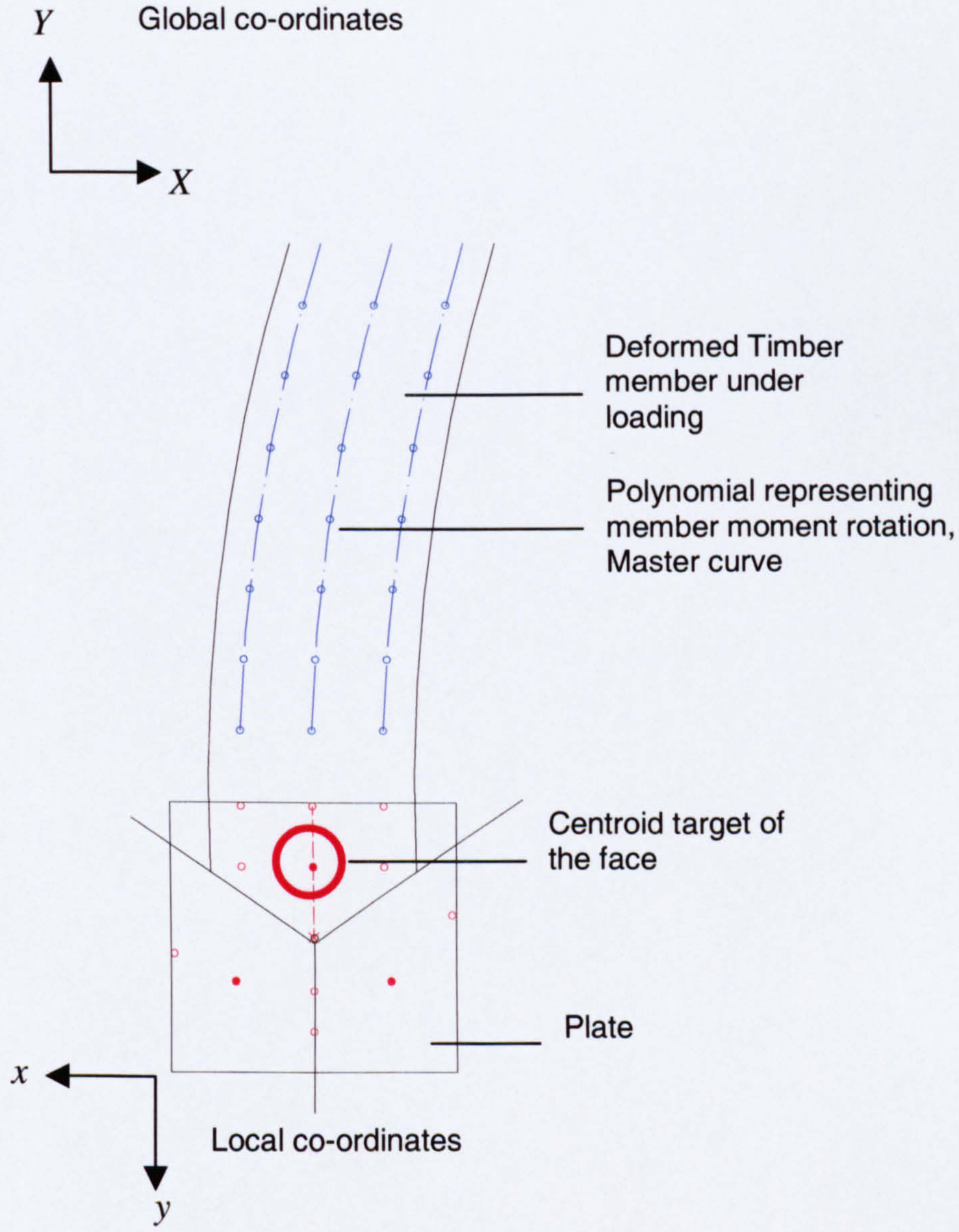

Fig. 3.5.1.1 - Rotation analysis

The target circled in red represents the centroid of the interface believed to be the mutual point of anchorage. It will be explained later that this point is central to our analysis for this face. What we are interested in is the relative rotational movement between the timber and the plate and the plate rotation. The step for semi-rigid moment rotation analysis is as follows.

A least square second degree polynomial regression curve can be drawn to fit the series of target co-ordinates in Fig. 3.5.1.1 and can be presented in the following form.

$$x = f(y) = ay^2 + by \qquad (3.5.1.1)$$

The significance of equation 3.5.1.1 is that the errors of the estimation are spread along the y-axis, and the curve would run along the member. This requires that co-ordinates of members, which are angled, be transformed to the vertical position before a regression curve is drawn.

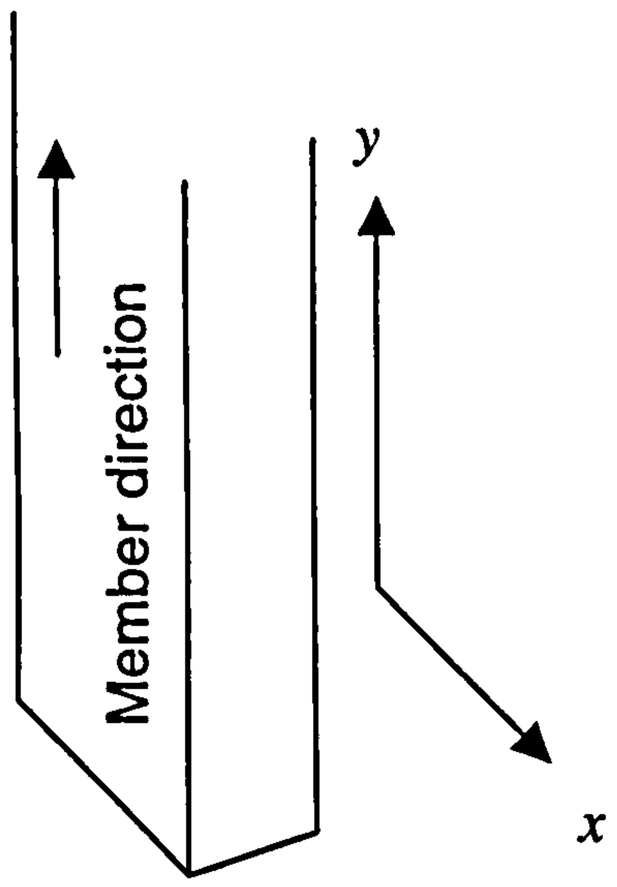

Fig. 3.5.1.2 – Local co-ordinate axis

A higher degree polynomial is not necessary because the curve inscribed is very shallow as one would imagine when the timber is bending. After establishing the equation for the curve, the curve can be extended to the plate thus, co-ordinates from the curve where the plate can be extrapolated, and the position of the timber behind the plate have effectively been predicted. The analysis will now be explained in more detail.

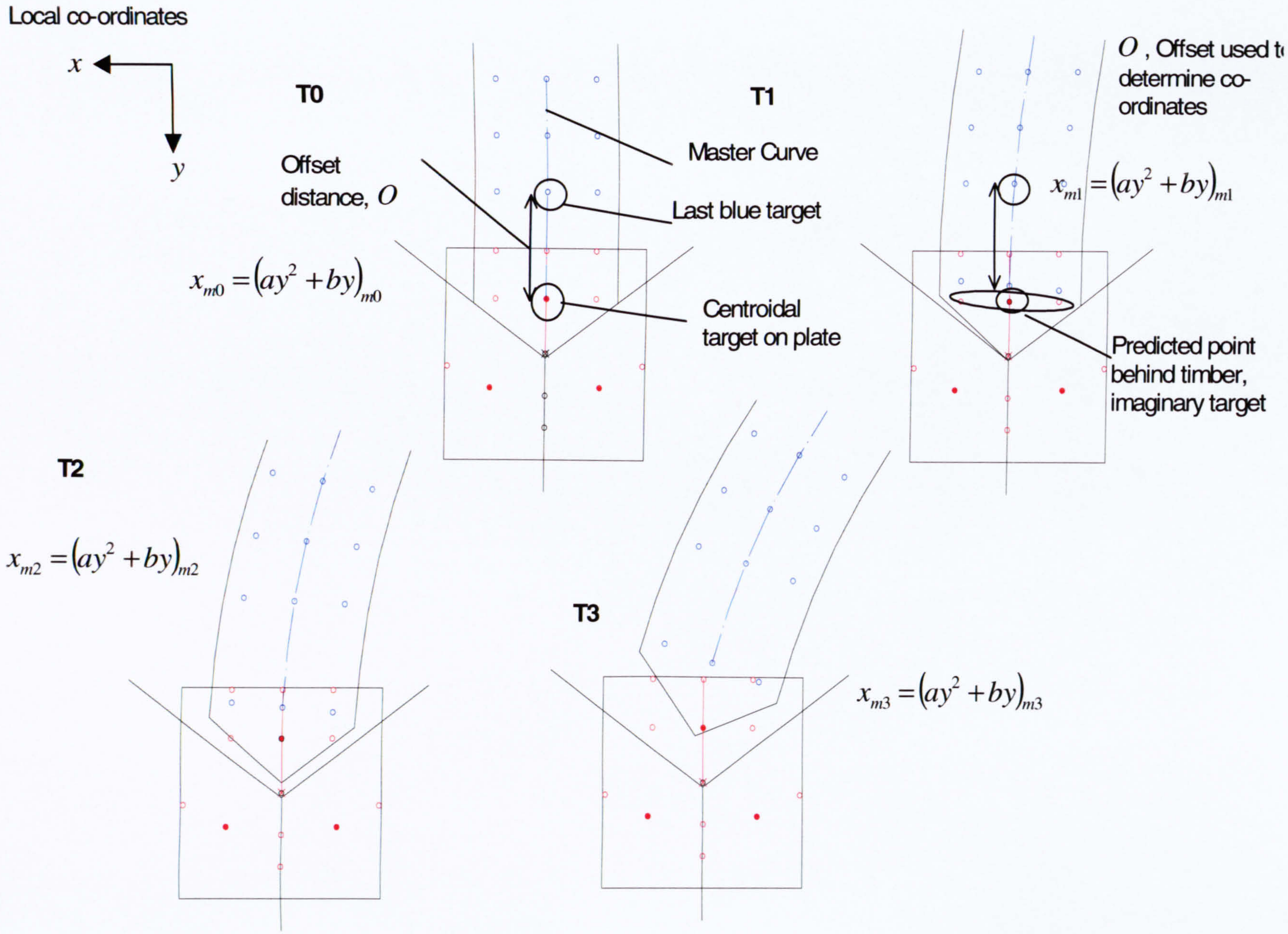

Fig. 3.5.1.3 – Semi-rigid moment rotation analysis

With reference to Fig. 3.5.1.3, the line of targets running nearest to the centroid of the plate is chosen for the moment rotation analysis as illustrated at time T0. The regression curve running through these targets will be referred to as the master curve. The targets at either side are ignored for now. At time T0 where no load is applied, the length of the offset distance O is the last (blue) target on the timber to the centroidal plate target (red). Throughout the description of the analysis, times T1 and T2 will be referred to. The curve and slope of the member at time T1 is given by the following equations respectively:

$$x_{m1} = a_{m1} y_{m1}^2 + b_{m1} y_{m1} \qquad \text{and} \qquad \frac{dx_{m1}}{dy_{m1}} = 2a_{m1} y_{m1} + b_{m1}$$

For simplicity, the equations will be expressed as

$$x_{m1} = \left(ay^2 + by\right)_{m1} \qquad (3.5.1.1a) \qquad \text{and} \qquad \left(\frac{dx}{dy}\right)_{m1} = \left(2ay + b\right)_{m1} \qquad (3.5.1.1b)$$

Extrapolating from the curve by offset distance O, from the last target, i.e. target closest to the plate, gives the y_{m1} co-ordinate of the imaginary target behind the plate. Substituting y_{m1} into the curve and slope equation 3.5.1.1a and 3.5.1.1b respectively gives the position of the target. The angle of the target is given by

$$\vartheta_{m1} = \tan^{-1}\left(\frac{dx}{dy}\right)_{m1} = \tan^{-1}\left(2ay + b\right)_{m1} \qquad (3.5.1.1c)$$

Similarly, at time T2

$$x_{m2} = \left(ay^2 + by\right)_{m2} \qquad (3.5.1.2a) \qquad \text{and} \qquad \left(\frac{dx}{dy}\right)_{m2} = \left(2ay + b\right)_{m2} \qquad (3.5.1.2b)$$

$$\vartheta_{m2} = \tan^{-1}\left(2ay + b\right)_{m2} \qquad (3.5.1.2c)$$

The relative rotational movement at time T2 can be found simply by the difference in slope angles in T2 and T1. i.e.

$$\vartheta_{m2-1} = \vartheta_{m2} - \vartheta_{m1} \qquad (3.5.1.3)$$

The assumption in the analysis is that O is always constant. This in reality, may not necessarily be the case. As illustrated in Fig. 3.5.1.4, when moment is applied, the timber bends, hence the vertical distance between the last co-ordinate and the imaginary co-ordinate would have changed. However, this change is negligible as the angle of rotation is small and negligible compared to distance O.

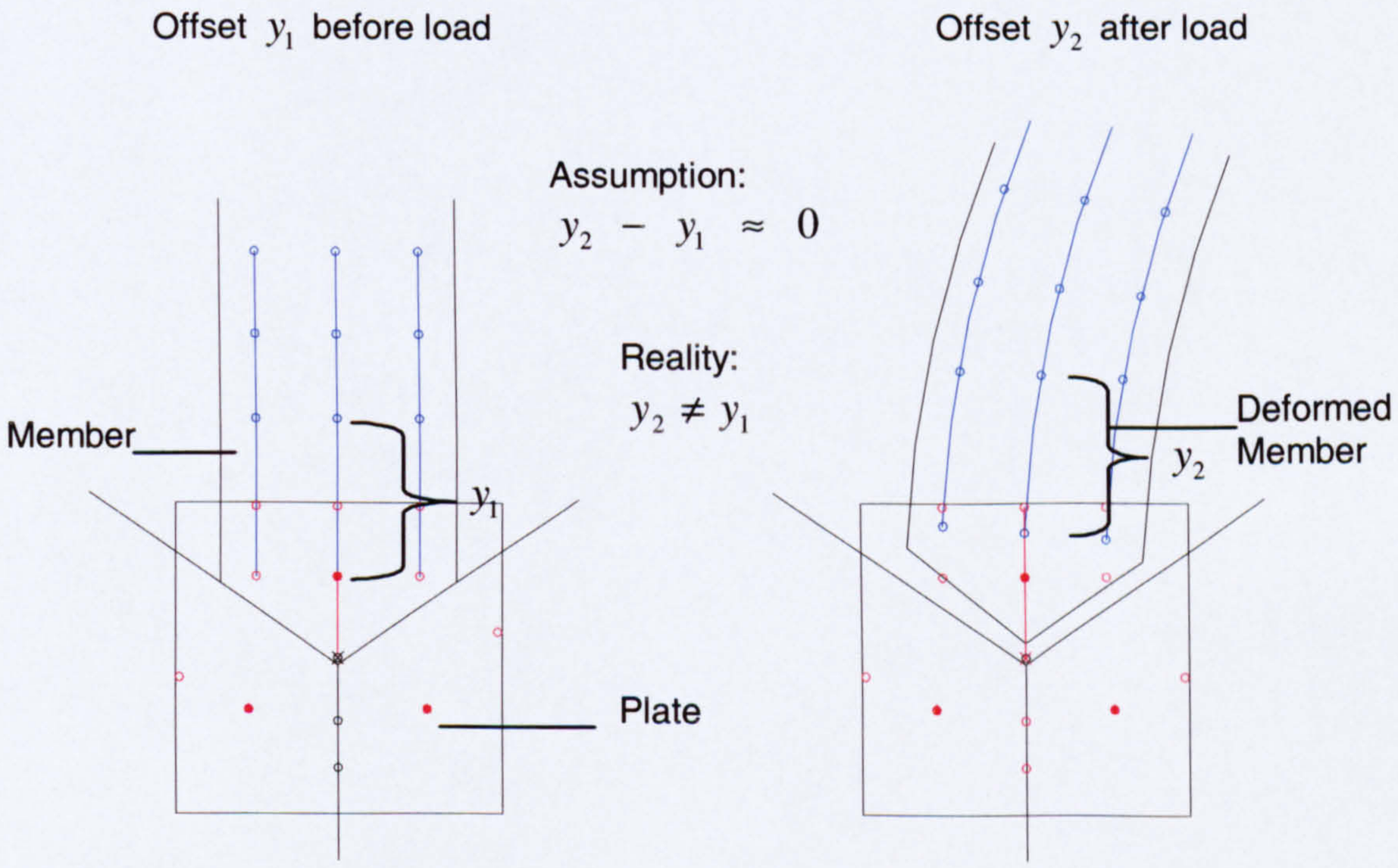

Fig. 3.5.1.4 – Offset distance constant throughout test

Plate deformation is part of semi-rigid behaviour of the plate. A similar concept is applied to the plate data to measure any plate deformation. A polynomial representing plate rotation is denoted by a red line as shown in Fig. 3.5.1.5 below.

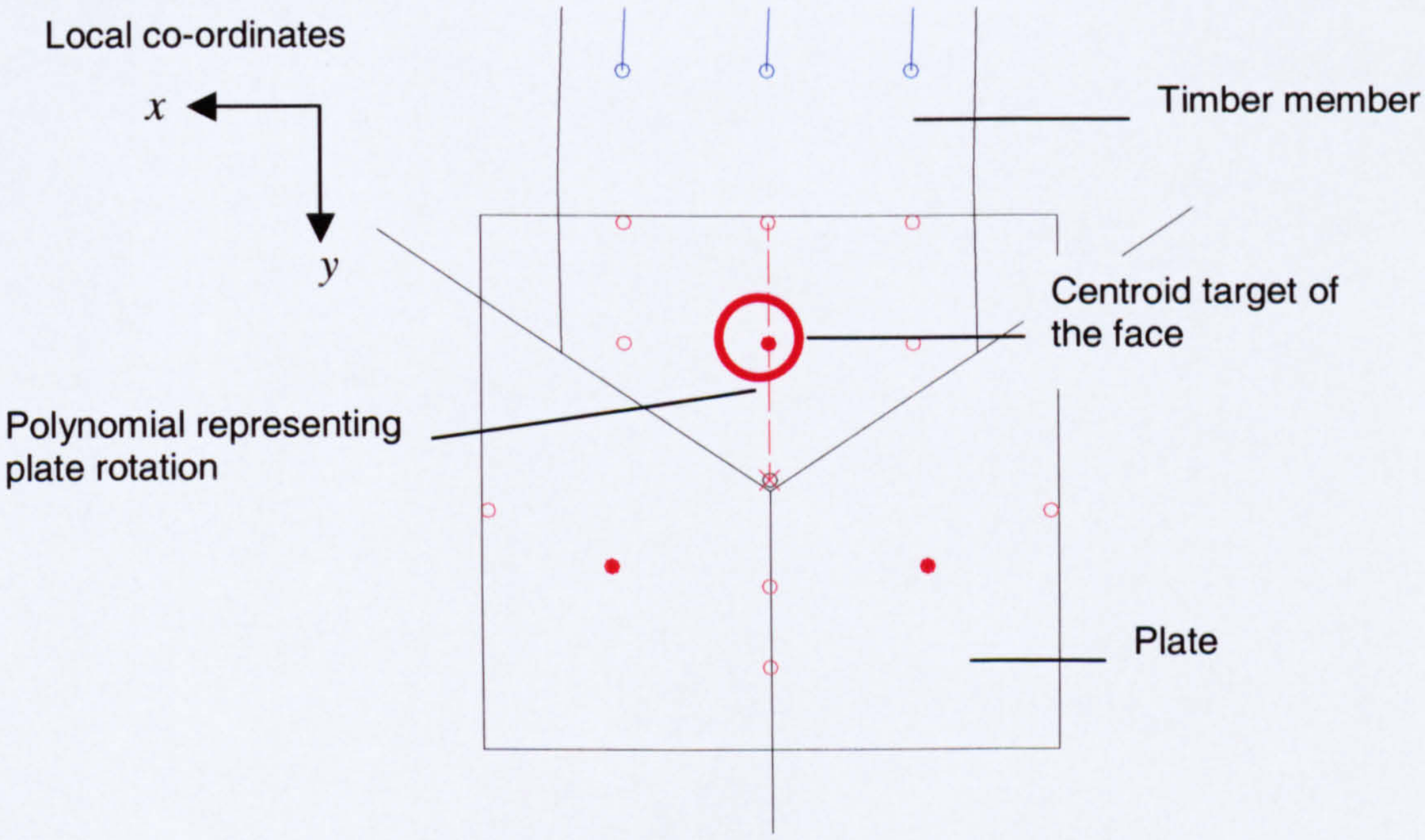

Fig. 3.5.1.5 – Plate Analysis

Fig. 3.5.1.6 shows how the plate may distort under load at time T0 to T3. The distortion is exaggerated to illustrate the deformation in the plate. The equations are the same as that of 3.5.1.1 to 3.5.1.2 but will represent the plate instead.

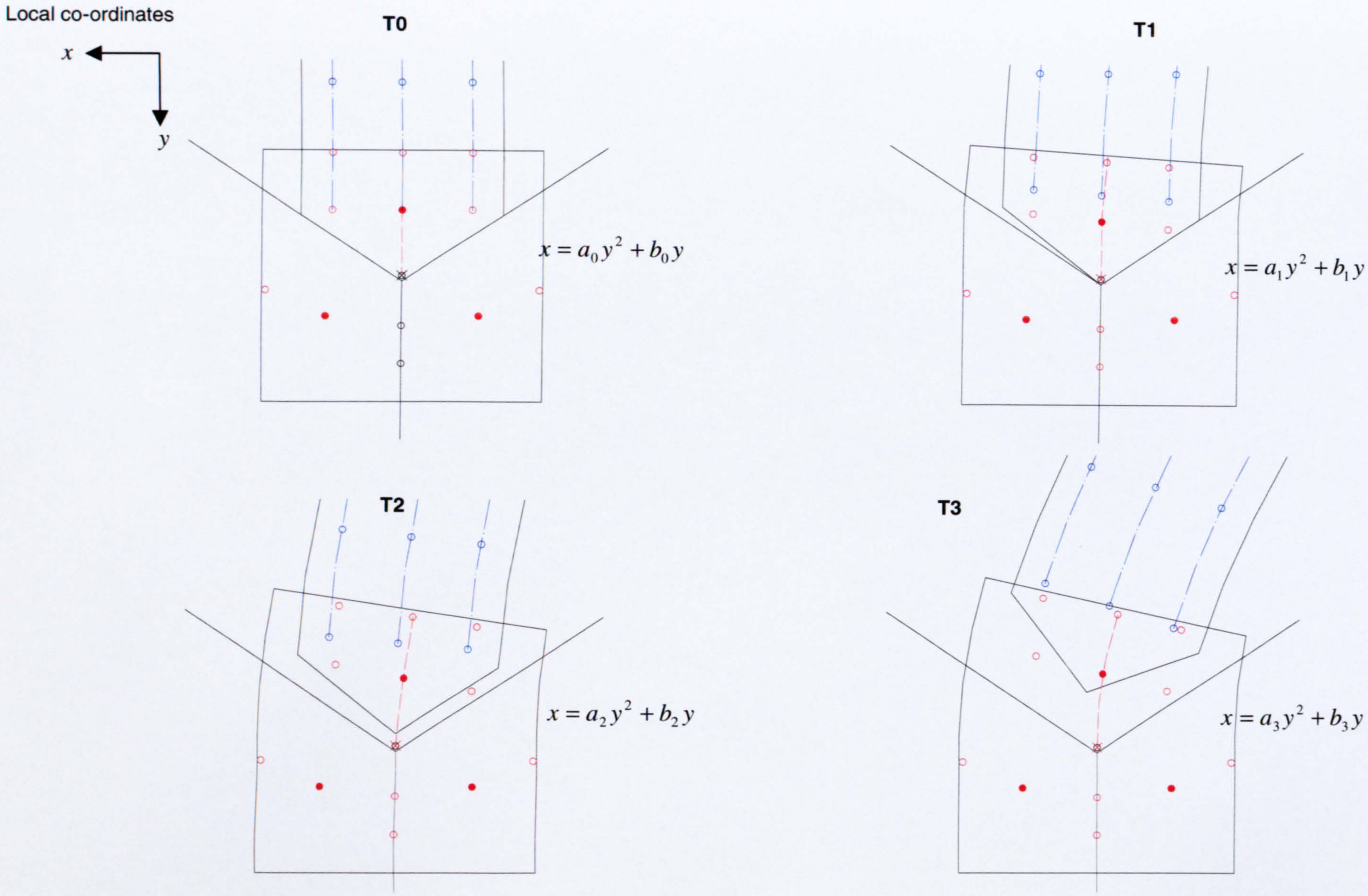

Fig. 3.5.1.6 - Plate distortion

At T1 the curve, slope of the curve and the angle at the centroid are

$$x_{p1} = \left(ay^2 + by\right)_{p1} \tag{3.5.1.4a}$$

$$\left(\frac{dx}{dy}\right)_{p1} = \left(2ay + b\right)_{p1} \tag{3.5.1.4b}$$

$$\vartheta_{p1} = \tan^{-1}\left(\frac{dx}{dy}\right)_{p1} = \tan^{-1}\left(2ay + b\right)_{p1} \tag{3.5.1.4c}$$

respectively.

For T2, the corresponding expressions are

$$x_{p2} = \left(ay^2 + by\right)_{p2} \tag{3.5.1.5a}$$

$$\left(\frac{dx}{dy}\right)_{p2} = \left(2ay + b\right)_{p2} \tag{3.5.1.5b}$$

$$\vartheta_{p2} = \tan^{-1}\left(\frac{dx}{dy}\right)_{p2} = \tan^{-1}\left(2ay + b\right)_{p2} \tag{3.5.1.5c}$$

Hence, the relative rotation of the plate at T2 is

$$\vartheta_{p2-1} = \vartheta_{p2} - \vartheta_{p1}$$

The analysis is repeated as before, however, unlike the member analysis there is no need for extrapolation because all the targets are visible. This leaves only the rotation at the centroid of the face on the plate to be determined.

As mentioned earlier semi-rigid displacement is the displacement of the plate and relative displacement between the plate and member. Therefore by definition, at T2

$$\vartheta_2 = \vartheta_{m2-1} + \vartheta_{p2-1} \tag{3.5.1.6}$$

3.5.2 Semi-rigid axial deformation

As for the semi-rigid rotation analysis, member and plate displacements are determined. The semi-rigid analysis is simple and is determined directly from the co-ordinates from the targets. Co-ordinates for plate displacement are directly obtainable, but co-ordinates for the member behind the plate are not. In the rotation analysis, we ignored the two lines of targets on either side of the member and used the middle one (master curve) only to measure rotation. Using the same method to extrapolate, we now use these targets on the side to predict two more points on the timber, behind the plate. The two curves drawn by these targets will be referred to as the slave curves. Hence, co-ordinates for two more points behind the plate are now known as indicated in Fig. 3.5.2.1 at T1. Axial displacement is movement measured in the direction of the member, i.e. the y-axis. Targets connected by the blue (dashed dot) and red (dashed) line are used for the analysis. As before, blue and red represent targets on the member and plate respectively.

Let the vertical (y-co-ordinate) mean of the 3 targets 1, 2 and 3 on the member be a_{m1} at T1 and for targets 7, 8 and 9 be a_{m2} at T2. Similarly, for the plate, targets 4, 5 and 6 for a_{p1} and 10, 11 and 12 for a_{p2}. Hence, the semi-rigid axial displacements are.

$$a_{m2-1} = a_{m2} - a_{m1} \qquad (3.5.1.7a)$$

and

$$a_{p2-1} = a_{p2} - a_{p1} \qquad (3.5.1.7b)$$

$$a_2 = a_{m2-1} + a_{p2-1}$$

In General terms

$$a_n = \left(a_{mn} - a_{m(n-1)}\right) + \left(a_{pn} - a_{p(n-1)}\right)$$ where, m is the time epoch

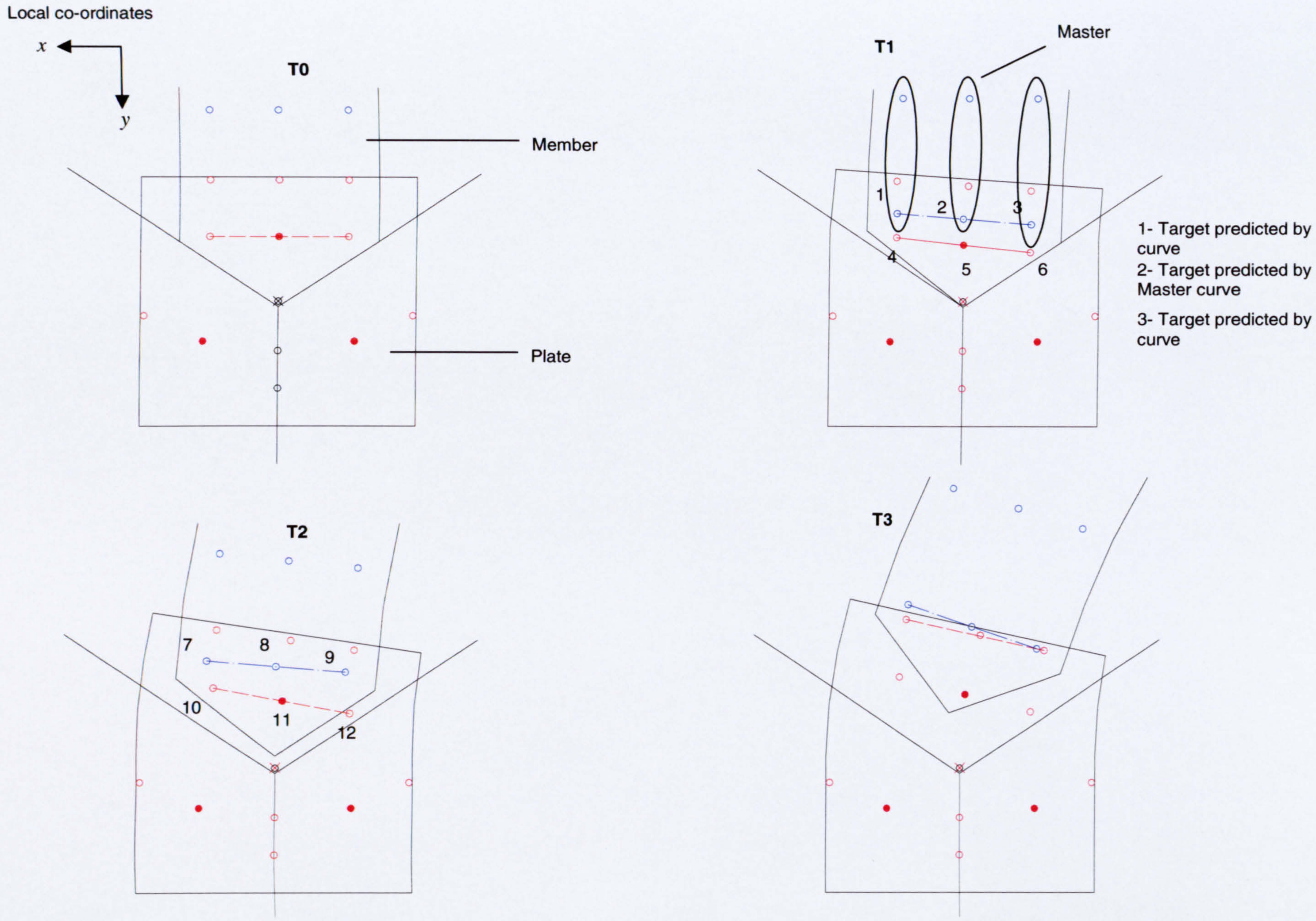

Fig. 3.5.2.1 – Semi-rigid axial displacements

3.5.3 Semi-rigid shear deformation

Shear is complex because it is difficult to measure in the presence of moments. Nevertheless, moment and axial displacement have been determined which makes it easier to determine shear displacements as it will now be described.

At this stage all co-ordinates for the member behind the plate have been predicted as determined in the semi-rigid rotational and axial displacement analysis, 3 points in total. Using least squares again, a regression curve can be drawn as before connecting these 3 predicted points. However, as illustrated in Fig 3.5.3.1 the orientation of the curves are different, therefore $y = f(x)$ will be used instead of $x = f(y)$. As before, blue targets are on the member and red targets are on the plate.

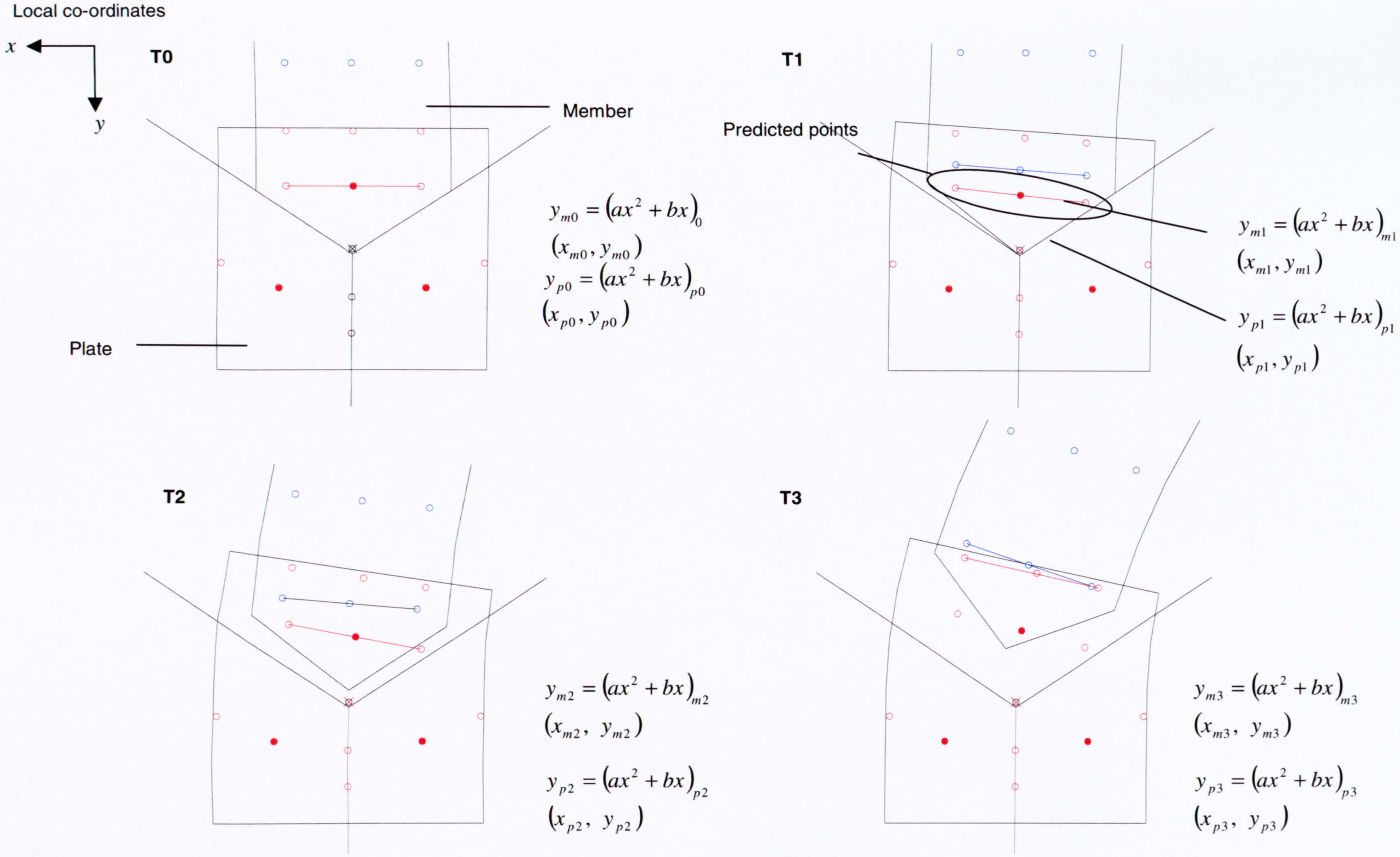

Fig. 3.5.3.1 – Semi-rigid shear displacement

Local co-ordinates

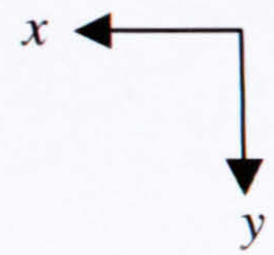

T1

T2

Plate

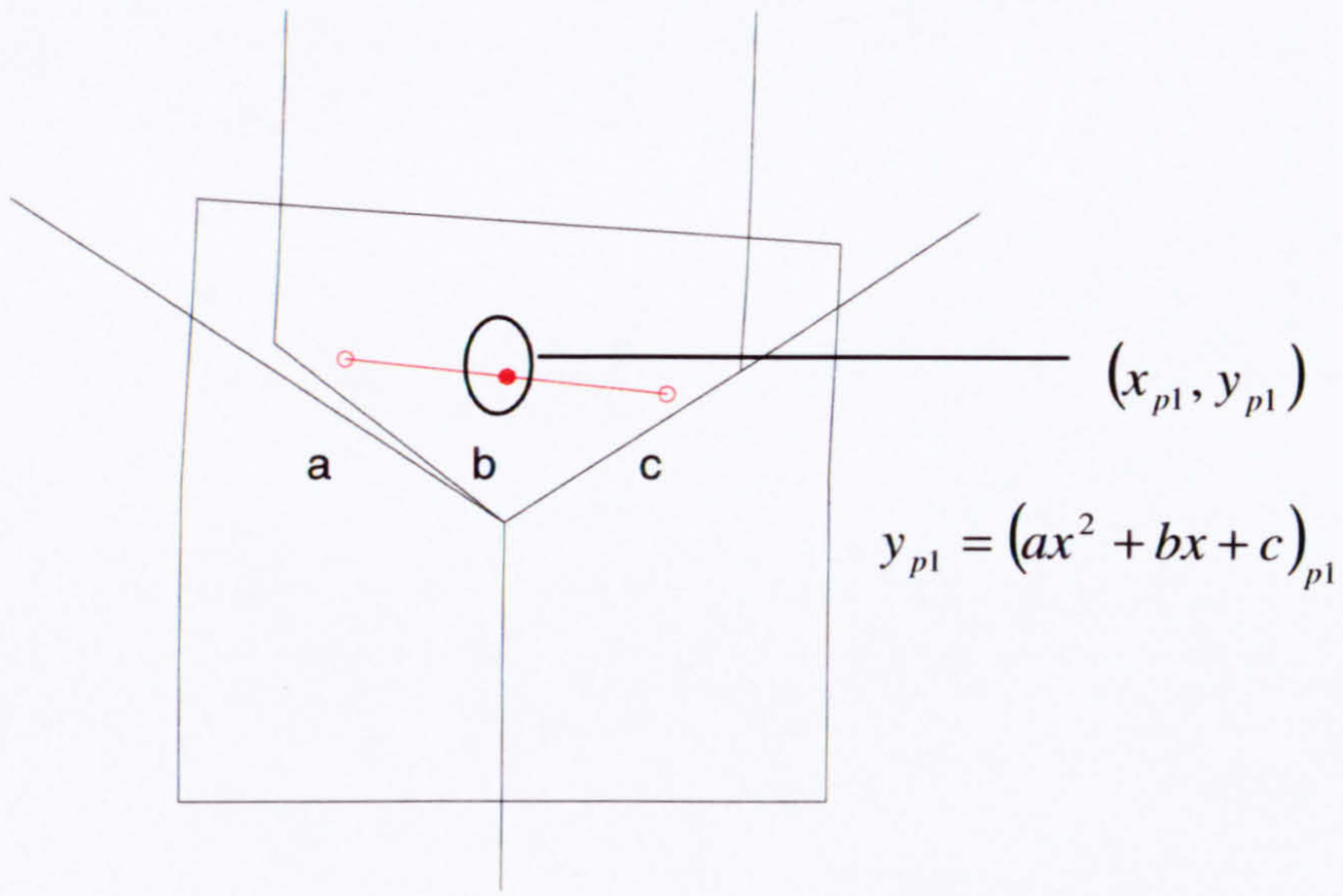

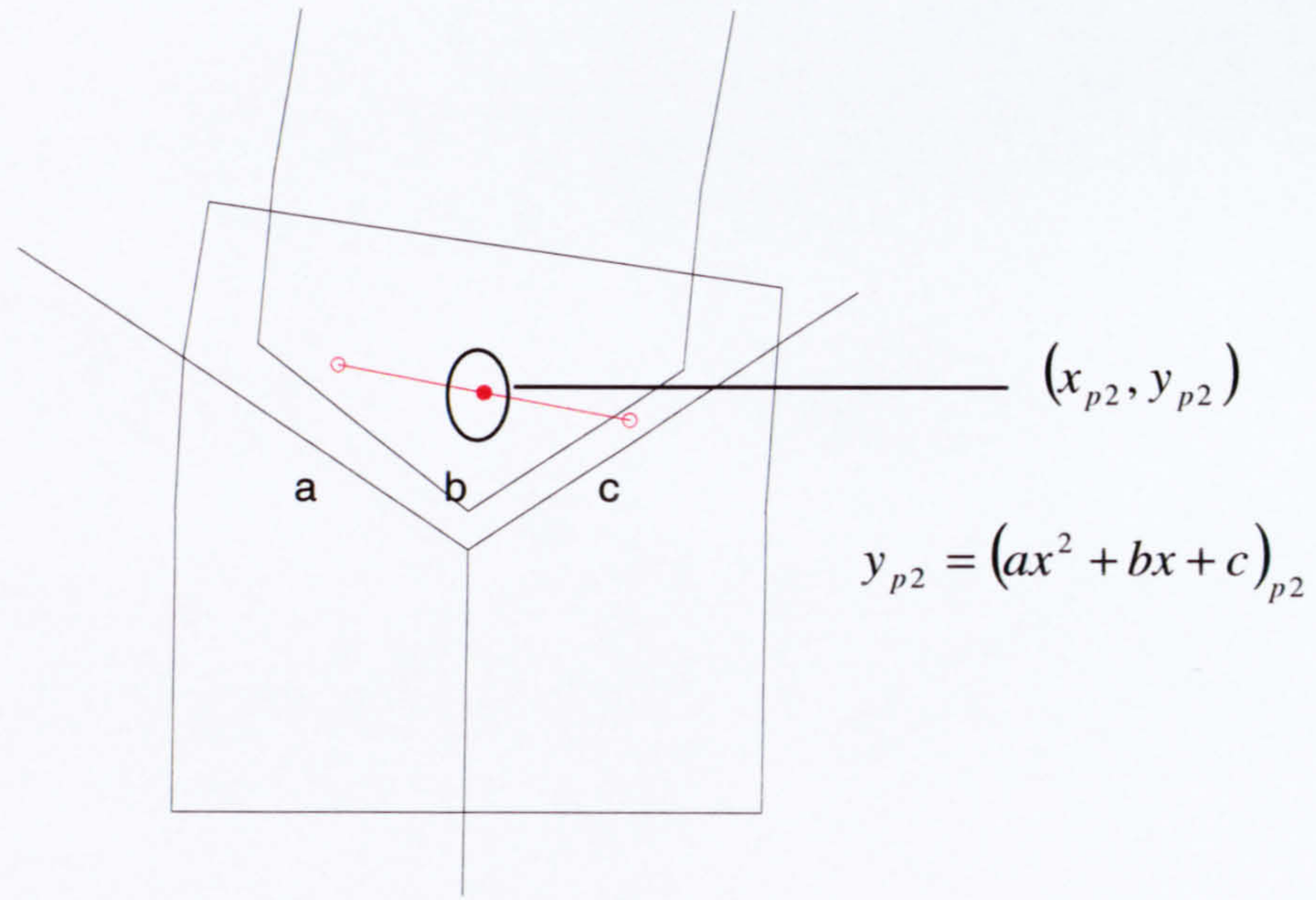

T1

T2

Member

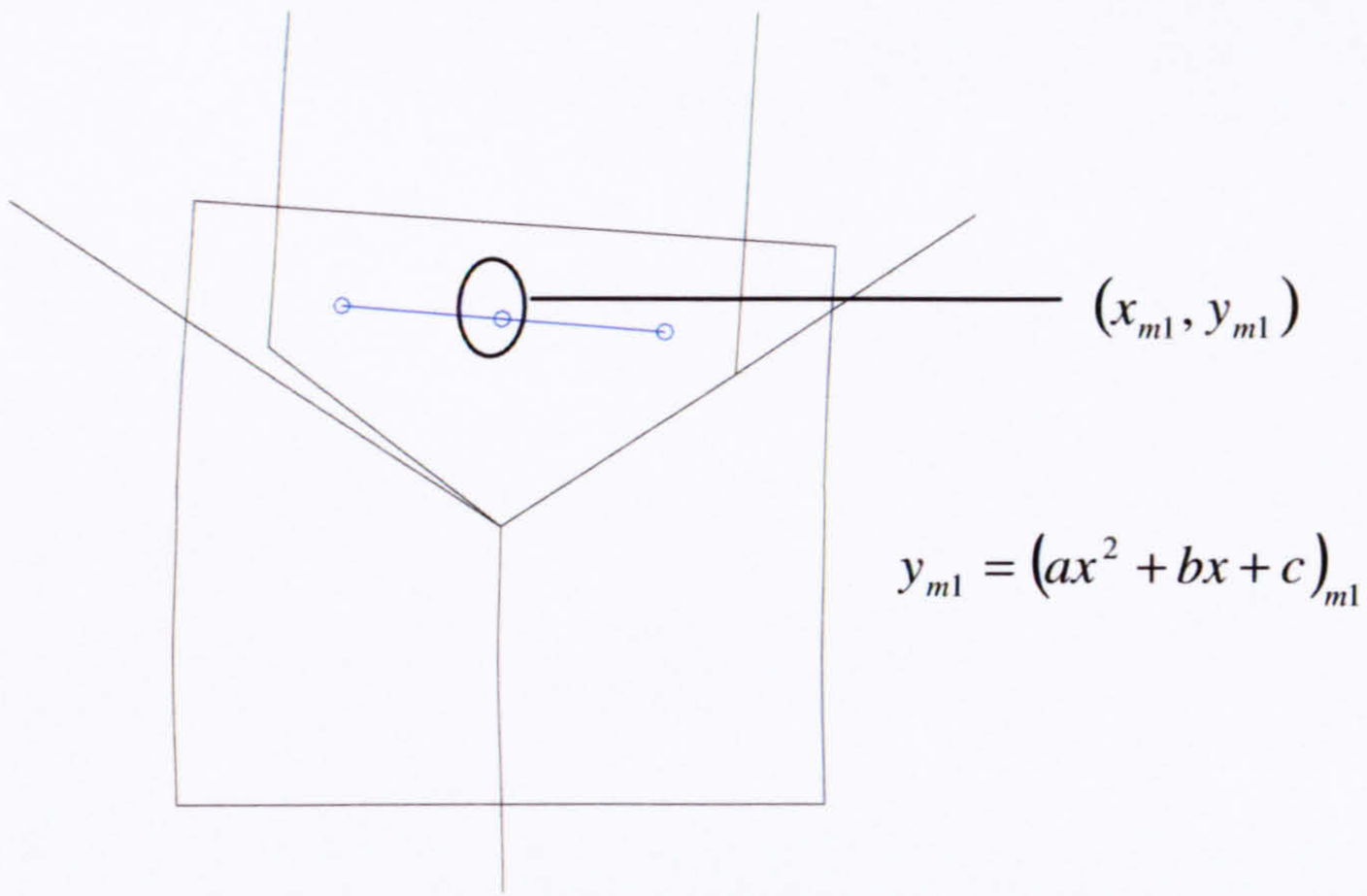

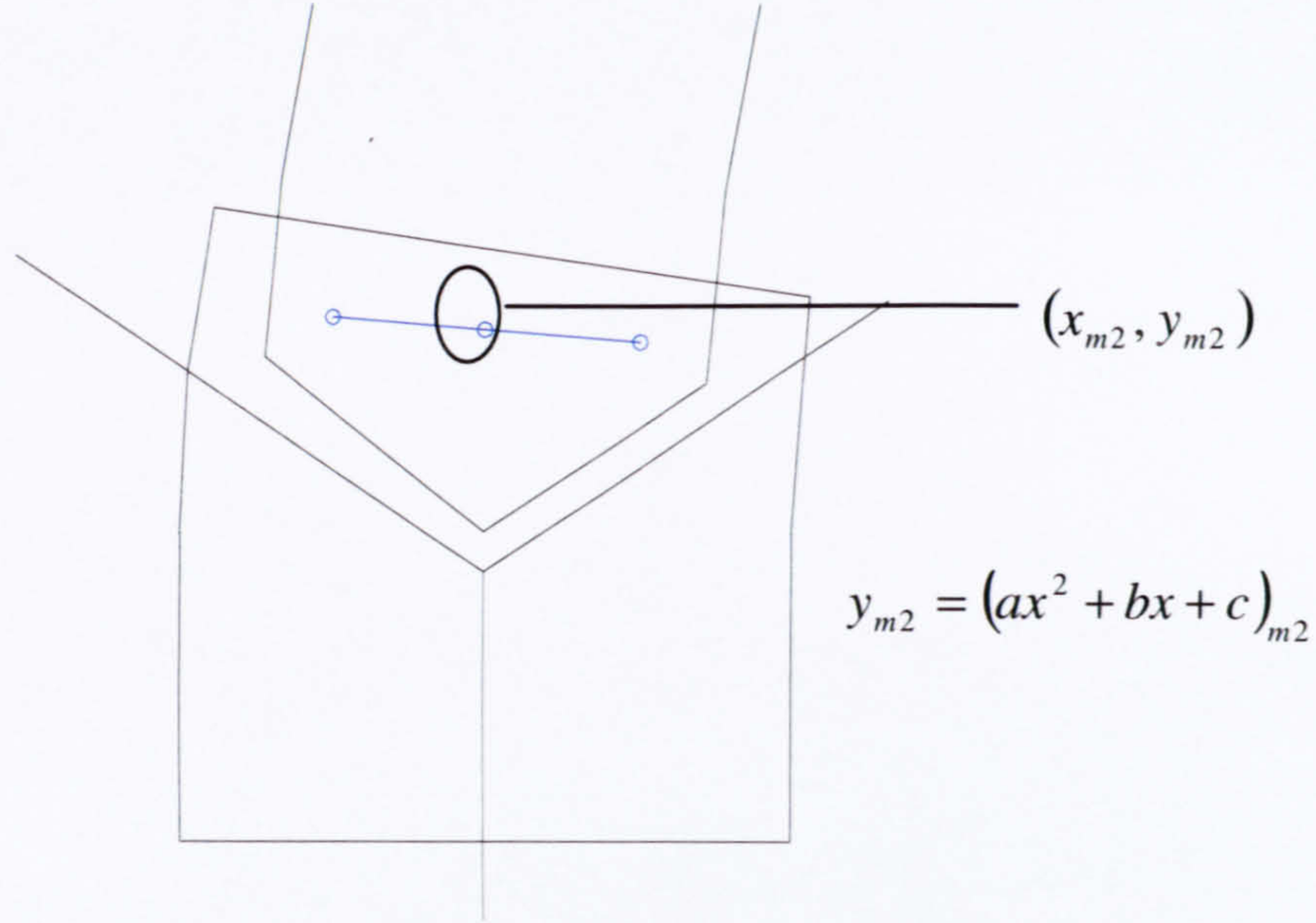

Fig. 3.5.3.2 – Break down of semi-rigid shear displacements

Again member and plate movement are treated separately. The illustration in Fig. 3.5.3.1 separates member and plate movement at times T1 and T2. What is being determined is how much of the movement is due to shear from one time to another. With reference to Fig. 3.5.3.3 the analysis is broken down into 4 parts from times T1 to T2.

At time T10/T1 – Initial stage

At time T11 – Axial displacement

At time T12 – Rotational displacement

At time T13/T2 – Shear displacement

At time T11, the first 1 represents time 1, the second suffix 1 denotes stage 1 as the analysis is broken down into 4 stages. The dotted lines represent previous movements whilst the line in bold represents current movement.

At time T11 – Axial displacement

The first part of the analysis requires the mean vertical displacement of the 3 points for the member which has already been determined in the axial semi-rigid displacement analysis given by Equation 3.5.1.7a,

Where $a_{m2-1} = a_{m2} - a_{m1}$.

At time T11:

Target a $\quad (x_{m10}, y_{m10} + a_{m2-1})_a = (x_{m11}, y_{m11})_a$

Target b $\quad (x_{m10}, y_{m10} + a_{m2-1})_b = (x_{m11}, y_{m11})_b$

Target c $\quad (x_{m10}, y_{m10} + a_{2-1})_c = (x_{m11}, y_{m11})_c$

Letting $y_{m11} = y_{m10} + a_{m2-1}$ and $x_{m10} = x_{m11}$, because no horizontal displacements due to shear are considered.

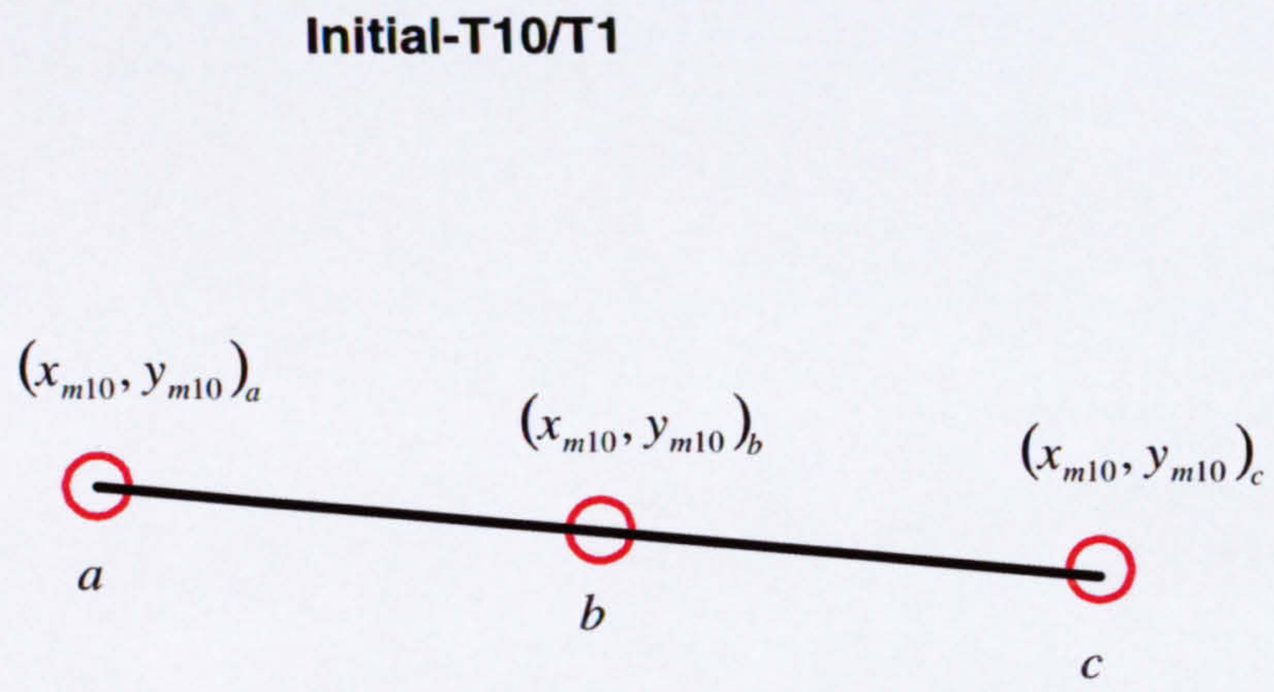

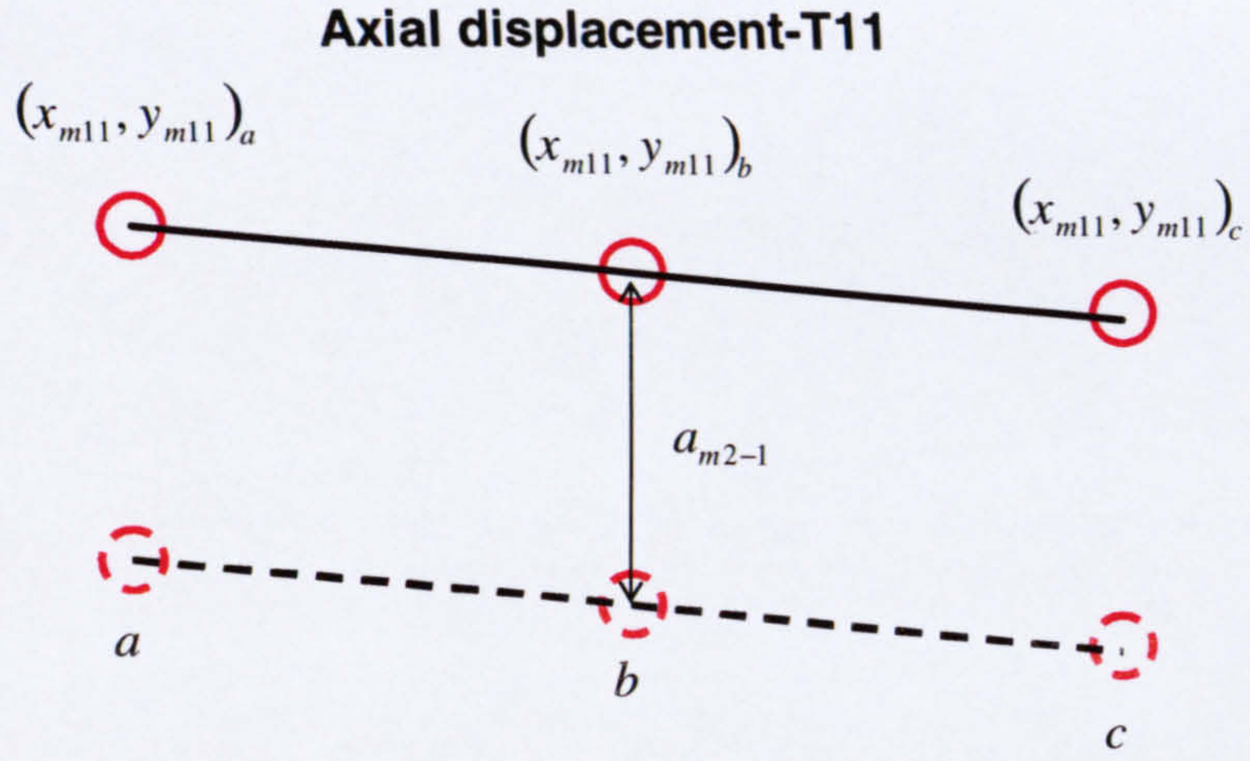

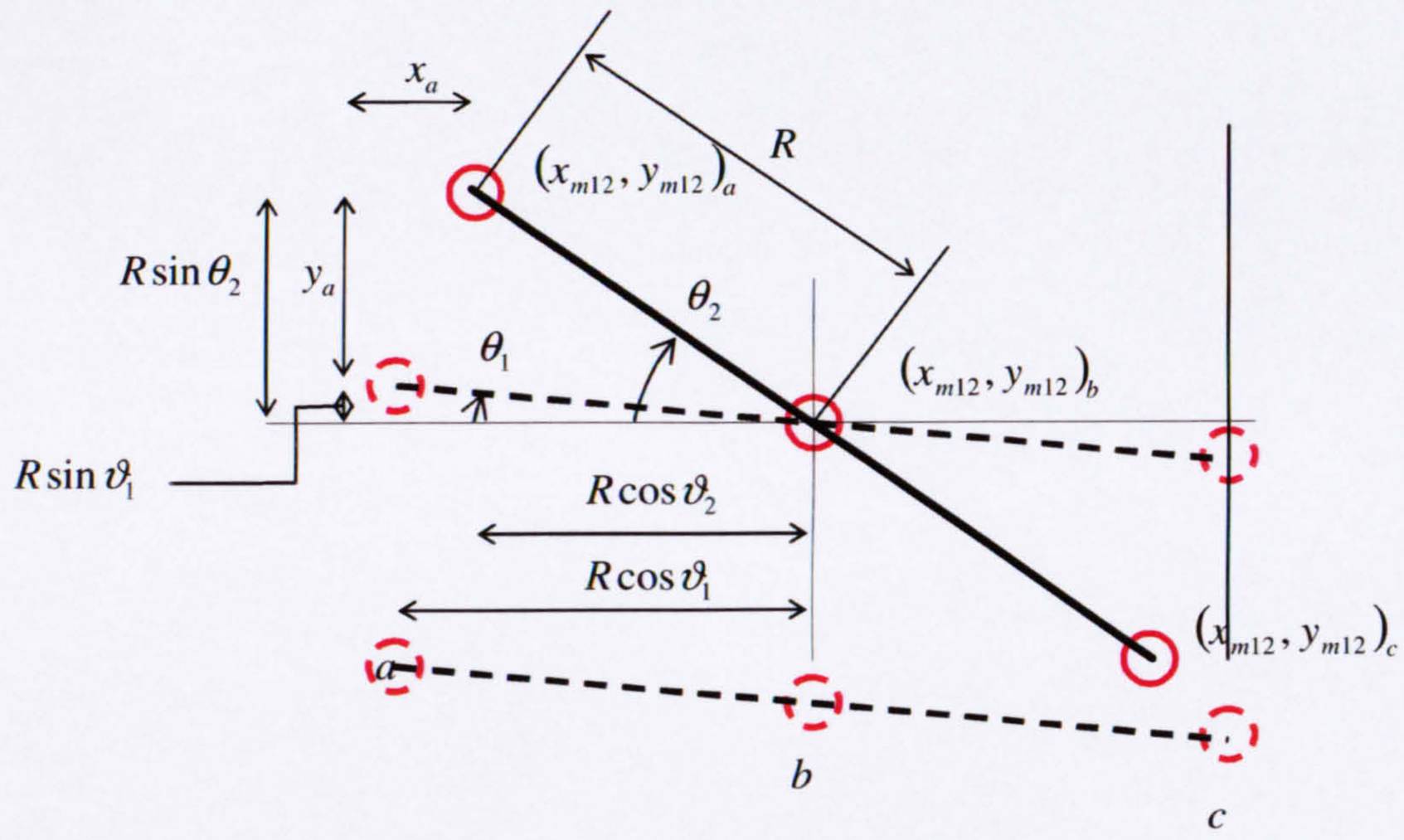

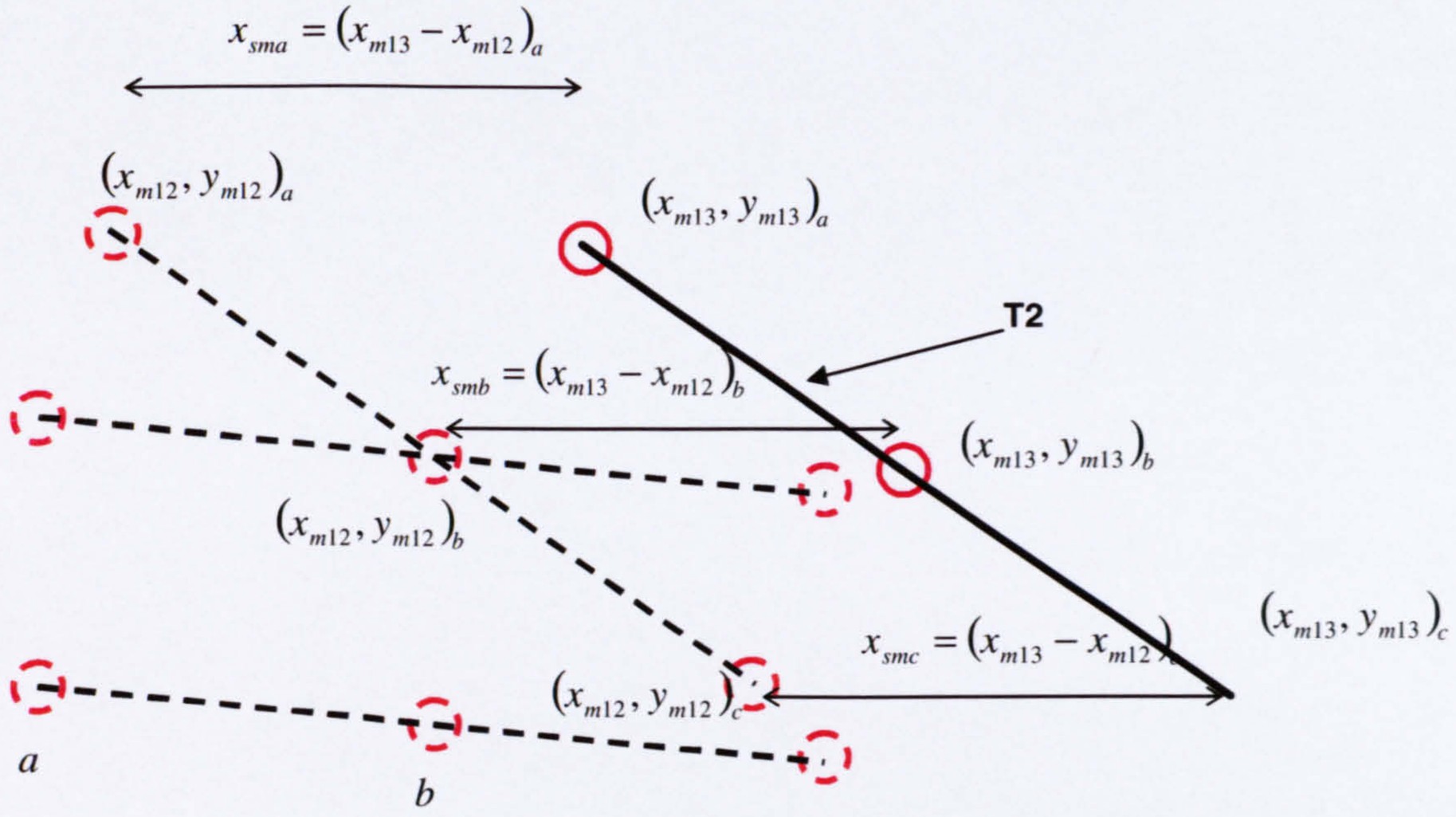

Horizontal displacement, $X = R(\cos\vartheta_{m2} - \cos\vartheta_{m1})$

Vertical displacement, $Y = R(\sin\vartheta_{m2} - \sin\vartheta_{m1})$

Fig. 3.5.3.3 – Step by step semi-rigid shear displacement analysis

Moment rotation-T12

Movement due to rotation is implemented next. Co-ordinates before rotation as shown at T11 are:

Target a $\quad (x_{m11}, y_{m11})_a$

Target b $\quad (x_{m11}, y_{m11})_b$

Target c $\quad (x_{m11}, y_{m11})_c$

Targets a and c are simply rotated clock-wise around target b. Recalling equations 3.5.1.1c and 3.5.1.2c for member rotation at times T1 and T2, which was already determined in the moment rotation analysis

$$\vartheta_{m1} = \tan^{-1}(2ay+b)_{m1} \qquad (3.5.1.1c)$$

$$\vartheta_{m2} = \tan^{-1}(2ay+b)_{m2} \qquad (3.5.1.2c)$$

The rotation is exaggerated in Fig 3.5.3.3 to illustrate the method. The distance between a and b is:

$$R_a = \sqrt{(x_{m11b} - x_{m11a})^2 + (y_{m11b} - y_{m11a})^2}$$

where x_{m11a} and x_{m11b} are x-co-ordinates on the member for target's a and b respectively at time T1 and ditto for y-co-ordinates. At time T12, there is vertical and horizontal displacement due to this rotation.

Vertical movement due to rotation

$$Y_a = R_a(\sin\vartheta_{m2} - \sin\vartheta_{m1})$$

Horizontal movement due to rotation

$$X_a = R_a(\cos\vartheta_{m2} - \cos\vartheta_{m1})$$

The new co-ordinates after rotation at a are

$$(x_{m11} + X_a, y_{m11} + Y_a) = (x_{m12}, y_{m12})_a$$

Letting $x_{m11} + X_a = x_{m12}$

Repeating the same for target c by determining X_c, Y_c and R_c

Gives

$$(x_{m11} + X_c, y_{m11} + Y_c) = (x_{m12}, y_{m12})_c$$

Again letting $y_{m11} + Y_c = y_{m12}$ and $x_{m11} + X_c = x_{m12}$

Note that target a and c is rotated clockwise, but target a is moving up whereas target c is moving down and therefore the displacement of c is in the opposing direction to a.

Shear movement-T13

The shear movement as illustrated at time T13 in Fig. 3.5.3.3 is the mean horizontal distance between targets at time T12 and T13, they are

At a $\quad s_{ma} = (x_{m13} - x_{m12})_a$

At b $\quad s_{mb} = (x_{m13} - x_{m12})_b$

At c $\quad s_{mc} = (x_{m13} - x_{m12})_c$

Hence the shear displacement for the member is

$$s_{m2} = \frac{s_{ma} + s_{mb} + s_{mc}}{3}$$

A similar analysis is repeated for semi-rigid plate shear. Referring back to Fig 3.5.3.3 the 3 member targets at time T10 are replaced by the 3 predicted member targets also shown in Fig. 3.5.3.2. The same procedure is applied over again with subscript m replaced by p. The point of rotation is naturally the centroidal target on the plate. Therefore the shear analysis for targets on the plate can be summarised as follows:

For axial displacement

At a $\quad (x_{p10}, y_{p10} + a_{p2\text{-}1})_a = (x_{p11}, y_{p11})_a$

At b $\quad (x_{p10}, y_{p10} + a_{p2\text{-}1})_b = (x_{p11}, y_{p11})_b$

At c $\quad (x_{p10}, y_{p10} + a_{p2\text{-}1})_c = (x_{p11}, y_{p11})_c$

For Moment rotation

$(x_{p11} + X_a, y_{p11} + Y_b)_a = (x_{p12}, y_{p12})_a \qquad (x_{p11} + X_a, y_{p11} + Y_a)_c = (x_{p12}, y_{p12})_c$

Letting $x_{p11} + X = x_{p12}$ and $y_{p11} + X = y_{p12}$ and so forth

For Shear displacement

At a $\quad s_{pa} = (x_{p13} - x_{p12})_a$

At b $\quad s_{pb} = (x_{p13} - x_{p12})_b$

At c $\quad s_{pb} = (x_{p13} - x_{p12})_b$

Hence the shear displacement for the plate at time T2 is:

$$s_{p2} = \frac{s_{pa} + s_{pb} + s_{pc}}{3}$$

From the analysis the shear displacement of the plate and member have been determined. Therefore the semi-rigid shear displacement at time T2 is:

$$s_{2\text{-}1} = s_{m2} - s_{p2} \qquad (3.5.1.8)$$

Which complete the data interpretation for semi-rigid displacement.

What follows is similar treatment of other connection types in the Queen truss as illustrated in Fig. 3.2.2. As in the crown joint analysis, the red and blue circles are targets on the plate and timber respectively with regression curves of the same colour code linking them. Each face/plate of a connection is represented by a dashed red cross. The dashed line parallel to the member is used for the moment rotation analysis on the plate, where the centre of the cross is denoted by a red (filled in) target. Three lines represent the member. One is a blue dashed dotted curve and the other two are dashed curve. The blue dashed dotted curve denoted by the number one is called the master target. Targets at the end of this curve, denoted by the number 4, are extrapolated and used for the member rotation analysis. The two blue dashed line represents the slave curve and are used to extrapolate data to determine the axial and shear displacement of the member. Note that for some joints, targets on slave curves are all visible thus there is no need for extrapolation. An example of this is the outer curve on leg 2, of the heel joint in Fig. 3.5.3.5. With some assistance from the legend below, illustrations of the regression curves and targets required for interpretation for each joint are presented. The targets for the Crown joint test has already been given in the analysis but will be illustrated again for completeness. The following legend can be referenced to view the illustrations from Fig. 3.5.3.1 to Fig 3.5.3.7.

Legend

1. Master Curve.

2/3 Slave curve 1/2.

4/5 Extrapolated targets from master/slave curves.

6. Centroid target on plate.

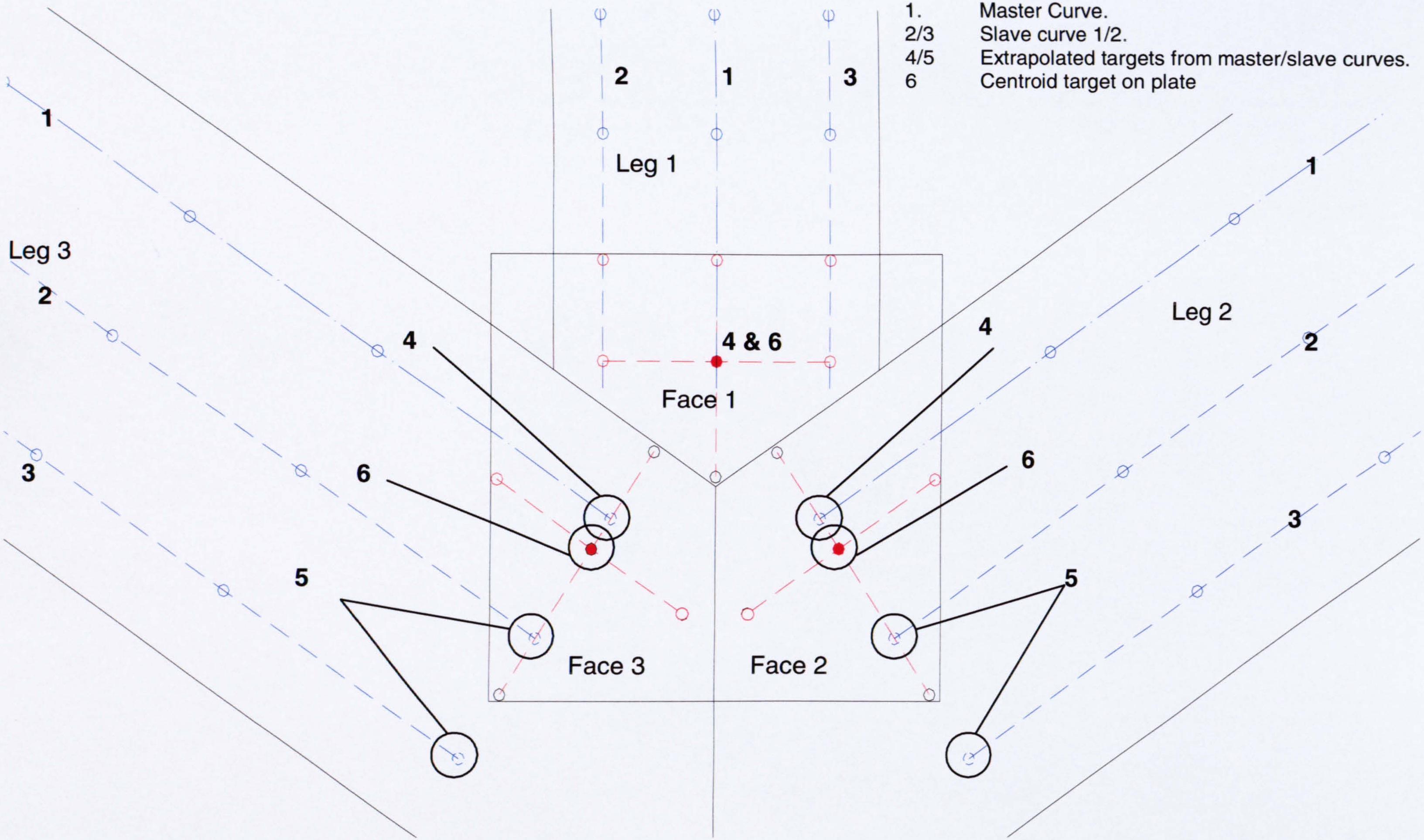

Fig.3.5.3.4 - Inverted Crown Joint

1. Master Curve.
2/3 Slave curve 1/2.
4/5 Extrapolated targets from master/slave curves.
6 Centroid target on plate

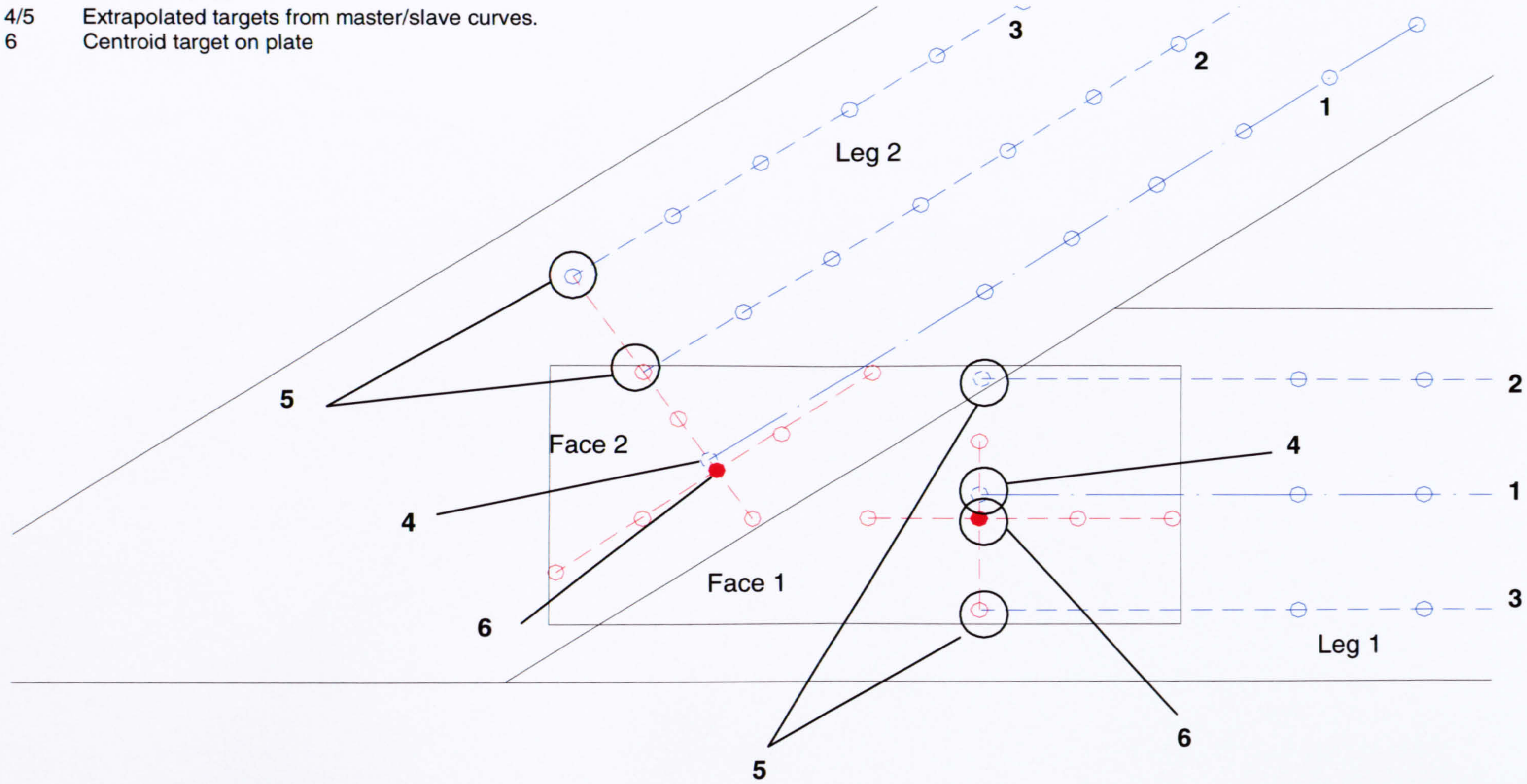

Fig. 3.5.3.5 – Heel Joint

1. Master Curve.
2/3 Slave curve 1/2.
4/5 Extrapolated targets from master/slave curves.
6 Centroid target on plate

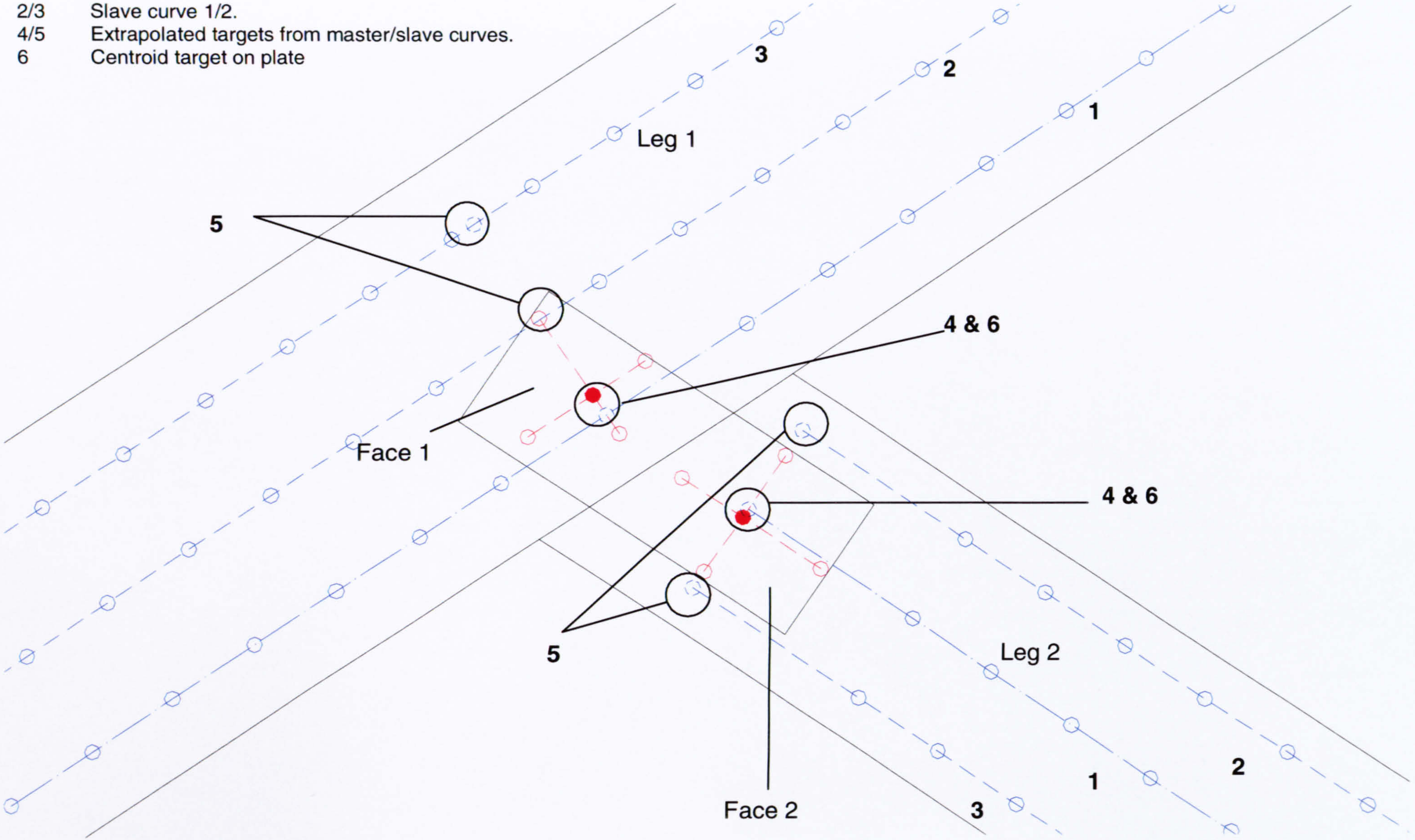

Fig. 3.5.3.6 - Top Chord Joint

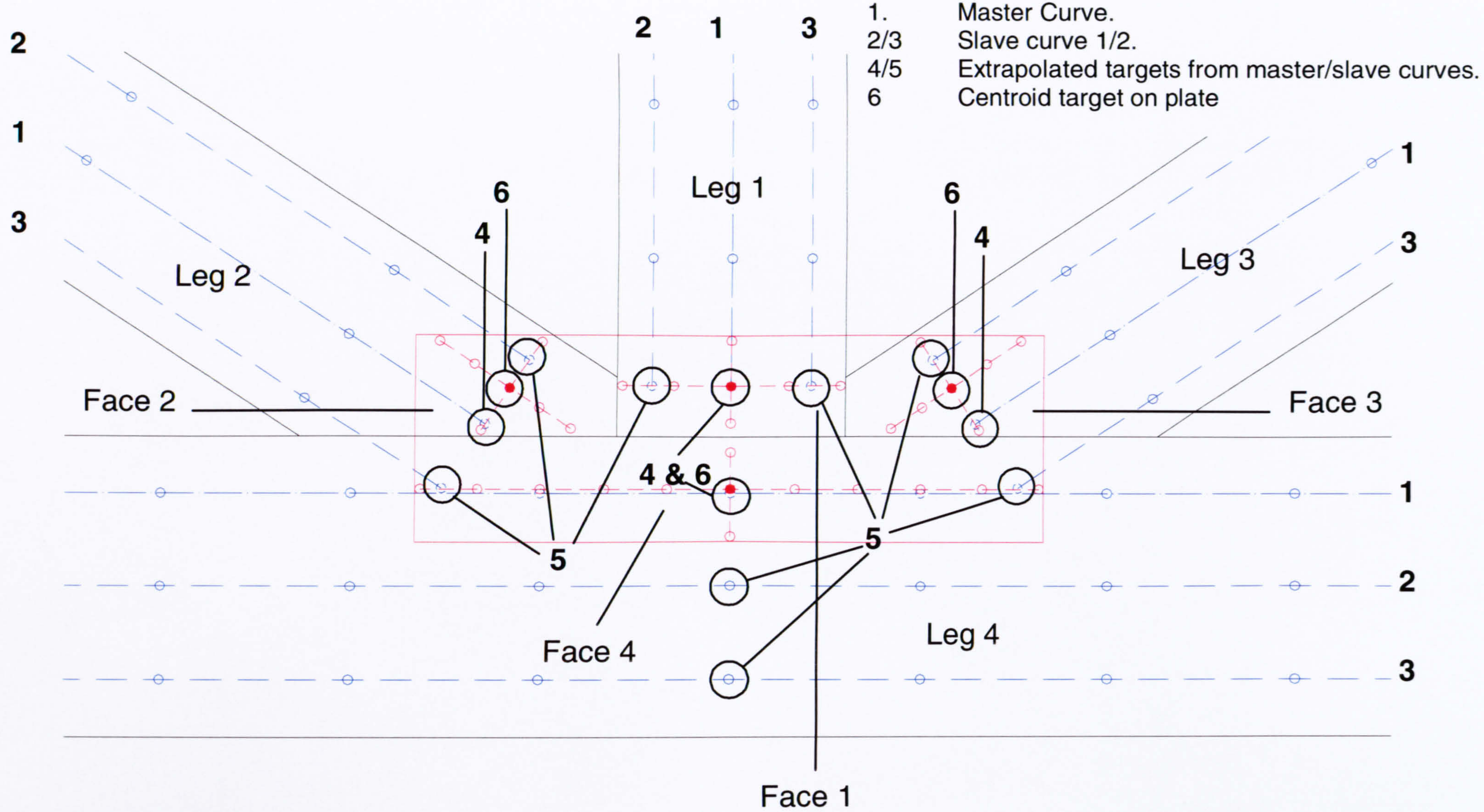

Fig. 3.5.3.7 – Bottom chord joint

The illustrations show how data will be extracted to determine semi-rigid rotation and deformation. It is understood that not all the data will be necessary. A connection is only as strong as its weakest link and it is this weakest link that will determine the strength of the connection. It is therefore only necessary to consider the weakest face in the joint. However, as illustrated, all faces are considered as there is no telling which face will fail first although in some connections, such as the bottom chord joint, it is obvious that face 1 will be the failure face as the web members are in compression and the bottom chord has a significant amount of bite area, i.e face size, than the centre web member. The heel joint is more difficult to predict.

The application to deal with this analysis was an on going development throughout the study. At the same time, the literature for the theory was written. After a few preliminary runs, some minor modifications to the theory were required. The second order polynomial described above was found to be too sensitive to target co-ordinates and frequently gave erroneous results in the moment rotation analysis. This is due to a number of reasons. The first is that the targets are not stuck in a perfectly straight line and can have a profound effect on curve slopes. The second reason is that if images taken are of bad quality, this can sometimes distort measurements of some targets. Some of the targets were obscured and required the camera to be placed in a less favourable position to capture them, which can affect image quality as experienced here. Subsequently, a less sensitive linear equation was adopted instead. However, the rest of the data interpretation process remains the same. The equation for the linear regression line and the angle of rotation is.

$$x_m = (ay + b)_m \qquad \tan^{-1}\left(\frac{dx_m}{dy}\right) = \tan^{-1} a_m$$

and

$$x_p = (ay + b)_p \qquad \tan^{-1}\left(\frac{dx_p}{dy}\right) = \tan^{-1} a_p$$

For the member and plate respectively.

The linear interpretation of the member is reasonable in the moment rotation analysis as the member remains quite rigid when loaded in the tests. Although the second order polynomial presented had not been adopted, it is kept in the body of the text to illustrate the aspects considered in developing the theory and the laboratory tests. The use of the second order polynomial was first adopted as it was thought that some curvature of the member was expected. A second order polynomial would be of better use if members were much longer and displayed significant curvature.

3.6 Loading arrangement

The preparation of the loading arrangements consumed a significant part of the test period. This was due to five different test arrangements, which encompassed 4 joint tests and one full scale tests. In addition many problems were encountered during the entire process of preparation and testing.

Although the timber was not conditioned, i.e. kept in a controlled environment, the storage environment was very similar to the testing environment. Typically the humidity was 40-65% and temperature 22-24°. Timber members were propped to avoid contact with the floor and gaps were also made between timber members to allow for air circulation. Measures were also made to prop the members at close proximity to discourage the possibility of warped members.

An existing steel frame was used to conduct the joint tests. The frame is approximately 2.5m wide and 3.0m high. Components were designed and drawn using AutoCAD R14 drawing package and then fabricated to accommodate the specimen, load cells and other various components in the frame. The frame dimensions ultimately dictated the lengths of the timber sections in these tests and posed difficulties in the design and fabrication stage when trying to accommodate inclined timber members within the square frame. Further problems were encountered due to the complexity of the loading regime, which required independent control of moment and axial loads without compromise to joint movement as demonstrated later. Several designs were considered before reaching the final one. .Because each test was different new components were required for each test.

The force component of each member in the truss under vertical load is illustrated in Fig. 3.6.1. These force components are maintained throughout the joint tests to simulate joint behaviour as part of a truss. Note that there is a tension splice joint near the left heel joint. The longest timber length available is 5.5 metres, which is below the width of the truss. The size of the splice plate is such that it can be assumed the bottom chord is continuous at that point. In addition, by locating the plate there the bending moment at the plate is reduced, whilst it is adequate under shear effects. The adequacy of the plate is observed in the structural tests as presented later.

There are 4 connection tests and one full scale truss test. The mechanics and moving components will be presented in detail for each test in the following order:

- Crown joint test
- Heel joint test
- Top chord joint test
- Bottom chord joint test
- Overall full scale truss test

Connection dimensions for the joint tests are now presented.

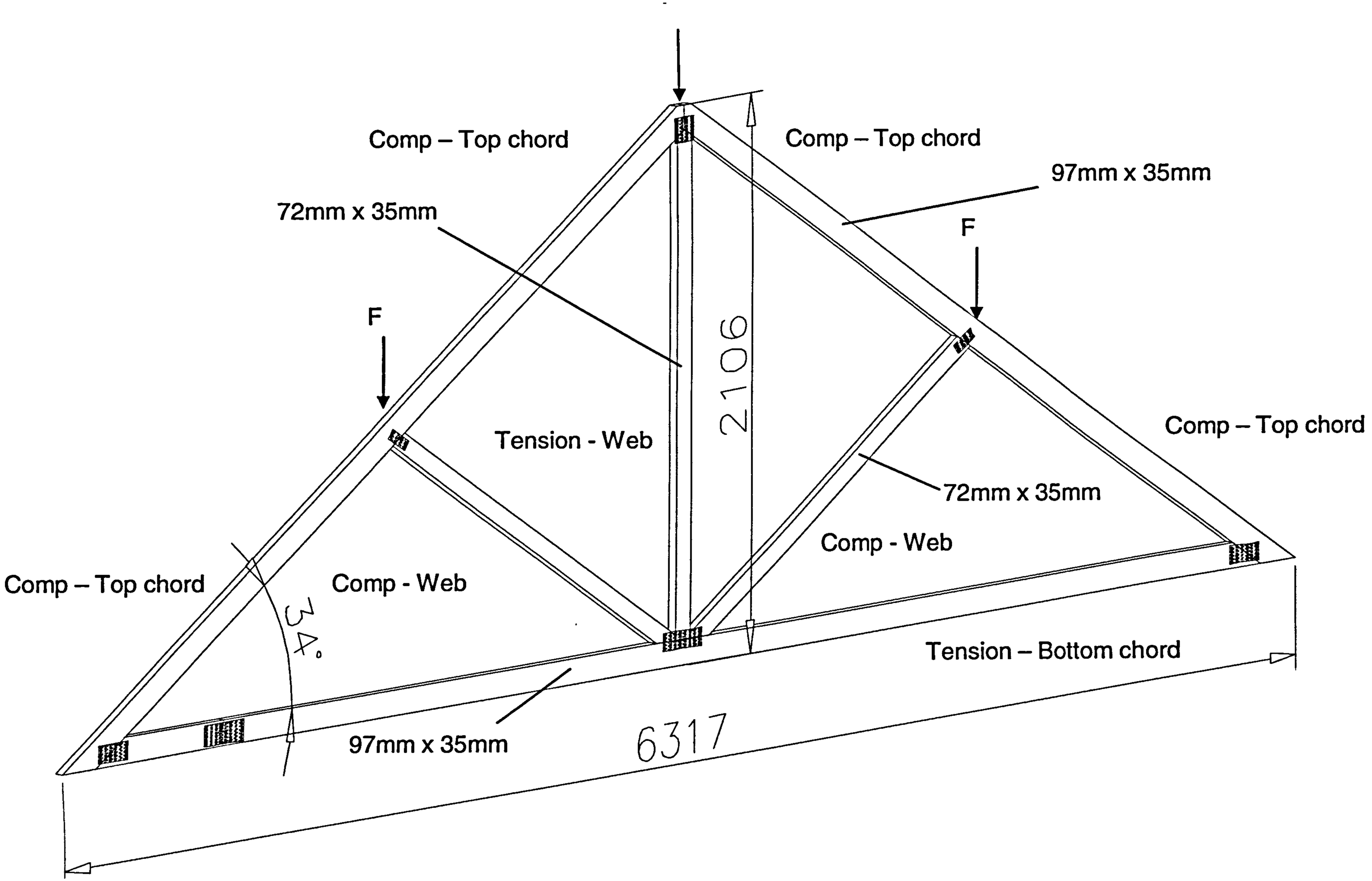

Fig. 3.6.1 – Force components of the truss

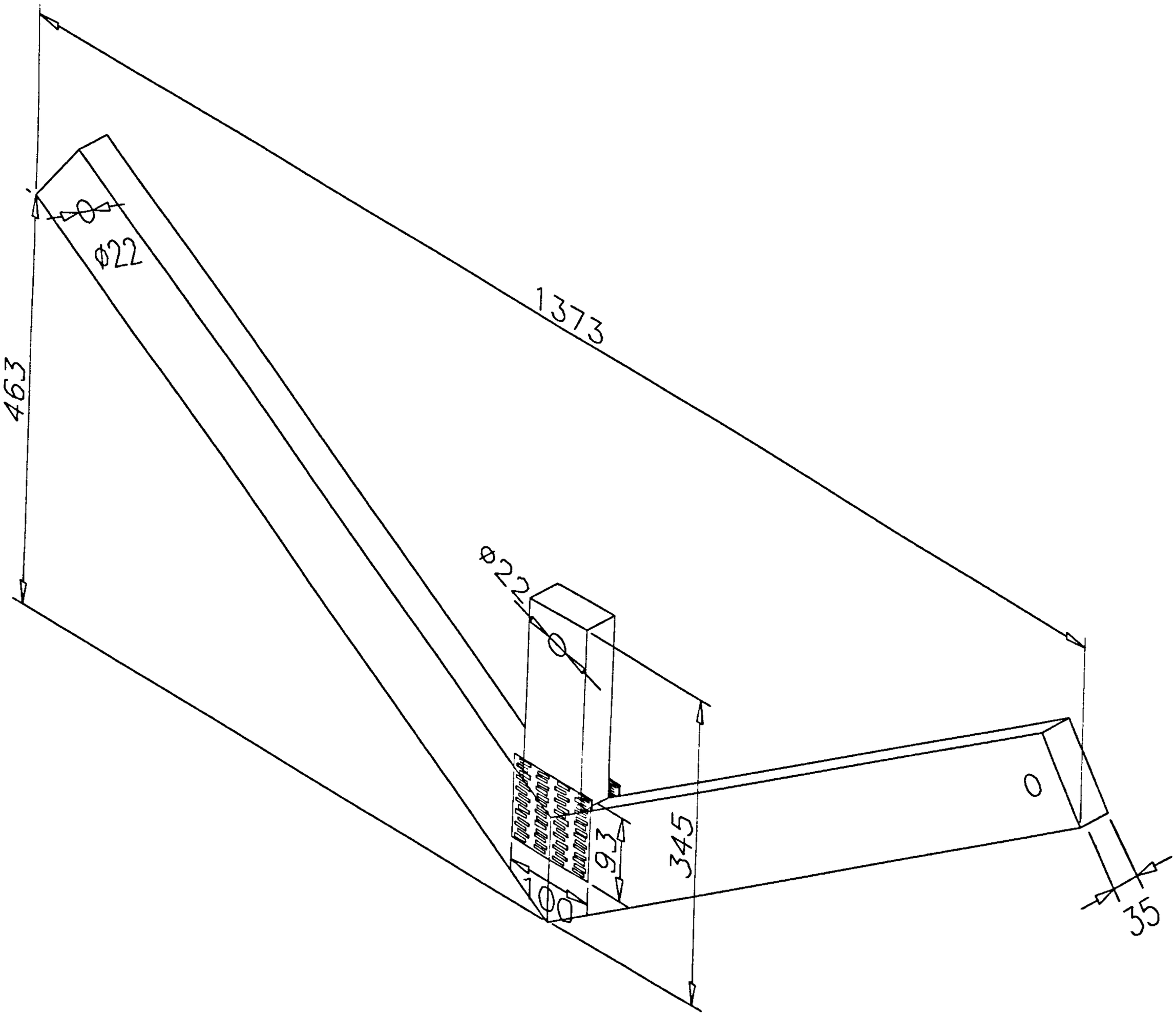

Fig. 3.6.2 – Crown Joint dimensions

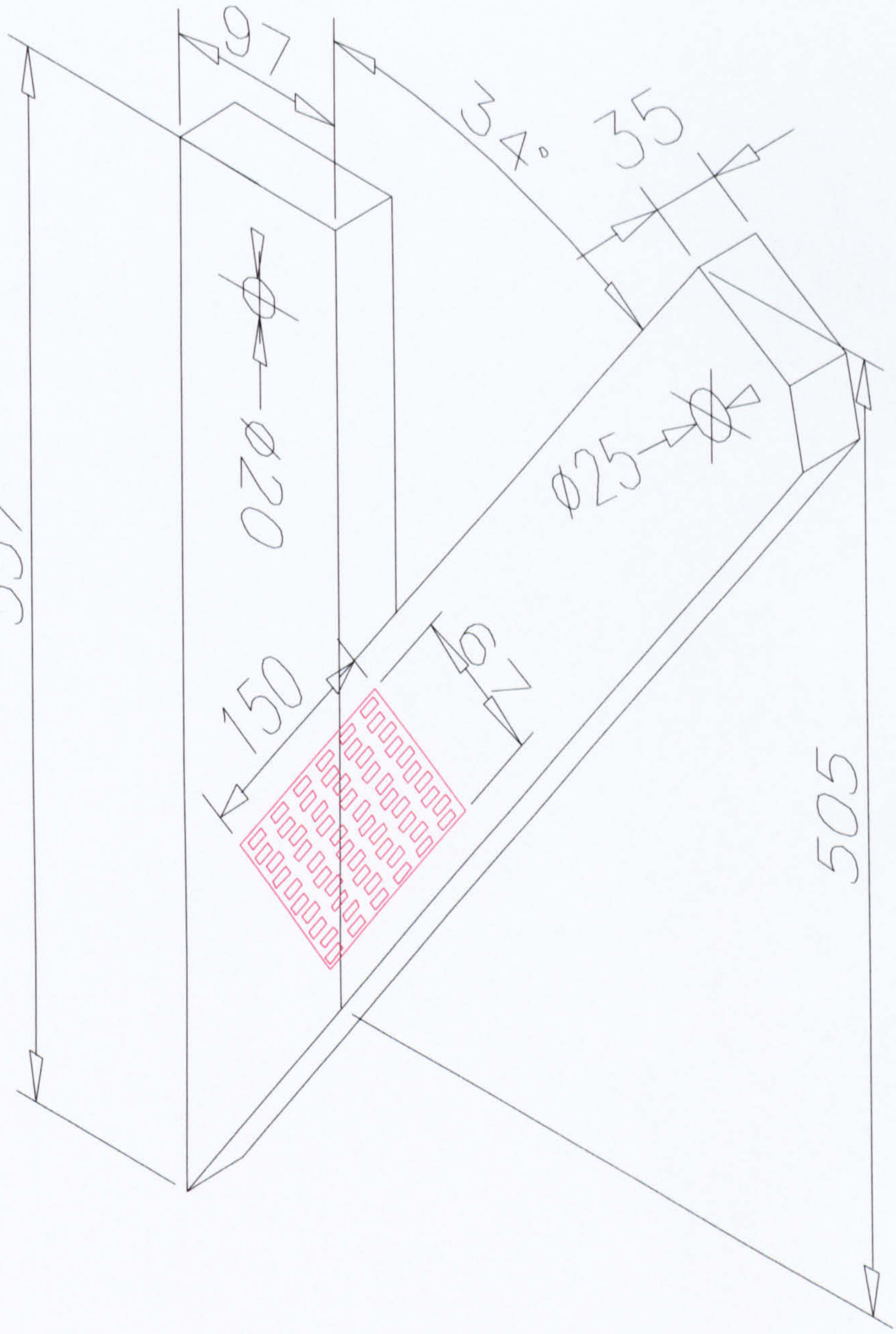

Fig. 3.6.3 – Heel Joint dimensions

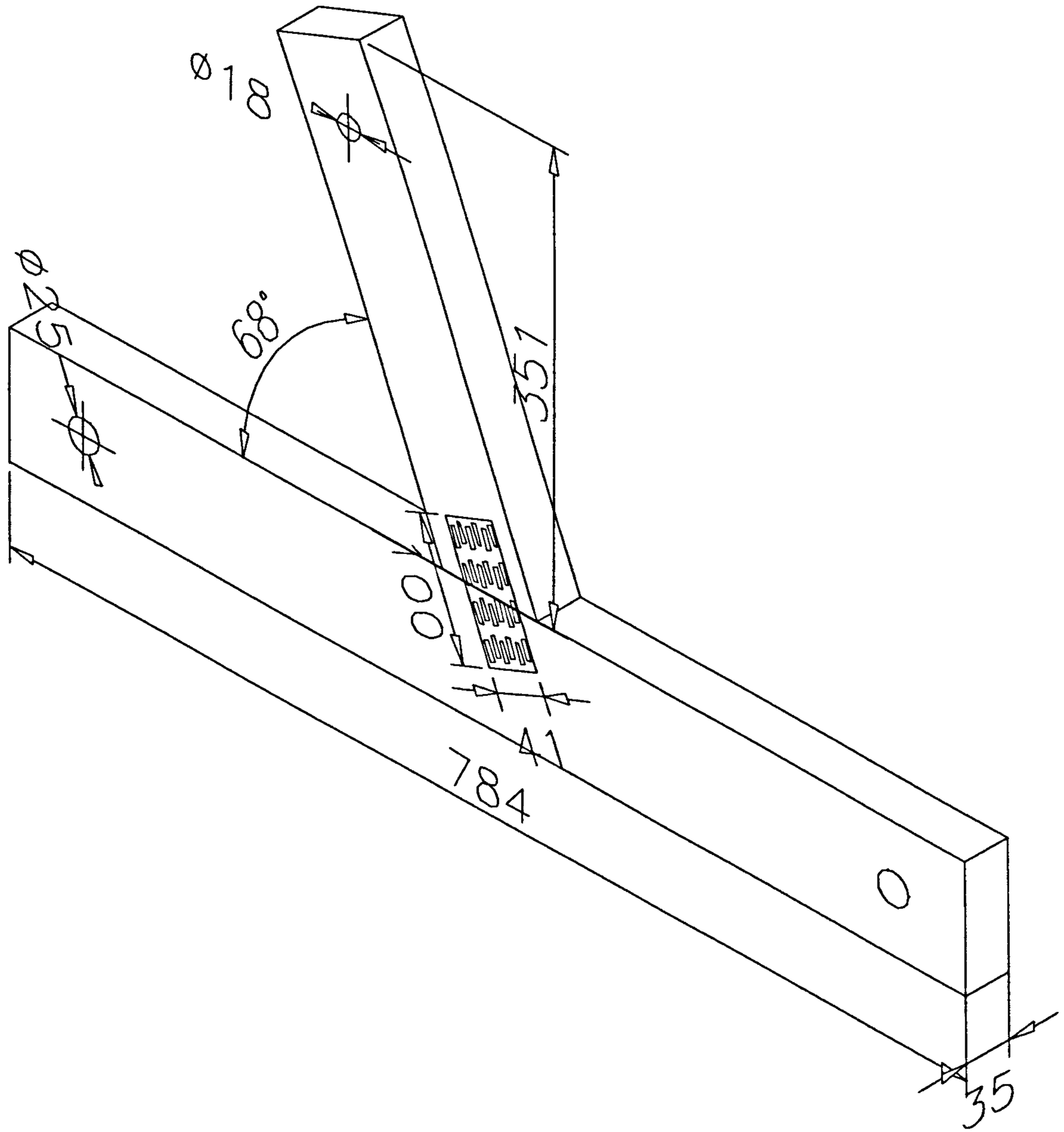

Fig. 3.6.4 – Top chord joint dimensions

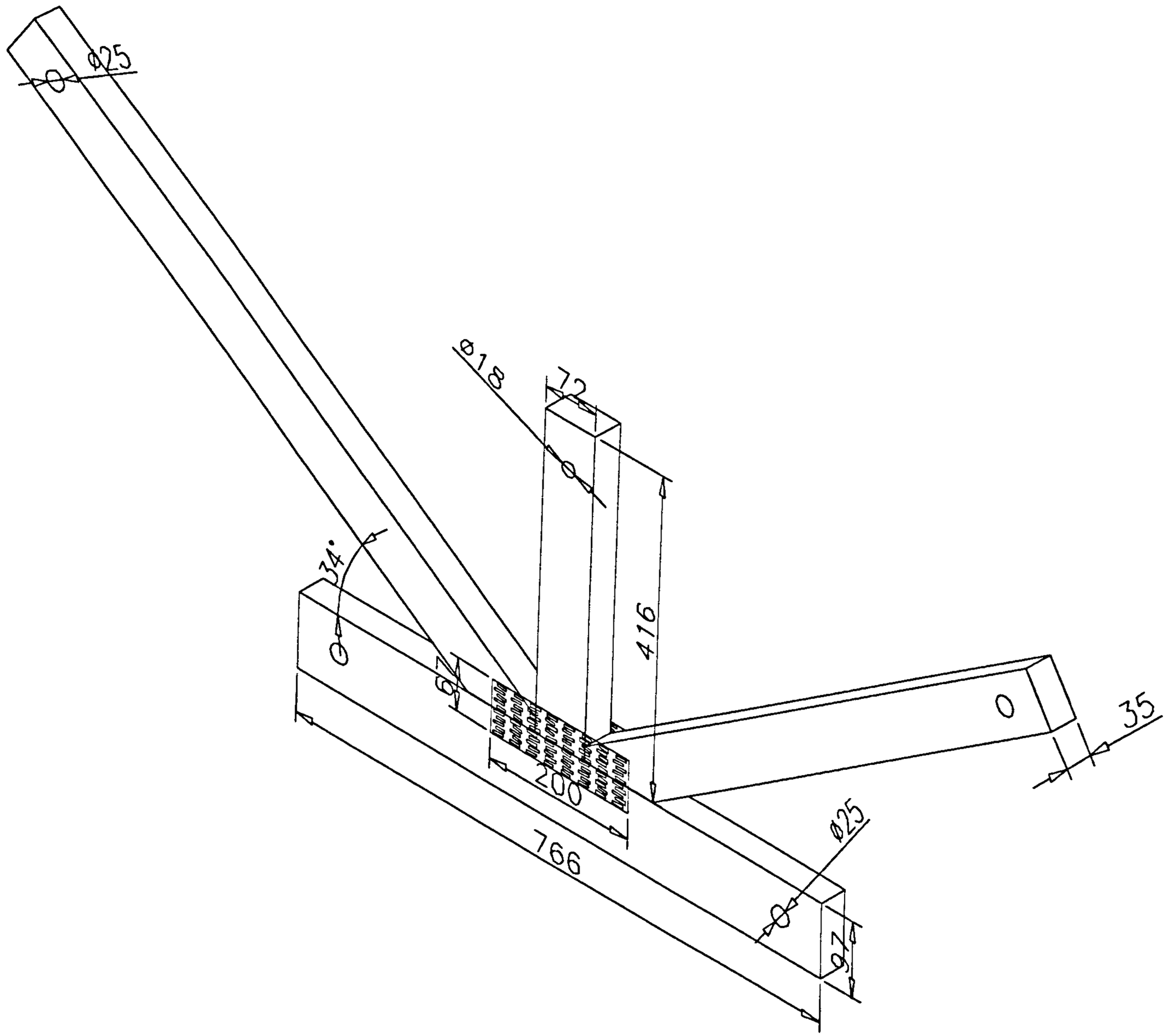

Fig. 3.6.5 – Bottom chord joint dimensions

The dimensions of each joint and their corresponding plate sizes are tabulated below.

Joint type	Member	Depth (mm)	Breadth (mm)	Plate size
Crown	Top chord Web	97 72	35 35	93x100
Heel	Top chord Bottom chord	97 97	35 35	67x150
Top chord	Top chord Web	97 72	35 35	41x100
Bottom chord	Bottom chord Web	97 72	35 35	67x200

Table 3.6.1 – Joint Dimensions

3.6.1 Crown Joint test

The crown joint test is illustrated in Fig. 3.6.1.1 on the next page. (See Fig, A4.1 for photograph). Because new load cells were required, the design was changed a few times either because load cell dimensions were not suitable or fittings for the load cells were difficult to adapt. Bolting components to the frame was made easy because of 22mm ∅ holes with 4" centres existed on the columns and beams of the frame. Initially it was thought that the height of the steel beam in the frame was adjustable. This would give some an advantage in designing subsequent tests if for example timber specimen members either needed to be reduced or increased for whatever reason. It later emerged that this was not possible due to the requirements of the close range photogrammetry where targets on the frame are used as fixed control point for the VMS afterwards. Slots as opposed to holes were drilled into most steel components to achieve a good fit and allow room for errors in machining. The frame was not perfectly square and this posed problems for components situated at the corners of the frame. As a result, the two brackets attached at the top corners of the frame were bolted to the frame first then tap welded in situ for a good fit. Some components were modified due to physical restrictions of machines in the fabrication process. The following legend is used to assist viewing of Fig. 3.6.1.1.

1. Top chord members
2. Web member through which axial and moment load is applied

3/4 Moment loads applied through a combination of dead weights, pulley and cable

5/6. Restraining points

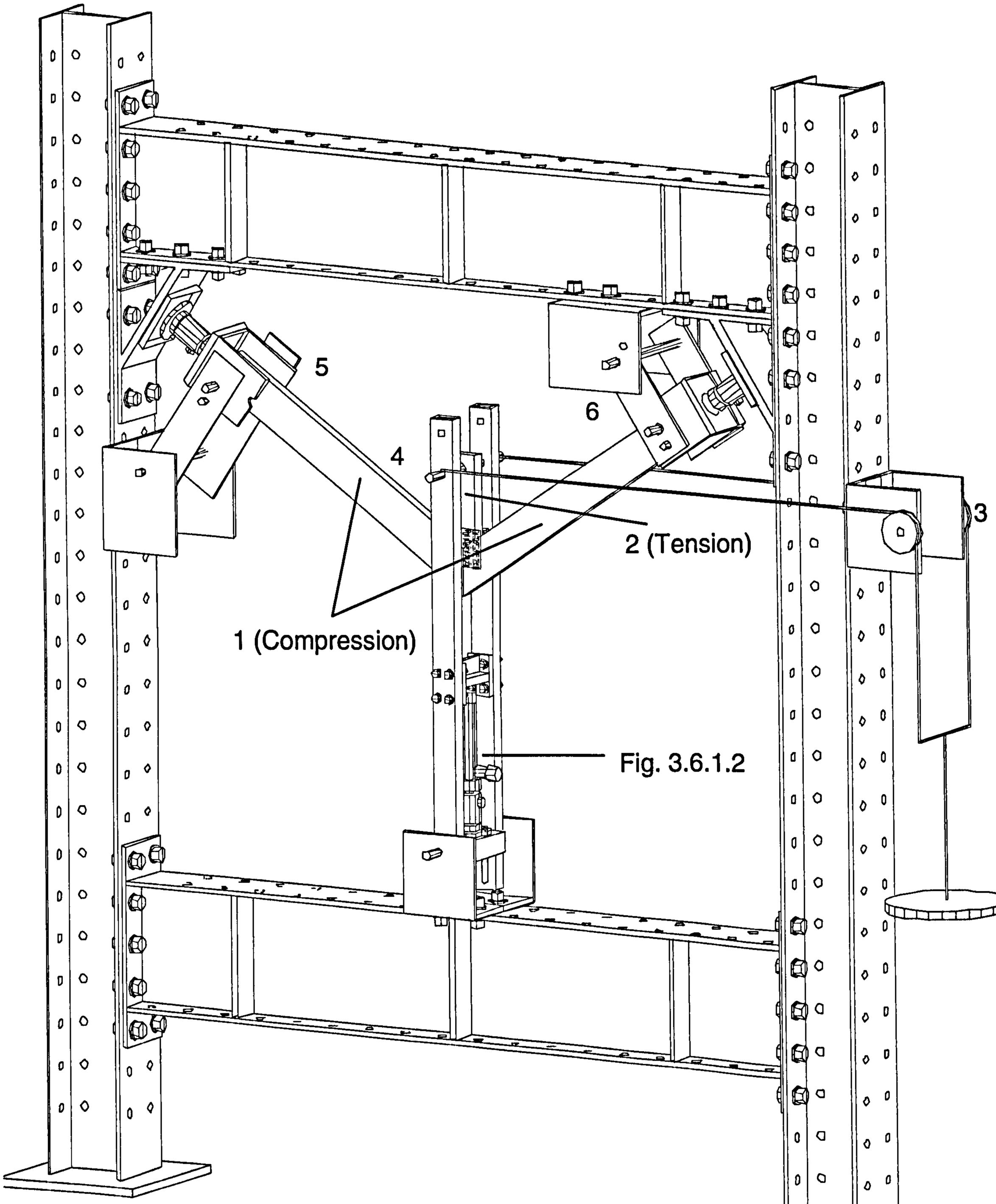

Fig. 3.6.1.1 - Crown Joint test

As illustrated in Fig 3.6.1.1, the joint is isolated and constrained such that no loads are shed on to the frame apart from reaction loads. Tensile and moment load are applied through the web member denoted by 4 on the sketch as the centre web member is in tension in the truss as illustrated in Fig 3.6.1. The moment load is applied through a pair of cables looped round the pin at 4, and rests on twin pulleys at either side of the flange of the column at 3. The cables are looped round another pin further down at the side. A hanger where dead weights can be placed, is hooked to the centre of this pin. The advantage of such a system is that the moment loading will be invariable because the applied dead weights are constant. The disadvantage is that the overloading of the hanger poses a safety problem. Also, manual work is involved when applying loads. Moment loads are isolated at the joint by holding the connection by bolts. When moment is applied to the connection via the web member, the connection will rotate. The reaction to this will also rotate the top chord members. In this particular loading arrangement the members will tend to rotate clock-wise under bending moment loads. The top chord members are restrained from rotating through steel components bolted to the left column and top beam for the left and right chord respectively as denoted by 5/6, thus confining moments at the connection.

The application of axial loads and moment loads are independent and lead to a design where the ram applying the axial load would rotate as well when moment loads were applied. As illustrated in the CAD drawing in Fig. 3.6.1.2, a hydraulic ram is used to apply axial loading through the web member at the centre of the frame via the T-block through to the twin hollow sections. When the ram is pumped the head pushes the T - Block which in turn pushes the twin

hollow sections, this force is transferred to the timber by a pin threaded through the hollow section and web further up, denoted by the number 4 in Fig. 3.6.1.1. The ram sits on top of the load cell, which is in turn bolted to a rotating platform. As illustrated in the diagram the ram is not restrained in anyway. The stability of the ram is established by applying a small load (less than 0.5KN) to temporarily keep it in position before testing. The rotating platform is supported by a pin threaded through it, which rests on a twin set of angled sections. A slot has been drilled into the hollow section to allow for axial movement. As illustrated in Fig. 3.6.1.3, this system permits the application of axial loads and free rotational movement when moment is exerted and vice versa.

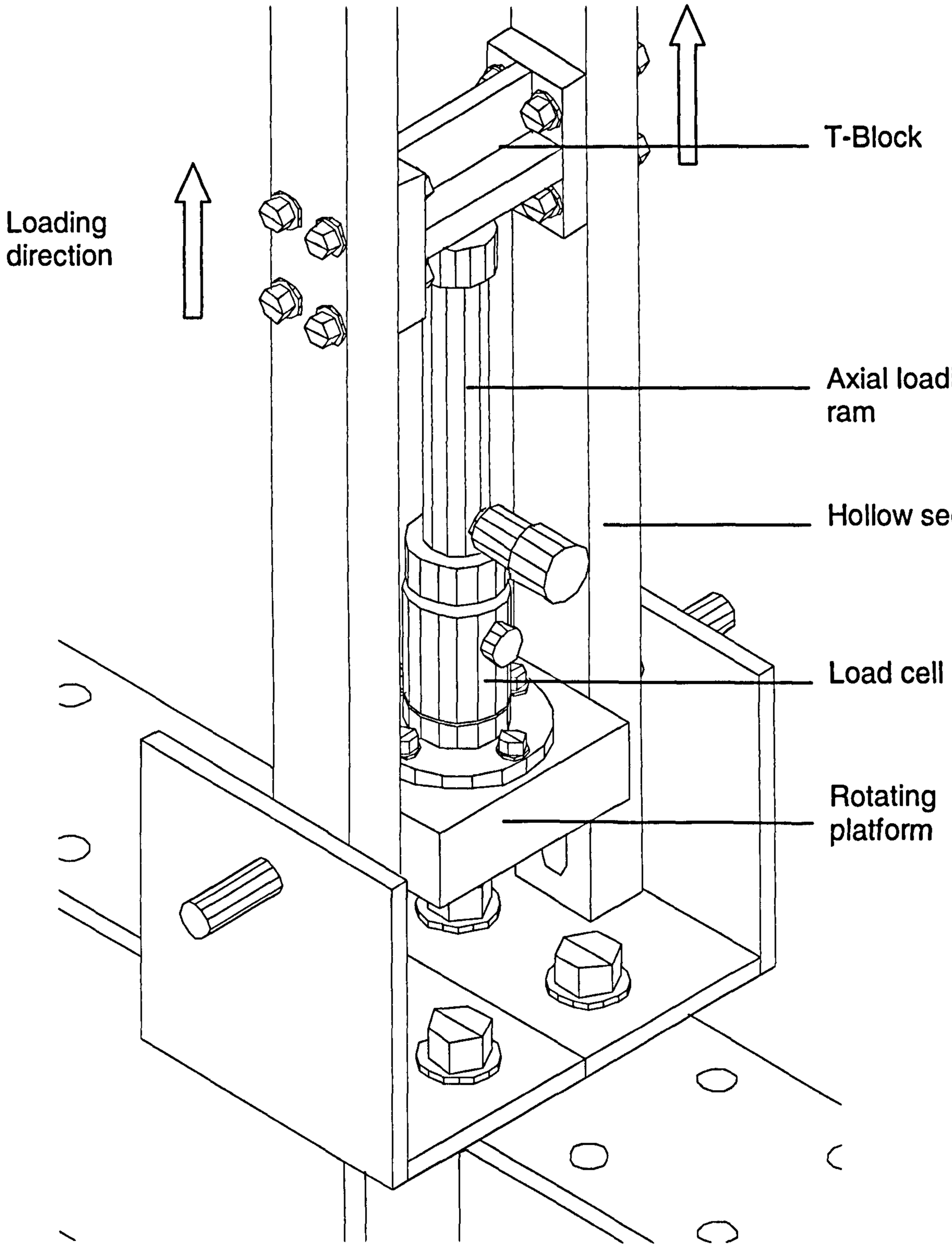

Fig. 3.6.1.2 – Axial load system

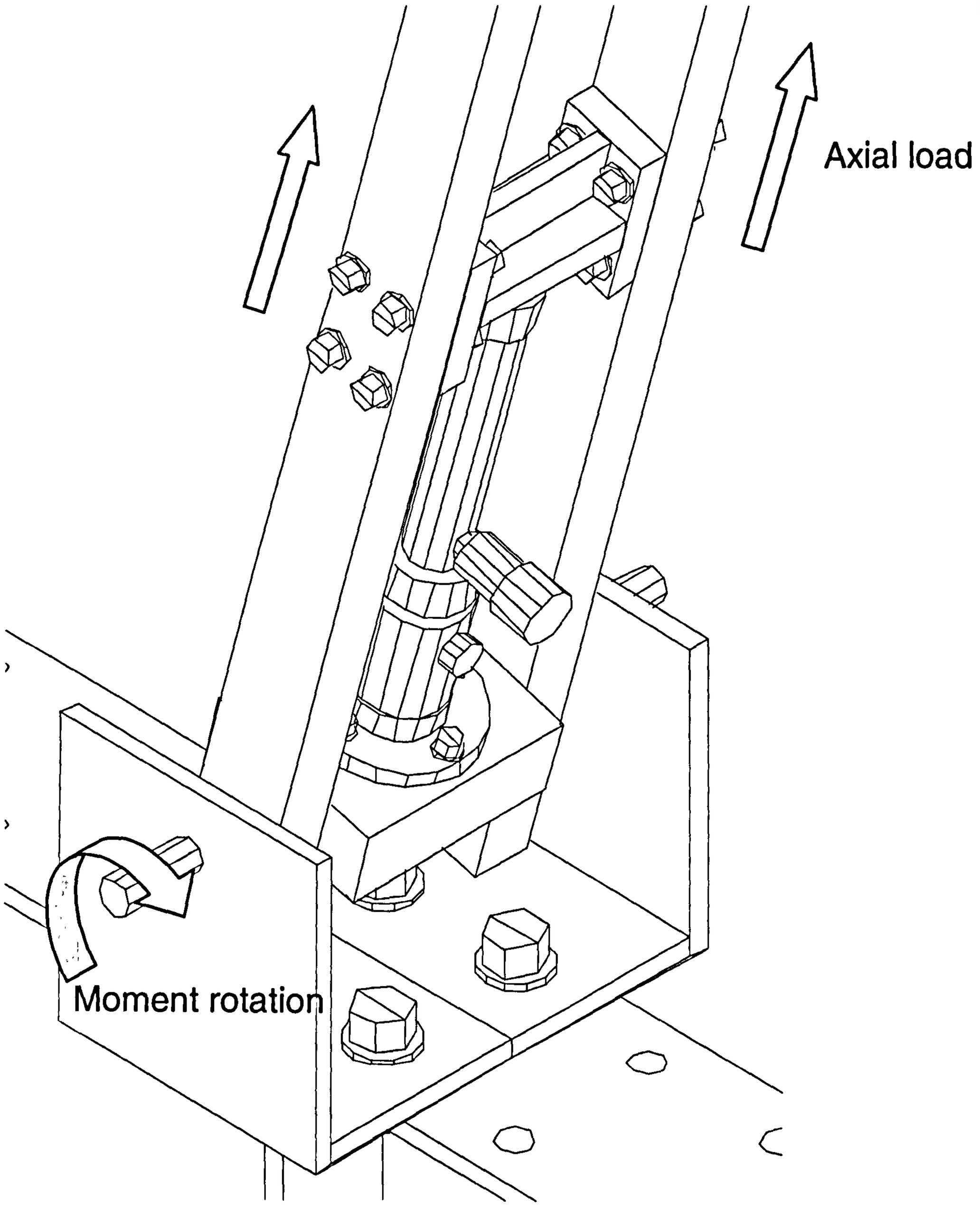

Fig. 3.6.1.3 – Axial load system with moment rotation

It was the intention of the loading arrangement to obtain independent control of axial and moment loads. However, from Fig. 3.6.1.1, one may identify that when a constant moment is applied and axial force is increased the joint will move in the upwards direction. Whilst this is happening the cable angle relative to the hollow-section will decrease, thus the moment load is no longer the same because the lever arm would have changed. In addition when moment loads are applied by the wire/pulley and the member rotates, there is a vertical and horizontal force component at the point of application. The other imperfection is when the member is rotated, pure axial load no longer exists as the hollow section is no longer perfectly parallel to the member, thus load is applied at a very small angle. However, the movement will be minimal as demonstrated in the test results thus the effects of these imperfections are small.

For the first loading arrangement, a mock test was conducted to try the frame and all the hardware involved in the tests. Although much effort was made for the tests to run smoothly there still were many problems encountered relating to the maintenance of the data logger and the availability of the cameras. In addition, because of the amount of hardware involved in these tests, much of the problem during the very first test was to orchestrate the sequence of data recording events as everything was operated manually by a single person. However, once the software were customised to, subsequent tests were easier to conduct.

3.6.2 Heel Joint test

The preparation for this test was faster than for the Crown joint test because it was possible to re-use some of the components from the crown joint test. However, some new components were made as shown in Fig. 3.6.2.1 (See Fig. A4.2 for photograph). The loading arrangement was simplified by orientating the heel connection. The method of applying axial load is similar to the crown joint test. As illustrated in Fig.3.6.2.2, the system is simply reversed to pull down instead of pushing up as the top chord member is in compression. The middle column near the centre of the frame provides the reaction for axial loads. The hollow sections were modified with extra slots. In this test, a steel support was made to provide support to the bottom chord and is bolted to the right column of the frame. The position of the support conforms to BS5268[38] to act as a wall plate underneath the heel joint in a truss with 5mm thick plate placed between the timber and support as detailed in Appendix A1 under wall plates. The length of the top chord member is short to accommodate the specimen, i.e. the lever arm is short. Furthermore, The heel joint retains a higher moment capacity than the crown joint. Originally, the moment loading system for the heel joint tests was adopted. It was therefore not surprising that half way through the tests, modifications were necessary to the moment loading system as there were insufficient dead weights to impose adequate bending moments. The system was subsequently changed and the force was applied through a hydraulic ram instead. As illustrated in Fig. 3.6.2.3 a buffer is bolted to the side of the frame providing the reaction for the ram. A load cell is sandwiched between the hydraulic ram and a steel platform welded to a steel rod. As before cables are hooked round the rod and connected to the specimen at the other end via a pulley.

Legend

1/2 Bottom chord and Top chord respectively.

3 Point of axial and bending moment load.

4 Restraining point

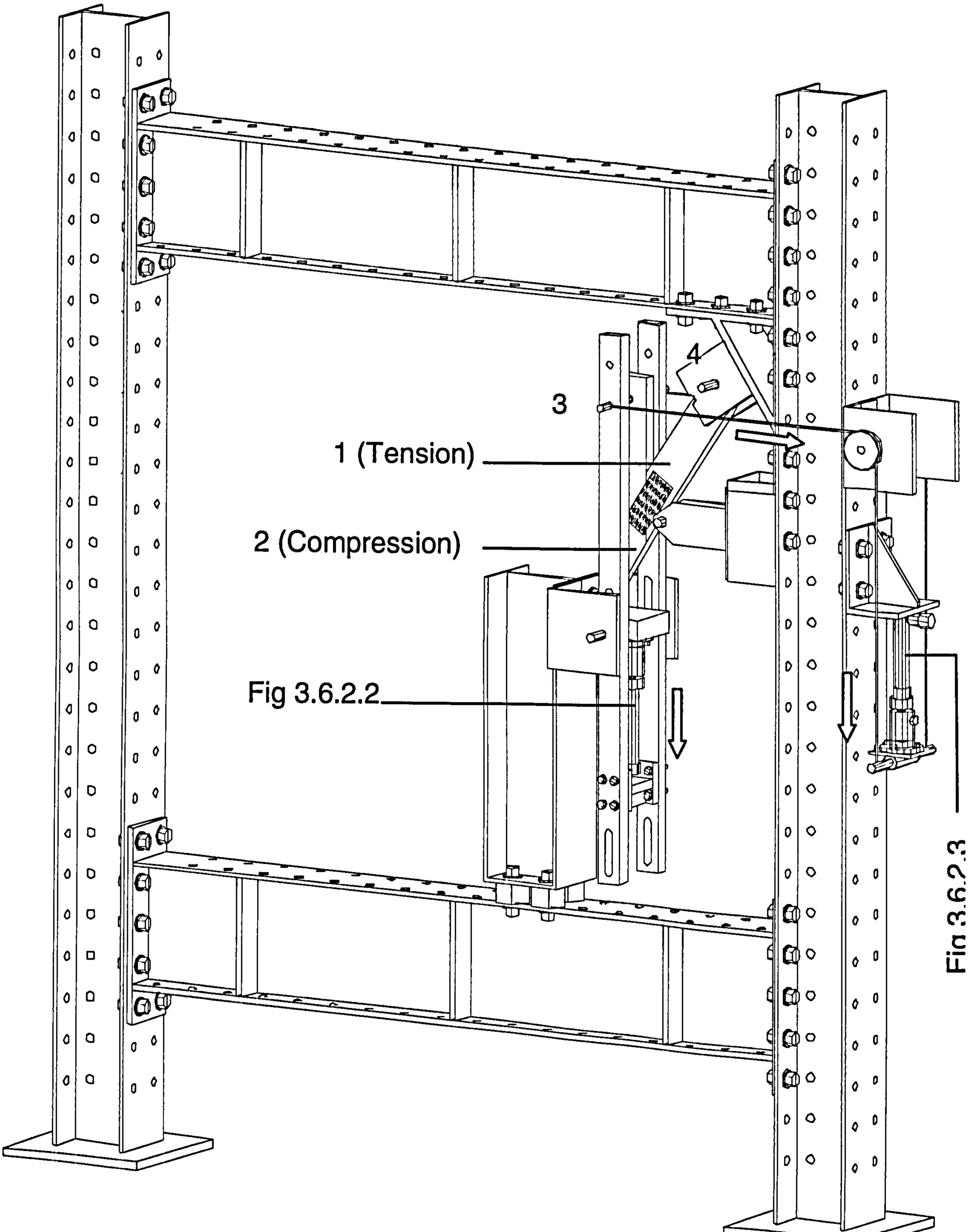

Fig. 3.6.2.1 – Heel Joint test

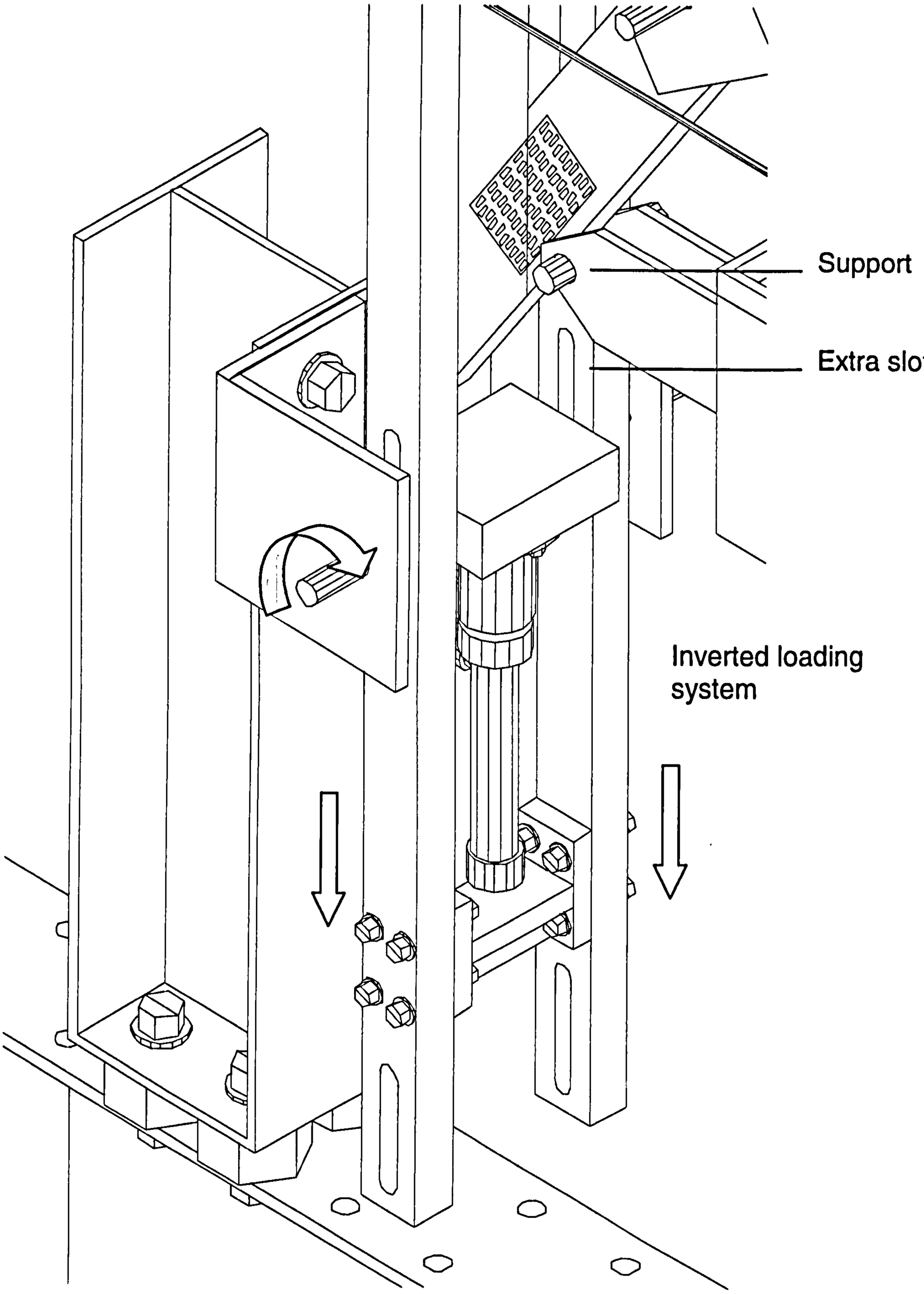

Fig. 3.6.2.2 – Inverted axial loading system

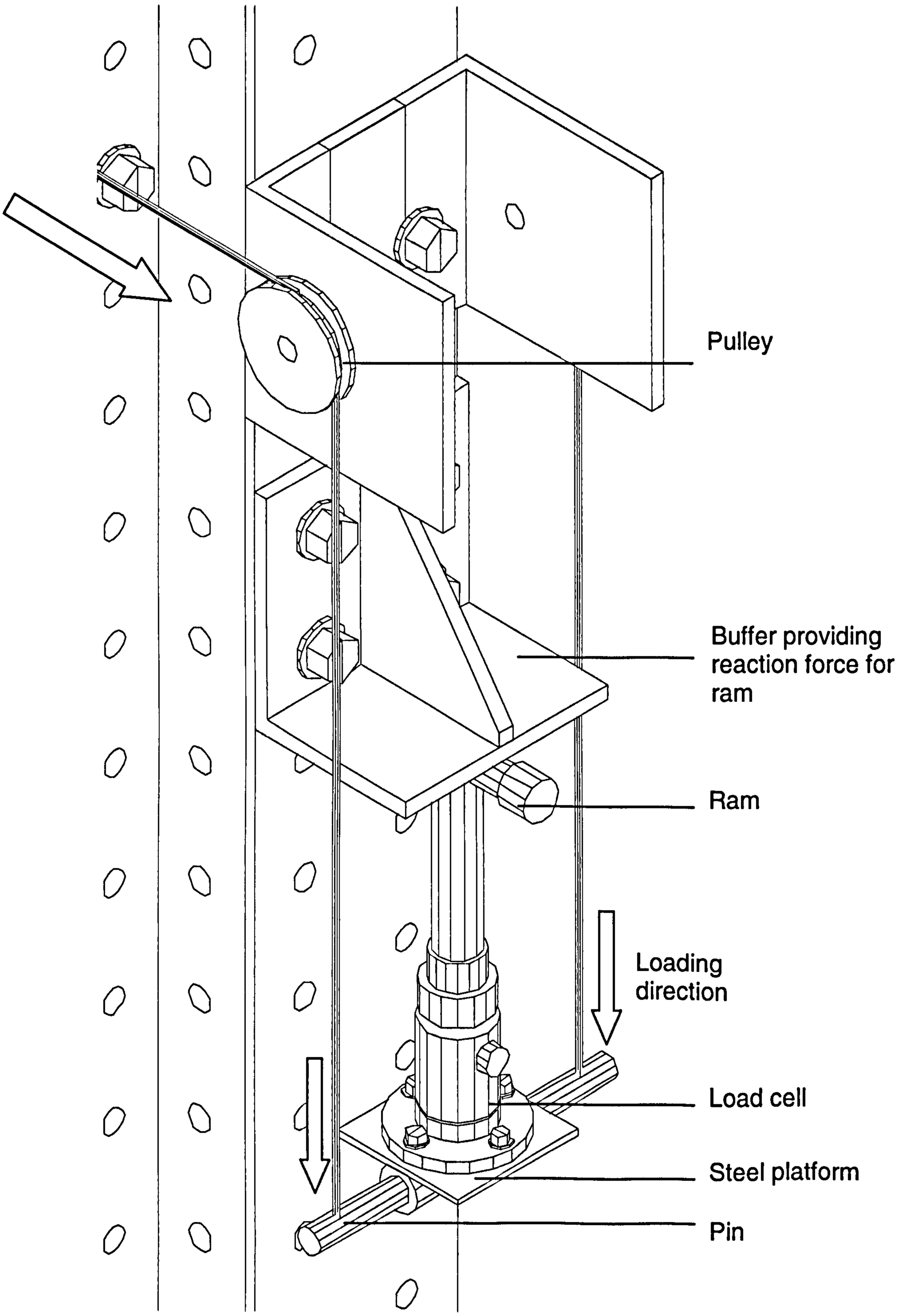

Fig. 3.6.2.3 - Moment loading system

3.6.3 Top Chord Joint test

Fig 3.6.3.1 shows the top chord test (See Fig A4.3 for photograph). In this particular test there are three load points, to simulate truss loads. These are: the axial loads parallel to the web, top chord compression force, and the moment load. To simplify the loading arrangement the joint is orientated such that the top chord is horizontal and the web is angled. The column and hollow section are simply moved near the centre of the frame. The axial loading system on the web is that of the Heel joint test but only inclined at a 22° to the vertical. To support the joint on the left, an inverted column is bolted to the top beam of the frame. The combination of a box section with and two plates bolted on both sides of the section is utilised to reach out and provide support the top chord at 3. As shown in Fig. 3.6.3.2, a load cell is fixed onto the box section horizontally and is sandwiched by a channel section used in previous tests. The specimen and channel are kept horizontal by the two plates. A pin threads through the plate, channel section, and the specimen. A slot is drilled into the plates to provide vertical support but allows force to be transferred to the load cell. Denoted by the number 4, at the other end, the compression load to the top chord is applied through a ram. A box section is bolted to the right column on the frame. The ram is fixed onto the box section where contact is made with another channel section at the tip of the ram. The specimen fits in the channel and is held there by a pin. Again, a plate is bolted to the box section, extending out to support the channel and specimen by the pin threading through. A slot is drilled to allow for movement for compression loads. With three load points there are many load combinations. It was therefore decided that the axial-moment test of the joint would be conducted as usual with an additional five

tests. The five tests will consist of different levels of compression loads at the top chord with constant axial and moment loads.

Legend

1/2 Web and Top chord member respectively.

3 Point of axial and bending moment load application.

4 Left restraining point.

5 Right restraining point and point of axial compression load.

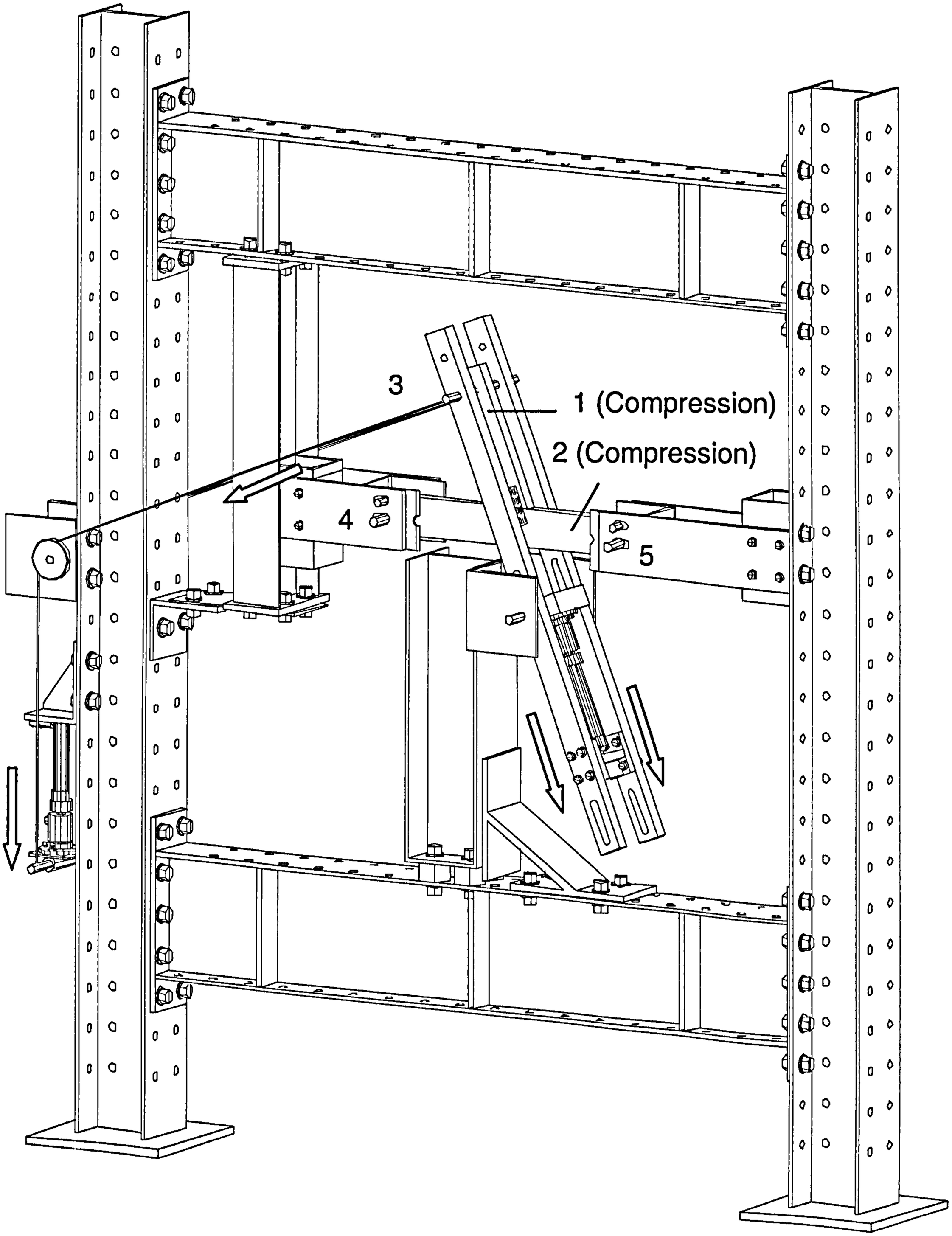

Fig. 3.6.3.1 – Top chord joint test

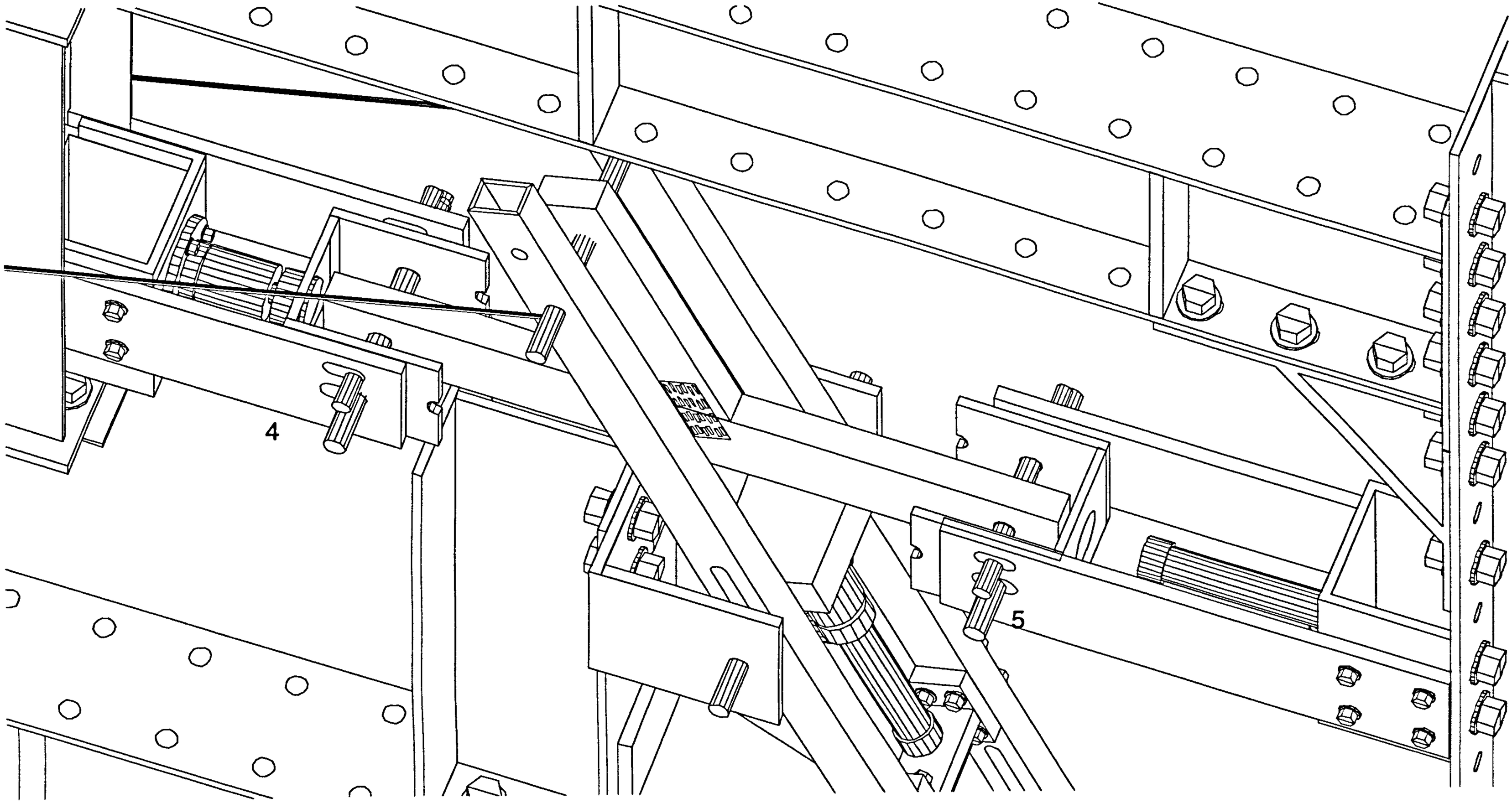

Fig. 3.6.3.2 – Compression load to the top chord

3.6.4 Bottom chord Joint test

The bottom chord test was left till last because it was anticipated that this would be the most difficult test to arrange. This proved very much so even with all the experience and components made up from the previous tests. There was little room for error as there are five restraint points (1, 2, 3, 4, and 5) and three load points as shown in Fig. 3.6.4.1 (See Fig. A4.4 for photograph). Even when the components were made fully adjustable the joint was difficult to fit and minor adjustments were necessary due to timber sizes and imperfections when making the connection. However, there are similarities between this test and the Crown joint tests. A tension load is again applied to the middle web member using the same loading system as before denoted by the number 1. The moment loading system is the same as that of Fig.3.6.2.3. At 4, the right side of the bottom chord a pin is threaded through restrained by a pair of plates bolted to a short column, which is in turn bolted to the lower beam of the frame. This plate extends out beyond the column on the other side. At the restraint, a pin is threaded through the plate and member, where a slot is made to provide support and movement for tension loading. A pair of steel cables is looped round the pin, leading to a pulley at 6. From there on the system is exactly the same as Fig 3.6.2.3, except this time a box section bolted between the plates provides the reaction force for the ram instead of the buffer. (See Fig A4.5 for closer details). The left side of the joint at 2 is simply restrained as in the Top Chord tests by plates extended from a box section, which is bolted to a column. However, the column has been propped by another box section at the bottom beam so as to achieve the right support height. Like the top chord joint test there are 3 load points. Therefore, the approach would be the same, i.e. the

standard combined load tests and an additional five load level compression to the bottom chord.

Legend

1. Restraint for left web member.

2. Left restraint.

3. Point of tension and moment load application through web member.

4. Right restraint.

5. Restraint for right web member.

6. Point of tension load application to bottom chord.

7/8 Web member tension and compression respectively.

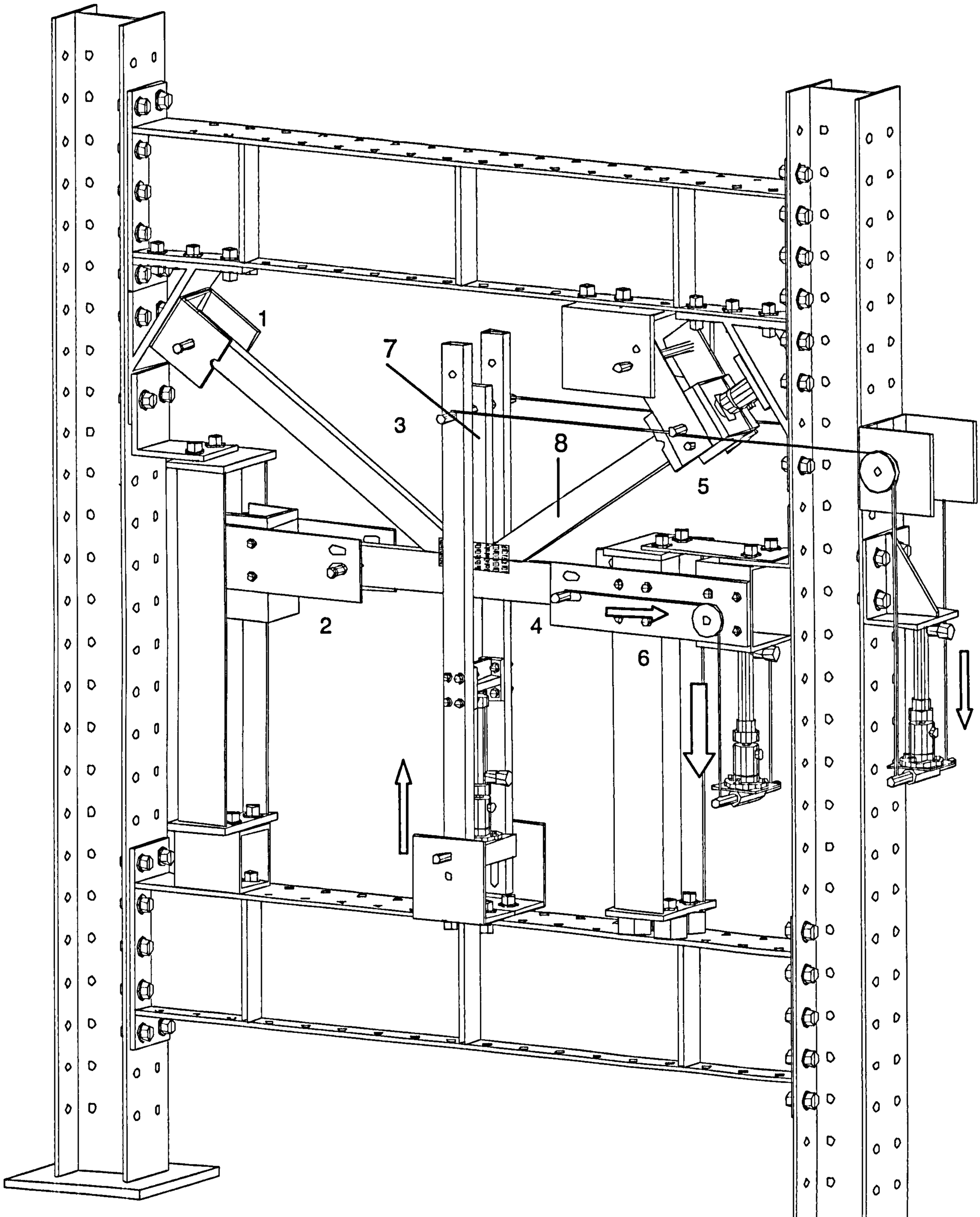

Fig. 3.6.4.1 – Bottom chord joint test

3.6.5 Full scale truss tests

The preparations for these tests included a parametric study for different load conditions, which included symmetrical and unsymmetrical load cases. To simplify testing arrangements, the study was limited to three load points for each load case where loads were applied vertically down. The purpose of this exercise was to gain an idea of how the joints would react under certain loads and thus, conduct tests, which would achieve useful results. For this, the semi-rigid joint truss program, STRUSS as explained in section 4.9, was used to determine displacement and internal forces of the truss. The connections were assumed to be rigid as at this stage the semi-rigid joint stiffness of each connection had not been determined. Nevertheless, the moment capacity of the connections at this stage was available from the joint tests. A rigid joint assumption would be adequate for linear behaviour and is more accurate than a pinned analysis. As illustrated below, 12 different load cases were simulated where in each case, 3, 10kN loads were applied at various points of the truss. It was found that when the truss was loaded symmetrically at the nodes/joints, there were little bending moment and shear forces at the nodes/joints but very high axial loads. Unsymmetrical truss loading at the nodes gave slightly higher moments. Moments at the joints were significantly higher when loads were applied on members at points between the joints. This further increased when loads were unsymmetrical. The moment forces were analysed and compared to the moment capacity of the joints, which was determined in the joint tests. Loading between joints, at the centre of the bay gave excessive bending moments and thus was not chosen as a connection may fail prematurely in the test. This also resulted in significant bending moments at the members and indicated the member may also fail prematurely if the connection does not.

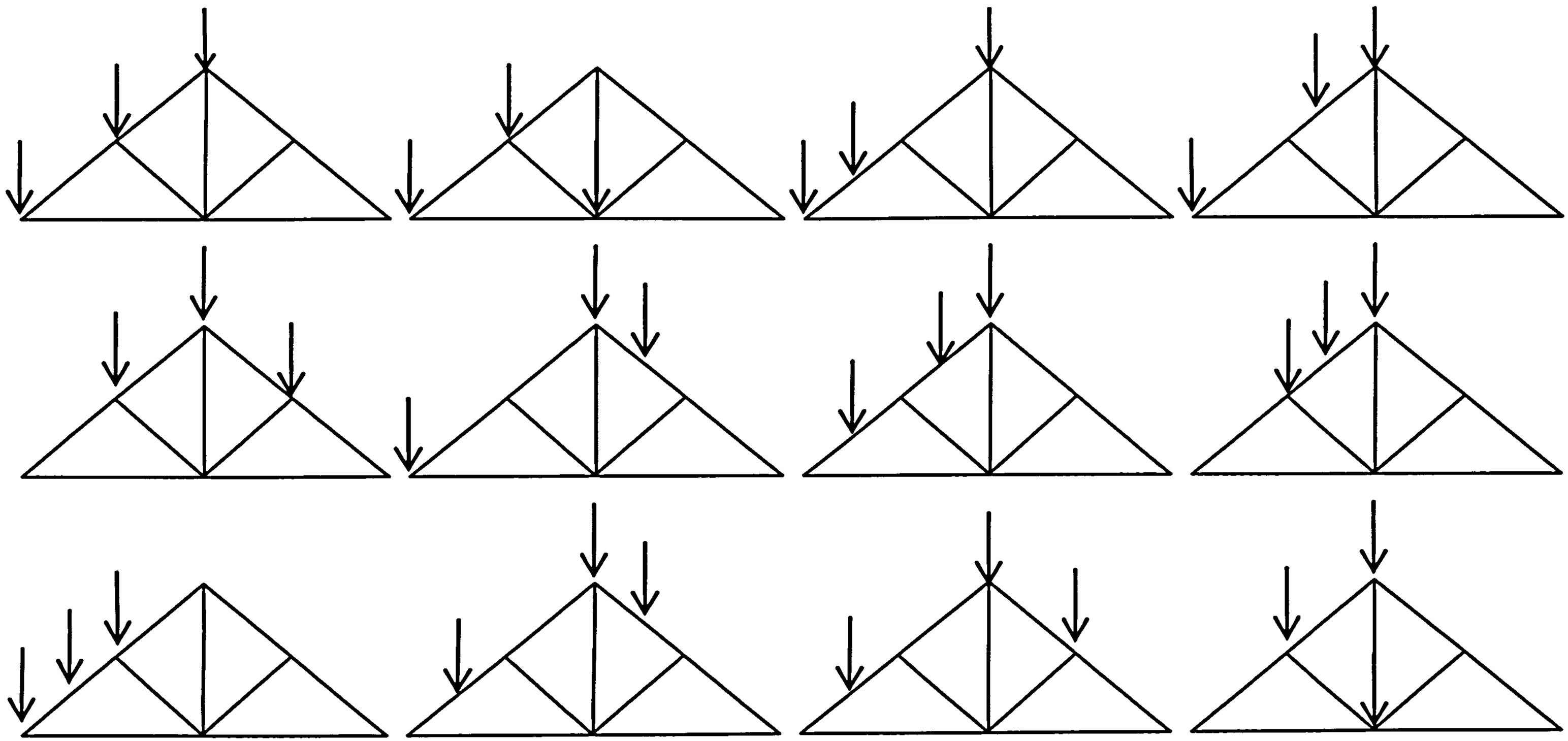

Fig. 3.6.5.1 – Truss load combinations

Both scenarios were to be avoided in order to conduct tests and produce results which would used to compare with analytical results. However, only loading on the members gave enough bending moments to the joint and the solution to this problem was to load the truss on the member but nearer to a connection.

Other loading arrangements were also possible but it was considered prudent to keep the arrangement simple. Simulating uniformly distributed loads would have certainly complicated the test arrangements. The loading arrangement could involve a series of pulleys on a test rig with several load points so that a uniformly distributed load can be applied to the whole span. Such arrangement has been used by Masse and Salinas[26]. Unlike the joint tests, it would be difficult to set up a test frame to accommodate such a span and to include the pulleys would complicate matters. Another example is to use fixed weights along the length of the bottom chord to simulate UDL's. However, this approach would be limited as loads would be difficult to increase but can be used to simulate dead loads. To simplify matters, one can assume point loads as illustrated below.

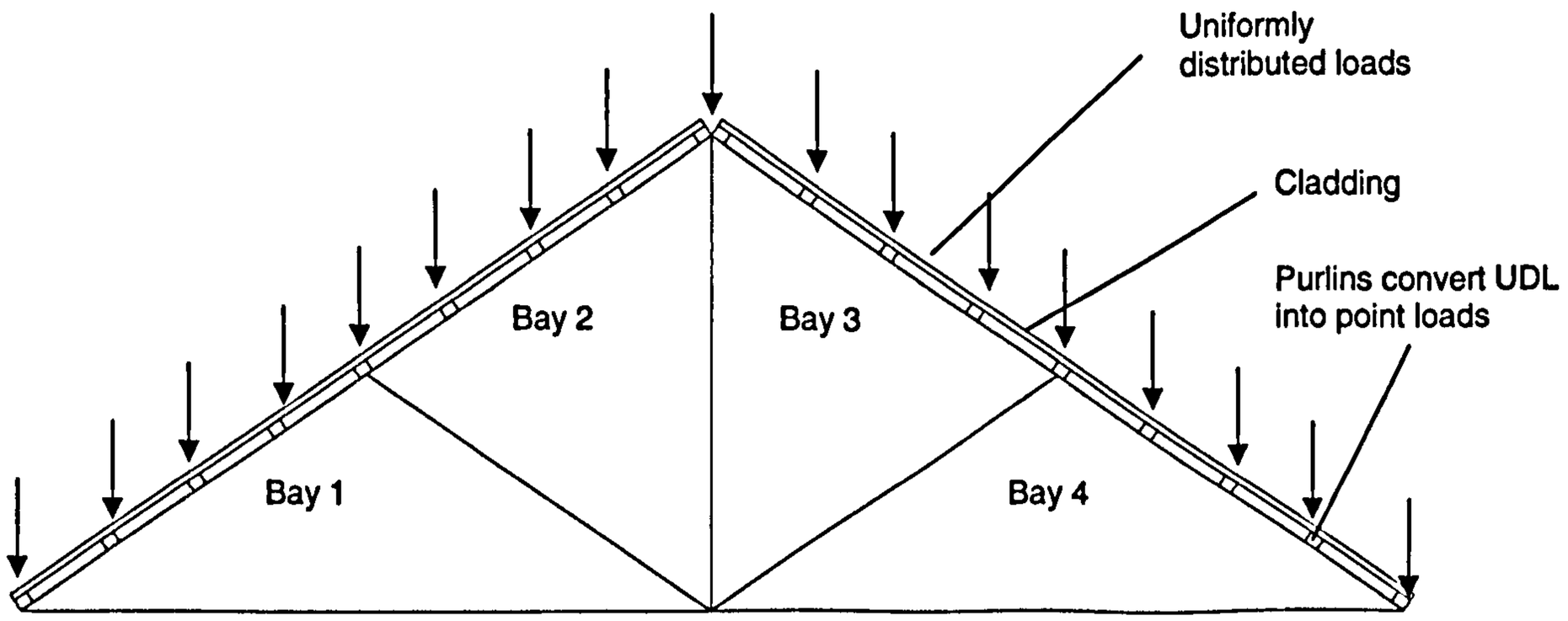

Fig. 3.6.5.2 - Loading of the truss

Whether it is a point load or a UDL, the load from the cladding will be transferred to the purlins and is then converted to point loads at the top chords of the truss and justifies the application of point loads in a truss. More complex loading arrangements such as wind loads are difficult to simulate as forces come from multiple directions.

After the parametric study it was decided to simulate three load conditions. These were symmetrical loading where load points were located at the two top chord joints and the crown joint. For this, two different simply supported conditions were tested. The support for the first and second test was located at the bottom and top chord respectively. The third test consists of an unsymmetrical loading arrangement. Loads were applied at the top chord and crown joint only where the support was located at the bottom chord. Details of the loading arrangements of these tests are given in the next section. A mock test was arranged where only loads were recorded. From this test a number of minor improvements to the loading arrangements were made. In addition to this, significant out of plane deformations are found at the top chord compression member before any signs of failure at the joint were noticed, hence the truss could not be loaded to its ultimate capacity. Scaffolds were erected to provide lateral restraints at the top chords. A truss system for a roof consists of many trusses lying parallel to each other at a specified distance. It is assumed that there are sufficient trusses connected by purlins in a roof system to counter the effects of lateral loads.

Symmetrical loading

The assemblage of the truss was similar to the connection tests, only at a larger scale. The members for the truss were cut first and then assembled together in the laboratory. The truss was clamped at each joint with a template at the bottom chord whilst a small moveable frame shown in Fig. 3.6.5.3 below at the back, was made up to compress the plate into the timber. The appropriate metal plates were compressed at each joint in succession after which the truss was turned over to repeat the procedure on the other side.

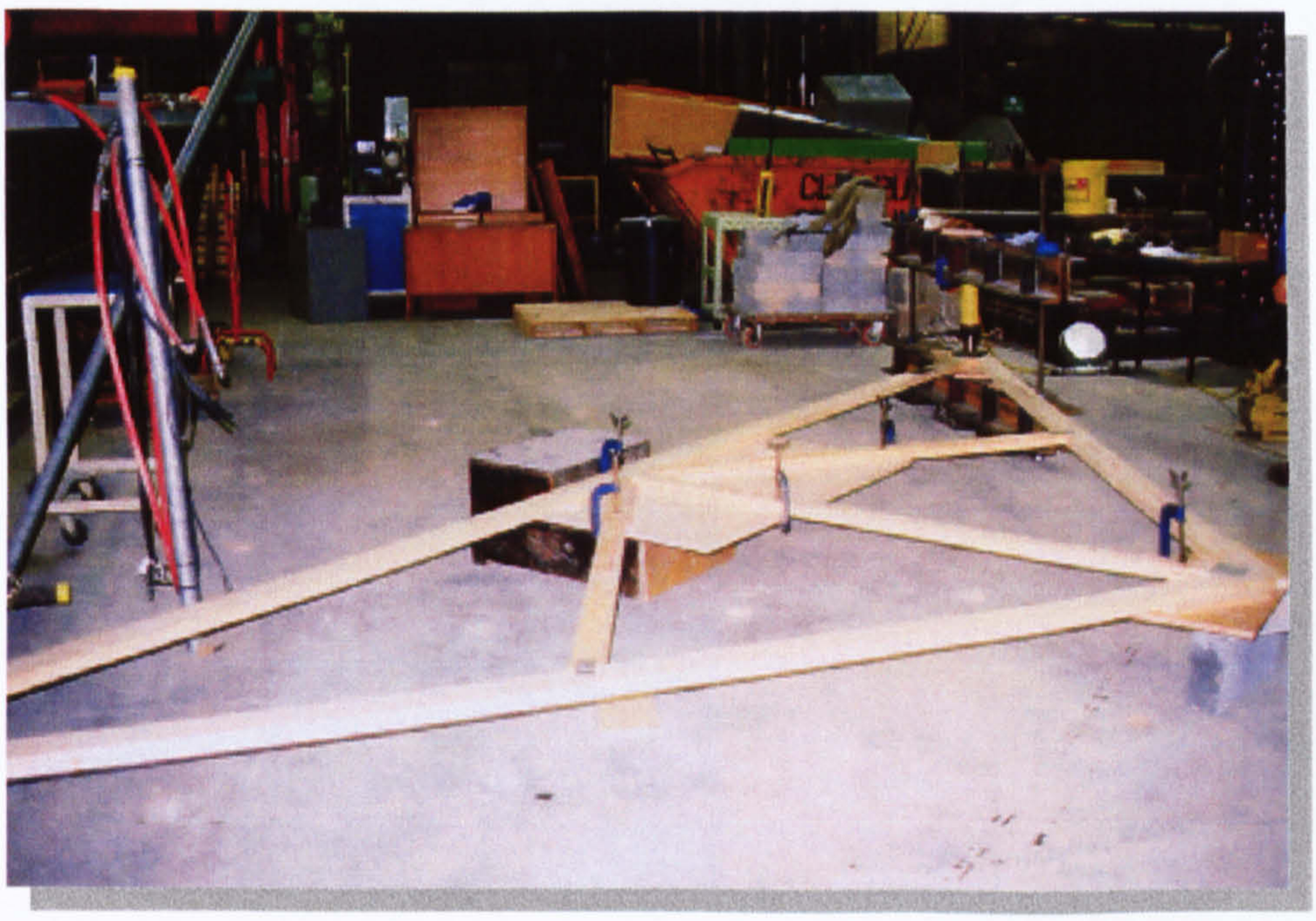

Fig. 3.6.5.3 – Assembling the truss

Fig. 3.6.5.4 illustrates the set up for symmetrical loading. The scaffolding used to provide out of plane support have been omitted for clarity. Images of the entire arrangement can be found in Fig. A4.6. Two bases approximately 6m apart consisting of large H sections are bolted together and to the strong floor. Only three vertical load points were selected for this in line with the number of available load cells.

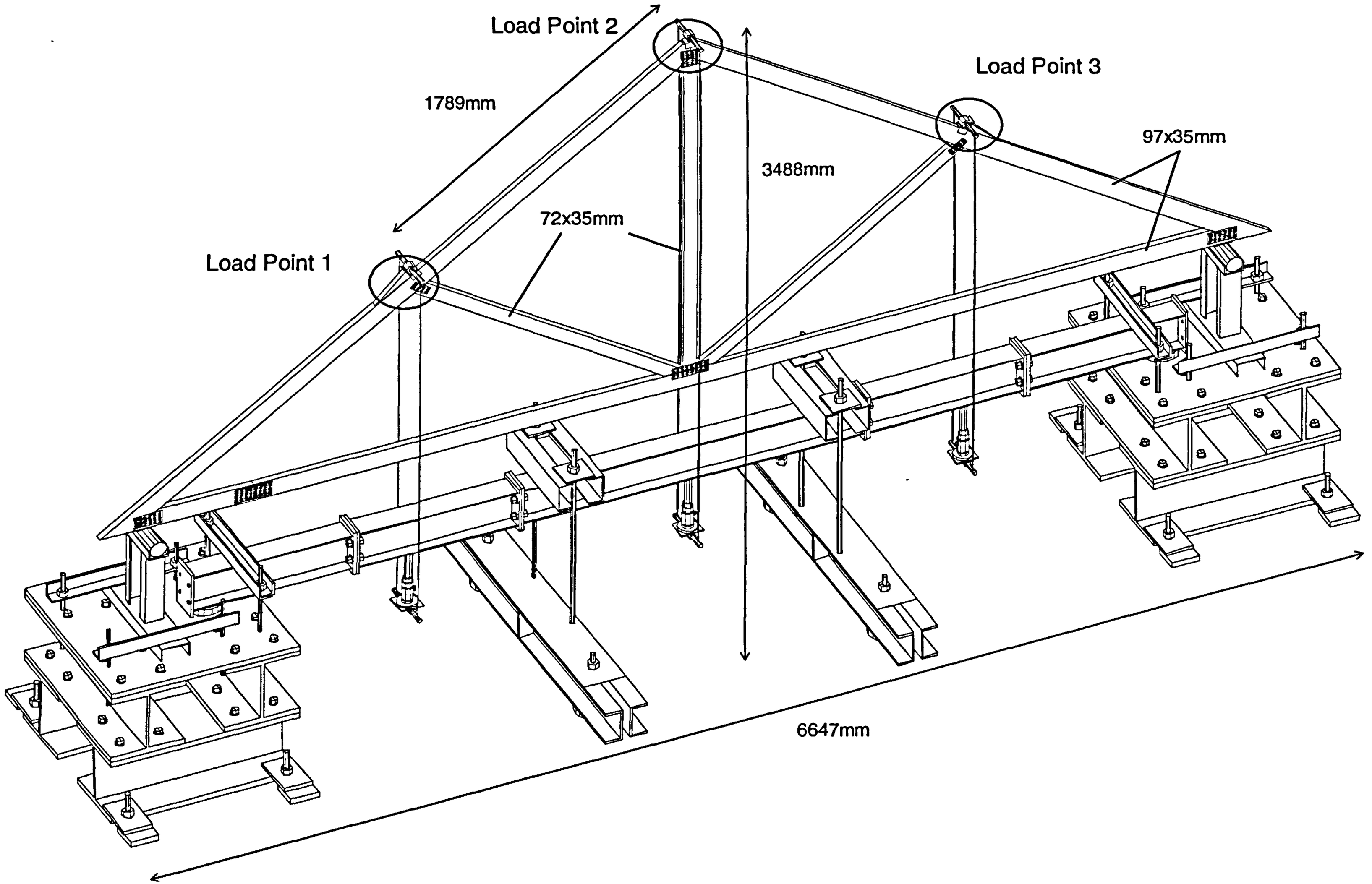

Fig. 3.6.5.4 – Test set-up for symmetrical loading

Minor alterations to the dimension of the truss were made. At load point 2, the apex of the truss, i.e. the crown joint, 25mm of timber was sliced off leaving a horizontal surface for a steel saddle as shown in Fig. 3.6.5.5a. The effect of this modification to the joint and ultimately the truss is negligible as both top chords are in compression. All crown joint tests showed that the critical area of this joint is at the web member and no signs of failure were observed in the top chords.

For the load point 1 & 3 at the top chord on either side of the truss, two more saddles were fabricated to sit on the top chord and were propped by a tapered piece of glued timber as illustrated in Fig. 3.6.5.5b. The tapered design minimises the effect of extra timber, but also provide adequate support for the loads. A thicker piece would have contributed to the stiffness of the chord or the joint and would have strengthened that part of the truss. The strength of the glue line was designed in excess of the capacity of the load, but on the other hand was kept to a minimum.

For all load points, a steel tube was welded onto each saddle with a pin threaded through allowing a steel cable to loop round the pin and lead down below the truss. The loading system is effectively the same as that for the moment loading in the Heel, Top chord and Bottom chord tests except that a beam replaces the buffer to provide reaction. Complications of this loading system were found during the mock test. The length of the cables contributed to the general instability of the loading system. In addition to this there were problems with keeping the pin horizontal due to instability at the saddle above. Clamping the saddle and attaching cable guides at the steel beam improved the stability.

As shown in Fig. 3.6.5.4, the extended support beam comprises 5 steel members bolted together and clamped to the bases at either end. The long member is further restrained at two points near the centre. At each point, a steel section sits on the member and is bolted down by to two steel rods. The restraint is completed by connecting the steel rods to a larger steel section which is bolted to the ground. This system and the clamp at the bases restrains the long beam from lifting when load is applied to the truss through the hydraulic rams.

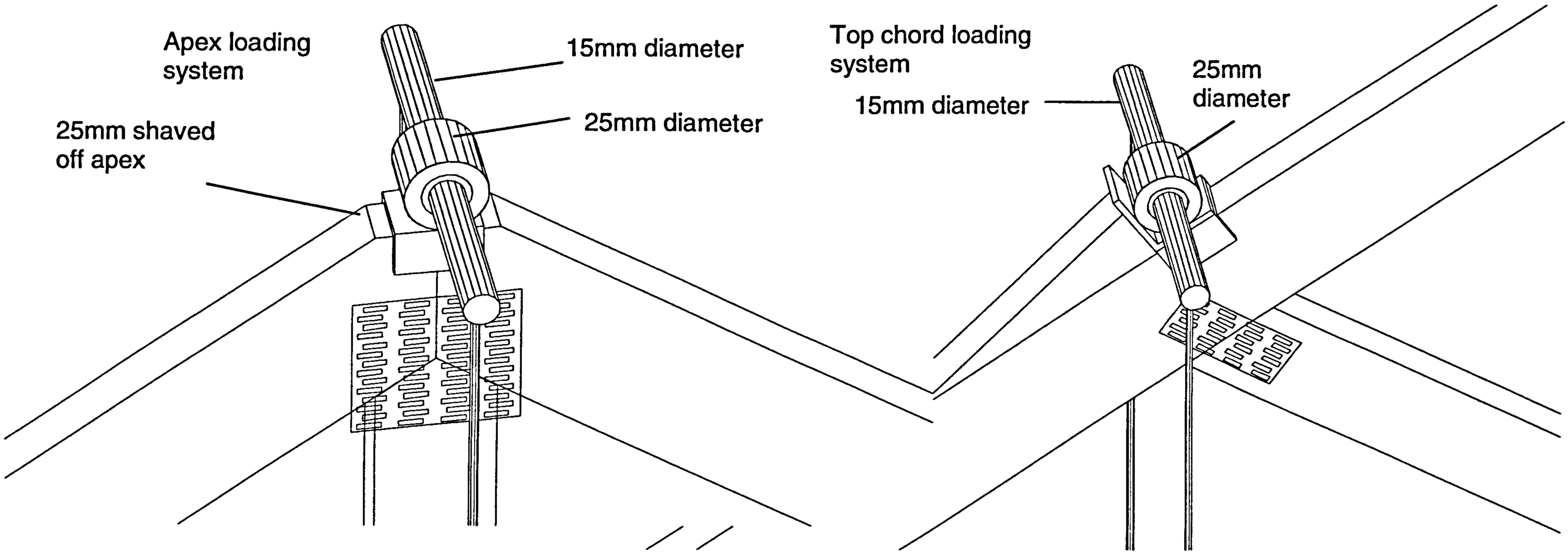

Fig. 3.6.5.5 – Truss loading system

For the second test arrangement, the supports at the heel joint are moved to the top chord as shown in Fig. 3.6.5.6b. As illustrated in Fig. 3.6.5.6a, initially this support was at the bottom chord. It was shown in the mock test that by locating the support on the bottom chord the plate is subjected to intense axial force parallel to the top chord, thus the heel joint failed through pull out first. As illustrated in Fig. 3.6.5.6, when load is applied on the crown and both the top chord joints, the top chord is in compression. The effect of this forces the top chord to slide in an outward direction at the heel joint. This is reacted at the heel joint and in turn loads the bottom chord in tension. The condition is eliminated when the support is moved to the top chord as illustrated in Fig. 3.6.5.6b. The compression force is now reacted by the support.

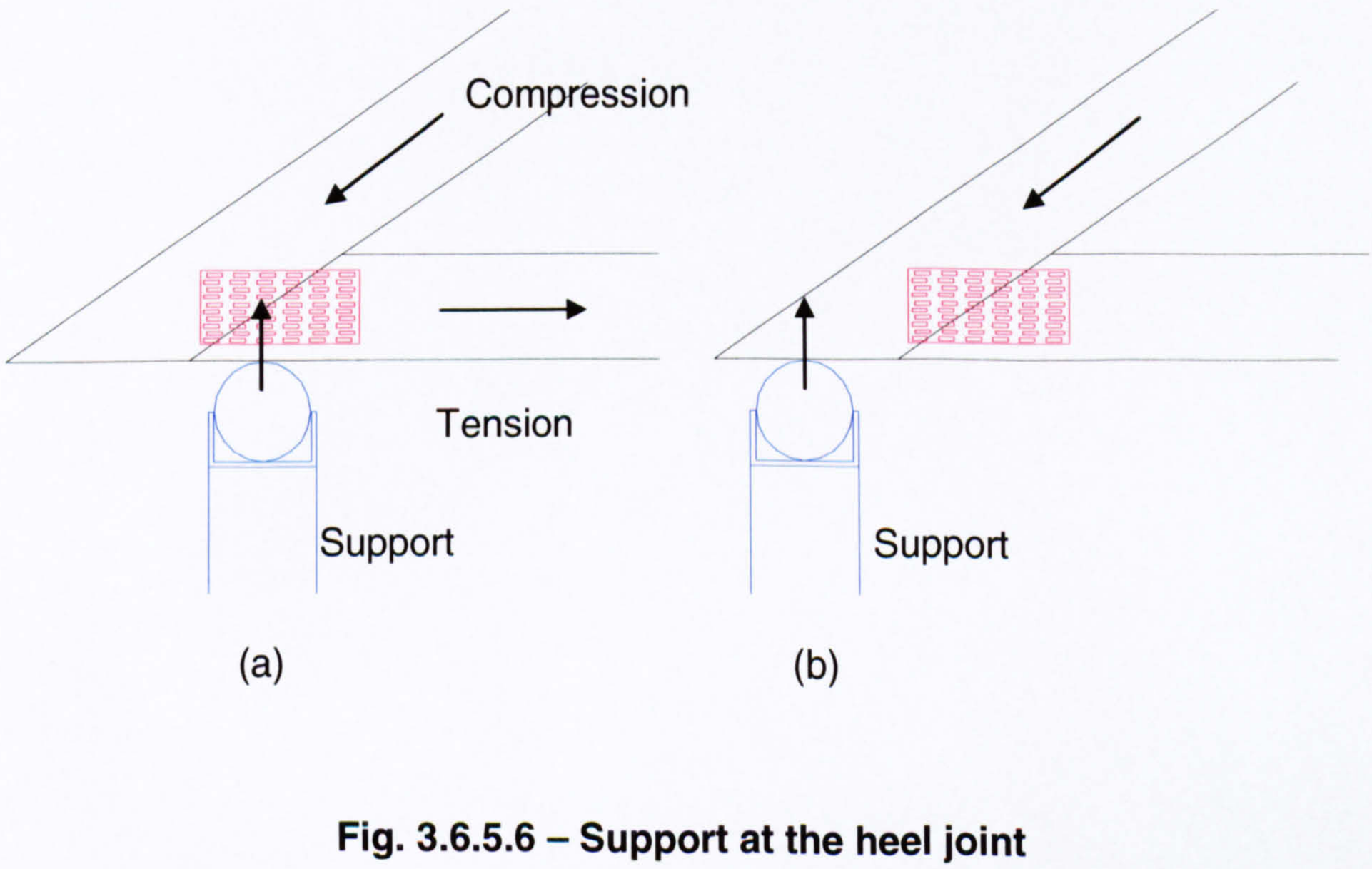

Fig. 3.6.5.6 – Support at the heel joint

Unsymmetrical loading

Since the symmetrical load system did not impose sufficient moments to any of the joints before the truss failed it was decided that the third test arrangement may achieve this by applying loads on the members (and not at the node points). However, according to the analysis carried out using the computer program described later, it was feared that this may lead to the member failing before the connection. This is because the members are rather slender and have low bending capacity. One possibility was to use layer members by gluing additional pieces of timber to the member, but this would have rendered the joint tests unusable for truss analysis. As discussed earlier, applying the load at the member but close to the joint reduced the moments on the member. After further analysis it was decided that loads would be applied at a sixth of the distance of the bay from the top chord joint as indicated in Fig. 3.6.5.7, load point 1 and 3, where by bending moment at the member is significantly reduced

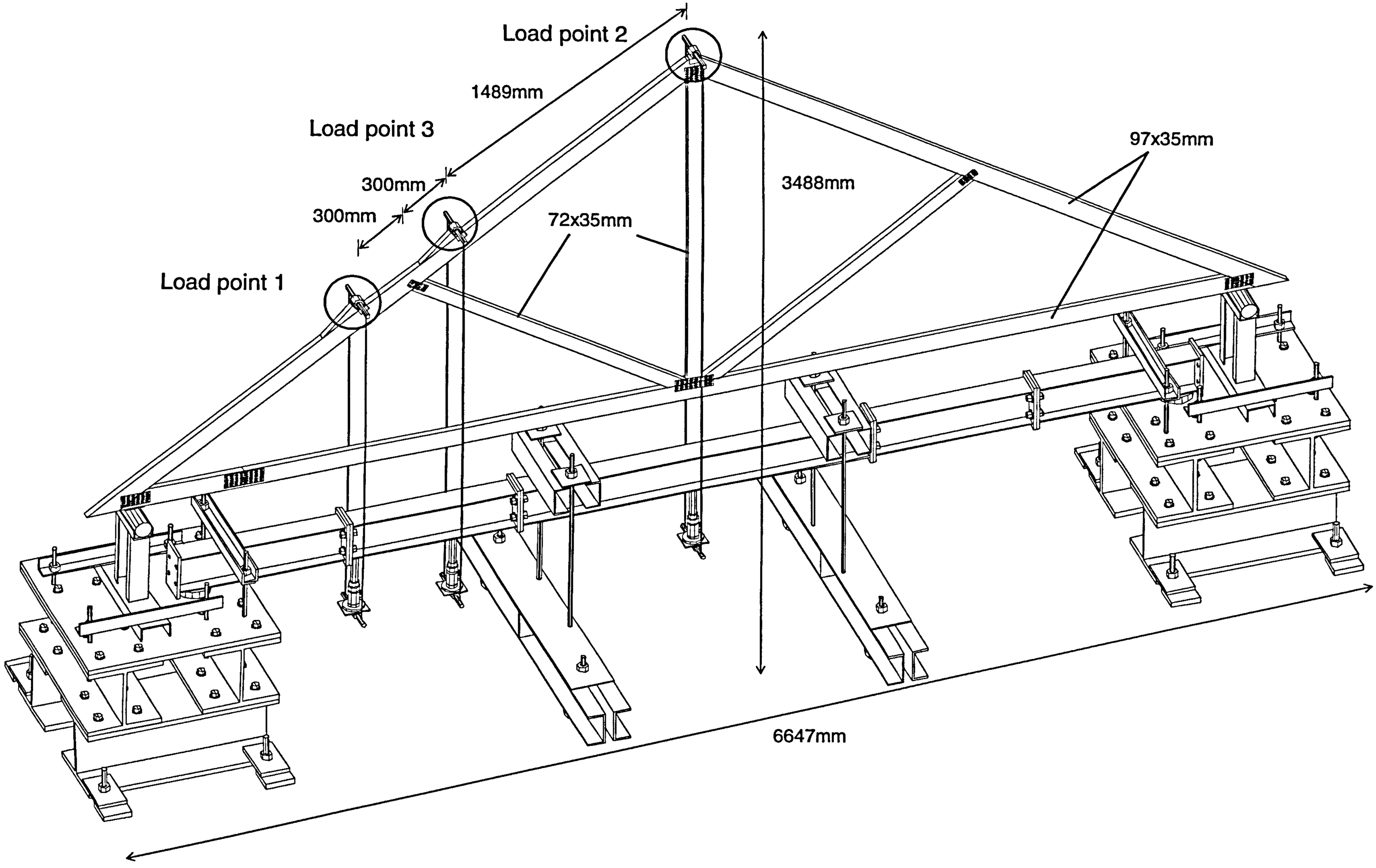

Fig. 3.6.5.7 – Test-set-up for symmetrical loading

3.7 Test procedure

In all tests, initial readings were taken from the load cells and displacement transducers before any loads were applied. For every reading made on the data acquisition software corresponding images are also taken from the cameras controlled by separate computers. In addition to this, pressure and displacement readings were manually taken from a pressure gauge and digital displacement transducer respectively.

For the joint tests, pure bending and axial tests were performed separately to establish axial and bending moment capacity. Once determined, 5 levels of axial and bending moment for the combination tests were decided. The load levels are selected such that the highest level is not too near capacity as in such a test the connection may fail before combined loads can be applied. Load levels are tabulated below but are repeated in Chapter 6 with the test results.

CJT		HJT		TCJT		BCJT	
	B/M Level (kNmm)		B/M Level (kNmm)		B/M Level (kNmm)		B/M Level (kNmm)
M1a	0.0	M5	0.0	M1	0.0	M1	0.0
M2	0.16	M1a	0.2	M2	0.1	M2	0.1
M3	0.19	M2	0.4	M6	0.2	M6	0.2
M4	0.35	M3	0.6	M3	0.3	M3	0.3
M5	0.42.0	M4	0.9	M5	0.3	M5a	0.5
	Axial load level (kN)		Axial load level (kN)		Axial load level (kN)		Axial load level (kN)
A1	0.0	A1e	0.0	5	0.0	A1	0.0
A2	3.0	A2	2.9	A2	4.3	A2	1.1
A3	4.4	A3	6.2	A3	4.9	A3	3.3
A4	6.0	A4	9.5	A4	9.9	A4	6.4
A5	8.4	A5	10.6	A6	13.0	A5	10.1

Table 3.7.1 – Load levels

All test equipment required manual operation and was therefore it was difficult to maintain a specified load rate. Images and observations were taken once movement had settled after each load increment. On some occasions this was not possible as either the transducer ran out of travel or slipped, or there was no transducer available. In such cases, a small time lapse is observed to allow the joint to settle before taking readings. Because of the timing of the readings being taken some kind of load rating was maintained. However, it was extremely difficult to sustain such timing near failure where the joint continuously deformed due to creep and the loads were difficult to maintain. At this point, sometimes more than one image and reading was taken per load increment. The load rate of timber is an important factor in timber strength. Generally, timber can sustain higher loads in short term loading and less load for long term loading. Nevertheless, tests described here are all short-term static tests and loads rates between tests were very close. Therefore load rating will be assumed to have had little effect on the results.

This chapter has focused on the details of the test procedure. Results from the tests are described in Chapter 6.

Chapter 4

Semi-rigid plane frame analysis

4.1 Introduction

Matrix analysis methods for skeletal frames were developed in the early 1960's. The simplest analysis is of 2-dimensional pin-jointed frames. For the analysis of trusses, in fact, 2-dimensional pin-jointed analysis is quite common in industry. Although analysis of 3-dimensional semi-rigid frames is perfectly feasible, the theoretical development here will be restricted to 2-dimensional frames.

In general, there are three types of semi-rigidity that can be defined for planar structures.

- Semi-rigidity associated with joint rotation
- Semi-rigidity associated with axial forces
- Semi-rigidity associated with shear forces

In this Chapter, these three types will be first defined. This will be followed by a summary of the stiffness matrix approach for rigid jointed frames. From this will be developed modifications to incorporate the three types of semi-rigidity mentioned above.

4.2 Assumptions

The following assumptions are made when conducting the 2D semi-rigid frame analysis

- Sections are prismatic, i.e. they have constant cross sectional area.
- The timber is assumed to have linear and isotropic properties.
- The centre line of the members all meet at a common point at the joint, hence there is no eccentric loading due to misalignment of the members.
- Connections are non-linear with eccentricity accounted for from joint test results
- No out of plane forces exists, that is the analysis is only 2 dimensional. Roof truss consists of several trusses working together and because of this there is sufficient out of plane support.

The following derivations are brief but full details can be found in Appendix B1

4.3 Rigid jointed frame analysis

We start by briefly presenting the elementary stiffness method of the rigid jointed case as illustrated in Fig. 4.3.1 and then proceed to the semi-rigid joint. This is described in detail in several text books[39,40,41]. The equations of a rigid jointed member are well documented and are shown below for completeness. The symbols have their usual meanings. They are also defined in the list of symbols.

$$M_i = \frac{4EI}{l}\vartheta_{mi} + \frac{2EI}{l}\vartheta_{mj} + \frac{6EI}{l^2}v_{mi} - \frac{6EI}{l^2}v_{mj} + M_i^F \qquad (4.3.1a)$$

$$M_j = \frac{4EI}{l}\vartheta_{mj} + \frac{2EI}{l}\vartheta_{mi} + \frac{6EI}{l^2}v_{mj} - \frac{6EI}{l^2}v_{mi} + M_j^F \qquad (4.3.1b)$$

$$S_i = \frac{6EI}{l^2}\vartheta_{mi} + \frac{6EI}{l^2}\vartheta_{mj} + \frac{12EI}{l^3}v_{mi} - \frac{12EI}{l^3}v_{mj} + \frac{M_i^F + M_j^F}{l} \qquad (4.3.2a)$$

$$S_j = -\frac{6EI}{l^2}\vartheta_{mi} - \frac{6EI}{l^2}\vartheta_{mj} - \frac{12EI}{l^3}v_{mi} + \frac{12EI}{l^3}v_{mj} - \frac{M_i^F - M_j^F}{l} \qquad (4.3.2b)$$

And

$$P_i = \frac{EA}{L}(u_i - u_j) \qquad (4.3.3a)$$

$$P_j = \frac{EA}{L}(u_j - u_i) \qquad (4.3.3b)$$

Using the derivations above, the stiffness matrix of a rigid jointed member in local co-ordinates can be written as

$$\begin{bmatrix} P_i \\ S_i \\ M_i \\ P_i \\ S_i \\ M_j \end{bmatrix} = \begin{bmatrix} \frac{EA}{L} & 0 & 0 & -\frac{EA}{L} & 0 & 0 \\ 0 & \frac{12EI}{L^3} & \frac{6EI}{L^2} & 0 & -\frac{12EI}{L^3} & \frac{6EI}{L^2} \\ 0 & \frac{6EI}{L^2} & \frac{4EI}{L} & 0 & -\frac{6EI}{L^2} & \frac{2EI}{L} \\ -\frac{EA}{L} & 0 & 0 & \frac{EA}{L} & 0 & 0 \\ 0 & -\frac{12EI}{L^3} & -\frac{6EI}{L^2} & 0 & \frac{12EI}{L^3} & -\frac{6EI}{L^2} \\ 0 & \frac{6EI}{L^2} & \frac{2EI}{L} & 0 & -\frac{6EI}{L^2} & \frac{4EI}{L} \end{bmatrix} \begin{bmatrix} U_{mi} \\ V_{mi} \\ \vartheta_{mi} \\ U_{mj} \\ V_{mj} \\ \vartheta_{mj} \end{bmatrix}$$

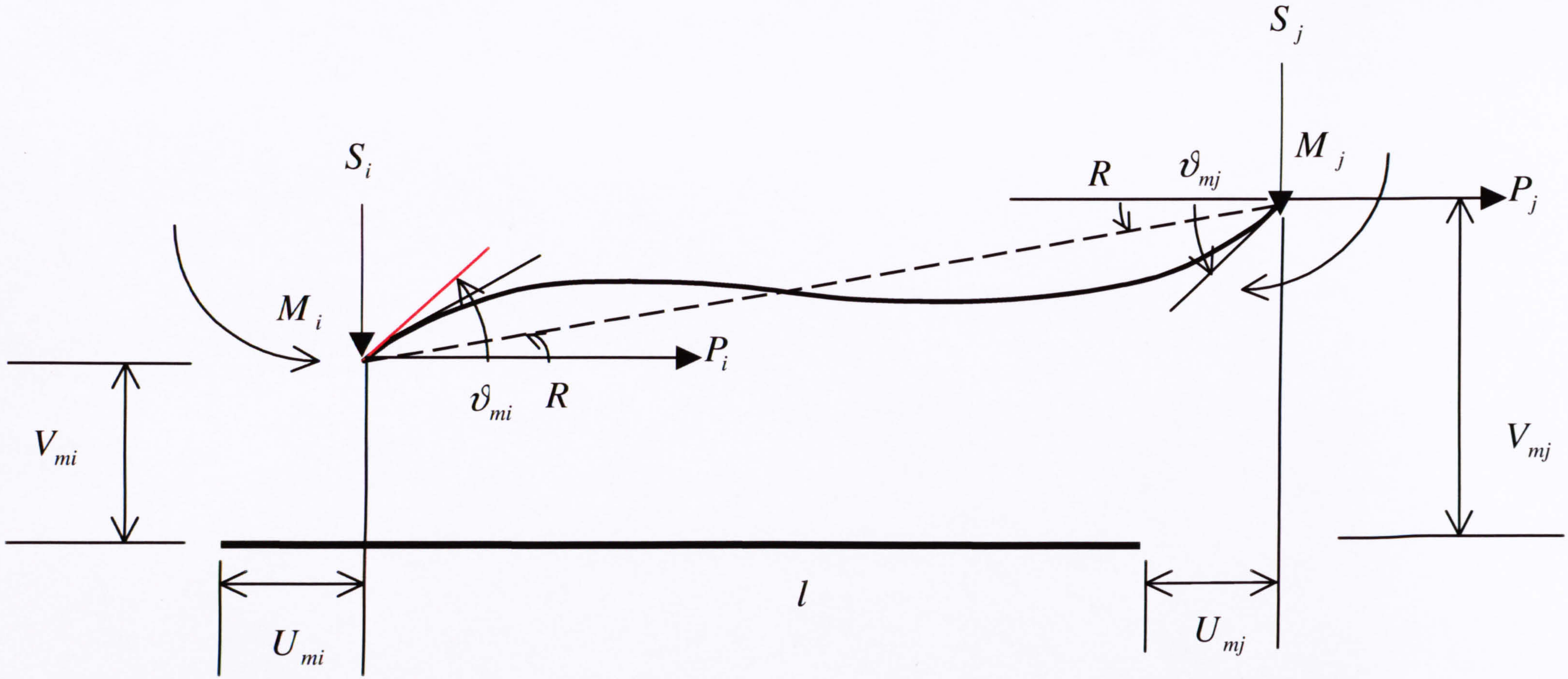

Fig. 4.3.1 - Rigid joint member

In global co-ordinates, the stiffness of the equation becomes

$$\{F\} = [T]^T [K][T]\{U\}$$

Where $[T]$ = Transformation matrix

And $[K]$ = Stiffness matrix

$$\begin{bmatrix} P_i \\ S_i \\ M_i \\ P_i \\ S_i \\ M_j \end{bmatrix} = \begin{bmatrix} c & -s & 0 & 0 & 0 & 0 \\ s & c & 0 & 0 & 0 & 0 \\ 0 & 0 & 1 & 0 & 0 & 0 \\ 0 & 0 & 0 & c & -s & 0 \\ 0 & 0 & 0 & s & c & 0 \\ 0 & 0 & 0 & 0 & 0 & 1 \end{bmatrix} \begin{bmatrix} \frac{EA}{L} & 0 & 0 & -\frac{EA}{L} & 0 & 0 \\ 0 & \frac{12EI}{L^3} & \frac{6EI}{L^2} & 0 & -\frac{12EI}{L^3} & \frac{6EI}{L^2} \\ 0 & \frac{6EI}{L^2} & \frac{4EI}{L} & 0 & -\frac{6EI}{L^2} & \frac{2EI}{L} \\ -\frac{EA}{L} & 0 & 0 & \frac{EA}{L} & 0 & 0 \\ 0 & -\frac{12EI}{L^3} & -\frac{6EI}{L^2} & 0 & \frac{12EI}{L^3} & -\frac{6EI}{L^2} \\ 0 & \frac{6EI}{L^2} & \frac{2EI}{L} & 0 & -\frac{6EI}{L^2} & \frac{4EI}{L} \end{bmatrix}$$

$$\begin{bmatrix} c & s & 0 & 0 & 0 & 0 \\ -s & c & 0 & 0 & 0 & 0 \\ 0 & 0 & 1 & 0 & 0 & 0 \\ 0 & 0 & 0 & c & s & 0 \\ 0 & 0 & 0 & -s & c & 0 \\ 0 & 0 & 0 & 0 & 0 & 1 \end{bmatrix} \begin{bmatrix} U_{mi} \\ V_{mi} \\ \vartheta_{mi} \\ U_{mj} \\ V_{mj} \\ \vartheta_{mj} \end{bmatrix}$$

This can be written in the form

The above stiffness matrix, $[K]$ will be relabelled $[S]$ when taking the semi-rigid behaviour into account the effective stiffness matrix $[S]$ will be obtained by modifying the stiffness matrix $[K]$ for rigid ended members. Thus, for rigid ended members

$$[K] = [S]$$

4.4 Semi-rigid joint rotational stiffness

This is idealised as a rotational spring[2] inserted between the end of the member and the joint as illustrated in Fig. 4.4.1 below.

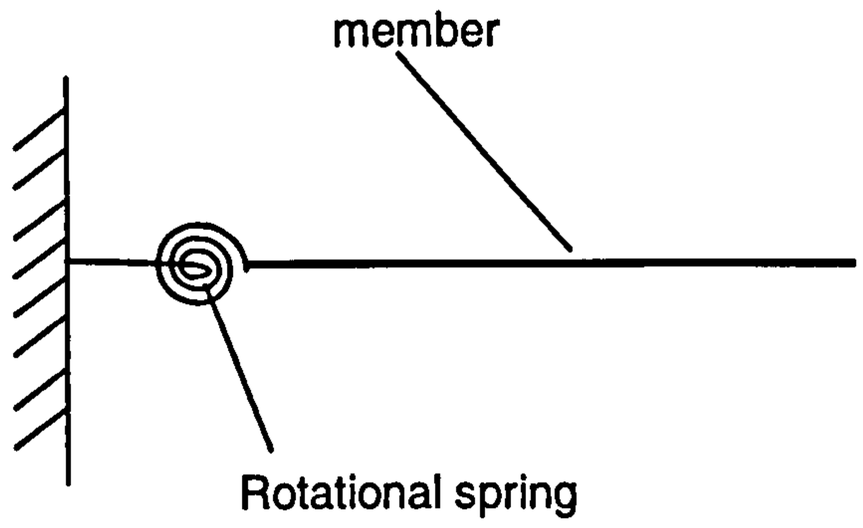

Fig. 4.4.1 – Semi-rigid rotational spring

The following derivation shows how joint semi-rigid rotation can be introduced into the slope deflection equations. Fig. 4.4.2 illustrates the member with a rotationally semi-rigid joint. Moments due to loading between nodes can be accounted for through M_i^F and M_j^F, the fixed end moments for nodes i and j respectively. All moments are taken as clock-wise positive.

$$M_i = \frac{4EI}{l}\vartheta_{mi} + \frac{2EI}{l}\vartheta_{mj} - \frac{6EI}{l^2}R + M_i^F \qquad (4.4.1a)$$

$$M_j = \frac{4EI}{l}\vartheta_{mj} + \frac{2EI}{l}\vartheta_{mi} - \frac{6EI}{l^2}R + M_j^F \qquad (4.4.1b)$$

$$R = \frac{(v_{mj} - v_{mi})}{l} \qquad (4.4.2)$$

With reference to Fig. 4.4.2 let ϑ_r and ϑ_m be the rotational displacement due to the spring and member respectively, therefore, the total rotational displacement is given by:

$$\vartheta_i = \vartheta_{mi} + \vartheta_{ri} \quad \therefore \quad \vartheta_{mi} = \vartheta_i - \vartheta_{ri} \qquad (4.4.3a)$$

$$\vartheta_j = \vartheta_{mj} + \vartheta_{rj} \quad \therefore \quad \vartheta_{mj} = \vartheta_j - \vartheta_{rj} \qquad (4.4.3b)$$

We define

λ_i, λ_j = Spring stiffness at joint i and j respectively.

Such that

$$\lambda_i = \frac{M_i}{\vartheta_{ri}} \qquad \lambda_j = \frac{M_j}{\vartheta_{rj}}$$

Substituting in Equation 4.4.1a and 4.4.1b for ϑ_{mi} and ϑ_{mj} and carrying out a series of algebraic manipulations gives

$$M_i = \frac{4EI}{l}\left[\frac{3r_i}{4-r_i r_j}\right]\vartheta_i + \frac{2EI}{l}\left[\frac{3r_i r_j}{4-r_i r_j}\right]\vartheta_j - \frac{6EI}{l^2}\left[\frac{r_i(2+r_j)}{4-r_i r_j}\right]v_{mj} + \frac{6EI}{l^2}\left[\frac{r_i(2+r_j)}{4-r_i r_j}\right]v_{mi} + \left[\frac{r_i}{4-r_i r_j}\right] - M_i^F(r_j-4) + M_j^F(2r_j-2) \quad (4.4.7a)$$

$$M_j = \frac{4EI}{l}\left[\frac{3r_j}{4-r_i r_j}\right]\vartheta_j + \frac{2EI}{l}\left[\frac{3r_i r_j}{4-r_i r_j}\right]\vartheta_i - \frac{6EI}{l^2}\left[\frac{r_j(2+r_i)}{4-r_i r_j}\right]v_{mj} + \frac{6EI}{l^2}\left[\frac{r_j(2+r_i)}{4-r_i r_j}\right]v_{mi} + \left[\frac{r_j}{4-r_i r_j}\right] - M_j^F(r_i-4) + M_i^F(2r_i-2) \quad (4.4.7b)$$

Where, M_i = Moment at joint i

and

$$r_i = \left(\frac{\lambda_i l}{\lambda_i l + 3EI}\right) \qquad r_j = \left(\frac{\lambda_j l}{\lambda_j l + 3EI}\right)$$

The original form of the slope deflection equation is kept for clarity and ease of implementing the new terms in the existing code, except of course rotations ϑ_i and ϑ_j are the full rotation, member and joint combined. The last term in the moment equation is moment due to member loads.

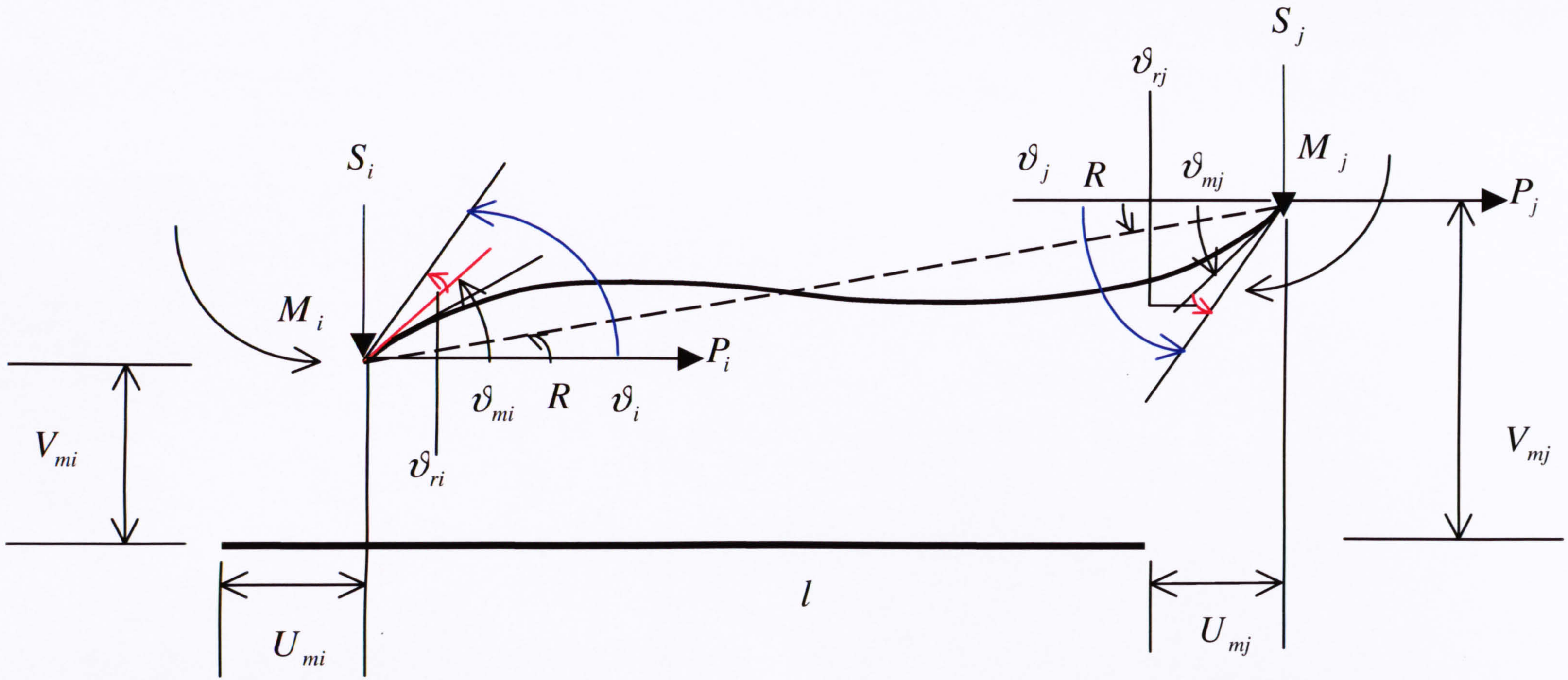

Fig. 4.4.2 – Rotationally semi-rigid jointed member

Internal Shear

With the aid of the diagram below the shear equation can be simply derived.

At i and j respectively.

$$M_i + M_j + S_j l = 0$$

$$M_j + M_i - S_i l = 0$$

Therefore,

$$S_i = \frac{M_j + M_i}{l} \qquad (4.4.8a) \qquad \text{and} \qquad -S_j = \frac{M_i + M_j}{l} \qquad (4.4.8b)$$

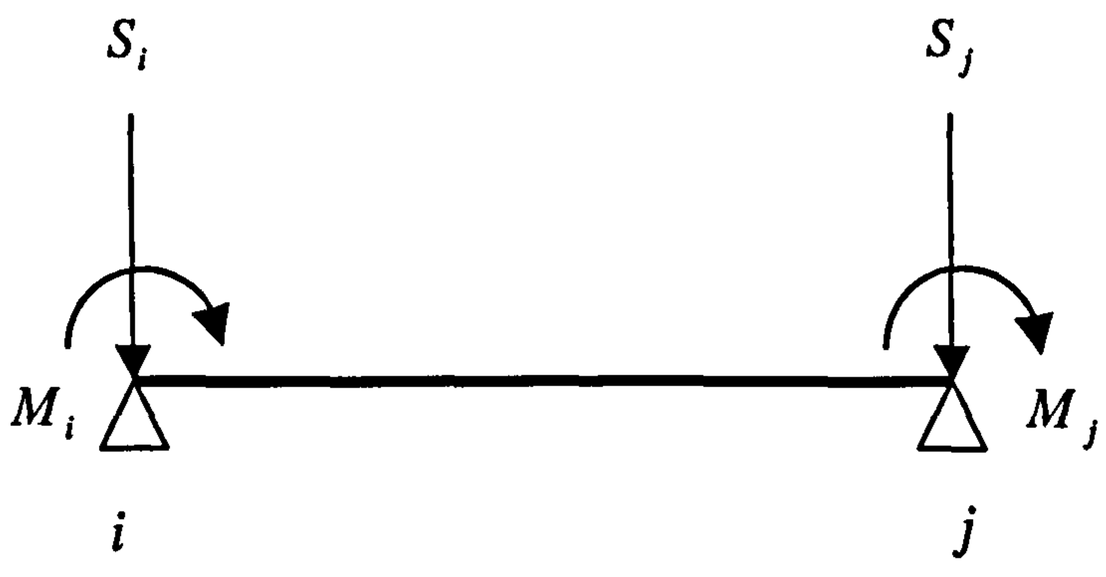

Fig 4.4.3 – Internal shear/reaction

By substituting the expressions for the moments, the following shear equations are deduced.

$$S_i = \frac{6EI}{l^2}\left[\frac{r_i(2+r_j)}{4-r_i r_j}\right]\vartheta_i + \frac{6EI}{l^2}\left[\frac{r_j(2+r_i)}{4-r_i r_j}\right]\vartheta_j + \frac{12EI}{l^3}\left[\frac{r_i + r_i r_j + r_j}{4-r_i r_j}\right]v_{mi}$$
$$-\frac{12EI}{l^3}\left[\frac{r_i + r_i r_j + r_j}{4-r_i r_j}\right]v_{mj} + \left[\frac{r_i r_j}{4-r_i r_j}\right]\frac{M_i^F\left(1+\frac{4}{r_j}-\frac{2}{r_i}\right)+M_j^F\left(1-\frac{2}{r_j}+\frac{4}{r_i}\right)}{l} \qquad (4.4.9a)$$

$$S_j = -\frac{6EI}{l^2}\left[\frac{r_i(2+r_j)}{4-r_i r_j}\right]\vartheta_i - \frac{6EI}{l^2}\left[\frac{r_j(2+r_i)}{4-r_i r_j}\right]\vartheta_j - \frac{12EI}{l^3}\left[\frac{r_i + r_i r_j + r_j}{4-r_i r_j}\right]v_{mi}$$
$$+\frac{12EI}{l^3}\left[\frac{r_i + r_i r_j + r_j}{4-r_i r_j}\right]v_{mj} - \left[\frac{r_i r_j}{4-r_i r_j}\right]\frac{M_i^F\left(1+\frac{4}{r_j}-\frac{2}{r_i}\right)+M_j^F\left(1-\frac{2}{r_j}+\frac{4}{r_i}\right)}{l} \qquad (4.4.9b)$$

The last term on the shear equation is shear due to member loads

Member axial forces

The member axial forces are also modified for member loads. Fig. 4.4.4 below illustrates the forces present due to the member being loaded, the fixed end moments having already been considered. The axial loads are denoted as w_i for node i, and similarly w_j for node j. w is denoted as the total load on the span. It is assumed reaction forces at the ends of the member are equal.

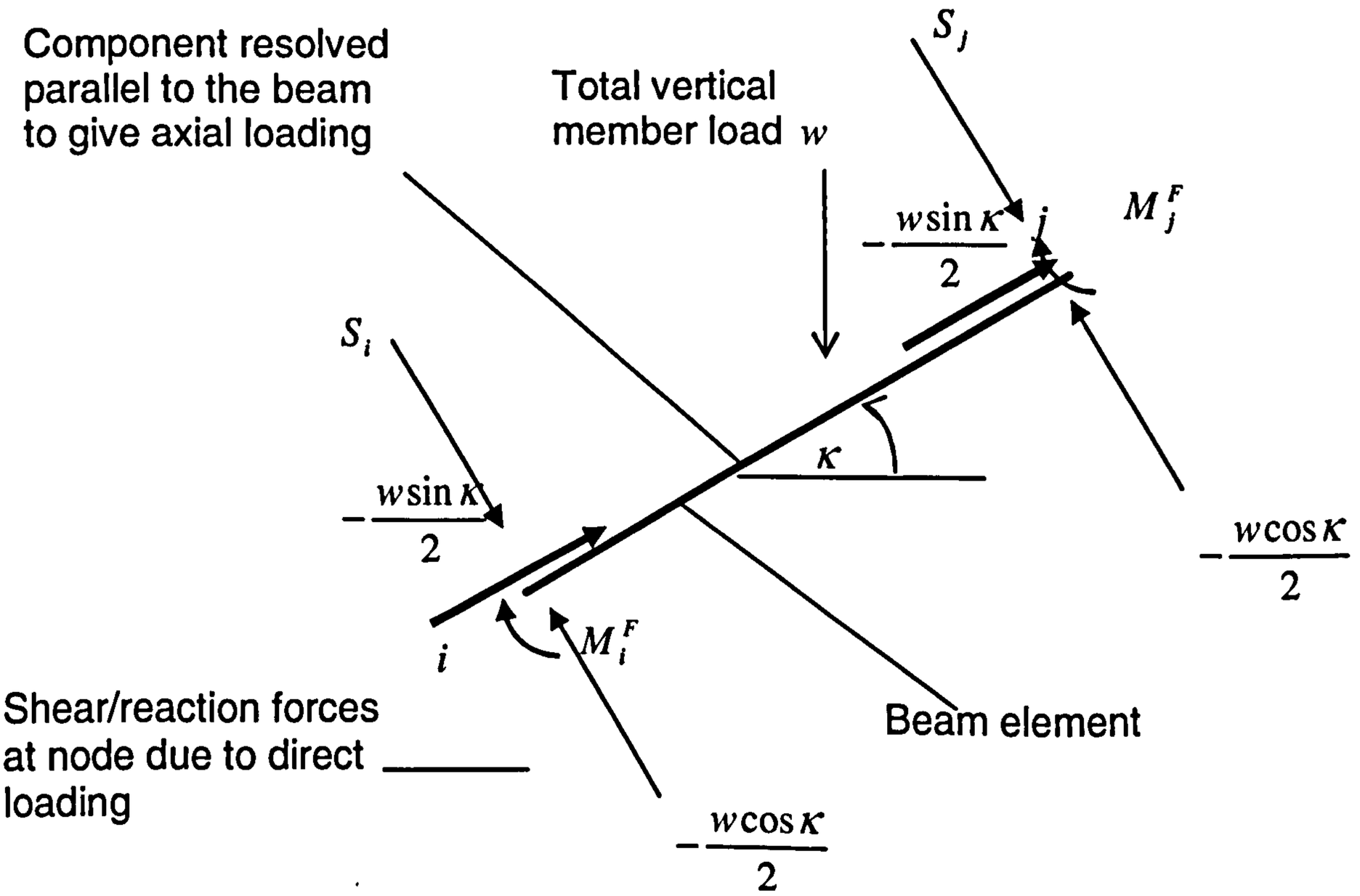

Fig.4.4.4 – Member load force diagram

For member axial force

At end i $P_i = \frac{EA}{l}(u_{mi} - u_{mj})$ (4.4.10a)

And

At end j $P_j = \frac{EA}{l}(u_{mj} - u_{mi})$ (4.4.10b)

Hence, the total member axial loading is :

$$P_i = \frac{EA}{l}(u_{mi} - u_{mj}) + \frac{w_i \sin\kappa}{2}$$

$$P_j = \frac{EA}{l}\left(u_{mj} - u_{mi}\right)\frac{+ w_j \sin\kappa}{2}$$

The total reaction/shear force due to member loads is

$$\left[\frac{r_i r_j}{4 - r_i r_j}\right]\frac{M_j^F\left(1+\frac{4}{r_j}-\frac{2}{r_i}\right)+M_i^F\left(1-\frac{2}{r_j}+\frac{4}{r_i}\right)}{l}+\frac{wl\cos\kappa}{2} \qquad (4.4.11a)$$

$$-\left[\frac{r_i r_j}{4 - r_i r_j}\right]\frac{M_j^F\left(1+\frac{4}{r_j}-\frac{2}{r_i}\right)+M_i^F\left(1-\frac{2}{r_j}+\frac{4}{r_i}\right)}{l}+\frac{wl\cos\kappa}{2} \qquad (4.4.11b)$$

for nodes i and j respectively.

The equations can now be expressed in matrix form. The stiffness matrix $[K]$ is now a combination of two components. This comprises the original stiffness matrix, $[S]$of the beam, but modified to include semi-rigid actions. The original form of S will be preserved, therefore, all new terms due to the semi-rigid joint rotational spring will be placed in a new matrix denoted as C. Hence, now,

$$[K] = [S][C]_R \qquad (4.4.12)$$

The suffix R, denotes joint semi-rigid rotation. In addition, the matrix modified to include forces induced by load between nodes, i.e. member load, will be denoted as $\bar{f}$, local member forces. Hence, the equation takes the form:

$$[f] = [S][u] + [\bar{f}]_R$$

Local forces are modified to:

$$[f] = [S][C]_R[u] + [\bar{f}]_R \qquad \text{or} \qquad [f] = [K][u] + [\bar{f}]_R \qquad (4.4.13)$$

Transformation of the local equation to global form is as follows:

$$[f] = [T][F]$$

$$\therefore$$

$$[T]\{F\} = [K]\{u\} + [\bar{f}]_R$$

Multiplying both sides by $[T]^{-1}$, Matrix T is orthogonal therefore $[T]^T = [T]^{-1}$

$$[T]^{-1}[T]\{F\}=[T]^{T}[K]\{u\}+[T]^{T}[\bar{f}]_{R}$$

For global to local displacement transformation $[u]=[T][U]$

$$\{F\}=[T]^{T}[K][T]\{U\}+[T]^{T}[\bar{f}]_{R} \qquad (4.4.14)$$

Where, $[K] = [S][C]_{R}$

The method to determine the new connection matrix, C_R is determined by utilising the flexibility matrix. The generation of the connection matrix is as follows.

Let us write the following equation

$$[K]=[S][C]$$

Where, $[K]$ = Full set of newly derived equations.

$[S]$ = Member stiffness matrix

$[C]$ = New connection matrix accounting for semi-rigid joint

Matrix $[K]$ is the new set of derivatives and $[S]$ is the stiffness matrix.

$[S]^{-1}[K]=[S]^{-1}[S][C]$ $[S]^{-1}$ and $[S]$ on the right side of the term cancel each other out therefore $[S]^{-1}[K]=[C]$

Where, $[S]^{-1}$= the reciprocal of the stiffness matrix, i.e. the flexibility matrix, which is well documented. Finally, the equations can be presented in matrix form where the stiffness matrix is preserved.

$$F = T \; S \; C_R$$

$$\begin{bmatrix} P_i \\ S_i \\ M_i \\ P_j \\ S_j \\ M_j \end{bmatrix} = \begin{bmatrix} c & -s & 0 & 0 & 0 & 0 \\ s & c & 0 & 0 & 0 & 0 \\ 0 & 0 & 1 & 0 & 0 & 0 \\ 0 & 0 & 0 & c & -s & 0 \\ 0 & 0 & 0 & s & c & 0 \\ 0 & 0 & 0 & 0 & 0 & 1 \end{bmatrix} \begin{bmatrix} \frac{EA}{l} & 0 & 0 & -\frac{EA}{l} & 0 & 0 \\ 0 & \frac{12EI}{l^3} & \frac{6EI}{l^2} & 0 & -\frac{12EI}{l^3} & \frac{6EI}{l^2} \\ 0 & \frac{6EI}{l^2} & \frac{4EI}{l} & 0 & -\frac{6EI}{l^2} & \frac{2EI}{l} \\ -\frac{EA}{l} & 0 & 0 & \frac{EA}{l} & 0 & 0 \\ 0 & -\frac{12EI}{l^3} & -\frac{6EI}{l^2} & 0 & \frac{12EI}{l^3} & -\frac{6EI}{l^2} \\ 0 & \frac{6EI}{l^2} & \frac{2EI}{l} & 0 & -\frac{6EI}{l^2} & \frac{4EI}{l} \end{bmatrix} \begin{bmatrix} 1 & 0 & 0 & 0 & 0 & 0 \\ 0 & \frac{4r_j - 2r_i + r_i r_j}{4 - r_i r_j} & \frac{-2Lr_i(1-r_j)}{4 - r_i r_j} & 0 & 0 & 0 \\ 0 & \frac{\frac{6}{L}(r_i - r_j)}{4 - r_i r_j} & \frac{3r_i(2-r_j)}{4 - r_i r_j} & 0 & 0 & 0 \\ 0 & 0 & 0 & 1 & 0 & 0 \\ 0 & 0 & 0 & 0 & \frac{4r_i - 2r_j + r_i r_j}{4 - r_i r_j} & \frac{-2Lr_j(1-r_i)}{4 - r_i r_j} \\ 0 & 0 & 0 & 0 & \frac{\frac{6}{L}(r_i - r_j)}{4 - r_i r_j} & \frac{3r_j(2-r_i)}{4 - r_i r_j} \end{bmatrix}$$

$$T \quad U \quad T^T \quad \bar{f}_R$$

$$\begin{bmatrix} c & s & 0 & 0 & 0 & 0 \\ -s & c & 0 & 0 & 0 & 0 \\ 0 & 0 & 1 & 0 & 0 & 0 \\ 0 & 0 & 0 & c & s & 0 \\ 0 & 0 & 0 & -s & c & 0 \\ 0 & 0 & 0 & 0 & 0 & 1 \end{bmatrix} \begin{bmatrix} u_{mi} \\ v_{mi} \\ \vartheta_i \\ u_{mj} \\ v_{mj} \\ \vartheta_j \end{bmatrix} + \begin{bmatrix} c & -s & 0 & 0 & 0 & 0 \\ s & c & 0 & 0 & 0 & 0 \\ 0 & 0 & 1 & 0 & 0 & 0 \\ 0 & 0 & 0 & c & -s & 0 \\ 0 & 0 & 0 & s & c & 0 \\ 0 & 0 & 0 & 0 & 0 & 1 \end{bmatrix} \begin{bmatrix} \frac{1}{(4 - r_i r_j)} \end{bmatrix} \begin{bmatrix} \frac{(4 - r_i r_j)\frac{w_i^{ext} \sin\kappa}{2}}{r_i r_j \left(\frac{M_j^F \left(1 + \frac{4}{r_j} - \frac{2}{r_i}\right) + M_i^F \left(1 - \frac{2}{r_j} + \frac{4}{r_i}\right)}{l} \right) + (4 - r_i r_j)\frac{-wl\cos\kappa}{2}} \\ r_i\left(-M_i^F(r_j - 4) + M_j^F(2r_j - 2)\right) \\ \frac{(4 - r_i r_j)\frac{w_j^{ext} \sin\kappa}{2}}{r_i r_j \left(-\frac{M_j^F \left(1 + \frac{4}{r_j} - \frac{2}{r_i}\right) + M_i^F \left(1 - \frac{2}{r_j} + \frac{4}{r_i}\right)}{l} \right) + (4 - r_i r_j)\frac{-wl\cos\kappa}{2}} \\ r_j\left(-M_j^F(r_i - 4) + M_i^F(2r_i - 2)\right) \end{bmatrix}$$

Fig. 4.4.5 – Matrix components of a rotationally semi-rigid joint member

It should be noted that by applying zero rotational stiffness, the equation should be reduced to that of a pinned truss analysis. On the opposite end, by applying infinite (or very high) rigidity, the equation should be reduced to that for the rigid jointed frame analysis.

For pinned joint we can assign the following value

λ_i = zero rotational stiffness

For rigid joint we can assign the opposite value

λ_i = Infinitely large rotational stiffness

The matrix can now deal with pinned joints, rigid joints, and semi-rigid joints.

4.5 Semi-rigid joint axial stiffness

A linear spring is used to model axial stiffness of a joint. The diagram in Fig. 4.5.1 below illustrates this spring along with the rotational spring.

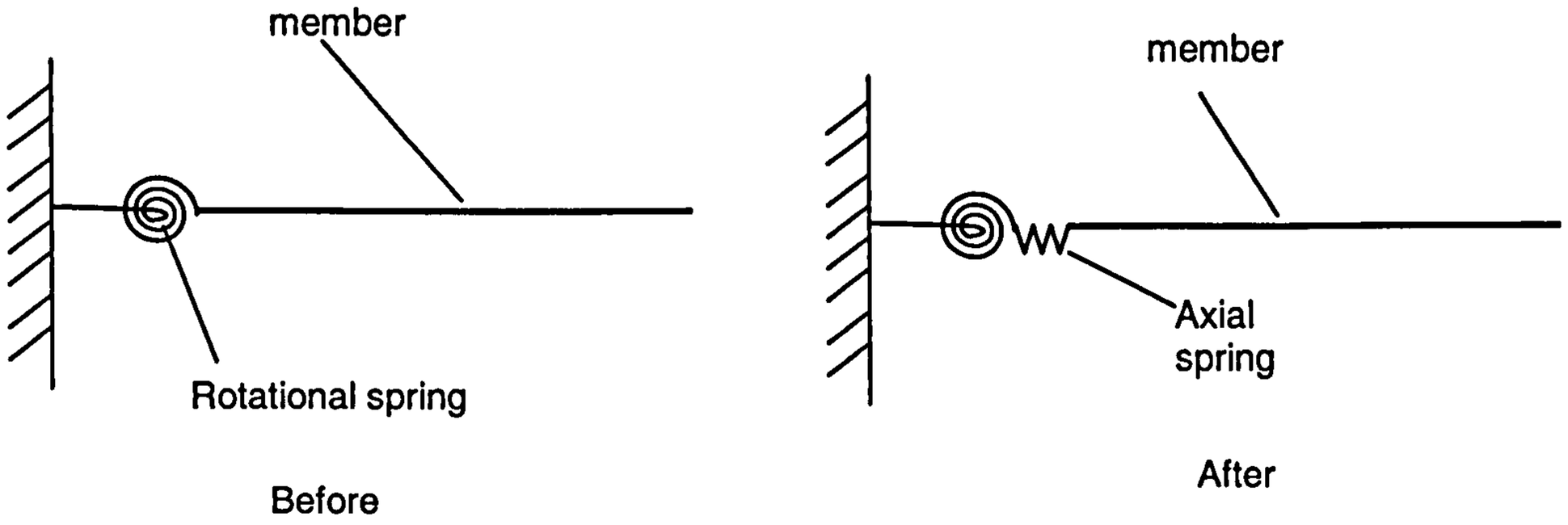

Fig. 4.5.1 – 2 D.O.F Semi-rigid joint representation

The axial displacement of a member is illustrated as shown below.

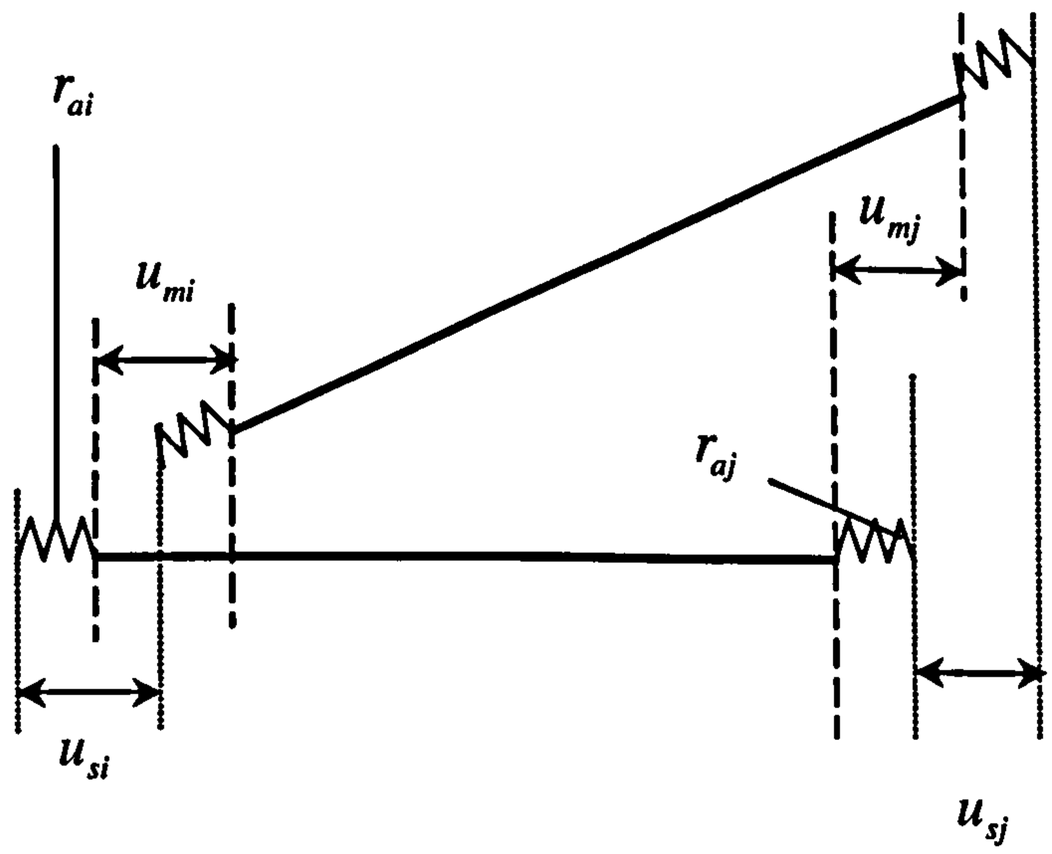

Fig. 4.5.2 – Axial spring and member displacements

u_{mi} =Local member horizontal displacement at node i

u_{mj} =Local member horizontal displacement at node j

u_{ai} =Local joint horizontal displacement at node i

u_{aj} =Local joint horizontal displacement at node j

u_i =Total horizontal displacement at i

u_j =Total horizontal displacement at j

The term u_i and u_j denotes horizontal displacement for ends i and j respectively. It now comprises two components, member and joint displacement. Hence, the following can be written

$$u_i = u_{mi} + u_{ai} \qquad \therefore \qquad u_{mi} = u_i - u_{ai}$$

$$u_j = u_{mj} + u_{aj} \qquad \therefore \qquad u_{mj} = u_j - u_{aj}$$

$$u_{ai} = \frac{P_i}{r_{ai}} \text{ and } u_{aj} = \frac{P_j}{r_{aj}}$$

Where r_{ai} =Axial spring stiffness at joint i

r_{aj} =Axial spring stiffness at joint j

We recall the axial force Equations 4.3.3a and 4.3.3b for member axial force.

$$P_i = \frac{EA}{L}(u_{mi} - u_{mj}) \text{ and } P_j = \frac{EA}{L}(u_{mj} - u_{mi})$$

for end i and j respectively.

Substituting for u_{mi} and u_{mj} we can arrive at the following after a series of algebraic manipulations.

$$P_i = \frac{EA}{l\rho}(u_i - u_j) \qquad (4.5.2a)$$

$$P_j = \frac{EA}{l\rho}(u_j - u_i) \qquad (4.5.2b)$$

Where,

$$\rho = \left(1 + \frac{EA}{lr_{aj}} + \frac{EA}{lr_{ai}}\right)$$

Horizontal displacement is now represented in terms of u_i and u_j, total displacement, member and joint combined. The stiffness matrix can now be modified to include equations 4.5.2a and 4.5.2b. Again, to preserve the original

form of the stiffness matrix, modifications are made to the connection, C matrix only.

Where, $[K]=[S][C]_{RA}$

The suffix A denotes semi-rigid axial connection stiffness. In global co-ordinates, the stiffness of the equation is shown in Fig. 4.5.3.

$$F = T \; S \; C_{RA}$$

$$\begin{bmatrix} P_i \\ S_i \\ M_i \\ P_j \\ S_j \\ M_j \end{bmatrix} = \begin{bmatrix} c & -s & 0 & 0 & 0 & 0 \\ s & c & 0 & 0 & 0 & 0 \\ 0 & 0 & 1 & 0 & 0 & 0 \\ 0 & 0 & 0 & c & -s & 0 \\ 0 & 0 & 0 & s & c & 0 \\ 0 & 0 & 0 & 0 & 0 & 1 \end{bmatrix} \begin{bmatrix} \frac{EA}{l} & 0 & 0 & -\frac{EA}{l} & 0 & 0 \\ 0 & \frac{12EI}{l^3} & \frac{6EI}{l^2} & 0 & -\frac{12EI}{l^3} & \frac{6EI}{l^2} \\ 0 & \frac{6EI}{l^2} & \frac{4EI}{l} & 0 & -\frac{6EI}{l^2} & \frac{2EI}{l} \\ -\frac{EA}{l} & 0 & 0 & \frac{EA}{l} & 0 & 0 \\ 0 & -\frac{12EI}{l^3} & -\frac{6EI}{l^2} & 0 & \frac{12EI}{l^3} & -\frac{6EI}{l^2} \\ 0 & \frac{6EI}{l^2} & \frac{2EI}{l} & 0 & -\frac{6EI}{l^2} & \frac{4EI}{l} \end{bmatrix} \begin{bmatrix} \frac{1}{\rho} & 0 & 0 & 0 & 0 & 0 \\ 0 & \frac{4r_j - 2r_i + r_i r_j}{4 - r_i r_j} & \frac{-2Lr_i(1-r_j)}{4 - r_i r_j} & 0 & 0 & 0 \\ 0 & \frac{\frac{6}{L}(r_i - r_j)}{4 - r_i r_j} & \frac{3r_i(2-r_j)}{4 - r_i r_j} & 0 & 0 & 0 \\ 0 & 0 & 0 & \frac{1}{\rho} & 0 & 0 \\ 0 & 0 & 0 & 0 & \frac{4r_i - 2r_j + r_i r_j}{4 - r_i r_j} & \frac{-2Lr_j(1-r_i)}{4 - r_i r_j} \\ 0 & 0 & 0 & 0 & \frac{\frac{6}{L}(r_i - r_j)}{4 - r_i r_j} & \frac{3r_j(2-r_i)}{4 - r_i r_j} \end{bmatrix}$$

$$T \quad U \quad T^T \quad \bar{f}_{RA}$$

$$\begin{bmatrix} c & s & 0 & 0 & 0 & 0 \\ -s & c & 0 & 0 & 0 & 0 \\ 0 & 0 & 1 & 0 & 0 & 0 \\ 0 & 0 & 0 & c & s & 0 \\ 0 & 0 & 0 & -s & c & 0 \\ 0 & 0 & 0 & 0 & 0 & 1 \end{bmatrix} \begin{bmatrix} u_i \\ v_{mi} \\ \vartheta_i \\ u_j \\ v_{mj} \\ \vartheta_j \end{bmatrix} + \begin{bmatrix} c & -s & 0 & 0 & 0 & 0 \\ s & c & 0 & 0 & 0 & 0 \\ 0 & 0 & 1 & 0 & 0 & 0 \\ 0 & 0 & 0 & c & -s & 0 \\ 0 & 0 & 0 & s & c & 0 \\ 0 & 0 & 0 & 0 & 0 & 1 \end{bmatrix} \left[\frac{1}{(4 - r_i r_j)} \right] \begin{bmatrix} (4 - r_i r_j) \frac{w_i^{ext} \sin \kappa}{2} \\ r_i r_j \left(\frac{M_j^F \left(1 + \frac{4}{r_j} - \frac{2}{r_i}\right) + M_i^F \left(1 - \frac{2}{r_j} + \frac{4}{r_i}\right)}{l} \right) + (4 - r_i r_j) \frac{-wl \cos \kappa}{2} \\ r_i \left(-M_i^F (r_j - 4) + M_j^F (2r_j - 2)\right) \\ (4 - r_i r_j) \frac{w_j^{ext} \sin \kappa}{2} \\ r_i r_j \left(-\frac{M_j^F \left(1 + \frac{4}{r_j} - \frac{2}{r_i}\right) + M_i^F \left(1 - \frac{2}{r_j} + \frac{4}{r_i}\right)}{l} \right) + (4 - r_i r_j) \frac{-wl \cos \kappa}{2} \\ r_j \left(-M_j^F (r_i - 4) + M_i^F (2r_i - 2)\right) \end{bmatrix}$$

Fig. 4.5.3 – Matrix components of an axial and rotational semi-rigid joint member

4.6 Semi-rigid joint shear stiffness

To implement shear stiffness the condition must be introduced to the vertical displacement component of the slope deflection equation. The new system is illustrated below in Fig. 4.6.1 with the joint semi-rigid shear spring.

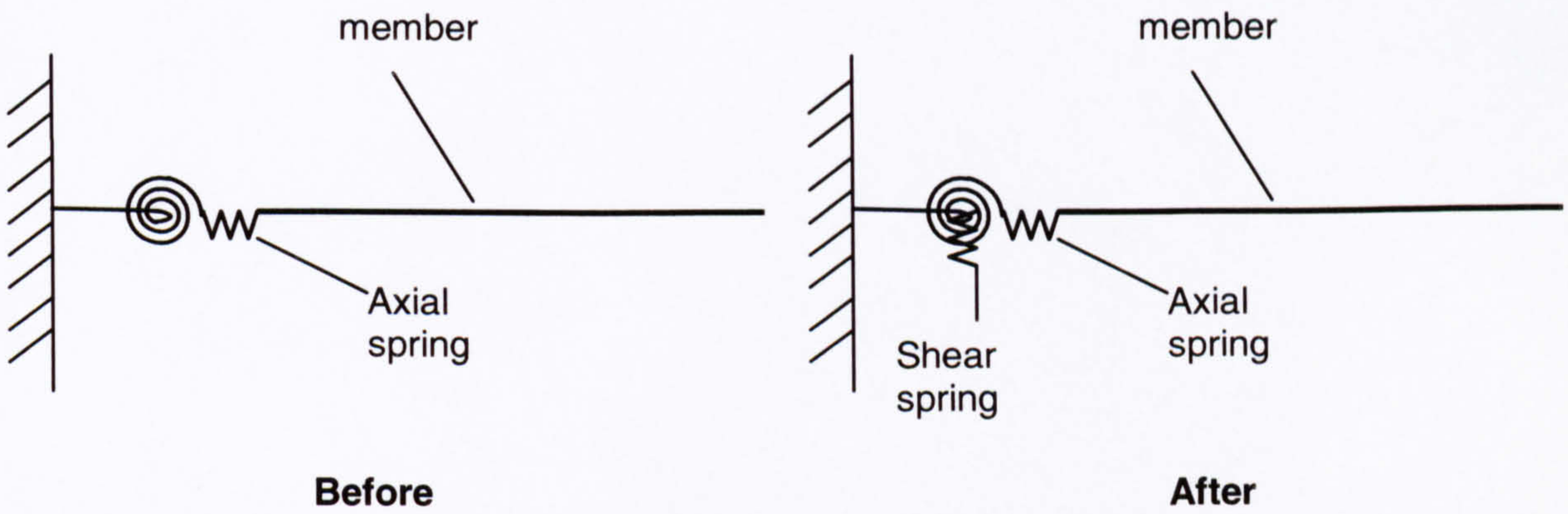

Fig. 4.6.1 – System of rotational, axial and shear semi-rigidity

A beam with the joint semi-rigid shear spring is shown below.

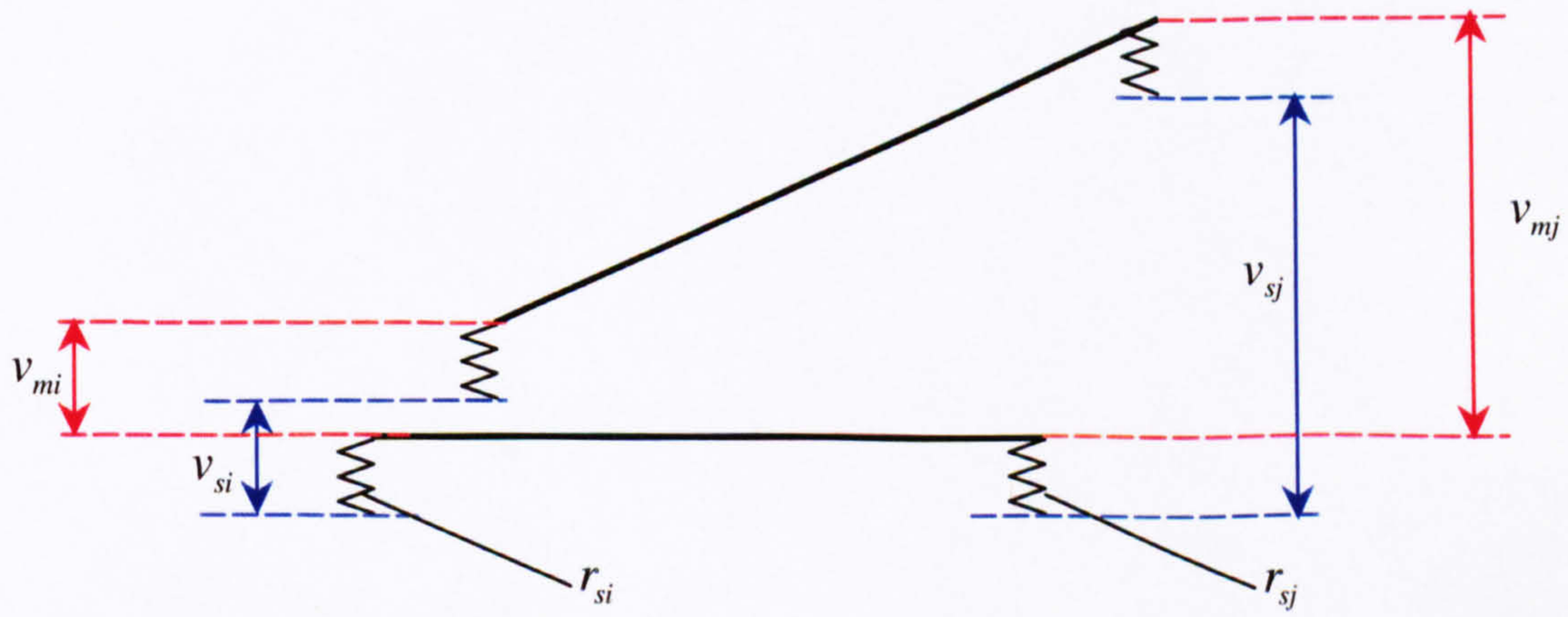

Fig. 4.6.2 – Displacement system of shear semi-rigidity

There are now 2 components for the vertical displacement as shown in the diagram above.

Where,

v_{mi} = Vertical member displacement at node I

v_{mj} = Vertical member displacement at node j

v_{si} = Shear spring displacement at node I

v_{sj} = Shear spring displacement at node j

r_{si} = Stiffness of shear spring at node I

r_{sj} = Stiffness of shear spring at node j

The term R of the slope deflection equation is modified because it is associated with the vertical movement of the equation, hence it can be expanded as follows.

We know $R = \frac{\Delta_m}{l} = \frac{v_{mj} - v_{mi}}{l}$

Denoting the following

$\Delta_t = v_j - v_i$ $\Delta_s = v_{sj} - v_{si}$ $\Delta_m = v_{mj} - v_{mi}$

where, Δ_t = Total vertical relative displacement

Δ_s = Spring relative displacement

Δ_m = Member relative displacement

v_i = Total vertical displacement at node i

v_j = Total vertical displacement at node j

Also,

$\Delta_t = \Delta_s + \Delta_m \ \therefore \quad \Delta_m = \Delta_t - \Delta_s$

Hence, $v_{mj} = v_j - v_{sj}$ $v_{mi} = v_i - v_{si}$

Therefore,

$$R = \frac{v_{mj} - v_{mi}}{l} = \frac{(v_j - v_{sj}) - (v_i - v_{si})}{l}$$

But $v_{si} = \frac{S_i}{r_{si}}$ and $v_{sj} = \frac{S_j}{r_{sj}}$

Where

$S_i = \frac{M_j + M_i}{l}$ and $S_j = -\frac{M_i + M_j}{l}$ as defined in (4.4.8a) and (4.4.8b)

respectively.

$\therefore \quad v_{mj} = v_j - \frac{S_j}{r_{sj}}$ and $v_{mi} = v_i - \frac{S_i}{r_{si}}$

Substituting the above v_{mj} and v_{mi} terms into equations (4.4.7a), (4.4.7b) for moments and (4.4.9a), (4.4.9b) for shear, followed by a series of algebraic manipulations gives us the following

$$M_i = \frac{4EI}{l}\left[\frac{3\alpha_i\alpha_j r_i}{4\varepsilon_i\alpha_i\alpha_j + 4\alpha_i\alpha_j - r_i r_j}\right]\vartheta_i + \left(-\frac{12(EI)^2}{l^2}\beta + \frac{2EI}{\alpha_i l}\right)\left[\frac{3\alpha_i\alpha_j r_i r_j}{4\varepsilon_i\alpha_i\alpha_j + 4\alpha_i\alpha_j - r_i r_j}\right]\vartheta_j$$
$$-\left(\frac{6EI}{l^2}\right)\left[\frac{\alpha_i\alpha_j r_i\left(2 + \frac{r_j}{\alpha_i} - \frac{6EIr_j\beta}{l}\right)}{4\varepsilon_i\alpha_i\alpha_j + 4\alpha_i\alpha_j - r_i r_j}\right]v_j + \left(\frac{6EI}{l^2}\right)\left[\frac{\alpha_i\alpha_j r_i\left(2 + \frac{r_j}{\alpha_i} - \frac{6EIr_j\beta}{l}\right)}{4\varepsilon_i\alpha_i\alpha_j + 4\alpha_i\alpha_j - r_i r_j}\right]v_i \qquad (4.6.7a)$$
$$-\left(r_j - 4\alpha_j - \frac{6EI\alpha_i\beta r_j}{l}\right)\left[\frac{r_i}{4\varepsilon_i\alpha_i\alpha_j + 4\alpha_i\alpha_j - r_i r_j}\right]M_i^F$$
$$+\left(2r_j - 2\alpha_j - \frac{12EI\alpha_i\beta r_j}{l}\right)\left[\frac{r_i}{4\varepsilon_i\alpha_i\alpha_j + 4\alpha_i\alpha_j - r_i r_j}\right]M_j^F$$

$$M_j = \frac{4EI}{l}\left[\frac{3\alpha_i\alpha_j r_j}{4\varepsilon_j\alpha_i\alpha_j + 4\alpha_i\alpha_j - r_i r_j}\right]\vartheta_j + \left(\frac{2EI}{\alpha_j l} - \frac{12(EI)^2}{l^2}\beta\right)\left[\frac{3\alpha_i\alpha_j r_i r_j}{4\varepsilon_j\alpha_i\alpha_j + 4\alpha_i\alpha_j - r_i r_j}\right]\vartheta_i$$
$$-\left(\frac{6EI}{l^2}\right)\left[\frac{\alpha_i\alpha_j r_j\left(2 + \frac{r_i}{\alpha_j} - \frac{6EIr_i\beta}{l}\right)}{4\varepsilon_i\alpha_i\alpha_j + 4\alpha_i\alpha_j - r_i r_j}\right]v_j + \left(\frac{6EI}{l^2}\right)\left[\frac{\alpha_i\alpha_j r_j\left(2 + \frac{r_i}{\alpha_j} - \frac{6EIr_i\beta}{l}\right)}{4\varepsilon_i\alpha_i\alpha_j + 4\alpha_i\alpha_j - r_i r_j}\right]v_i \qquad (4.6.7b)$$
$$+\left(2r_i - 2\alpha_i - \frac{12EIr_i\alpha_j\beta}{l}\right)\left[\frac{r_j}{4\varepsilon_j\alpha_i\alpha_j + 4\alpha_i\alpha_j - r_i r_j}\right]M_i^F$$
$$-\left(r_i - 4\alpha_i - \frac{6EI\beta\alpha_j r_i}{l}\right)\left[\frac{r_j}{4\varepsilon_j\alpha_i\alpha_j + 4\alpha_i\alpha_j - r_i r_j}\right]M_j^F$$

$$S_i = \frac{6EI}{l^2}\left[\frac{\alpha_i\alpha_j r_i\left(2-\frac{6EI\beta r_j}{l}+\frac{r_j}{\alpha_j}\right)}{4\varepsilon_j\alpha_i\alpha_j+4\alpha_i\alpha_j-r_i r_j}\right]\vartheta_i+\frac{6EI}{l^2}\left[\frac{\alpha_i\alpha_j r_j\left(2+\frac{r_i}{\alpha_i}-\frac{6EI\beta r_i}{l}\right)}{4\varepsilon_j\alpha_i\alpha_j+4\alpha_i\alpha_j-r_i r_j}\right]\vartheta_j$$

$$-\left(\frac{12EI}{l^3}\right)\left[\frac{\alpha_i\alpha_j\left(r_i\frac{r_i r_j}{2}\left(\frac{1}{\alpha_i}+\frac{1}{\alpha_j}\right)+r_j-\frac{6EIr_i r_j\beta}{l}\right)}{4\varepsilon_i\alpha_i\alpha_j+4\alpha_i\alpha_j-r_i r_j}\right]R' \qquad (4.6.8a)$$

$$+\left[\frac{r_i r_j}{4\varepsilon_j\alpha_i\alpha_j+4\alpha_i\alpha_j-r_i r_j}\right]\left[\frac{1}{l}\right]$$

$$\left\{\left(1+\frac{4\alpha_j}{r_j}-\frac{2\alpha_i}{r_i}+\frac{6EI\beta(\alpha_i-2\alpha_j)}{l}\right)M_i^F+\left(1+\frac{4\alpha_i}{r_i}-\frac{2\alpha_j}{r_j}+\frac{6EI\beta(\alpha_j-2\alpha_i)}{l}\right)M_j^F\right\}$$

$$S_j = -\frac{6EI}{l^2}\left[\frac{\alpha_i\alpha_j r_i\left(2-\frac{6EI\beta r_j}{l}+\frac{r_j}{\alpha_j}\right)}{4\varepsilon_j\alpha_i\alpha_j+4\alpha_i\alpha_j-r_i r_j}\right]\vartheta_i-\frac{6EI}{l^2}\left[\frac{\alpha_i\alpha_j r_j\left(2+\frac{r_i}{\alpha_i}-\frac{6EI\beta r_i}{l}\right)}{4\varepsilon_j\alpha_i\alpha_j+4\alpha_i\alpha_j-r_i r_j}\right]\vartheta_j$$

$$+\left(\frac{12EI}{l^3}\right)\left[\frac{\alpha_i\alpha_j\left(r_i+\frac{r_i r_j}{2}\left(\frac{1}{\alpha_i}+\frac{1}{\alpha_j}\right)+r_j-\frac{6EIr_i r_j\beta}{l}\right)}{4\varepsilon_i\alpha_i\alpha_j+4\alpha_i\alpha_j-r_i r_j}\right]R' \qquad (4.6.8b)$$

$$-\left[\frac{r_i r_j}{4\varepsilon_j\alpha_i\alpha_j+4\alpha_i\alpha_j-r_i r_j}\right]\left[\frac{1}{l}\right]$$

$$\left\{\left(1+\frac{4\alpha_j}{r_j}-\frac{2\alpha_i}{r_i}+\frac{6EI\beta(\alpha_i-2\alpha_j)}{l}\right)M_i^F+\left(\frac{6EI\beta(\alpha_j-2\alpha_i)}{l}+1-\frac{2\alpha_j}{r_j}+\frac{4\alpha_i}{r_i}\right)M_j^F\right\}$$

Where, $\beta = \left(\frac{1}{l^2 r_{sj}}+\frac{1}{l^2 r_{si}}\right)$

$$\alpha_i = 1+\frac{3EIr_i\beta}{l} \qquad \text{and} \qquad \alpha_j = 1+\frac{3EIr_j\beta}{l}$$

$$\gamma_j = \frac{3EIr_j}{\alpha_j l} \text{ and } \gamma_i = \frac{3EIr_i}{\alpha_i l}$$

The new terms are introduced to the correction matrix. The matrices where shear rigidity will be implemented is in the $[C]_{RA}$ and $[\bar{f}]$ matrix.

$$[F] = [T]^T[K][T][U]+[T]^T[\bar{f}]_{RAS} \qquad \text{where, } [K] = [S][C]_{RAS}$$

$$\begin{bmatrix} P_i \\ S_i \\ M_i \\ P_j \\ S_j \\ M_j \end{bmatrix} = \begin{bmatrix} c & -s & 0 & 0 & 0 & 0 \\ s & c & 0 & 0 & 0 & 0 \\ 0 & 0 & 1 & 0 & 0 & 0 \\ 0 & 0 & 0 & c & -s & 0 \\ 0 & 0 & 0 & s & c & 0 \\ 0 & 0 & 0 & 0 & 0 & 1 \end{bmatrix} \begin{bmatrix} \frac{EA}{l} & 0 & 0 & -\frac{EA}{l} & 0 & 0 \\ 0 & \frac{12\,EI}{l^3} & \frac{6EI}{l^2} & 0 & -\frac{12\,EI}{l^3} & \frac{6EI}{l^2} \\ 0 & \frac{6EI}{l^2} & \frac{4EI}{l} & 0 & -\frac{6EI}{l^2} & \frac{2EI}{l} \\ -\frac{EA}{l} & 0 & 0 & \frac{EA}{L} & 0 & 0 \\ 0 & -\frac{12\,EI}{l^3} & -\frac{6EI}{l^2} & 0 & \frac{12\,EI}{l^3} & -\frac{6EI}{l^2} \\ 0 & \frac{6EI}{l^2} & \frac{2EI}{l} & 0 & -\frac{6EI}{l^2} & \frac{4EI}{l} \end{bmatrix}$$

$$\begin{bmatrix} \frac{1}{\rho} & 0 & 0 & 0 & 0 & 0 \\ 0 & \frac{\alpha_i\alpha_j\left[4r_j - 2r_i + r_ir_j\left(\frac{2}{\alpha_j} - \frac{1}{\alpha_i} - \frac{6EI\beta}{l}\right)\right]}{4\varepsilon_i\alpha_i\alpha_j + 4\alpha_i\alpha_j - r_ir_j} & \frac{\alpha_i\alpha_j\left[-2lr_i\left(1 - \frac{r_j}{\alpha_j}\right) - 12\,EI\beta r_ir\right]}{4\varepsilon_i\alpha_i\alpha_j + 4\alpha_i\alpha_j - r_ir_j} & 0 & 0 & 0 \\ 0 & \frac{\alpha_i\alpha_j\left[\frac{6}{l}\left(r_i - r_j - r_ir_j\left(\frac{1}{\alpha_j} - \frac{1}{\alpha_i}\right)\right)\right]}{4\varepsilon_i\alpha_i\alpha_j + 4\alpha_i\alpha_j - r_ir_j} & \frac{\alpha_i\alpha_j\left[3r_i\left(2 - \frac{r_j}{\alpha_j} + \frac{6EI\beta r_j}{l}\right)\right]}{4\varepsilon_i\alpha_i\alpha_j + 4\alpha_i\alpha_j - r_ir_j} & 0 & 0 & 0 \\ 0 & 0 & 0 & \frac{1}{\rho} & 0 & 0 \\ 0 & 0 & 0 & 0 & \frac{\alpha_i\alpha_j\left[4r_i - 2r_j + r_ir_j\left(\frac{2}{\alpha_i} - \frac{1}{\alpha_j} - \frac{6EI\beta}{l}\right)\right]}{4\varepsilon_i\alpha_i\alpha_j + 4\alpha_i\alpha_j - r_ir_j} & \frac{\alpha_i\alpha_j\left[2lr_j\left(1 - \frac{r_i}{\alpha_i}\right) + 12\,EI\beta r_ir_j\right]}{4\varepsilon_i\alpha_i\alpha_j + 4\alpha_i\alpha_j - r_ir_j} \\ 0 & 0 & 0 & 0 & \frac{\alpha_i\alpha_j\left[\frac{6}{l}\left(r_i - r_j + r_ir_j\left(\frac{1}{\alpha_i} - \frac{1}{\alpha_j}\right)\right)\right]}{4\varepsilon_i\alpha_i\alpha_j + 4\alpha_i\alpha_j - r_ir_j} & \frac{\alpha_i\alpha_j\left[3r_j\left(2 - \frac{r_i}{\alpha_i} + \frac{6EI\beta r_i}{l}\right)\right]}{4\varepsilon_i\alpha_i\alpha_j + 4\alpha_i\alpha_j - r_ir_j} \end{bmatrix}$$

$$\begin{bmatrix} c & s & 0 & 0 & 0 & 0 \\ -s & c & 0 & 0 & 0 & 0 \\ 0 & 0 & 1 & 0 & 0 & 0 \\ 0 & 0 & 0 & c & s & 0 \\ 0 & 0 & 0 & -s & c & 0 \\ 0 & 0 & 0 & 0 & 0 & 1 \end{bmatrix} \begin{bmatrix} u_i \\ v_i \\ \vartheta_i \\ u_j \\ v_j \\ \vartheta_j \end{bmatrix} +$$

$$T$$

$$\begin{bmatrix} c & -s & 0 & 0 & 0 & 0 \\ s & c & 0 & 0 & 0 & 0 \\ 0 & 0 & 1 & 0 & 0 & 0 \\ 0 & 0 & 0 & c & -s & 0 \\ 0 & 0 & 0 & s & c & 0 \\ 0 & 0 & 0 & 0 & 0 & 1 \end{bmatrix} \left[\frac{1}{\left(4\varepsilon_i\alpha_i\alpha_j + 4\alpha_i\alpha_j - r_ir_j\right)} \right]$$

$$\bar{f}_{RAS}$$

$$\begin{bmatrix} \left(4\varepsilon_i\alpha_i\alpha_j + 4\alpha_i\alpha_j - r_ir_j\right)\frac{w_i^{ext}\sin\kappa}{2} \\ r_ir_j\left(\frac{M_i^F\left(1+\frac{4\alpha_j}{r_j}-\frac{2\alpha_i}{r_i}+\frac{6EI\beta\left(\alpha_i-2\alpha_j\right)}{l}\right)+M_j^F\left(1-\frac{2\alpha_j}{r_j}+\frac{4\alpha_i}{r_i}+\frac{6EI\beta\left(\alpha_j-2\alpha_i\right)}{l}\right)}{l}\right)+\left(4-r_ir_j\right)\frac{-wl\cos\kappa}{2} \\ r_i\left(-M_i^F\left(r_j-4\alpha_j-\frac{6EI\alpha_i\beta r_j}{l}\right)+M_j^F\left(2r_j-2-\frac{12EI\alpha_i\beta r_j}{l}\right)\right) \\ \left(4\varepsilon_i\alpha_i\alpha_j + 4\alpha_i\alpha_j - r_ir_j\right)\frac{w_j^{ext}\sin\kappa}{2} \\ -r_ir_j\left(\frac{M_i^F\left(1+\frac{4\alpha_j}{r_j}-\frac{2\alpha_i}{r_i}+\frac{6EI\beta\left(\alpha_i-2\alpha_j\right)}{l}\right)+M_j^F\left(1-\frac{2\alpha_j}{r_j}+\frac{4\alpha_i}{r_i}+\frac{6EI\beta\left(\alpha_j-2\alpha_i\right)}{l}\right)}{l}\right)+\left(4-r_ir_j\right)\frac{-wl\cos\kappa}{2} \\ r_j\left(-M_j^F\left(r_i-4\alpha_i-\frac{6EI\beta\alpha_jr_i}{l}\right)+M_i^F\left(2r_i-2\alpha_i-\frac{12EIr_i\alpha_j\beta}{l}\right)\right) \end{bmatrix}$$

Fig. 4.6.3 – Matrix components of 3-DOF semi-rigid joint member

Member and Joint displacements

With the introduction of the semi-rigid effects, the displacement at the member ends now comprises member and joint displacement components. The local displacements of these two components can be determined once global displacements have been transformed. Local and global displacements are denoted by lower and upper case respectively, assuming the global displacements are obtained. Local internal displacements are obtained by the following. The total displacements, i.e. the global displacements are:

$$U = \begin{bmatrix} U_i \\ V_i \\ \vartheta_i \\ U_j \\ V_j \\ \vartheta_j \end{bmatrix}$$

Transforming the global displacement to the local displacement requires the following transformation

$$\{\delta\} = [T]\{U\}$$

$$\begin{bmatrix} u_i \\ v_i \\ \vartheta_i \\ u_j \\ v_j \\ \vartheta_j \end{bmatrix} = \begin{bmatrix} c & s & 0 & 0 & 0 & 0 \\ -s & c & 0 & 0 & 0 & 0 \\ 0 & 0 & 1 & 0 & 0 & 0 \\ 0 & 0 & 0 & c & s & 0 \\ 0 & 0 & 0 & -s & c & 0 \\ 0 & 0 & 0 & 0 & 0 & 1 \end{bmatrix} \begin{bmatrix} U_i \\ V_i \\ \vartheta_i \\ U_j \\ V_j \\ \vartheta_j \end{bmatrix}$$

The internal member displacements need to be determined now. The equations for local forces in general form are:

$$\{f\} = [K]\{\delta\} + \{\bar{f}\}$$

The force at the member end is given as,

$$\{F\}_{mem} = [S]\{\delta\}_{mem} + \{\bar{f}\}_{mem} \qquad (4.6.9)$$

The force for entire system is given as

$$\{F\} = [S][C]_{RAS}\{\delta\} + \{\bar{f}\}_{RAS} \qquad (4.6.10)$$

Where

$\{S\}$ = Stiffness matrix

$[C]_{RAS}$ = Connection matrix

$\{\delta\}_{mem}$ = Member displacement.

$\{\bar{f}\}_{mem}$ = Internal force due to member loads.

$\{\delta\}$ = Total local displacement

$\{F\}_{mem}$ = Force due to member loads.

By conservation of energy, that is, no loss in energy through the system, therefore force for the entire system and member have to be in equilibrium.

$\{F\} = \{F\}_{mem}$ and $\{\bar{f}\} = \{\bar{f}\}_{mem} = \{f\}_{RAS}$.

By equating Equations 4.6.9 and 4.6.10 $\therefore \{\delta\}_{mem} = [C]_{RAS}\{\delta\}$

With reference to Fig. 4.6.4 the local displacement of the rotational, axial and shear semi-rigid connection can be found by

$\{\delta\} = \{\delta\}_{Con} + \{\delta\}_{mem} \therefore \quad \{\delta\}_{con} = \{\delta\} - \{\delta\}_{mem}$

where $\{\delta\}_{con} = \begin{bmatrix} \vartheta_r \\ u_{si} \\ v_s \end{bmatrix}$

Substituting $\{\delta\}_{mem}$ into equation 4.6.9 and determine $\{\bar{f}\}_{RAS}$ as detailed in Fig. 4.6.3, hence, $\{F\}_{mem}$ is found. Fig. 4.6.4 below can be used to visualise the member, connection and total displacements. The physical presence of the

springs in the sketch bears no resemblance to the geometry of the connection and is only for illustration purposes.

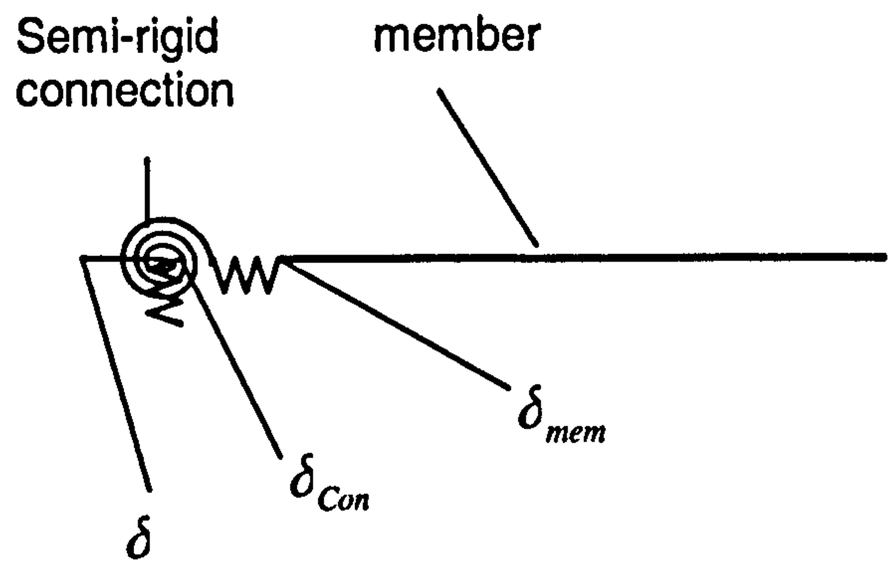

Fig.4.6.4 – Semi-rigid joint model

4.7 Stability functions

The analysis can be modified to include the effects of the instability of the members. Stability functions are available in text books[42] and are only briefly mentioned here for completeness. More fundamentally, it is how the function is implemented into the current analysis. The instability of a structure occurs when compressive forces are present. As the axial loads increase the rotational stiffness reduces because as the member bends eccentricity increases and loads applied axially are converted into bending moments. The bending moments reduce the rotational stiffness of the member. The effects of instability are particularly important for slender members subject to compressive loads. Stability functions are used to quantify the effect of axial force on stiffness and work by reducing the stiffness of the member which is dependent on the end conditions, material properties, length of the member and the axial load. The frame analysis is based on the assumption that when the Euler load is reached stiffness is zero. The function is implemented into the stiffness matrix as follows.

Recalling the slope deflection equation 4.3.1a and 4.3.1b

$$M_i = \frac{4EI}{l}\vartheta_{mi} + \frac{2EI}{l}\vartheta_{mj} + \frac{6EI}{l^2}v_{mi} - \frac{6EI}{l^2}v_{mj} + M_i^F \qquad (4.3.1a)$$

$$M_j = \frac{4EI}{l}\vartheta_{mj} + \frac{2EI}{l}\vartheta_{mi} + \frac{6EI}{l^2}v_{mj} + \frac{6EI}{l^2}v_{mi} + M_j^F \qquad (4.3.1b)$$

The derivation of the following equations which includes the effect of the axial force and member rotational stiffness is found in text books and will not be repeated here.

$$M_i = s\frac{EI}{l}\vartheta_{mi} + sc\frac{EI}{l}\vartheta_{mj} + s(1+c)\frac{EI}{l^2}v_{mi} - s(1+c)\frac{EI}{l^2}v_{mj} + M_i^F \qquad (4.7.1a)$$

$$M_j = s\frac{EI}{l}\vartheta_{mj} + sc\frac{EI}{l}\vartheta_{mi} - s(1+c)\frac{EI}{l^2}v_{mj} + s(1+c)\frac{EI}{l^2}v_{mi} + M_j^F \qquad (4.7.1b)$$

$$S_i = (s - sc)\left[\frac{EI}{l^2}\vartheta_{mi} + \frac{EI}{l^2}\vartheta_{mj}\right] + 2s(1+c)\left[\frac{EI}{l^3}v_{mi} - \frac{EI}{l^3}v_{mj}\right] + \frac{M_i^F + M_j^F}{l} \quad (4.7.2a)$$

$$S_j = -(s - sc)\left[\frac{EI}{l^2}\vartheta_{mi} + \frac{EI}{l^2}\vartheta_{mj}\right] - 2s(1+c)\left[\frac{EI}{l^3}v_{mi} - \frac{EI}{l^3}v_{mj}\right] - \frac{M_i^F + M_j^F}{l} \quad (4.7.2b)$$

Where, $s = \dfrac{\alpha(1 - 2\alpha\cot 2\alpha)}{(\tan\alpha - \alpha)}$ and $c = \dfrac{2\alpha - \sinh 2\alpha}{\sinh 2\alpha - 2\alpha\cosh 2\alpha}$

These are called the stiffness and carry over function respectively.

Where, $\alpha = \dfrac{\pi\sqrt{|\rho|}}{2}$ and $\rho = \dfrac{P}{P_E}$

Where P is the member load

P_E is the Euler load

$$P_E = \frac{\pi^2 EI}{l^2}$$

The stiffness matrix is modified as follows

$$S = \begin{bmatrix}
\frac{EA}{l} & 0 & 0 & -\frac{EA}{l} & 0 & 0 \\
0 & 2s(1+c)\frac{EI}{l^3} & (s-sc)\frac{EI}{l^2} & 0 & -2s(1+c)\frac{EI}{l^3} & (s-sc)\frac{EI}{l^2} \\
0 & s(1+c)\frac{EI}{l^2} & s\frac{EI}{l} & 0 & -s(1+c)\frac{6EI}{l^2} & s\frac{EI}{l} \\
-\frac{EA}{l} & 0 & 0 & \frac{EA}{L} & 0 & 0 \\
0 & -2s(1+c)\frac{EI}{l^3} & -(s-sc)\frac{EI}{l^2} & 0 & 2s(1+c)\frac{EI}{l^3} & -(s-sc)\frac{EI}{l^2} \\
0 & s(1+c)\frac{EI}{l^2} & s\frac{EI}{l} & 0 & -s(1+c)\frac{EI}{l^2} & s\frac{EI}{l}
\end{bmatrix}$$

Hence, the stiffness matrix is now a function of axial compression load. By using this matrix, rather than the matrix in Fig. 4.6.3, the instability effects due to axial compression can be included.

4.8 Non-linear connection behaviour

The connection function utilises joint experimental data to describe the behaviour of the joint from elastic through to plastic. The method is described below.

Assuming a typical example is taken from a joint test, the results may look like the following plotted graph for a given joint.

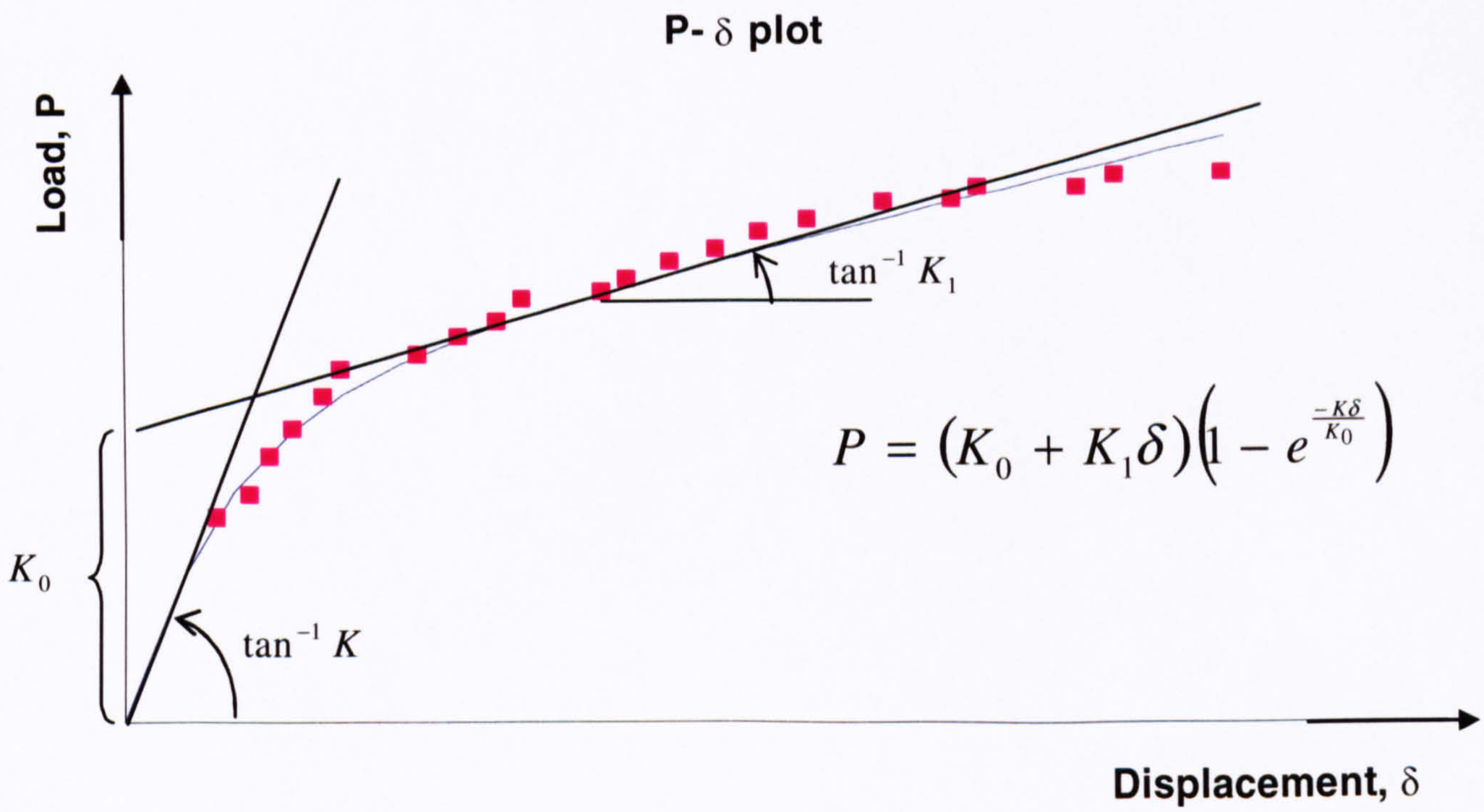

Fig. 4.8.1 – Foschi Power function

Fig. 4.8.1, shows the Foschi[12] exponential function being fitted to a set of experimental data. Load P, can be bending moment, axial force or shear force. Similarly, δ can be a rotation or a translational displacement.

Where,

K	Initial stiffness
K_0,	Asymptotic to Tangent stiffness
K_1	Tangent Stiffness
δ	Semi-rigid displacement

By experimenting with the different parameters a function for non-linear semi-rigid response for a joint can be determined and implemented into frame analysis. Therefore further modifications to the semi-rigid equations are required.

Recalling the semi-rigid rotational stiffness equations

$$\lambda_i = \frac{M_i}{\vartheta_{ri}} \text{ and } \lambda_i = \frac{M_i}{\vartheta_{ri}}$$

Let Foschi's exponential function for moment rotational stiffness be modified to

$$M = (K_0 + K_1\vartheta)\left(1 - \exp\left(\frac{-K\vartheta}{K_0}\right)\right) \qquad (4.8.1)$$

The non-linear stiffness is therefore:

$$\lambda = \frac{dM}{d\vartheta} = \exp\left(\frac{-K\vartheta}{K_0}\right)\left[K - K_1 + K_1\frac{\vartheta K}{K_0}\right] + K_1$$

Hence

$$\lambda_i = \frac{dM_i}{d\vartheta_{ri}} = \exp\left(\frac{-K\vartheta_{ri}}{K_0}\right)\left[K - K_1 + K_1\frac{\vartheta_{ri}K}{K_0}\right] + K_1$$

and

$$\lambda_j = \frac{dM_j}{d\vartheta_{rj}} = \exp\left(\frac{-K\vartheta_{rj}}{K_0}\right)\left[K - K_1 + K_1\frac{\vartheta_{rj}K}{K_0}\right] + K_1 \qquad (4.8.2)$$

The above equations apply for joint i and j of a beam element and similarly, for axial and shear semi-rigid stiffness. The Foschi parameters are determined from directly using the values through trial and error in an Excel spreadsheet until a good fit, judged visually was established. The alternative method is to use a least square fit to the power function. However, this was not implemented due to time pressures. In addition, the benefit of the visual method is that rogue values can be spotted and neglected immediately.

4.9 Computational procedure

The mentioned theory of the analysis has been programmed in FORTRAN 90 to obtain truss failure loads and deflections. Using an existing Fortran program from Brebbia[43] as a starting point, the program STRUSS, was developed to include geometrical non-linearity and non-linear semi-rigid rotation, axial and shear connection response. STRUSS uses an incremental load procedure. At each load increment out of balance forces are iteratively reduced to a specified convergence criterion using the constant stiffness matrix method. After convergence at each load increment, loads and displacements are accumulated where co-ordinates are updated, setting the truss for the next load increment. At each stage a linear analysis is performed. As this type of analysis is well documented, details have been left out.

A flow chart of STRUSS is presented on the next page. The steps are typical of an incremental load analysis. Some details of each step are presented on the following page.

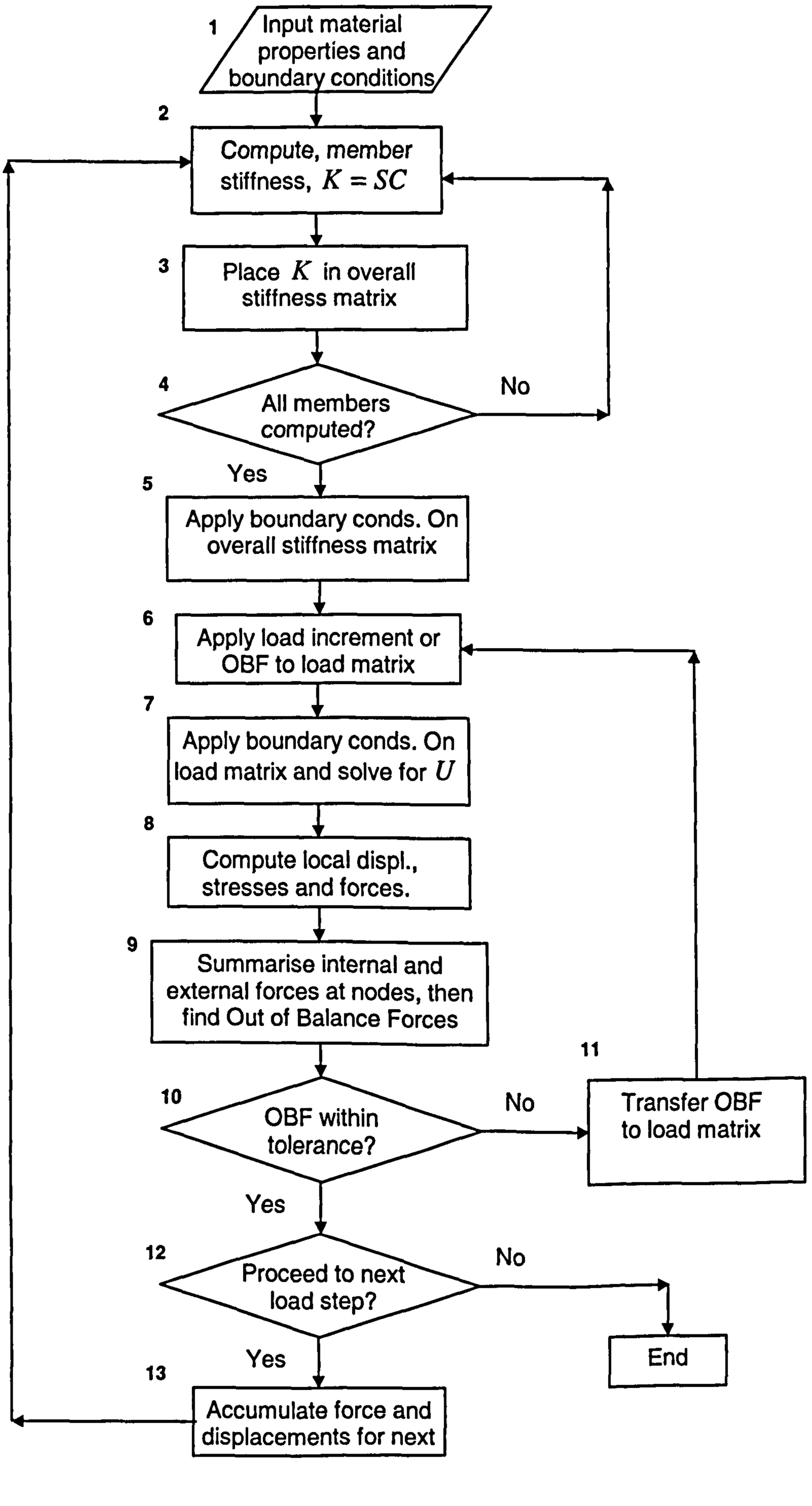

Fig.4.9.1 – STRUSS program flow chart

1. Read in number of nodes and timber beam lengths, beam cross sections and properties, non-linear connection properties and boundary conditions.
2. First compute member stiffness matrix S, which is dependent on stability functions. Next compute connection matrix C, derived from the Foschi power function for non-linear semi-rigid connection which is a function of local nodal displacement. For the first increment and iteration, initial stiffness is used. Finally compute stiffness matrix, $K = SC$
3. Place stiffness matrix, K into overall stiffness matrix.
4. Repeat steps 2-3 until all members computed.
5. Apply boundary conditions to overall stiffness matrix.
6. Read in Nodal and member loads. If in the middle of an iteration apply Out of Balance Forces.
7. Apply boundary conditions to load matrix and use Gauss elimination to solve for global displacement, U. Accumulate displacement.
8. Use global displacements transform to local displacements to find local member forces.
9. For each node, summarise internal and external forces and determine out of balance forces.
10. Is out of balance forces within specified tolerance?
11. If out of balance forces out of tolerance, transfer forces in to the load matrix.
12. Proceed to the next load increment if not the last.
13. If yes, accumulate member forces and displacements for the next load increment.

Chapter 5

Finite element analysis

5.1 Introduction

This chapter presents details of the finite element model used to calculate the local response of the connections. The 2-D beam analysis described in Chapter 4 can predict the overall response of the truss through displacements, member forces, and other semi-rigid parameters at the joint. However, it does not provide details of the stresses within the members and the connection. Such results, if available, would provide data for detailed analysis in the truss and individual connections. In particular stress distribution data of the nail plate would be valuable for plate designers and various plate models as mentioned in the literature review.

The entire process of the finite element is conducted in ANSYS, a commercially available finite element package.

5.2 Assumptions

The following assumptions are made in the analysis

- For the same reasons as the 2-D beam element analysis, the 2-D and 3-D finite element model is assumed to be laterally adequate and effects of lateral forces are negligible. Timber is an anisotropic material but is assumed to be orthotropic in the x-y plane for simplicity. Forces are dominantly in this plane whilst z plane forces are negligible.
- Timber members are assumed to be linearly elastic throughout the load history.
- Timber is known for its different properties in tension and compression, whether parallel or perpendicular to the grain. The tensile and compression modulus of the timber perpendicular and parallel to the grain are assumed to be equal.
- The critical parts of the truss are at the joints as the connection will fail before the timber. This is evident in the connection and full scale truss test mentioned later. In fact, timber member capacity is never breached. Therefore the preceding two assumptions are reasonable.
- The strength properties of the nail plate are dependent on the angle at which it is loaded. However, values derived for the connections already accounts for nail load at an angle. Therefore connection strength properties are assumed to be isotropic.
- The moment rotation data is not applied to the FE model as rotational parameters cannot be applied to the elements. Rotation parameters are dependent on the isotropic properties of the element which is determine through direct axial loading test.

5.3 Finite element model

Before any values were given to the material properties in the timber a 2-D model was drawn in ANSYS. This is a standard procedure in ANSYS for defining areas to be meshed. To save computational time and the size of the database, coarse meshing was used for the main timber member as stress distribution is simple in these areas. As the members approached the connections the mesh density was gradually increased. Each member is treated as a separate entity and only has a relationship through the connection model as explained later. The process of drawing the model for the timber first involved plotting key points to form lines. Using the lines, areas are established so meshing can proceed. This was done for half of the truss due to symmetry. Key points were designated such that it would coincide with the shape of the plate at each connection and also allow a gradual reduction of mesh density away from the connection. The model was then mirrored at the centre and nodes merged at the bottom chord joint of the truss for a continuous member.

Timber is an anisotropic material, however, as frequently adopted to simplfy analysis it is assumed to be orthotropic. This reduces the original 21 independent coefficients for anisotropic materials to 9 as illustrated for the 3-D body in Fig, 5.3.1 below.

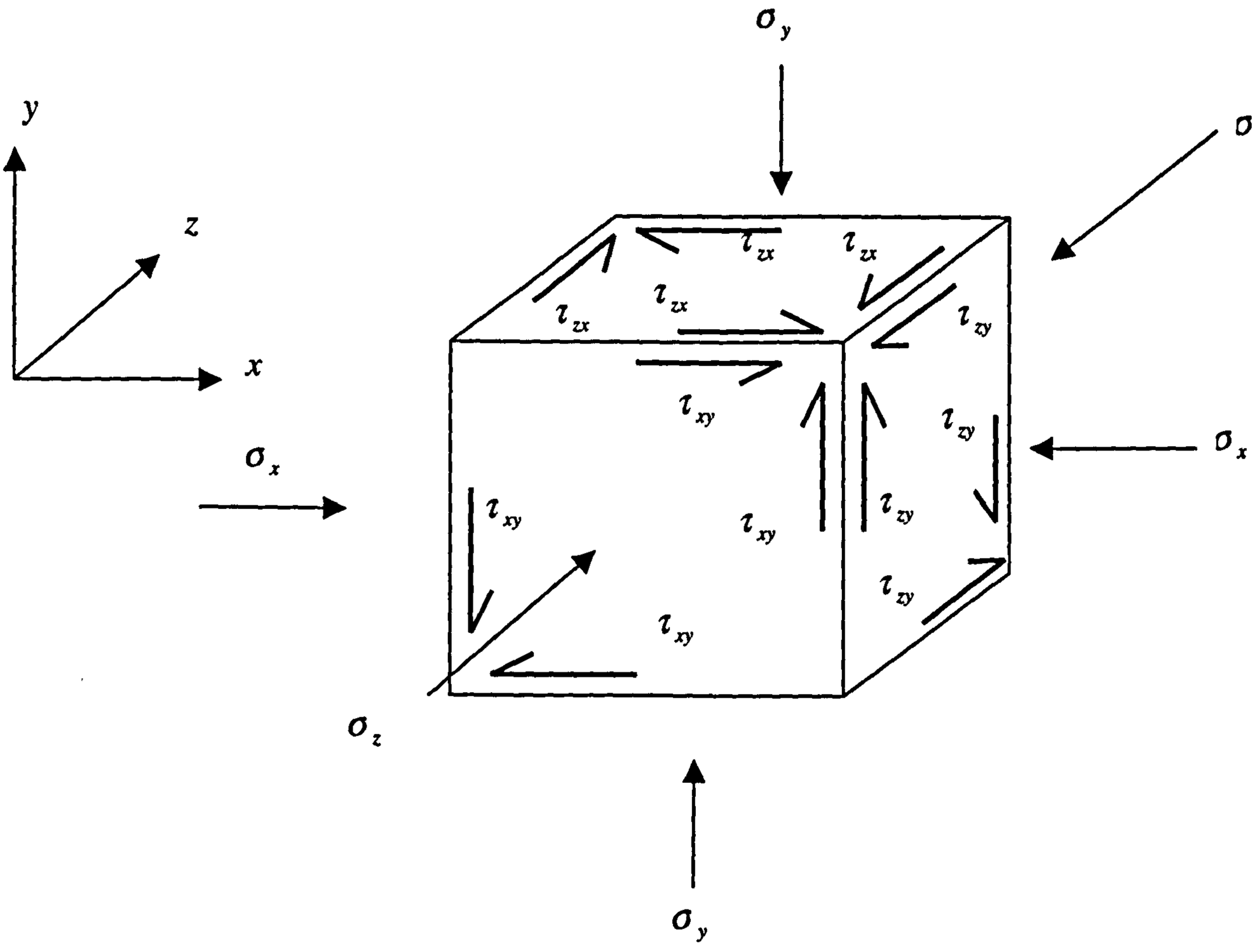

Fig. 5.3.1 – Stress state of 3-D body

The orthotropic material constitutive relationship adopted is as follows:

$$\begin{Bmatrix} \varepsilon_x \\ \varepsilon_y \\ \varepsilon_z \\ \gamma_{xy} \\ \gamma_{yz} \\ \gamma_{zx} \end{Bmatrix} = \begin{bmatrix} \frac{1}{E_x} & -\frac{\nu_{yx}}{E_y} & -\frac{\nu_{zx}}{E_z} & 0 & 0 & 0 \\ -\frac{\nu_{xy}}{E_x} & \frac{1}{E_y} & -\frac{\nu_{zy}}{E_z} & 0 & 0 & 0 \\ -\frac{\nu_{xz}}{E_x} & -\frac{\nu_{yz}}{E_y} & \frac{1}{E_z} & 0 & 0 & 0 \\ 0 & 0 & 0 & \frac{1}{G_{xy}} & 0 & 0 \\ 0 & 0 & 0 & 0 & \frac{1}{G_{yz}} & 0 \\ 0 & 0 & 0 & 0 & 0 & \frac{1}{G_{zx}} \end{bmatrix} \begin{Bmatrix} \sigma_x \\ \sigma_y \\ \sigma_z \\ \tau_{xy} \\ \tau_{yz} \\ \tau_{zx} \end{Bmatrix}$$

$$\{\varepsilon\} = [C] \{\sigma\}$$

Where

$$G_{xy} = \frac{E_{xy}}{2(1+\nu_{xy})}, \qquad G_{xy} = \frac{E_{yz}}{2(1+\nu_{yz})} \qquad \text{and} \qquad G_{xy} = \frac{E_{zx}}{2(1+\nu_{zx})}$$

However, because the model is 2-D, z terms are cancelled and matrix C is reduced to the following.

$$\begin{Bmatrix} \varepsilon_x \\ \varepsilon_y \\ \gamma_{xy} \end{Bmatrix} = \begin{bmatrix} \frac{1}{E_x} & -\frac{\nu_{yx}}{E_y} & 0 \\ -\frac{\nu_{xy}}{E_x} & \frac{1}{E_y} & 0 \\ 0 & 0 & \frac{1}{G_{xy}} \end{bmatrix} \begin{Bmatrix} \sigma_x \\ \sigma_y \\ \tau_{xy} \end{Bmatrix} \qquad (5.3.1)$$

$$\{\varepsilon\} = [C] \{\sigma\}$$

Hence, there are now only 4 independent terms E_x, E_y, G_{xy} and poisson's ratio, $\nu_{xy} = \nu_{yx}$ are required. The strength values assigned to the timber are obtained from BS5268 Part II[38].

Modulus of timber parallel to the grain $E_{T//} = 7400 Nmm^{-2}$

In the absence of test data the modulus of timber perpendicular to the grain is assumed to be a 20th of the modulus parallel to the grain[44], therefore

$$E_{T\perp} = \frac{7400}{20} = 370 Nmm^{-2}$$

Therefore,

$E_{T\perp} = E_y$ and $E_{T//} = E_x$

The poisson's ratio $\nu_{xy} = \nu_{yx} = 0$ are assumed as there is no data available for this parameter. The timber is assumed to be linear throughout the load history therefore no plastic laws are implemented into this material. Plane 42 type element is used to mesh the timber, which has 2 degrees of freedom per node. The mesh design for the timber at all 4 connections are presented at the end of this chapter in Fig. 5.3.6 – 5.3.9. At this stage the timber members have no relationship with each other and the model is incomplete and connected via the joint as presented next.

Connection model

Shell elements used to represent the connections are established using existing nodes on the mesh, i.e. elements representing timber. The total area of elements is exactly that of the area of the plate as shown in Fig. 5.3.6 – 5.3.9 by a thick black line. The connection is idealised as shell elements because the physical nature of the protruding nails resembles a thin plate. The shell elements are used to represent the overall behaviour of the semi-rigid joint. The strength parameters of the shell elements are derived from joint test results and will be a bilinear model representing the initial strength moduli, yield stress and tangent modulus of the joint. A sample of the derivation from the heel joint test is now presented.

For the heel joint, the failed face is at the top chord and the calculation is as follows:

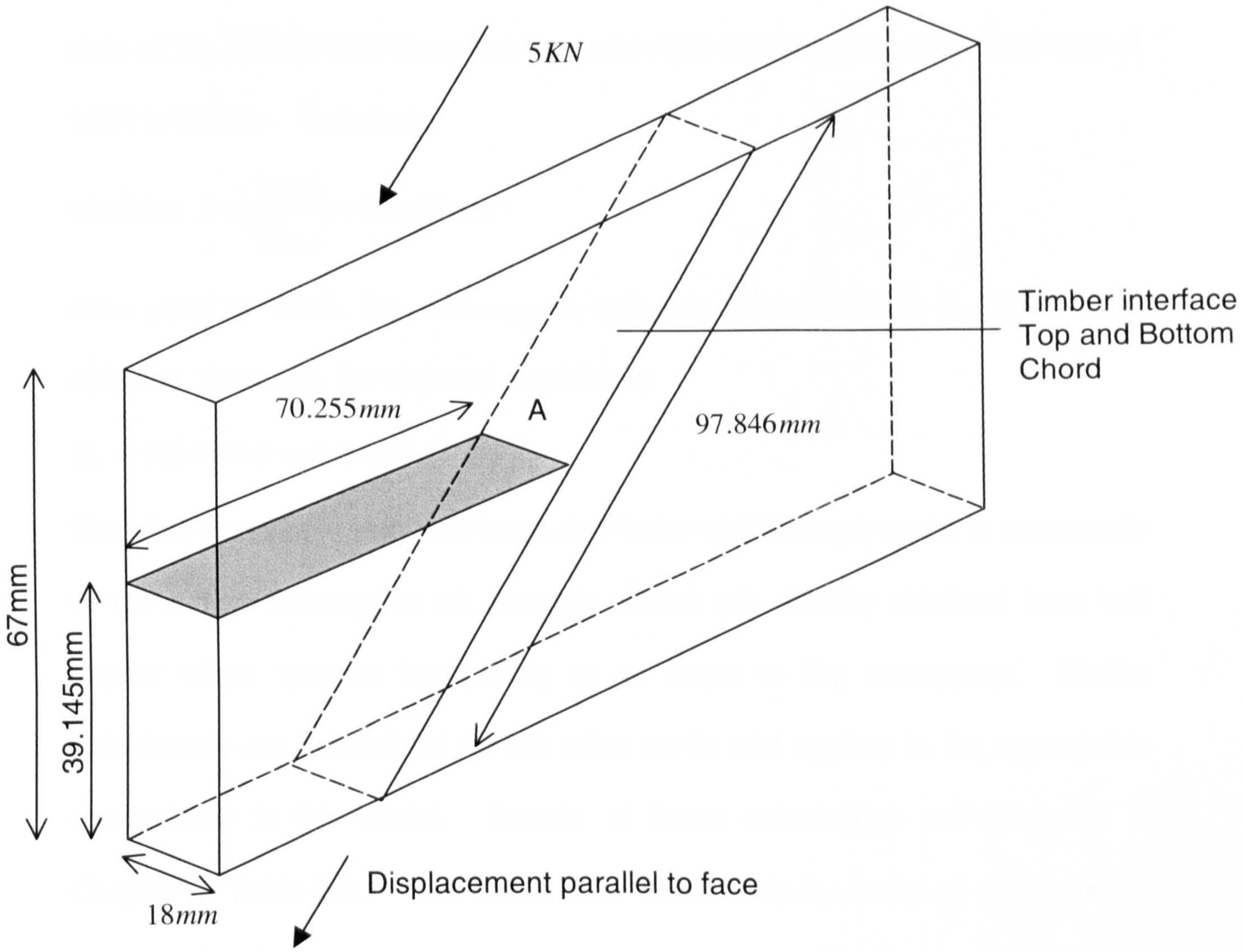

Fig. 5.3.2 – Nail plate interaction shell idealisation

As presented in the results in Chapter 6, Fig. 6.3.2, the yield load for the heel joint test (HJTM5) subjected to pure axial loading is 10KN. The thickness of 18mm represents the total length of the nails on 2 plates, i.e. 9mm per plate as detailed in Appendix B2.

Hence,

Yield stress on shaded area A, $\sigma_y = \frac{10\times10^3}{18\times70.255} = 7.908 Nmm^{-2}$

The distance, 39.145mm from the bottom of the plate to area A is considered to be the mutual point, i.e. the y centroidal distance. As indicated, the length of interface between the top and bottom chord is 97.8mm. Load displacement plots of the HJTM5 test show that the semi-rigid displacement at an axial load of 10kN is 3.5mm. Therefore,

Modulus $E = \frac{7.908}{3.5/97.846} = 221.1 Nmm^{-2}$

After yield at 10kN, the subsequent stiffness of test HJTM5 is 0.2 of initial stiffness, therefore, the reduced modulus is

$E_T = 221.1 \times 0.2 = 44.2 Nmm^{-2}$

The shell element is assumed to be non-linear and isotropic and it is reasonable to make this assumption as strength values are directly obtained from test results which account for loading at an angle to the connection. Similar calculations are carried out for the other joints and applied to the appropriate connections in the model. Results of these calculations are tabulated in Chapter 6, Table 6.9.1. The constitutive relationship for the shell elements are presented as follows:

Referring back to Equation 5.3.1 for an orthotropic material, the C matrix is simplified. Only stress in xy plane are considered, these are the dominant stresses in the connection. Furthermore, for an isotropic material

$E = E_x = E_y = E_z$ and $\nu = \nu_{xy} = \nu_{xz} = \nu_{yz}$

Therefore, $G = G_{xy} = G_{xz} = G_{yx}$

Hence, there are only 2 independent coefficients for a 2-D isotropic material and C matrix can be written as

$$\begin{Bmatrix} \varepsilon_x \\ \varepsilon_y \\ \varepsilon_z \\ \gamma_{xy} \\ \gamma_{yz} \\ \gamma_{zx} \end{Bmatrix} = \begin{bmatrix} \frac{1}{E} & -\frac{\nu}{E} & -\frac{\nu}{E} & 0 & 0 & 0 \\ -\frac{\nu}{E} & \frac{1}{E} & -\frac{\nu}{E} & 0 & 0 & 0 \\ -\frac{\nu}{E} & -\frac{\nu}{E} & \frac{1}{E} & 0 & 0 & 0 \\ 0 & 0 & 0 & \frac{1}{G} & 0 & 0 \\ 0 & 0 & 0 & 0 & \frac{1}{G} & 0 \\ 0 & 0 & 0 & 0 & 0 & \frac{1}{G} \end{bmatrix} \begin{Bmatrix} \sigma_x \\ \sigma_y \\ \sigma_z \\ \tau_{xy} \\ \tau_{yz} \\ \tau_{zx} \end{Bmatrix}$$

$$\{\varepsilon\} = [C] \{\sigma\}$$

Again, omitting stresses in components in the z direction for 2-D analysis gives

$$\begin{Bmatrix} \varepsilon_x \\ \varepsilon_y \\ \gamma_{xy} \end{Bmatrix} = \begin{bmatrix} \frac{1}{E} & -\frac{\nu}{E} & 0 \\ -\frac{\nu}{E} & \frac{1}{E} & 0 \\ 0 & 0 & \frac{1}{G} \end{bmatrix} \begin{Bmatrix} \sigma_x \\ \sigma_y \\ \tau_{xy} \end{Bmatrix}$$

(5.3.2)

$$\{\varepsilon\} = [C] \{\sigma\}$$

$$G = \frac{E}{2(1+\nu)}$$

Thus E is the initial modulus of the connection. The poisson's ratio $\nu = 0$ as there is no data available for the poisson ratio of the plate with holes associated with punched nails.

Where non-linear plastic behaviour is observed in the connection the following plastic laws are implemented to account for this response. ANSYS provides built-in plastic laws to model plastic behaviour in materials. The connection at hand is not a material as such and requires an examination of $\sigma - \varepsilon$ curves to suit results presented in Chapter 6. For this the BKIN function for bilinear

kinematic hardening is used. This is a bilinear $\sigma - \varepsilon$ curve as presented in Fig. 5.3.3 used to represent plastic behaviour.

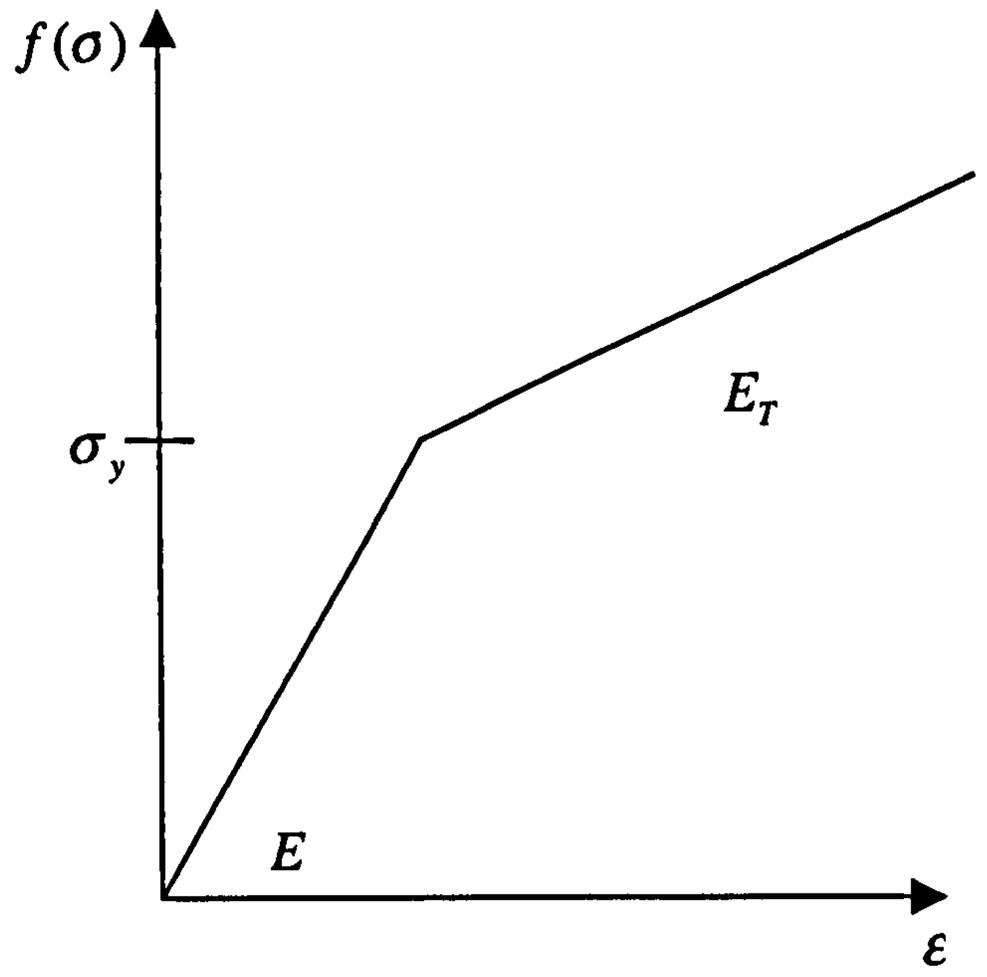

Fig. 5.3.3 – Bilinear Kinematic model

BKIN uses the von Mises failure criterion to locate the general failure stresses, σ. This criterion determines whether the material has reached its yield point or not and can be plotted onto a 2-D stress space as illustrated in Fig. 5.3.4.

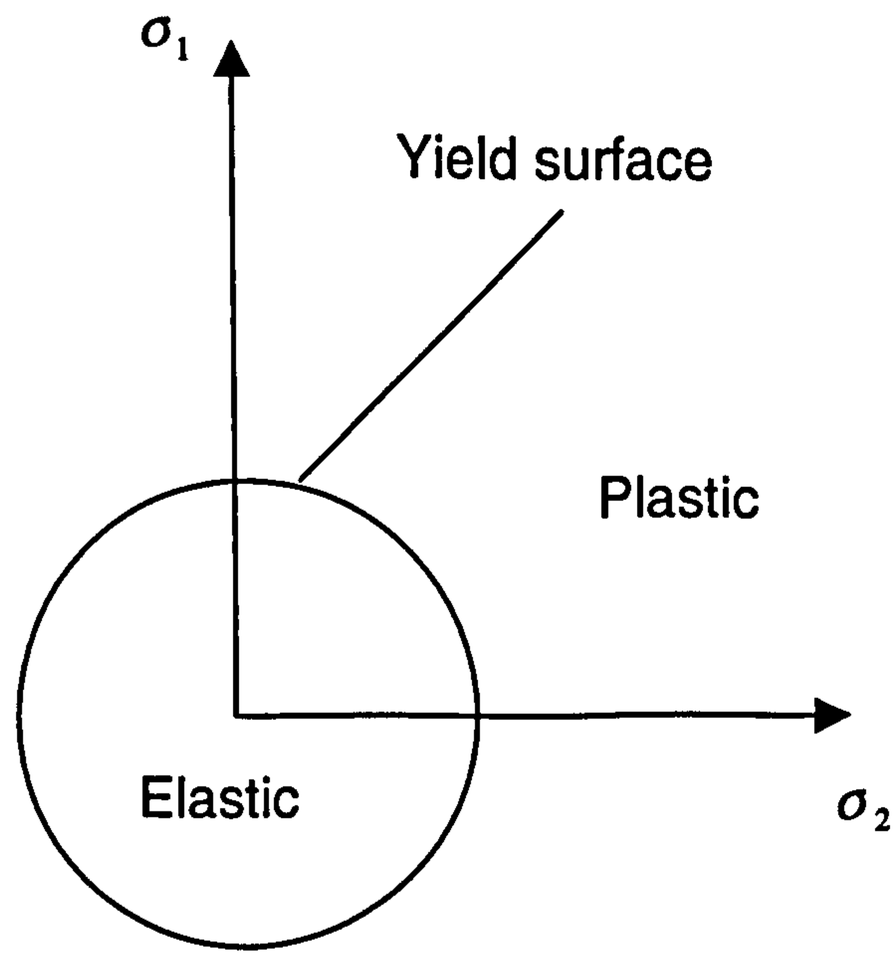

Fig. 5.3.4 – Von Mises failure surface

The equation for this criterion is:

$$F = \left[\frac{3}{2}(\{s\}-\{\alpha\})^T [M](\{s\}-\{\alpha\})\right]^{\frac{1}{2}} - \sigma_y = 0$$

where the Deviatoric stress vector,

$$\{s\} = \{\sigma\} - \sigma_m [1 \quad 1 \quad 0 \quad 0 \quad 0 \quad 0]^T$$

The mean stress, $\sigma_m = \frac{1}{2}(\sigma_x + \sigma_y)$

And yield surface shift $\alpha = \int C\{d\varepsilon^{pl}\}$

C is the constitutive relationship as established in Equation 5.3.2.

Any stress state inside the circle is elastic and analysis can continue as normal. However, once the stress state reaches the circle or beyond, i.e. $F = 0$ or $F > 0$, the yield criterion is no longer valid and a new criterion is formed for subsequent stress states, i.e. material behaviour beyond yielding as indicated by σ_y in Fig. 5.3.3. Part of the formation of this new circle is determined through a hardening law. In this particular model, kinematic hardening is used. This simply involves shifting the circle as shown below.

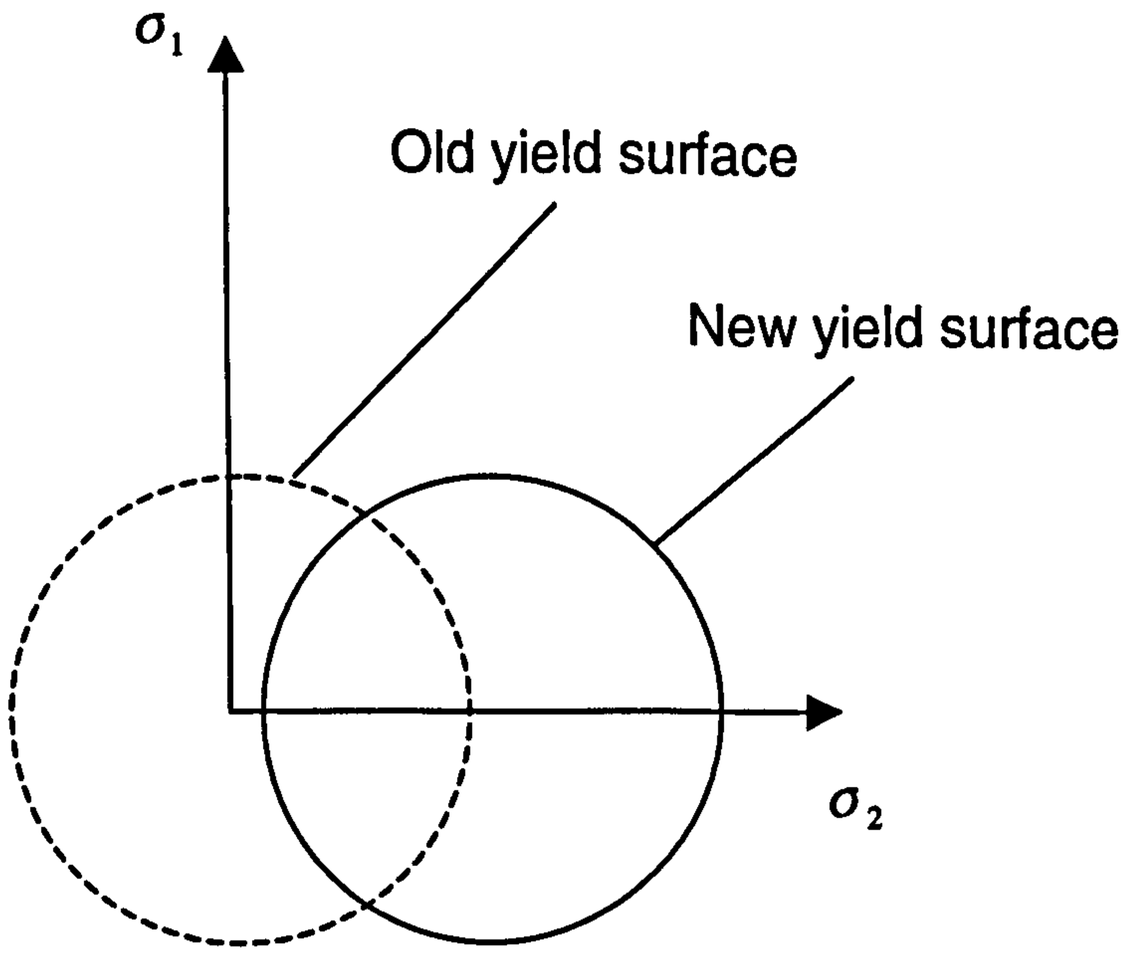

Fig. 5.3.5 – Kinematic Hardening

The direction in which the circle shifts is determined by an associated flow rule.

$$\frac{\partial F}{\partial \sigma} = \frac{3}{2\sigma_e}(\{s\} - \{\alpha\})$$

The direction of the movement is normal to the yield surface and is defined as the plastic strain. The above equations are implemented by ANSYS program[46].

Contact model

The length of the gaps of abutting joints at the connection are assumed to be zero as this is the case in the tests. The connections are made to fit exactly to rule out any effects of gaps between members. Whilst tensile loads are not affected by gaps, compression members certainly are. This could complicate analysis as the plate may buckle near or at the gap and thus may require a more complex plastic theory. Potentially, gaps can also weaken the strength of the joint. The effect of abutting joints and friction between these members are accounted for in the model. Contact elements are placed between nodes on one member to another at every joint in the truss where potentially compression and friction can occur.

The contact 12 element is used to model contact behaviour. This is a node to node contact where an element with stiffness and friction properties is defined between abutting members at the nodes. The following properties are used for the contact element.

The bearing strength across the grain of the timber is the compression stress perpendicular to the grain and similarly for parallel to the grain. The contact surface angles varies for each connection and an appropriate value of compression strength for each surface depending on the angle can be calculated using the Hankinsons formula[33].

Hence,

Compression parallel to the grain[38] $\sigma_{//} = 8.2 Nmm^{-2}$

Compression perpendicular to the grain[38] $\sigma_{\perp} = 2.5 Nmm^{-2}$

The Hankinson's formula is normally used to determine loads at angles to the grain, but here it is used for stresses at angle to the grain instead and can be presented as follows:

$$\sigma_{\alpha} = \frac{\sigma_{//}\sigma_{\perp}}{\sigma_{//}\sin^2\alpha + \sigma_{\perp}\cos^2\alpha}$$

α is the angle to the grain. This bearing angle can be determined. However, because connections have different member angles faces abutting, the weaker stress angle is adopted. Only abutting members in compression are considered. The bearing angles for the respective connection is tabulated as follows:

Joint Type / Member	Heel		Crown	Top chord		Bottom chord			
	Bottom Chord	Top Chord	Top Chord	Top Chord	Web	Centre Web	Side Web	Side Web	Bottom Chord
α	0	34	0	68	0	56	0	0	34
σ_{α}	8.200	**4.787**	**8.200**	**2.770**	8.200	**3.194**	8.200	8.200	**4.787**
Contact area(mm^2)		6071.3	4095.105	2717.9		672.221			3509.9
No of contacts		14	8	13		4			8
Contact strength(N)		2076	4197.483	579.18		536.823			2100.3

Table 5.3.1 – Contact element parameters

The selected contact stress is then multiplied by the contact area then divided by the number of contact nodes in that area. Since there is no data available for timber friction a value of 0.4 for Coulomb coefficient of friction is adopted from Eshbach as published in Vatovec *et al*[6]. The red lines in the following illustrations show where contact elements are placed at each connection

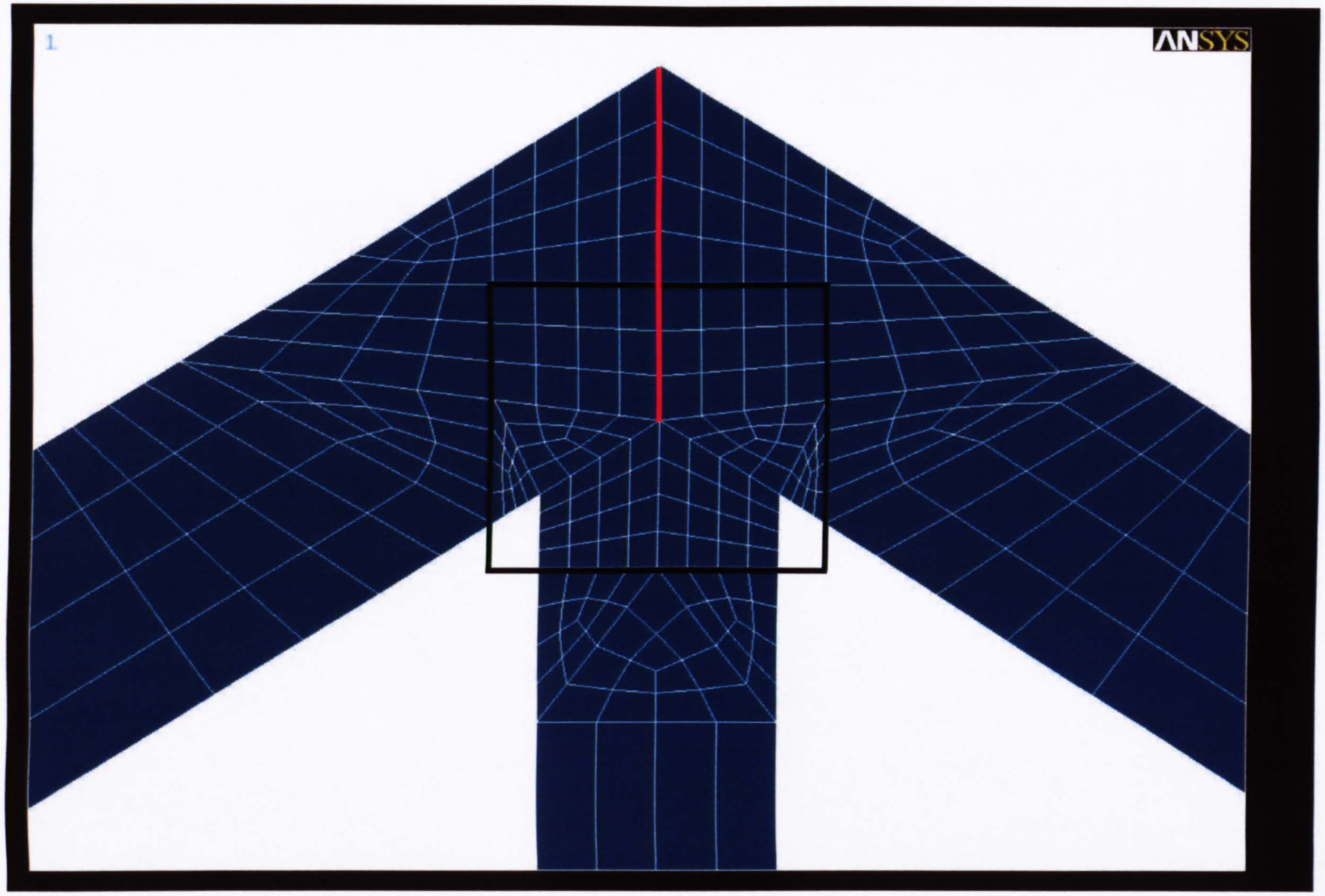

Fig.5.3.6 – Crown joint finite element model

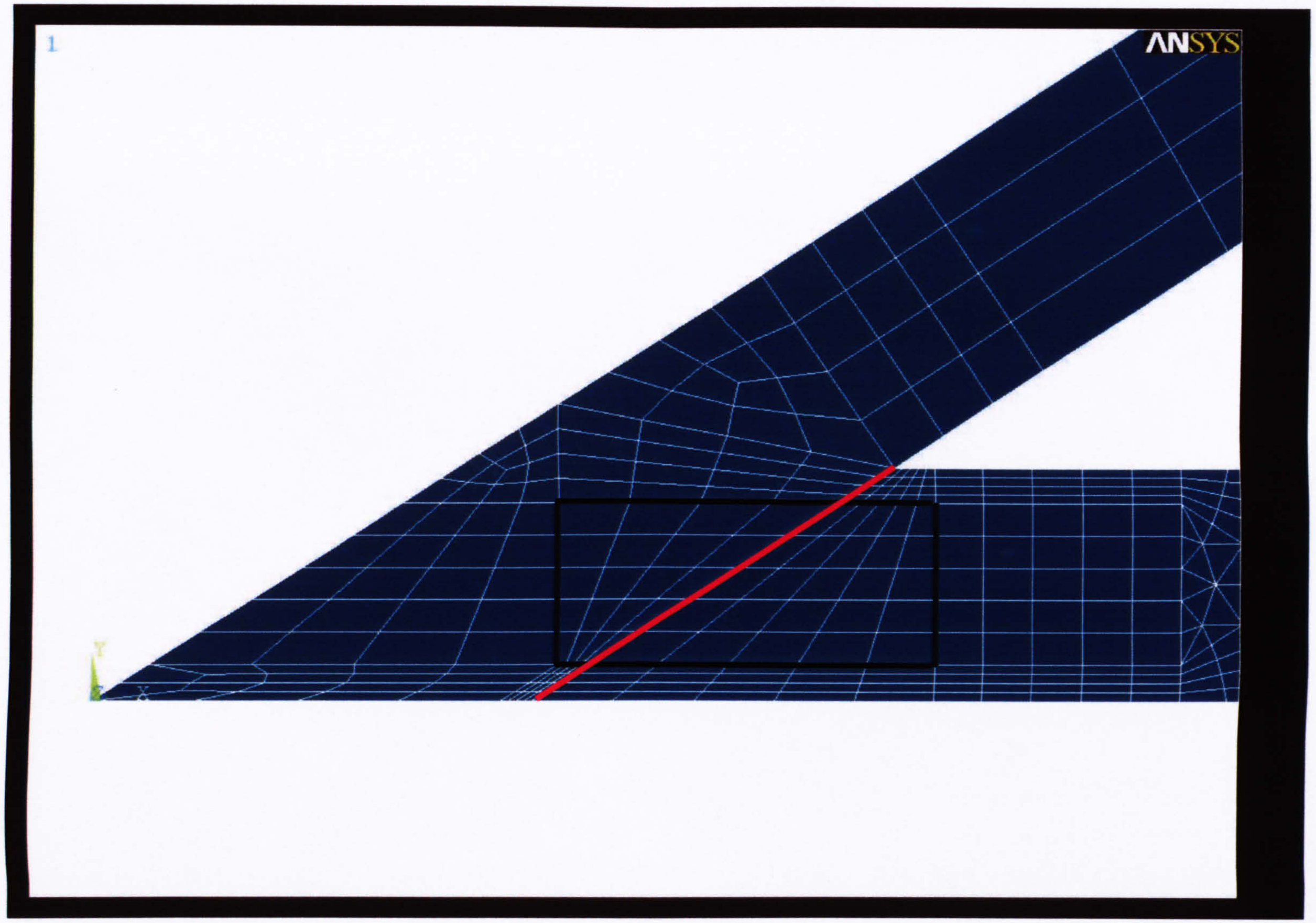

Fig. 5.3.7 – Heel Joint Finite element model

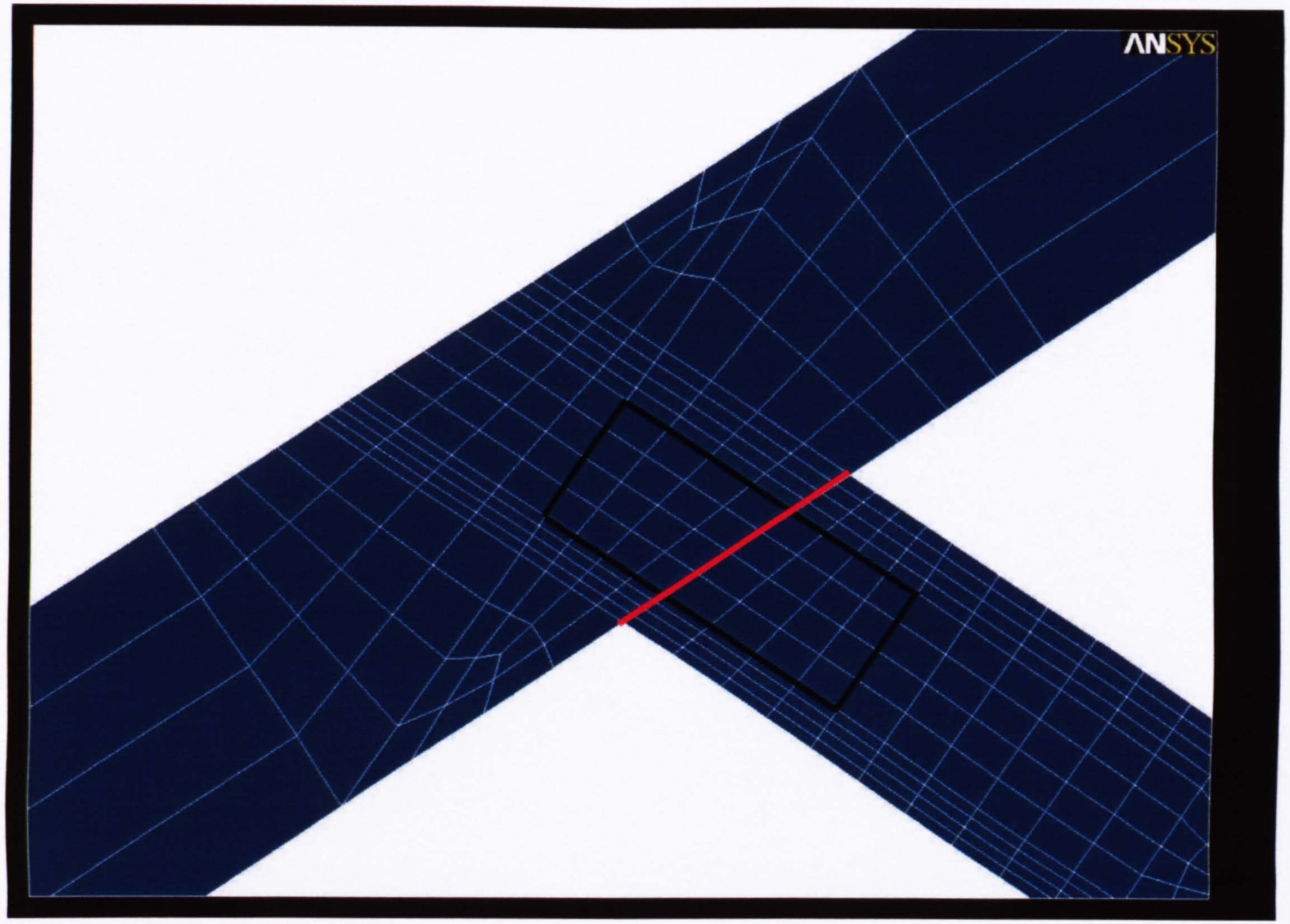

Fig, 5.3.8 – Top chord joint Finite element model

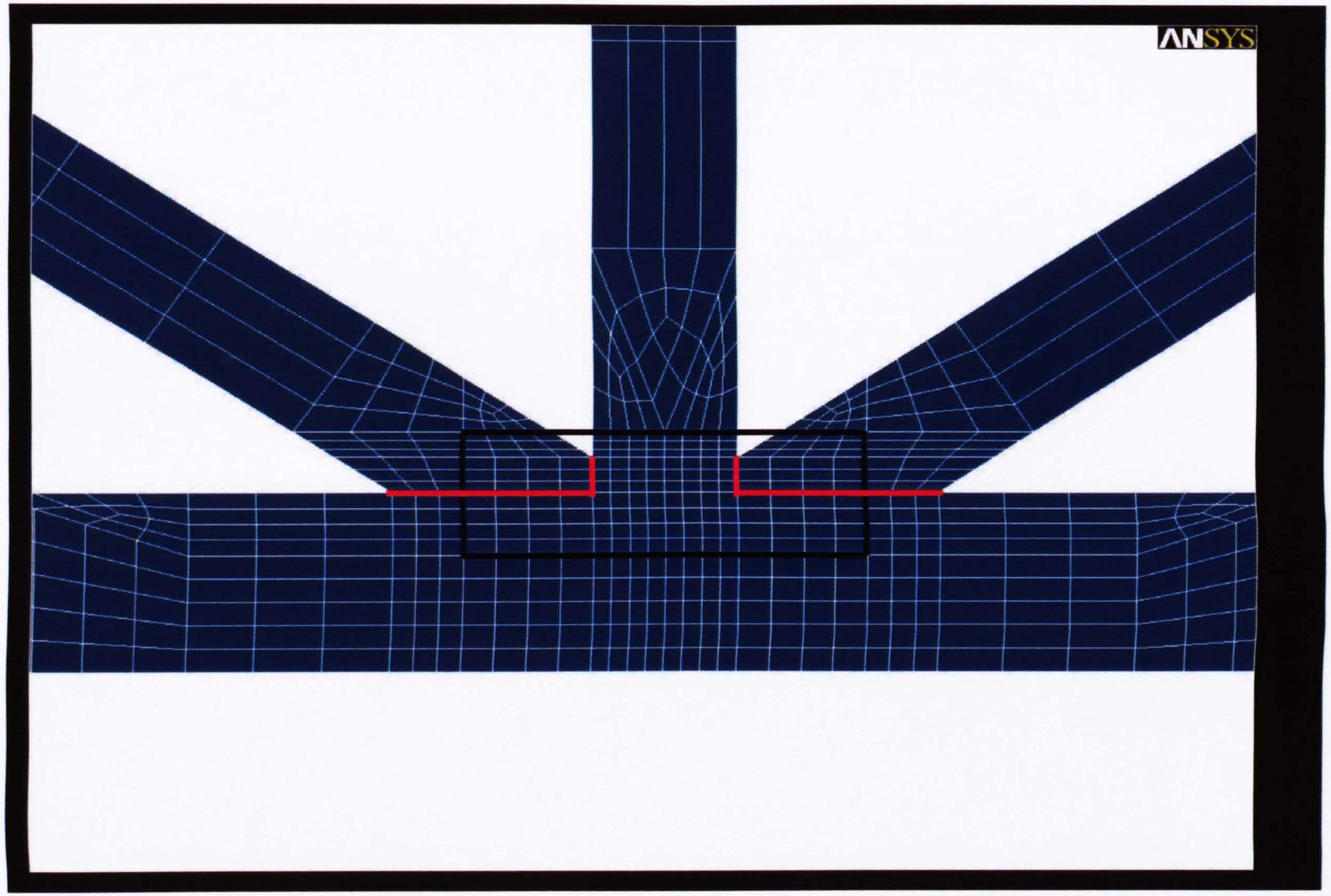

Fig 5.3.9 – Bottom chord joint Finite element model

This Chapter described the finite element idealisation model. The results are presented in the next Chapter.

Chapter 6

Results and Discussion

6.1 Laboratory Experimental test

This Chapter presents the results of the joint tests and full scale truss test. Two types of tests are conducted for each joint. The first is the constant bending moment test, where bending moment is applied to the joint to a desired level and then held. This is followed by the application of axial loads until failure. For the second type of test, axial loads are increased to a desired level and held, followed by an increase in bending moment until failure. For the two tests, 5 levels of bending moment and axial loads are selected for the constant bending moment and constant axial load tests respectively, which includes pure bending moment and pure axial load tests. The truss test consists of the application of three vertical load points to failure as discussed in Chapter 3.

The failures modes of these tests are discussed along with the effects of combined loads. A comparison of results of the full scale truss tests are made with the 2 models proposed in Chapter 3 and 4 followed by a conclusion.

It is emphasised that the primary aim of the joint tests was to obtain average rotational, axial and possibly shear stiffness, and not to define the true characteristics of the connections

6.2 Crown Joint test

Constant bending moment tests – CJTM series

The load pattern for each constant bending moment test is tabulated below. Bending moment is increased to the values indicated and held constant. Axial load is then increased till failure as indicated in the table. Tests CJTM1a is a pure axial loading test.

Test	CJTM1a	CJTM2	CJTM3	CJTM4	CJTM5
Constant B/M x 10^3(KNmm)	0	0.16	0.19	0.35	0.42
Max. Axial load (kN)	13.59	10.36	12.88	10.49	12.04

Table 6.2.1 – CJTM series test programme

Fig. 6.2.1 shows a typically deformed plate for test series CJTM. In the image what remains is the top chord member of the crown joint. The web member has been detached under tensile loads. The nails at the edge of the plate failed by pull out, but more resistance was exhibited away from the edge through small chunks of timber taken out from the web member. Nail bending is more heavily displayed away from the edge of the plate with pairs of nails bending towards each other. The anchorage area of this face of the joint is very small which may explain the relatively low level of damage to the nails and the timber. The behaviour of the Crown joint in axial tension can be described as brittle as there is little warning of failure in the test as shown in Fig. 6.2.2. All the tests exhibit a relatively constant 'elastic' stiffness followed by sudden failure. This maybe explained by the interaction between the nails and the timber. The connection under such load in this configuration relies on the nails to stay straight. Once the nails bend at the edge of the plate, out-of-plane forces at the nail/timber occur. The only resistance to loads at these nails is the friction between the nail and timber. Once this is exceeded, continued failure progress throughout the nails in the plate occurs until no additional load can be sustained. These results

show that there is little influence of moment load on axial displacement and that axial stiffness remains mainly unaffected regardless of the level of bending moment. However, axial capacity decreases with increased bending moment although a firm pattern is not established. In tests CJTM3 and CJTM5, there is evidence of some embedding shortly after the application of load, shown by significant displacement, but less so in other tests. Embedding could be caused by loose contact between the tooth and the timber at parts of the joint.

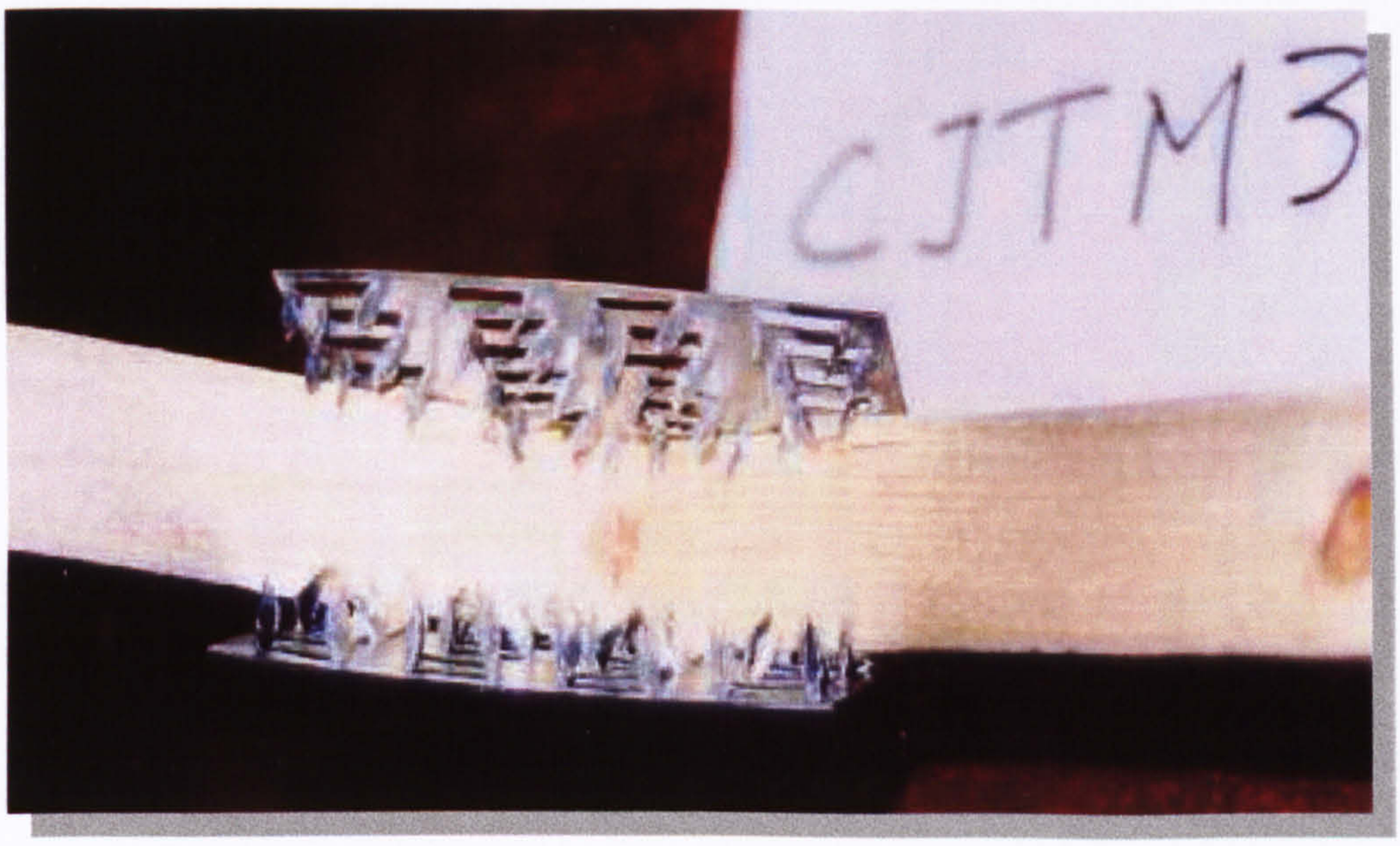

Fig. 6.2.1 – Tensile axial load failure

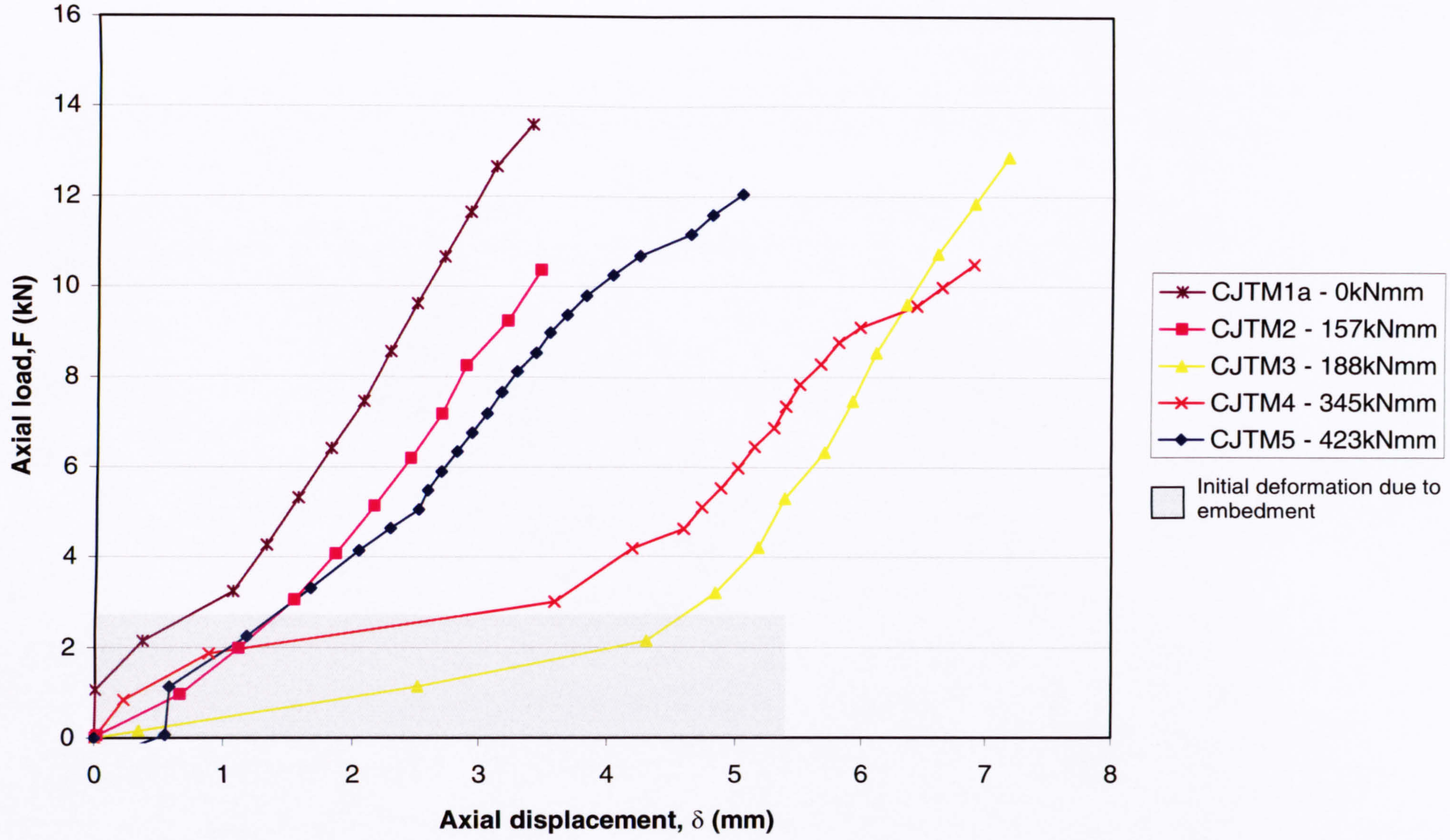

Fig.6.2.2 – Effect of bending moments on axial stiffness for Crown Joints

Constant axial load tests – CJTA series

In these tests the axial load remains constant where the bending moment is increased until failure. The axial load levels are tabulated below for each test with the failure bending moment. Test CJTA1 is a pure bending moment test.

Test	CJTA1	CJTA2	CJTA3	CJTA4	CJTA5
Constant Axial load (kN)	0.0	3.0	4.4	6.0	8.4
Max. B/M x10^3(kNmm)	0.51	0.53	0.47	0.53	0.58

Table 6.2.2 – CJTA series test programme

For the CJTA fixed axial loads test, more nail bending was displayed, which was in the direction of the bending moments. At failure, larger pieces of timber were fractured from the web member, some of which was from the nails at the edge of the plate, as shown in Fig. 6.2.3. However, as the results in Fig. 6.2.4 show, the behaviour is quite different from the CJTM tests. The curves show clearly ductile behaviour as indicated by the continued decrease in stiffness exhibited in all the tests. The stiffness represents the resistance by a group of nails interacting with the timber against the rotation of the joint. Once the capacity between the nail and timber is exceeded the connection yielded. The capacity of the nails in the timber progressively fails throughout the connection until no additional load is sustainable. This increased rate of movement towards the end gave clear warning of failure in the CJTA series tests more than that for the CJTM tests. However, tests CJTA3 exhibited brittle behaviour, which could possibly be contributed by some inconsistency in the timber strength.

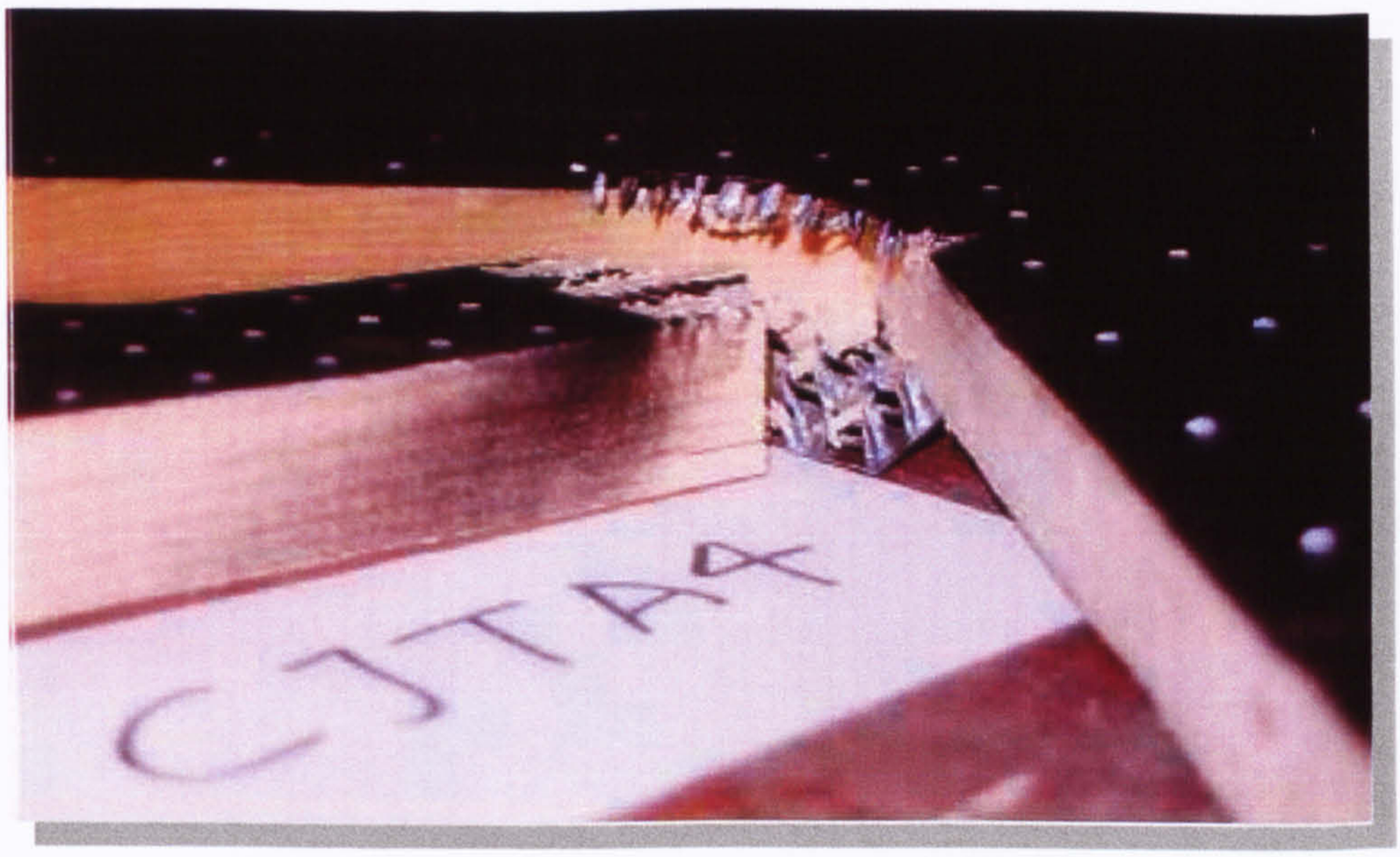

Fig. 6.2.3 – Bending moment load failure

There is some influence of axial loads on bending moments during the later stages of the tests. In fact tests with higher axial loading retain higher rotational stiffness and bending moment capacity during the latter stages of the test.

Dead weights of different magnitude (5kg, 10kg etc.) were used to apply bending moments. With the load increments available loads were gradually increased using different weight combinations which sometimes involved taking partial load off at times and reloading to avoid large load increments. For example, if the load was at 50kg and the next increment required was 55kg, a load of maybe 5kg would be taken off first. Subsequently, a load of 10kg would put on to make 55kg, thereby loading and unloading to achieve the right load increment. This was necessary due to the lack of dead weight increments. This occasional reduction in load is represented by kinks along the curve, for example test CJTA1.

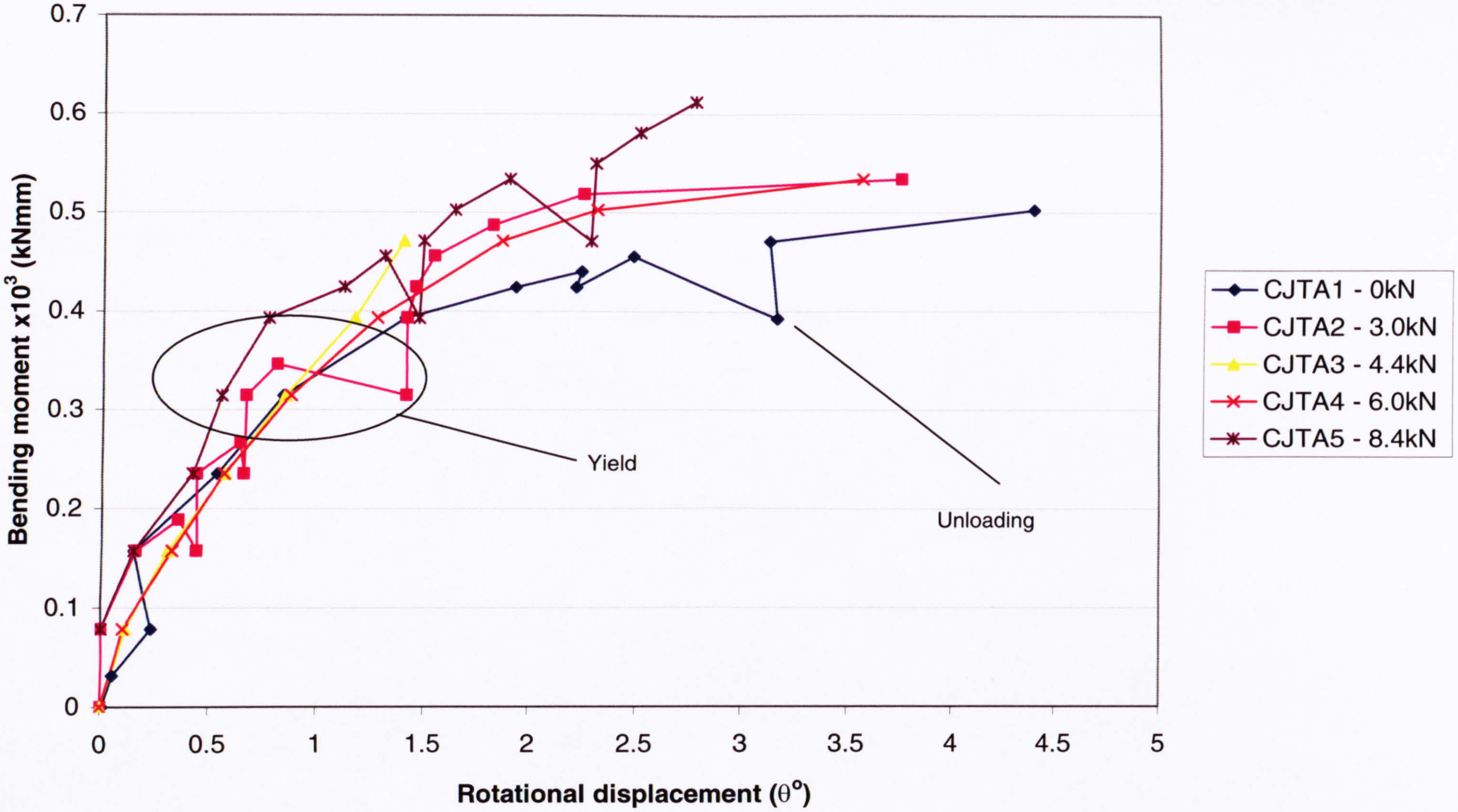

Fig.6.2.4 – Effect of axial loads on rotation stiffness for Crown Joints

6.3 Heel Joint Test

Constant bending moment tests – HJTM series

A similar test programme is adopted here as tabulated below for the constant bending moment test. Again the desired bending moment is achieved, followed by an increase in axial load until failure.

Test	HJTM5	HJTM1a	HJTM2	HJTM3	HJTM4
Constant B/M x10^3(kNmm)	0.0	0.2	0.4	0.6	0.9
Max. Axial load (kN)	12.11	15.88	17.66	15.23	23.32

Table 6.3.1 – HJTM series test programme

Plate failure was exhibited in all HJTM series tests. This is marked by a vertical snap from the top of the plate where the two members meet as shown below.

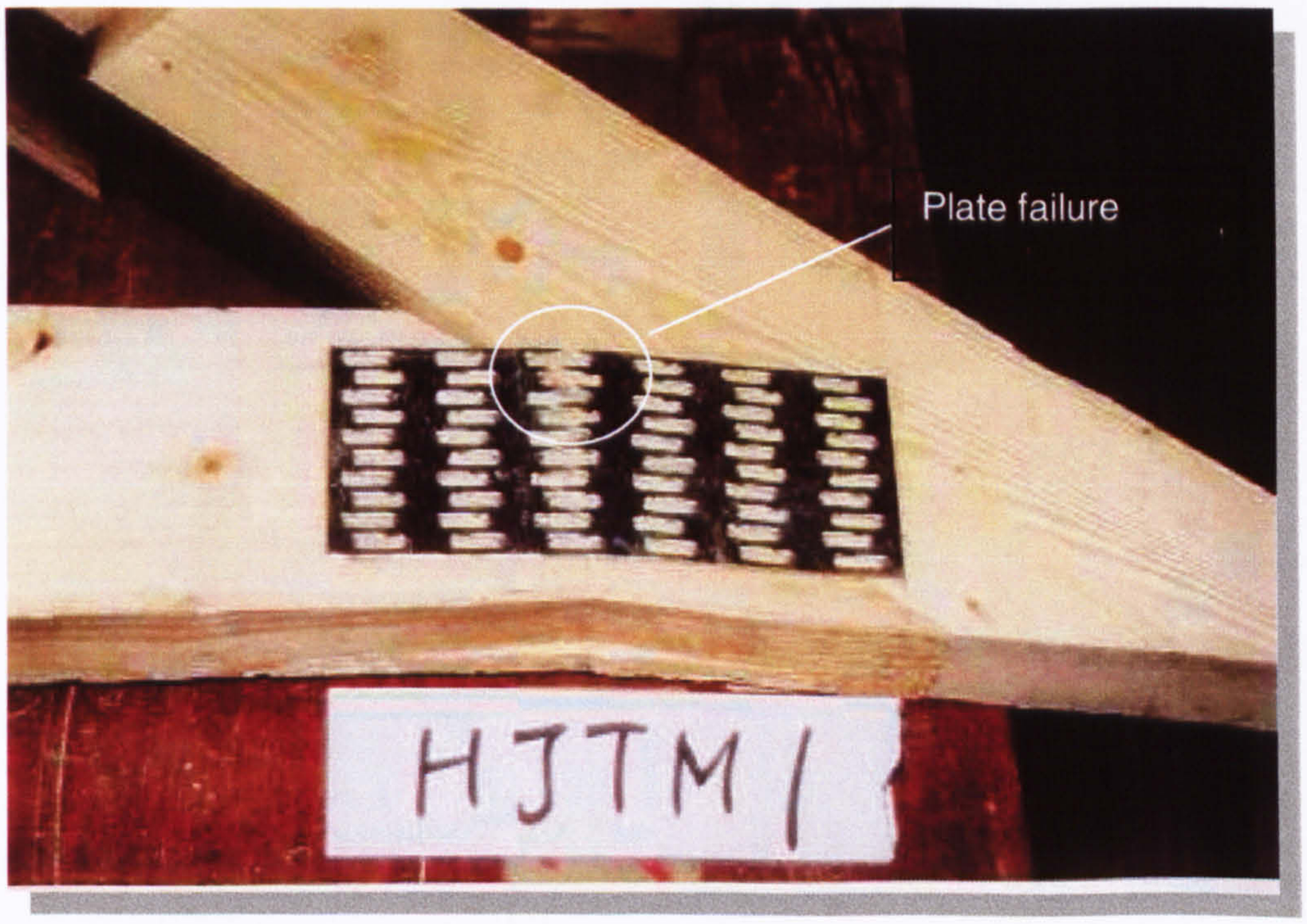

Fig. 6.3.1 – Typical plate failure for HJTM series test

In the crown joint test, axial loads produced a brittle response, whereas the same loads for the heel joint produced a ductile response. The explanation for this is that nails at the heel joint provide adequate strength for axial loads, which forces the failure to be at the plate, thus producing the ductile effect. The yield point in Fig. 6.3.2 is actually the plate yielding until such point, at the end of the curve, the plate snaps. The results of the HJTM series tests show that there is

some effect of bending moments on axial stiffness. As indicated in Fig. 6.3.2 the initial stiffness of all the tests are similar up to approximately 10–12.5kN. There is generally a kink at this point, which can be considered as the point where the connection yields and behaves in a plastic manner under a weaker axial stiffness for each joint. From this point, there is an increase in axial stiffness for connections with larger bending moments. A marked difference in stiffness between tests HJTM4 and HJTM5 is observed. Specimens in between the limits have similar stiffness. There is also generally an increase in the axial capacity of the heel joint. According to these results bending moment actually contributes to axial stiffness and capacity.

Although, in general it was observed that failure was initiated by pull out of the nails, in this instance, little or no pull out was exhibited. The failure of the plate suggests that nail strength was adequate as far as axial stiffness is concerned. Plate failure occurred at the point where the amount of material was minimal, i.e. in between the slots on the steel plate. Test HJTM3 and HJTM4 also exhibited similar failure characteristics but with the bottom and top chord torn off respectively. As seen in Fig. 6.3.1, the plate has only failed at the top.

The location of the wall plate is detailed in Appendix A1 Truss design in the wall plate design.

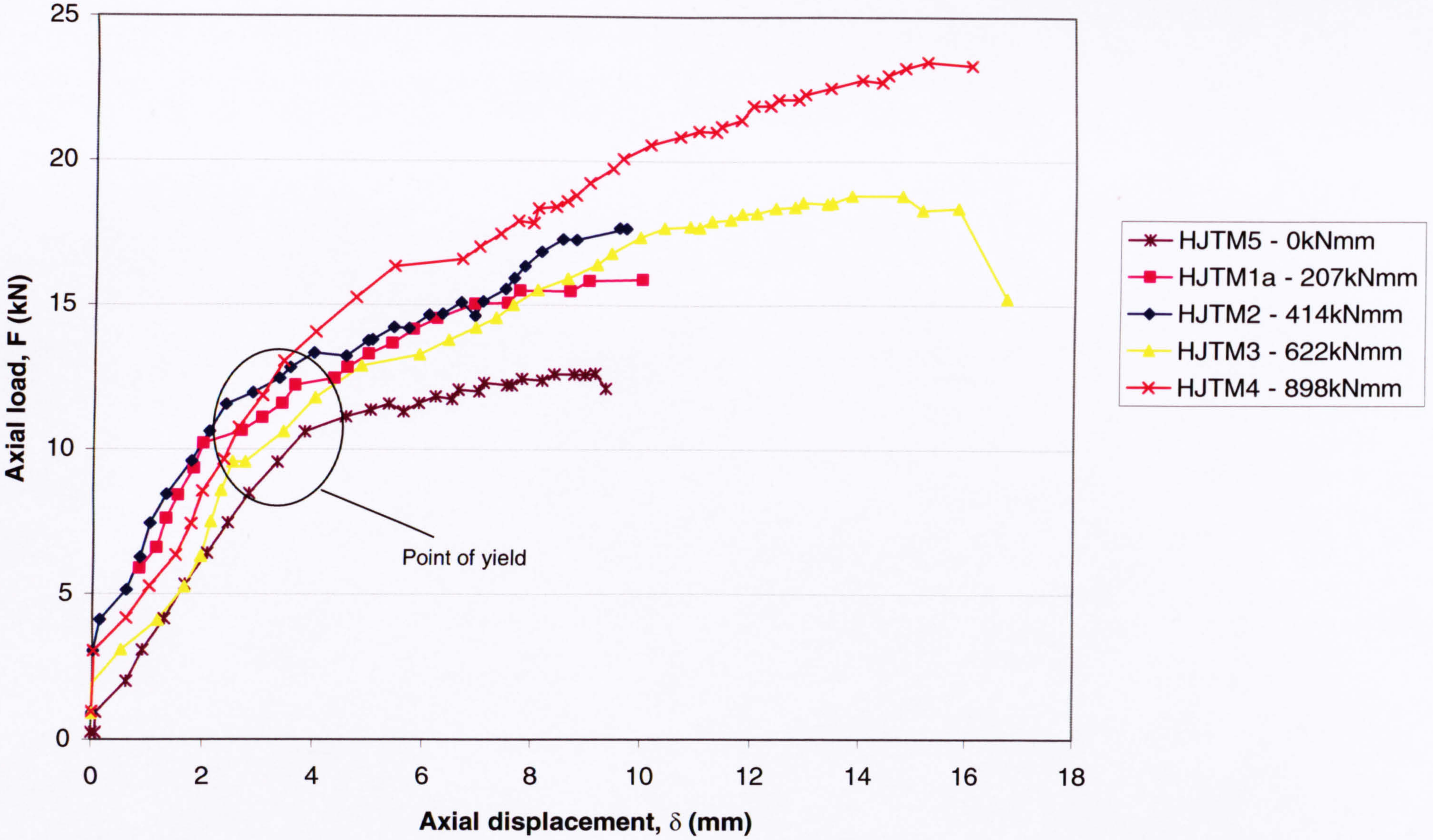

Fig. 6.3.2 – Effect of bending moments on Axial stiffness for Heel Joints

Constant axial load tests – HJTA series

The following test programme for the Heel joint constant axial load test is adopted.

Test	HJTA1e	HJTA2	HJTA3	HJTA4	HJTA5
Constant Axial load (kN)	0.0	2.9	6.2	9.5	10.6
Max. B/M x10^3(kNmm)	1.25	1.50	1.59	1.63	1.74

Table 6.3.2 – HJTA series test programme

The damage to the connection was predominantly at the top chord of the timber as shown in Fig. 6.3.3. Small deformation is observed at the corner of the plate. The mode of failure was splitting of the top chord member caused by tensile forces acting perpendicular to the grain situated near the corner of the plate due to the direction of the applied moments. It is postulated that the nails at this corner of the plate provide a weak point in the connection as far as bending moment is concerned. The direction of the bending moment encourages tensile forces to act perpendicular to the grain. Timber is very weak in this respect and the nail, which essentially introduces a void in the timber fibres encourages cracks to form.

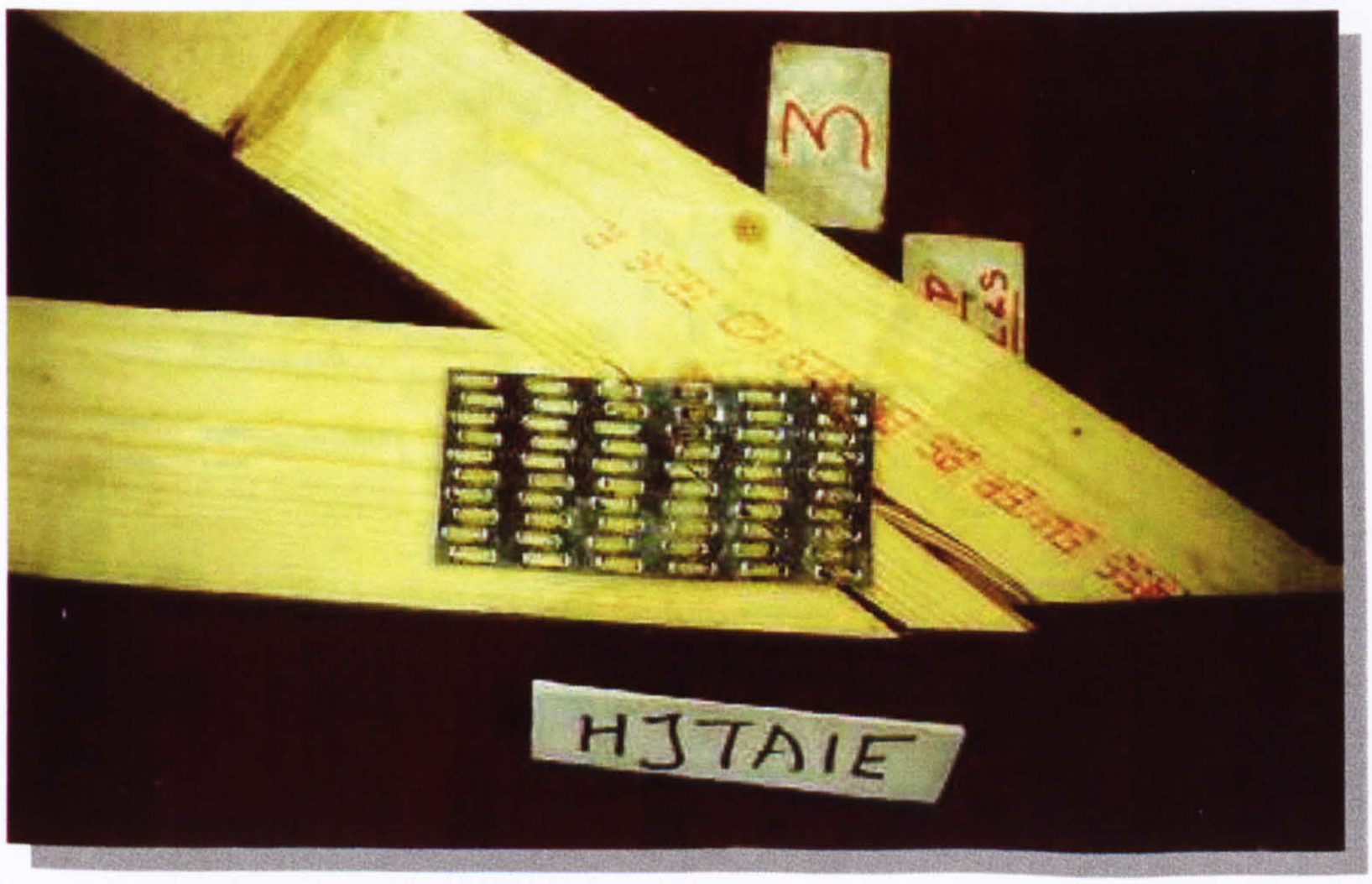

Fig. 6.3.3 – Failure mechanism for HJTA series test

The location of the crack was always near the corner of the plate because away from the corner of the plate, timber is held together by the increased number of nails. Thus, timber at the inner part of the plate is being held together by the nail plate. There was also some deformation of the plate as the nails bend as well. In general, the results in Fig. 6.3.4 show that the connection behaves in a ductile manner under bending moments. During the latter stages of the test, as bending moment level increases, a gradual decrease in rotational stiffness is observed.

There is some effect of axial loads on rotational stiffness. Initially, the tests exhibit similar rotational stiffness. As axial loads increase, the difference in rotational stiffness is more obvious. The failure loads shows distinctly the difference between the tests. The difference in axial load capacity of HJTA1e and HJTA5 is approximately 600kNmm.

Problems were encountered for the pure bending moment test HJTA1 and the test was subsequently repeated 4 times from HJTA1C through HJTA1F to test for strength consistency in the timber. Failure was consistently at a bending moment of 1.2kNmm. The results of all these tests are similar and can be found in Appendix C1. Only one sample from the test namely HJTA1e, has been used to represent pure bending moments in Fig. 6.3.3.

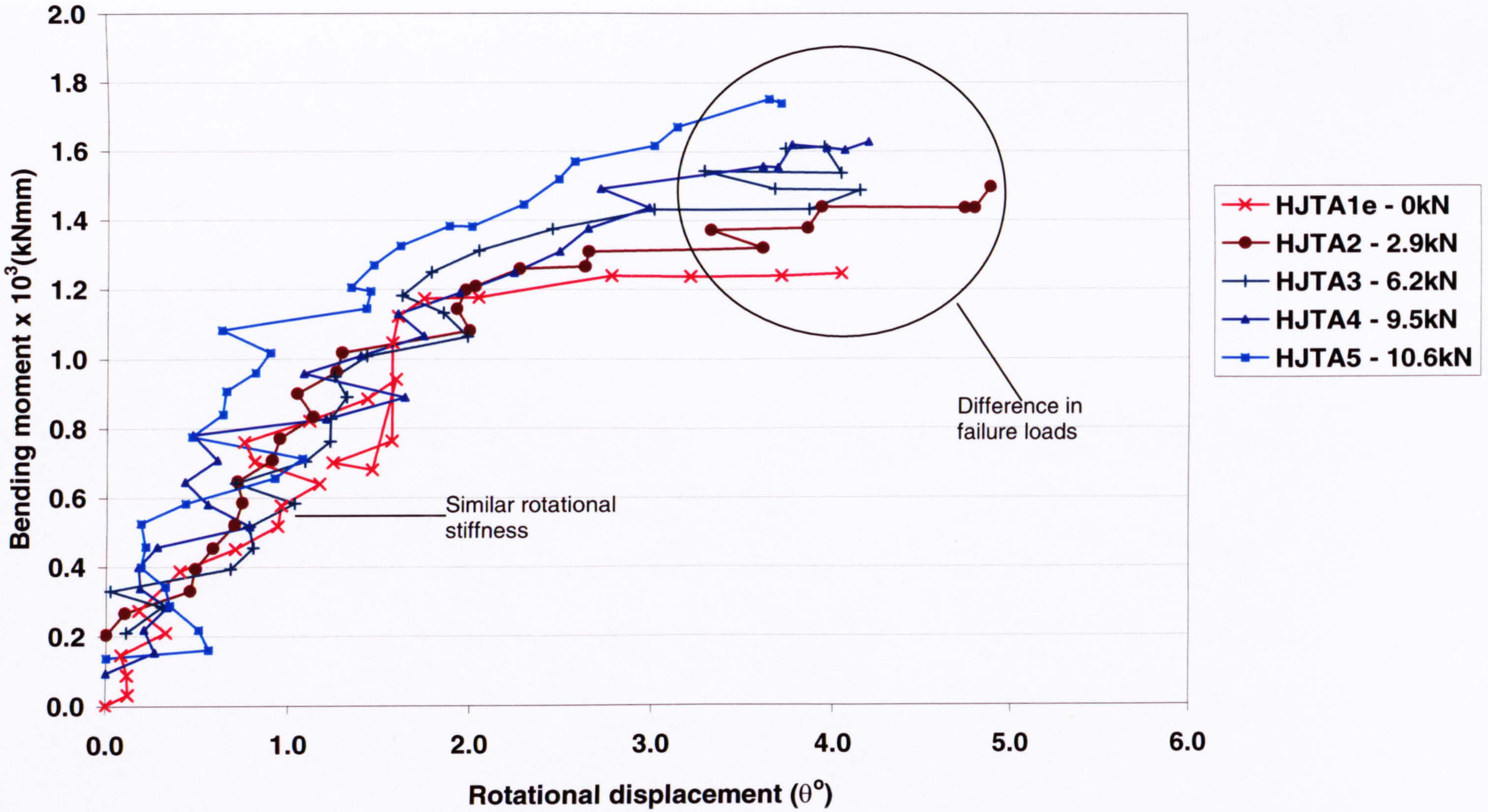

Fig. 6.3.4 – Effect of axial loads on rotation stiffness for Heel Joints

6.4 Top Chord Joint test

Constant bending moment tests – TCJTM series

Constant bending moment tests are conducted as tabulated below.

Test	TCJTM1	TCJTM2	TCJTM6	TCJTM3	TCJTM5
Constant B/M x10^3(kNmm)	0.00	0.14	0.20	0.26	0.30
Max. Axial load (kN)	13.87	14.4	17.42	7.86	4.39

Table 6.4.1 – TCJTM series test programme

For the TCJTM series with constant bending moment test, the failure was located at the top chord. The nail plate served more as shear connectors stopping the web from sliding as the axial loads were reacted by abutting members. However, as soon as crushing was about to occur some axial forces were distributed through the plate. A marked difference in axial load was observed for tests TCJTM1, TCJTM2, TCJTM6 compared to TCJTM3 and TCJTM5. Test TCJTM6 did not go with the trend, which is due to some variation in timber strength. The first three tests were literally direct bending moment test on the top chord with little bending moments at the joint as axial compression load was applied to the web member. The top chord failed in these tests and therefore dictated the capacity. The last two tests were subject to larger bending moments, which decreased the axial load capacity caused by tooth withdrawal and splitting of the timber but axial stiffness remains relatively the same for all the tests as seen in Fig. 6.4.2. The axial failure load is much lower for TCJTM5 due to large bending moments. The connection was probably close to failure in bending moment already, before the axial loads were applied. The results of all these tests, show a relatively linear response followed by a peak where yielding occurs except for test TCJTM5 where a brittle response is observed. The axial stiffness for these tests are consistent, which shows that bending moment has little effect of the axial stiffness of the joint.

But there is profound difference in the axial load capacity due to the difference in failure modes as discussed. As bending moment increases, the axial load capacity is reduced.

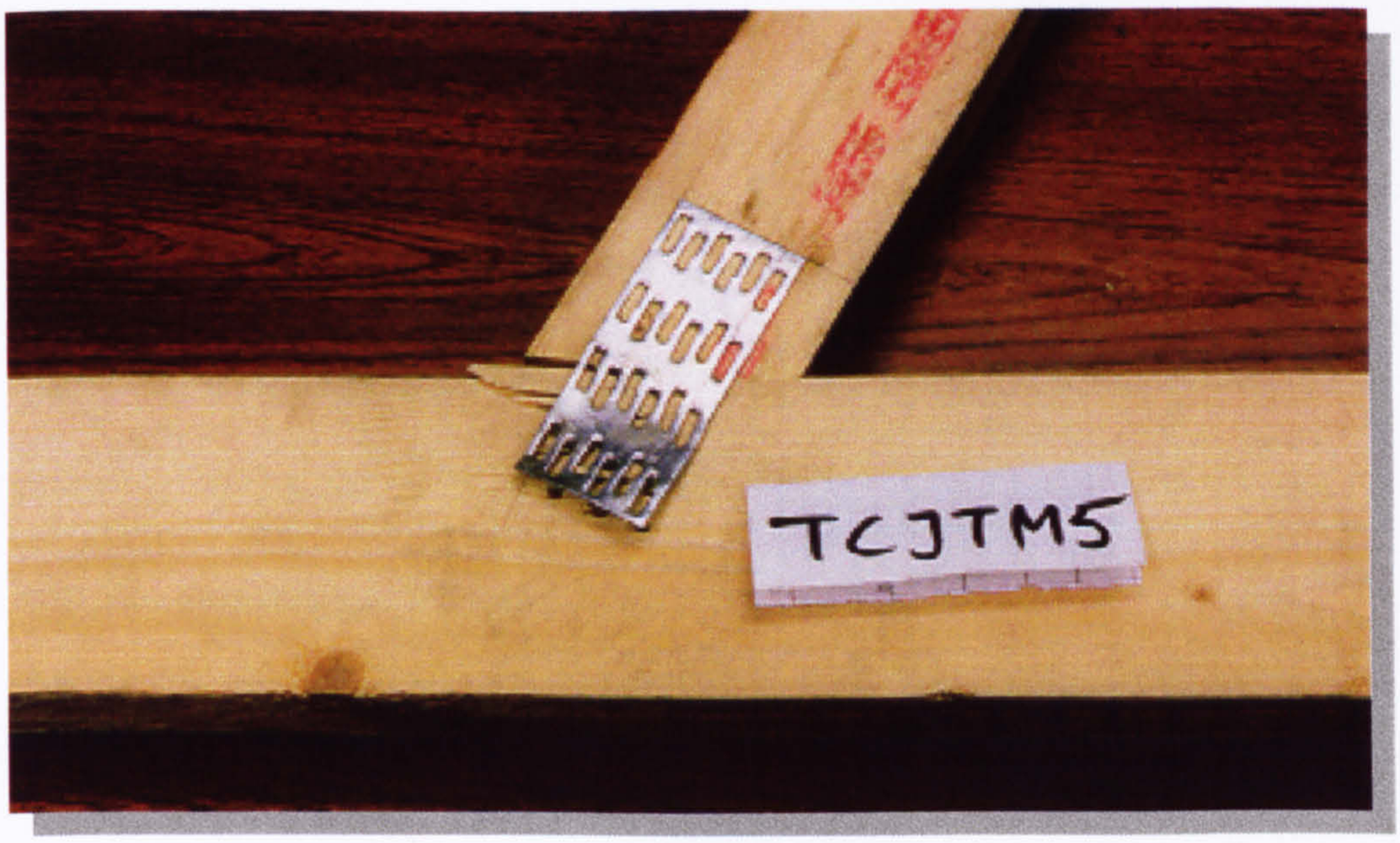

Fig. 6.4.1 – Failed test specimen from TCJTM5

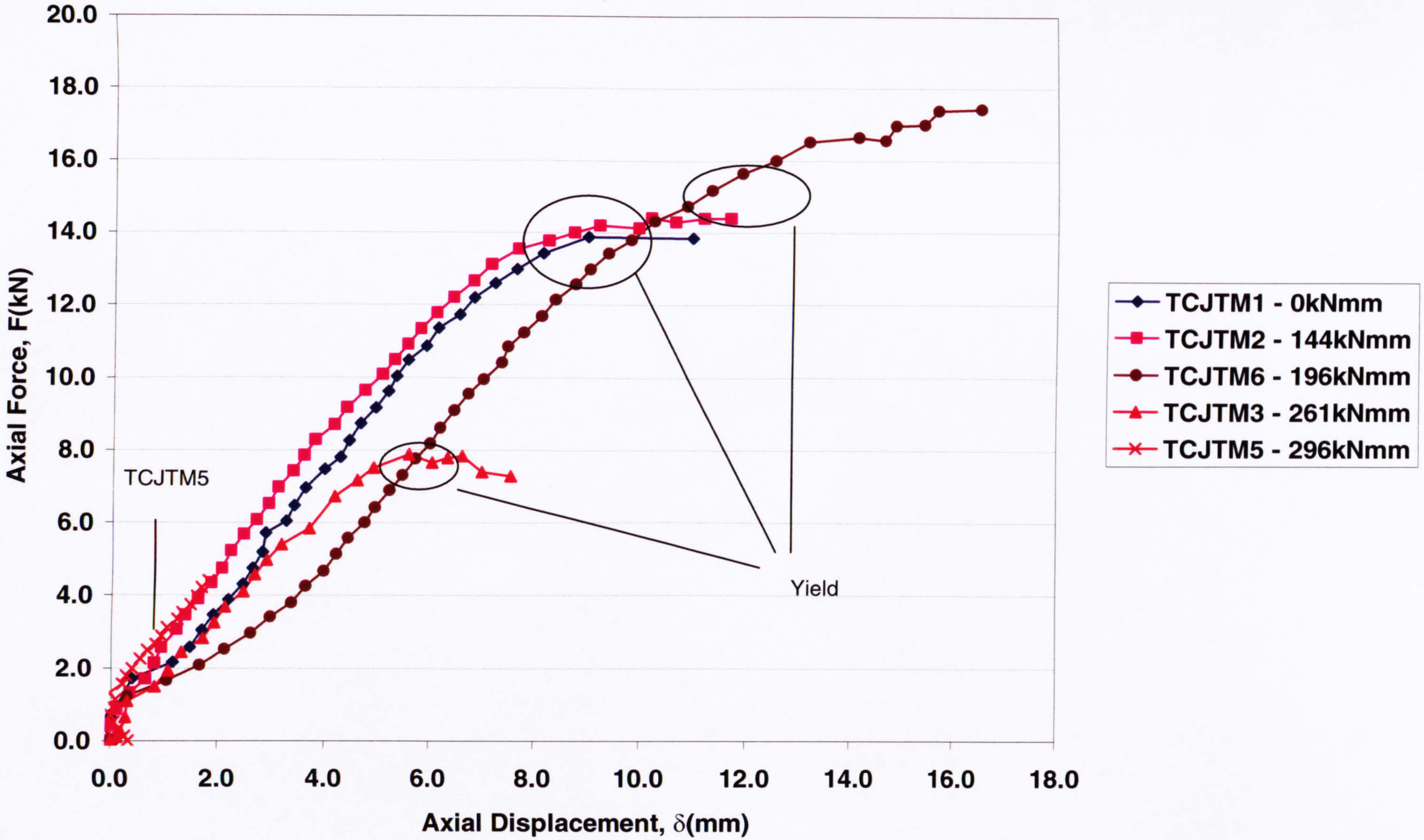

Fig. 6.4.2 - Effect of bending moment on axial stiffness for Top chord Joints

Constant axial load tests – TCJTA series

Constant axial load tests are conducted as tabulated below.

Test	TCJT5	TCJTA2	TCJTA3	TCJTA4	TCJTA6
Constant Axial load (kN)	0.0	4.3	4.9	9.9	13.0
Max. B/M x10^3(kNmm)	0.29	0.27	0.27	0.22	0.32

Table 6.4.2 – TCJTA series test programme

For the TCJTA series tests, plate failure in the form of buckling and tensile failure was observed at the plate. All tests exhibited tooth withdrawal and increased levels of timber crushing for increased axial loads. Fig. 6.4.3 shows a typical mode of failure where tensile failure occured at the plate.

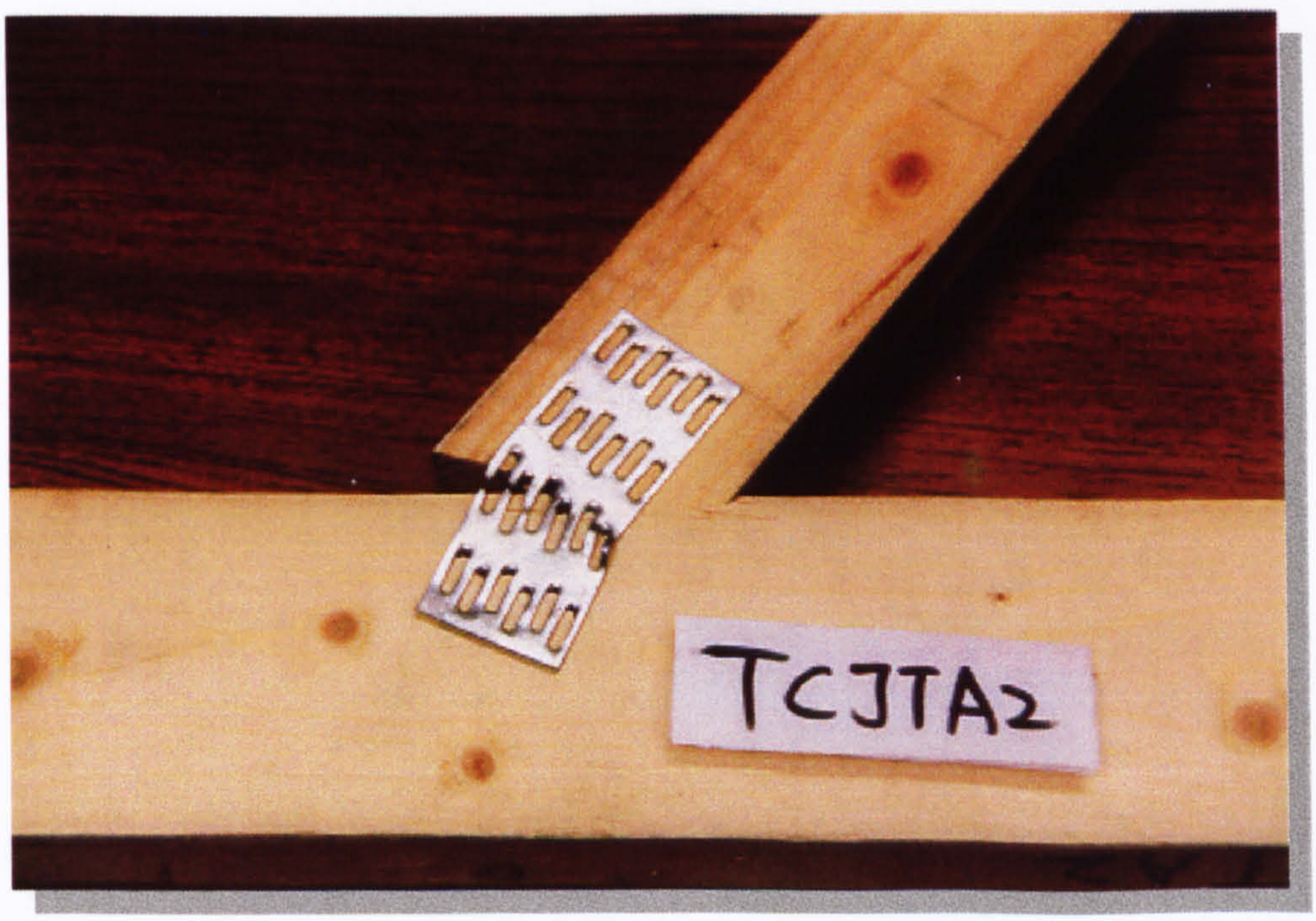

Fig. 6.4.3 – TCJTA2 connection failure

The results in Fig. 6.4.4 show that axial loads have only a little effect on the initial rotational stiffness of the connection. The connection initially acts linearly as the plate sustains the bending moment. It is observed from the figure that the point of yield for the plate is at approximately 225-250KNmm. Once the plate fails, timber crushing is initiated. This was followed by a decline in the stiffness due to the gradual crushing of the timber. It is in this region that the effects of axial load on rotational stiffness are noted. The rotational stiffness

decreases for higher levels of axial loads as increased axial loads encouraged timber crushing. In fact this behaviour had little to do with the joint itself as the mentioned trend is due to timber crushing under larger axial load where the connection has actually failed already at yield. The results show that the joint behaves in a ductile manner.

The result of test TCJTA6 differed from the set trend. Stiffness is initially higher followed by higher yield strength. The difference is due to the strength properties of the connection, which may be caused by variations in the strength of the timber. Further, variability was demonstrated in two other tests. The results of tests TCJTA4 and TCJTA5, which were repetitive, are compared in Fig. C1.1. The results of these two tests differ, even with identical load patterns with marked difference in capacity.

In addition to the tests reported, a brief investigation of the effects of compression load at the top chord to the axial stiffness of the member was carried out. Results shown in Fig C1.44 are inconclusive due to different response, which is possibly due to timber variations.

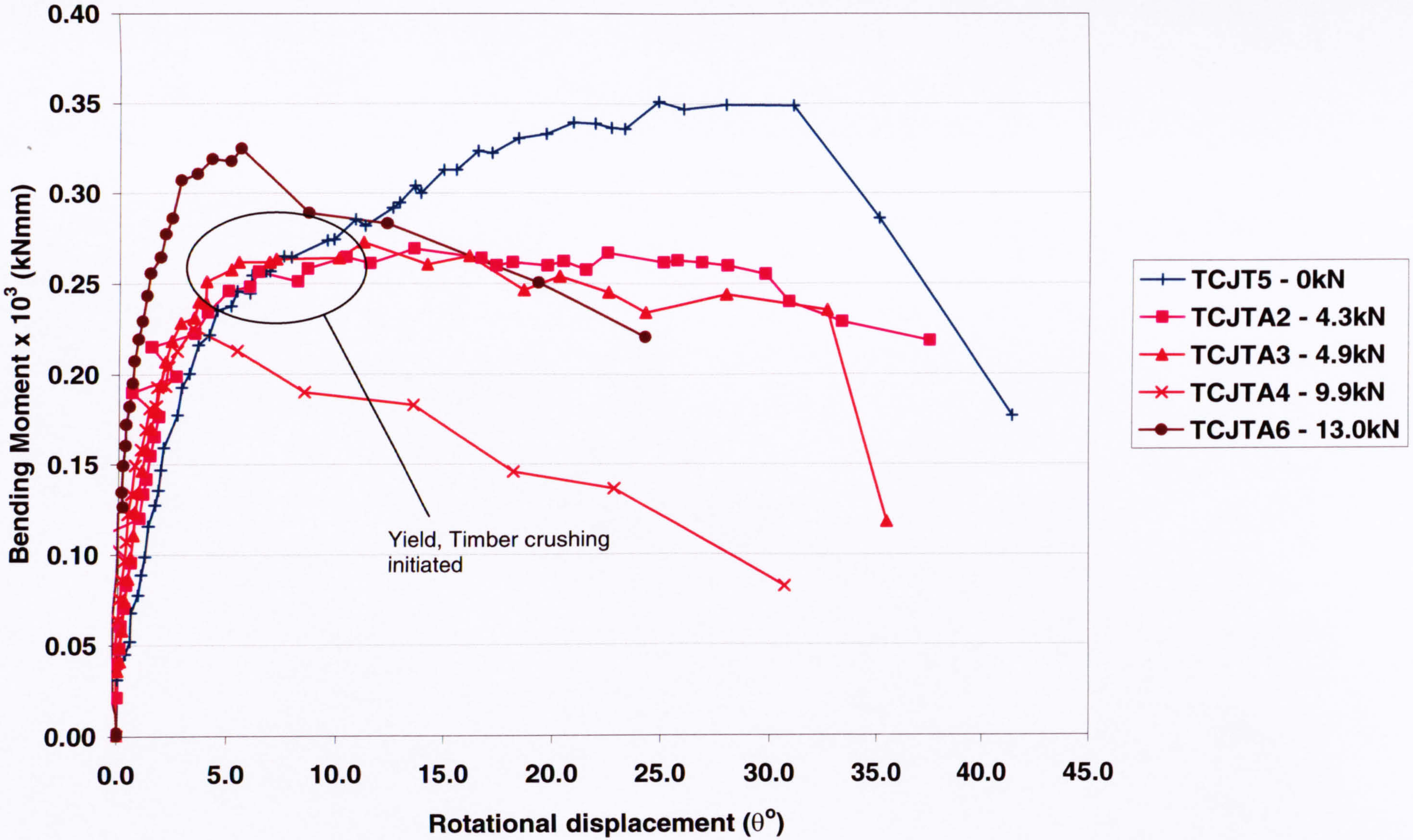

Fig. 6.4.4 – Effect of axial loads on rotation stiffness for Top chord Joints

6.5 Bottom Chord Joint test

Constant bending moment tests – BCJTM series

Test	BCJTM1	BCJTM2	BCJTM6	BCJTM3	BCJTM5a
Constant B/M x10^3(kNmm)	0.00	0.09	0.22	0.33	0.45
Max. Axial load (kN)	12	12.03	11.48	6.84	8.14

Table 6.5.1 – BCJTM series test programme

The constant bending moment tests were conducted as detailed in the table above. In this series all failures occurred at the web member where the load was applied. As shown in Fig. 6.5.1, the separated web member showed less damage to the timber at the edge of the plate. This suggests that the nails had little resistance and that the main cause of failure at this part of the joint was nail pull out, which lead to the greatest deformation in the plate. In addition to the pull out and bending of the nails, some timber damage was exhibited. Timber residue was found attached to the nails away from the edge of the plate, which indicated the strength of the nail bite compared to at the edge of the plate. As results show in Fig. 6.5.3 the connection behaves in a brittle manner.

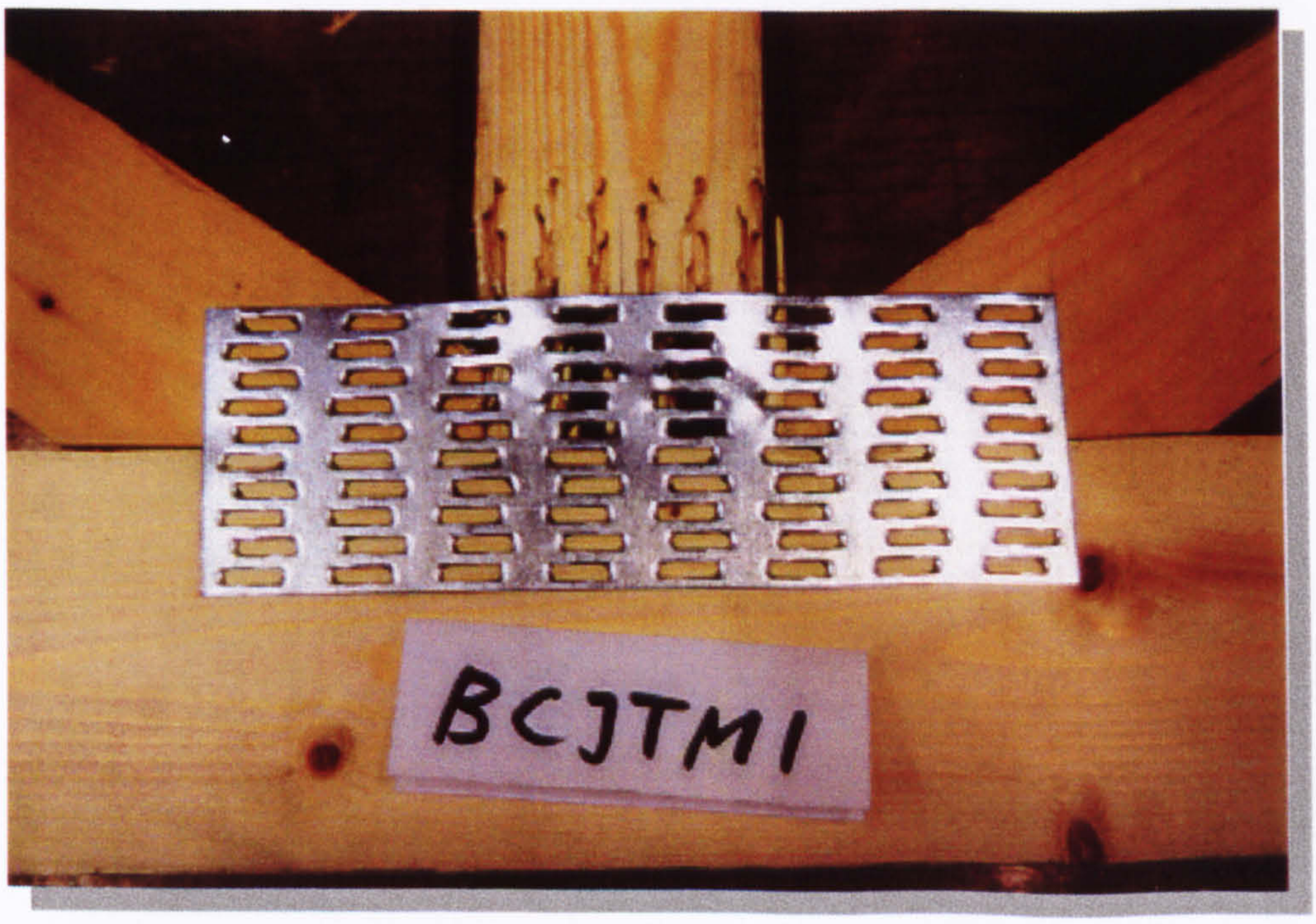

Fig. 6.5.1 – Typical failure of BCJTM test series

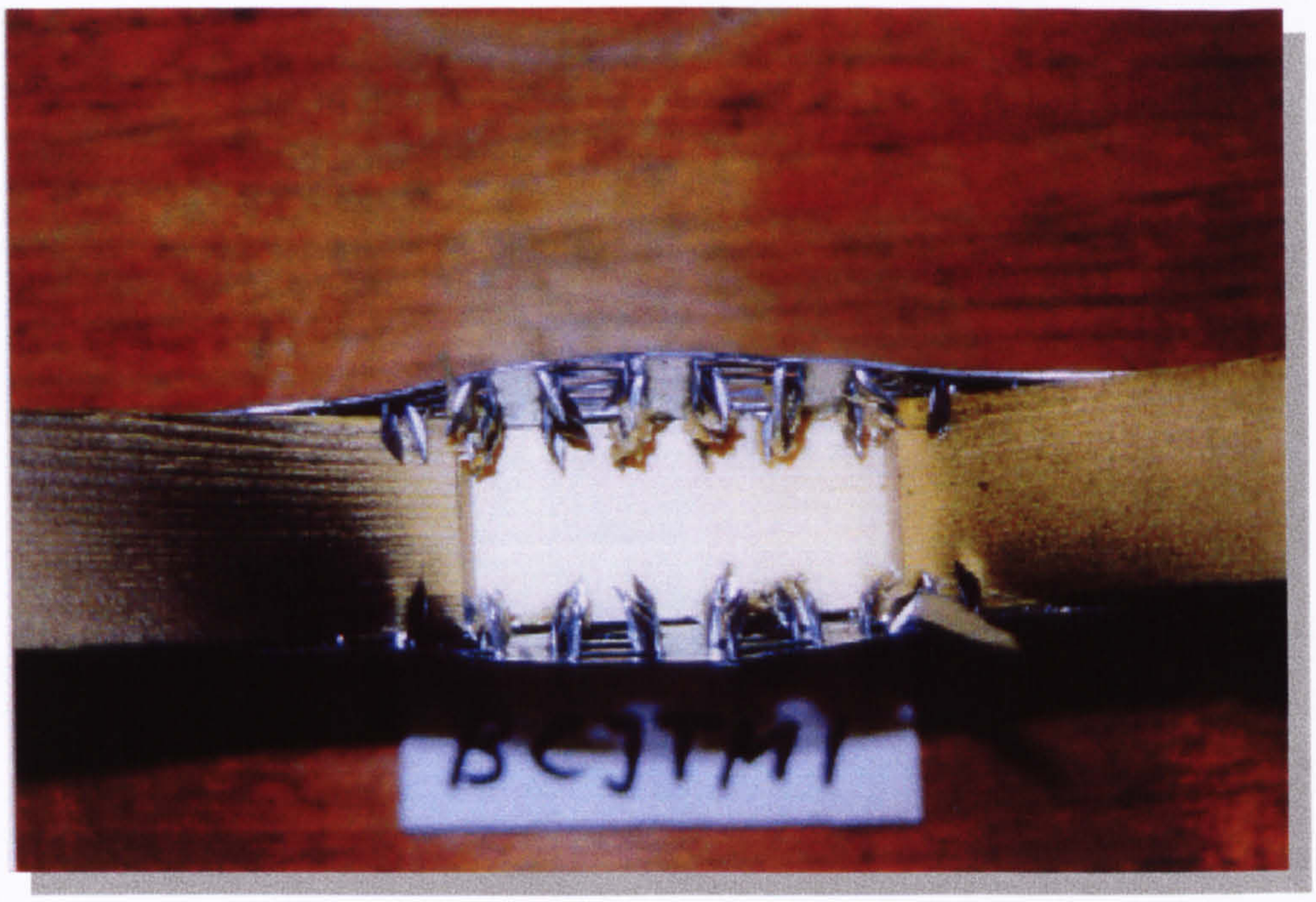

Fig. 6.5.2 – Nail and plate deformation of BCJTM series

The axial stiffness and strength capacity of specimens BCJTM1, BCJTM2 and BCJTM3 remains un-affected by bending moments and exhibits brittle behaviour shown by constant axial stiffness followed by an almost abrupt failure at approximately 12KN. Tests BCJTM4 and BCJTM5a shows ductility is encouraged by bending moments. They show that large bending moments reduce the axial stiffness of the connection and axial capacity although the strength capacity of test BCJTM5a is not consistent with the trend, i.e. BCJTM5a shows a higher axial load capacity than BCJTM4.

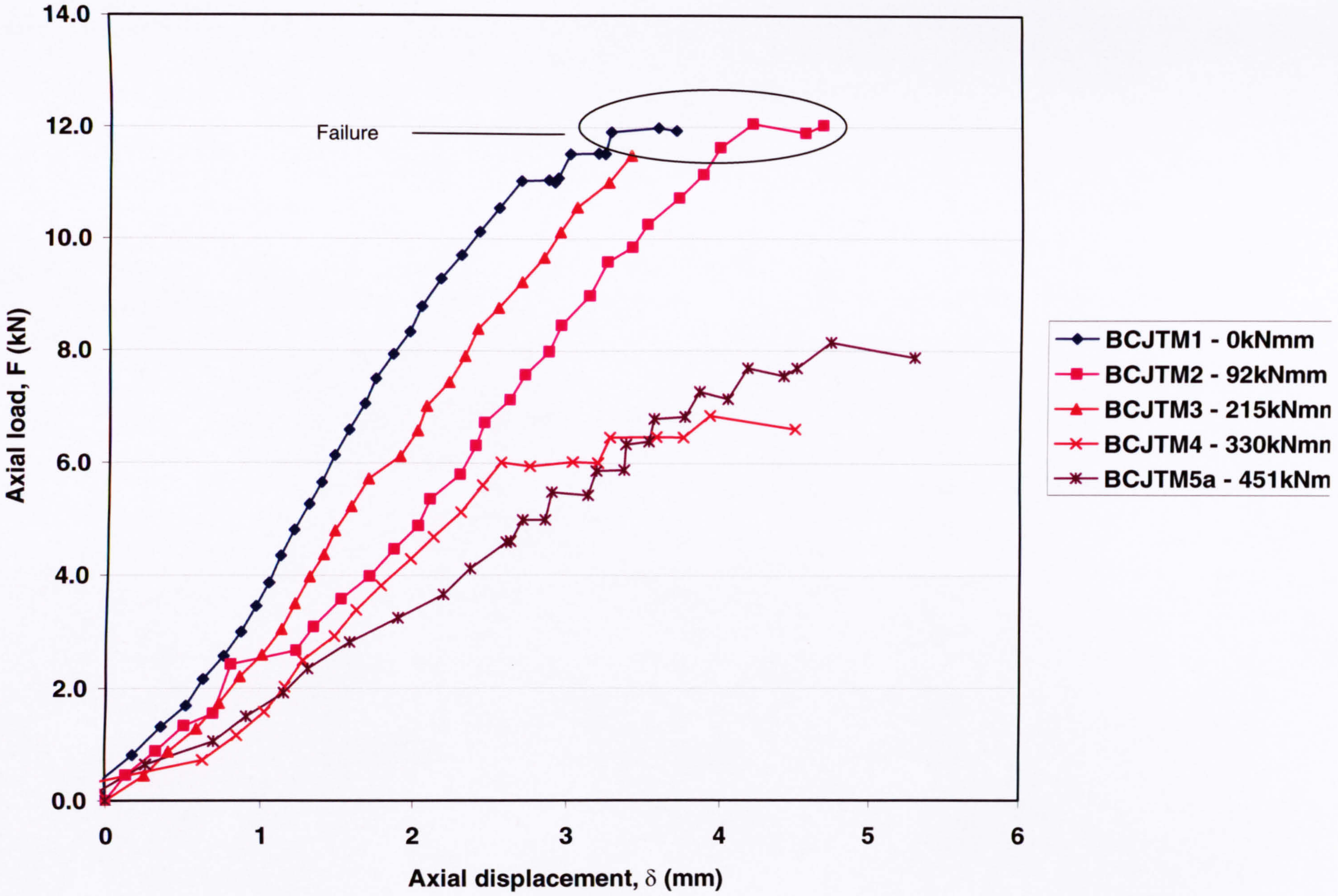

Fig. 6.5.3 – Effect of bending moment on axial stiffness of Bottom chord joints

Constant axial load tests – BCJTA series

The loading of the bottom chord test was conducted as tabulated below.

Test	BCJTA1	BCJTA2	BCJTA3	BCJTA4	BCJTA5
Constant Axial load (kN)	0.0	1.1	3.3	6.4	10.1
Max. B/M x10^3(kNmm)	0.52	0.53	0.54	0.46	0.24

Table 6.5.2 – BCJTA series test programme

The nails at the edge of the plate initiated failure and was evident from the withdrawal. Nail deformation was towards the load direction. The response of the connection under bending moment is of a ductile connection. The connection is similar to the crown joint where a similar failure mechanism was seen. The difference is seen in the curve characteristics, which depend on the configuration of the joint. Clearly the crown joint configuration is different from the bottom chord. The strength of the group of nails in the joint is described by the initial linear stiffness of the joint. Yielding occurs once the contact capacity between the nail and timber is exceeded for a sufficient number of nails at the edge of the plate. The rate of displacement increases when loading continues beyond yield point. The capacity of the nails in the timber progressively fails from the edge of the plate until no load is further sustainable, which is shown by large movements i.e. low stiffness. The results show that the bending moment stiffness is affected by high axial loads. Tests BCJTA4 shows an earlier decline in stiffness than BCJTA1-BCJTA3. This decline in stiffness is even more profound for test BCJTA5, where yielding is almost half that for the first three tests and with less ductility. There is only a little influence of axial loads on rotational stiffness and capacity except for higher axial load levels, i.e. BCJTA4 and BCJTA5. A significant decline in rotational capacity is exhibited in test BCJTA5 for a higher axial load level.

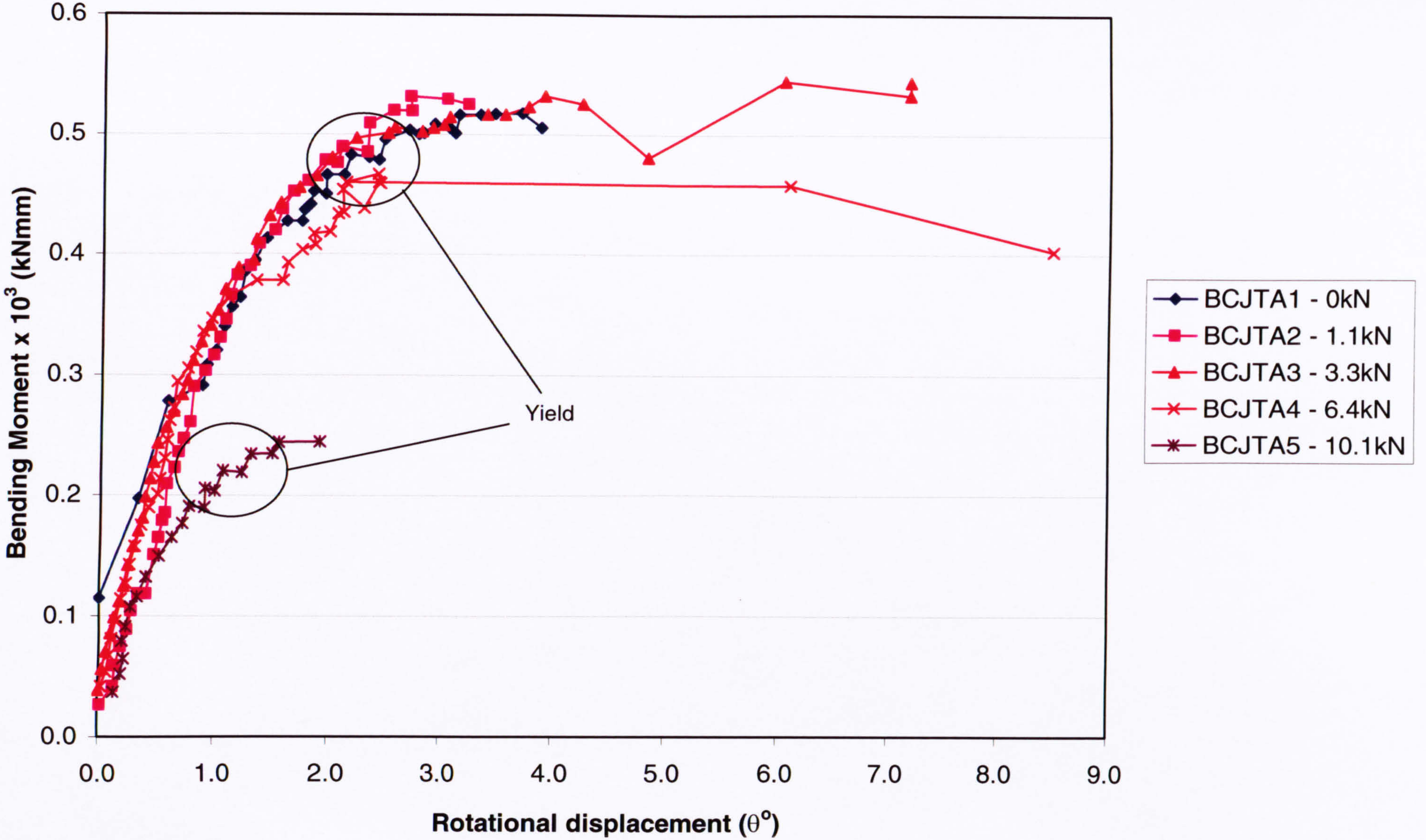

Fig. 6.5.4 – Effect of axial loads on rotation stiffness for Bottom chord joints

6.6 Joint test summary

The joint tests are now briefly summarised. Tensile axial loading of the plates perpendicular to the length of the plate produced a brittle response where pull out was the primary cause of failure. However, the angled load in the HJTM test series produced a non-linear and more ductile response. Although there are signs of frictional resistance between the top and bottom chord, these contribute little to the strength as loads are predominantly vertical. In addition, plate failure, which was the cause of the ductile response was exhibited in these tests. The BCJT and the CJT tests look visually similar sharing the same failure anchorage area at the web. Adjacent members connected to the plate are in compression and abutting either to each other (CJT), or to other members (BCJT). The plate-nail to member orientation is the same but results are different. All joints gave a ductile response under bending moment loads.

When pull out is the initiation of failure, it is usually exhibited at the edge of the plate with more resistance away from the edge. This indicates that strength is not consistent throughout the plate.

The results confirm that there is generally effect of combined bending and axial loads on the stiffness of the joint and the failure load. The effects of this phenomenon vary between connections and there is no linear relationship.

After the joint tests, samples were cut from one of the member of each joint from where density and moisture content were measured. The density and moisture content of the timber was typically between 8.8–10.8% and 0.37-0.50mg/mm^3 respectively, details of which are presented in Appendix C1.

In the joint tests an attempt to measure shear in the presence of moments has been difficult. Results are difficult to interpret and therefore have not been used. A sample from test HJTA1e is given in Appendix C1.

Displacement results of the joint tests have been successfully measured using digital photogrammetry. Fig. C2.1 shows a typical image from the HJTA1 tests with reflective dots. This is one of four images taken around the object. The co-ordinate of each dot is measured through VMS and then processed using EngVis to produce a displacement diagram as shown in Fig. C2.2. The results presented above are only the data required for purposes of this thesis. However, close range photogrammetry produced much more data than reported. Because targets were measured in 3-D cartesian co-ordinates, out of plane movement can also be measured. As discussed before, this indicates potential for nail plate analysis such as pull out as reported in the tests in this thesis, although it was not the purpose of this thesis to investigate this subject intensively.

The results of the joint tests can be summarised below in Table 6.6.1.

Joint	Test Code	Constant B/M x10^3 (kNmm)	Max. Axial load (kN)	Constant Axial (kN)	Max.B/M x10^3 (kNmm)	Failure mode
Crown	CJTM1a	0	13.6	-	-	Pull out
	CJTM2	0.2	10.4	-	-	Pull out
	CJTM3	0.2	12.9	-	-	Pull out
	CJTM4	0.3	10.5	-	-	Pull out
	CJTM5	0.4	12	-	-	Pull out
	CJTA1	-	-	0	0.5	Pull out
	CJTA2	-	-	3	0.5	Pull out
	CJTA3	-	-	4.4	0.5	Pull out
	CJTA4	-	-	6	0.5	Pull out
	CJTA5	-	-	8.4	0.6	Pull out
Heel	HJTM5	0	12.1	-	-	Plate failure
	HJTM1a	0.2	15.9	-	-	Plate failure
	HJTM2	0.4	17.7	-	-	Pull out and bottom chord detached
	HJTM3	0.6	15.2	-	-	Pull out and top chord detached
	HJTM4	0.9	23.3	-	-	Plate failure
	HJTA1e	-	-	0	1.3	Top chord split
	HJTA2	-	-	2.9	1.5	Top chord split
	HJTA3	-	-	6.2	1.6	Top chord split
	HJTA4	-	-	9.5	1.6	Top chord split
	HJTA5	-	-	10.6	1.7	Top chord split
Top Chord	TCJTM1	0	13.9	-	-	Timber bending
	TCJTM2	0.1	14.4	-	-	Timber bending
	TCJTM6	0.2	17.4	-	-	Timber bending
	TCJTM3	0.3	7.9	-	-	Pull out
	TCJTM5	0.3	4.4	-	-	Pull out
	TCJT5	-	-	0	0.3	Plate failure
	TCJTA2	-	-	4.3	0.3	Plate failure
	TCJTA3	-	-	4.9	0.3	Plate failure
	TCJTA4	-	-	9.9	0.2	Plate failure
	TCJTA6	-	-	13	0.3	Plate failure
Bottom Chord	BCJTM1	0	12	-	-	Pullout
	BCJTM2	0.1	12	-	-	Pullout
	BCJTM6	0.2	11.5	-	-	Pullout
	BCJTM3	0.3	6.8	-	-	Pullout
	BCJTM5a	0.5	8.1	-	-	Pullout
	BCJTA1	-	-	0	0.5	Pullout
	BCJTA2	-	-	1.1	0.5	Pullout
	BCJTA3	-	-	3.3	0.5	Pullout
	BCJTA4	-	-	6.4	0.5	Pullout
	BCJTA5	-	-	10.1	0.2	Pullout

Table 6.6.1 – Summary of joint test results

6.7 Full Scale Truss test

The following table summarises the full scale truss test conducted

	Test code					
	FST1	**FST2**	**FST3**	**FST4**	**FST5**	**FST6**
Load	Sym	Sym	Sym	Unsym	Unsym	Unsym
Support	B/C	B/C	Rafter	B/C	B/C	B/C

Table 6.7.1 – Full scale truss test programme

Key

Sym – Symmetrical load, Fig. 3.6.5.3

Unsym – Unsymmetrical load, Fig. 3.6.5.6

B/C – Support at the Bottom chord, Fig. 6.6.3a

Rafter – Support at the rafter, Fig. 6.6.3b

As described in section 3.6.5, the symmetrical load with the supports at the heel joint, under the bottom chord was tested twice, four times including the mock test. Although displacement measurements were not recorded for the mock test, the failure was recorded and found to be similar to the other tests. In all three tests the truss failed at the heel joint, but the mode was quite different depending upon where the supports were. As designed, by placing the supports at the bottom chord the mode of failure obtained was as shown in Fig. 6.7.1. The principal mode of failure observed was the pull out of the nails. However, test FST3 was a slightly different test. As explained in section 3.6.5, the truss is supported at the top chord as oppose test FST1 and FST2 at the bottom chord. As shown in Fig. 6.7.4, the failure load for FST4 is 16KN and shows a significant difference of 10KN in capacity, although the stiffness remains similar. Furthermore, the mode of failure was also different. Here, the principal cause of the failure was splitting of the timber parallel to the grain at the top chord as shown in Fig. 6.7.2.

Fig. 6.7.1 – Failure mode for support at the bottom chord

Fig. 6.7.2 – Failure mode for support at the rafter for test FST3

The mode of failure can be explained by illustrations in Fig. 6.7.3. The cause of failure is through tension forces from the bottom chord, which applies tension load perpendicular to the grain at the top chord. In test FST1 and FST2, the reaction from the support at the bottom chord reduced the tension load perpendicular to the top chord and the cause of failure was simply pull out. Whilst in FST3 a similar load was applied but there was no support at the

bottom chord. Therefore, the top chord was being directly loaded in tension, perpendicular to the grain and resulted in a far inferior strength than test FST1 and FST2. More fundamentally, timber is weak in tension perpendicular to the grain and this dictated the truss capacity.

The results in Fig. 6.7.4 show that the truss behaved in quite a linear fashion. The failure of the truss can be described as brittle with very little ductility.

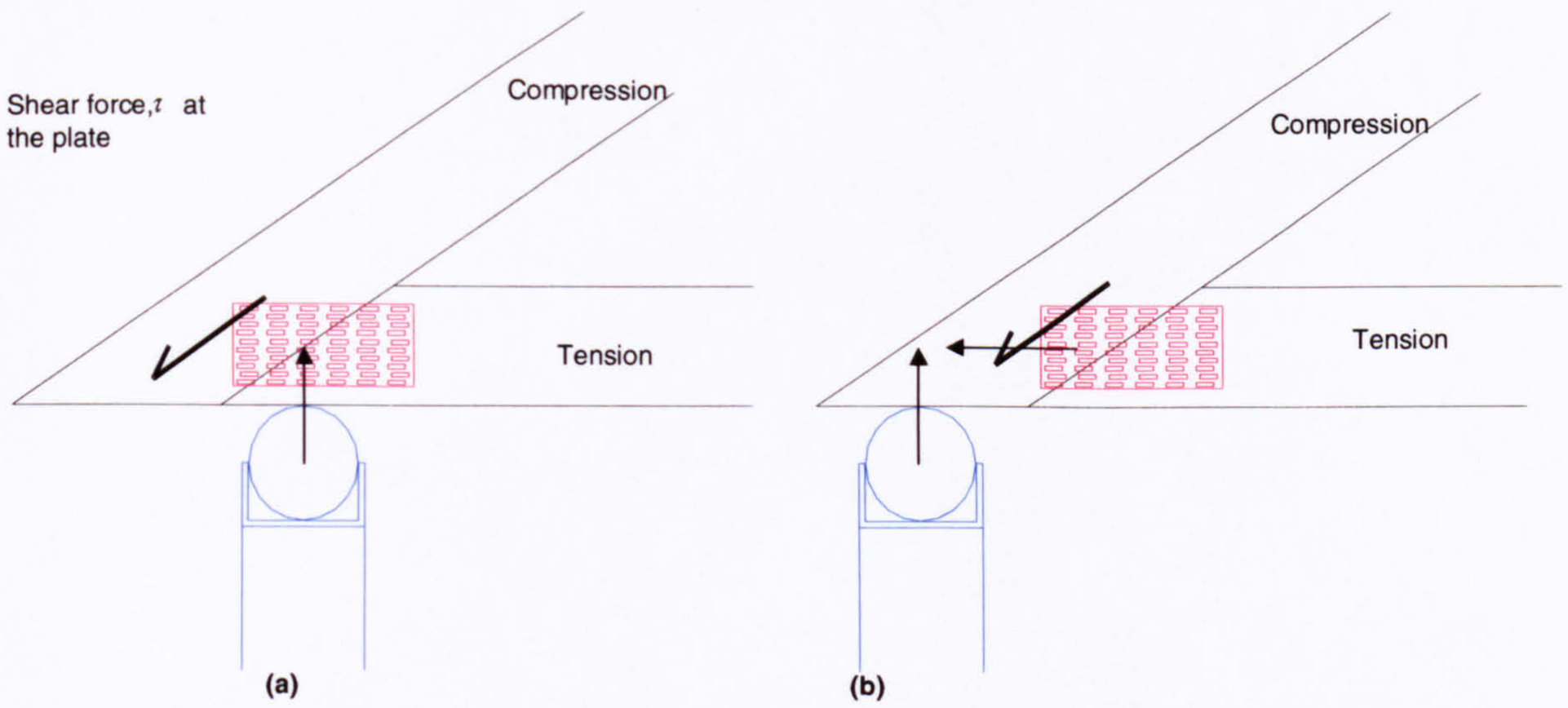

Fig. 6.7.3 – Failed heel joint for two different support points

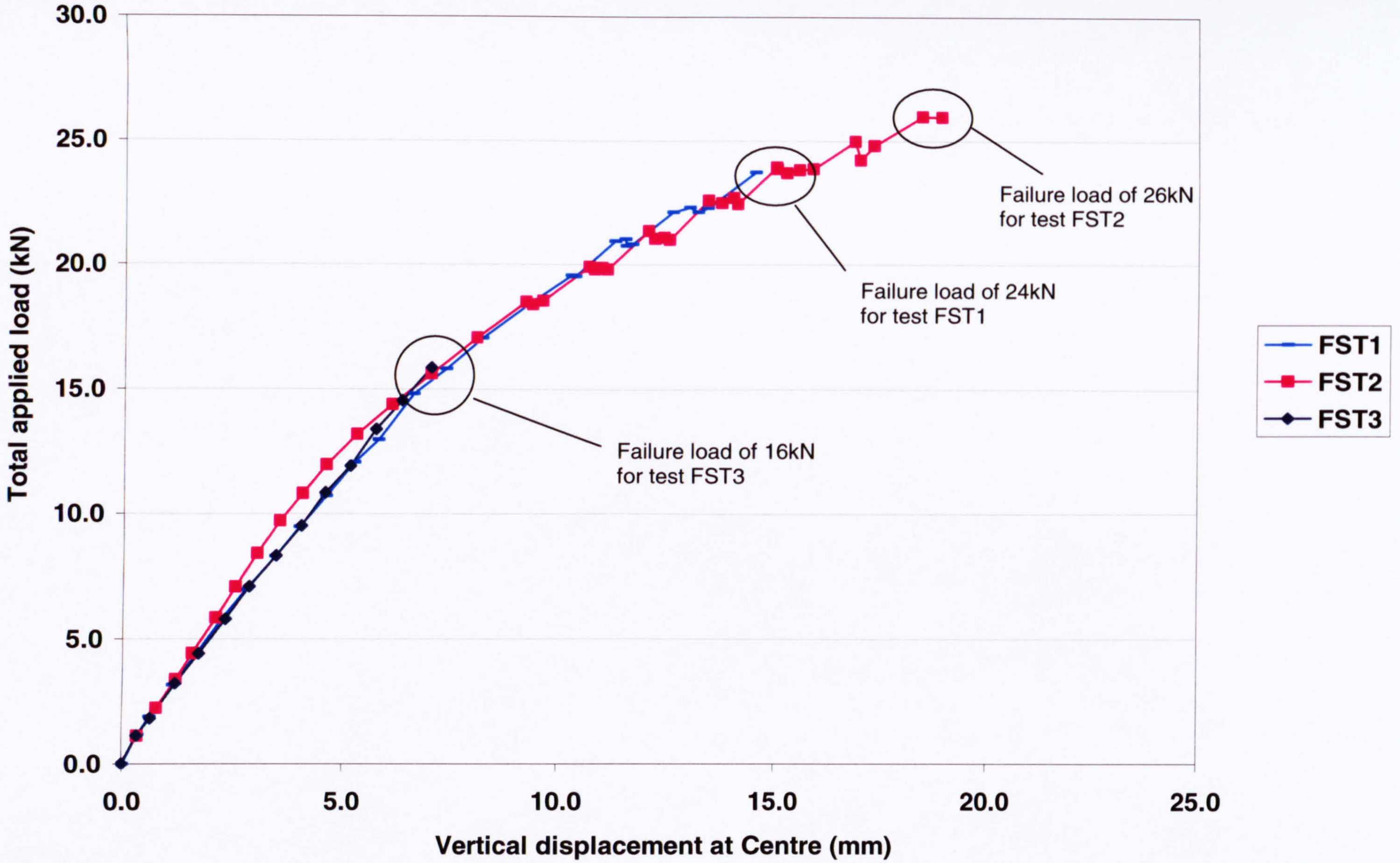

Fig. 6.7.4 – Results of the Symmetrical full scale truss test

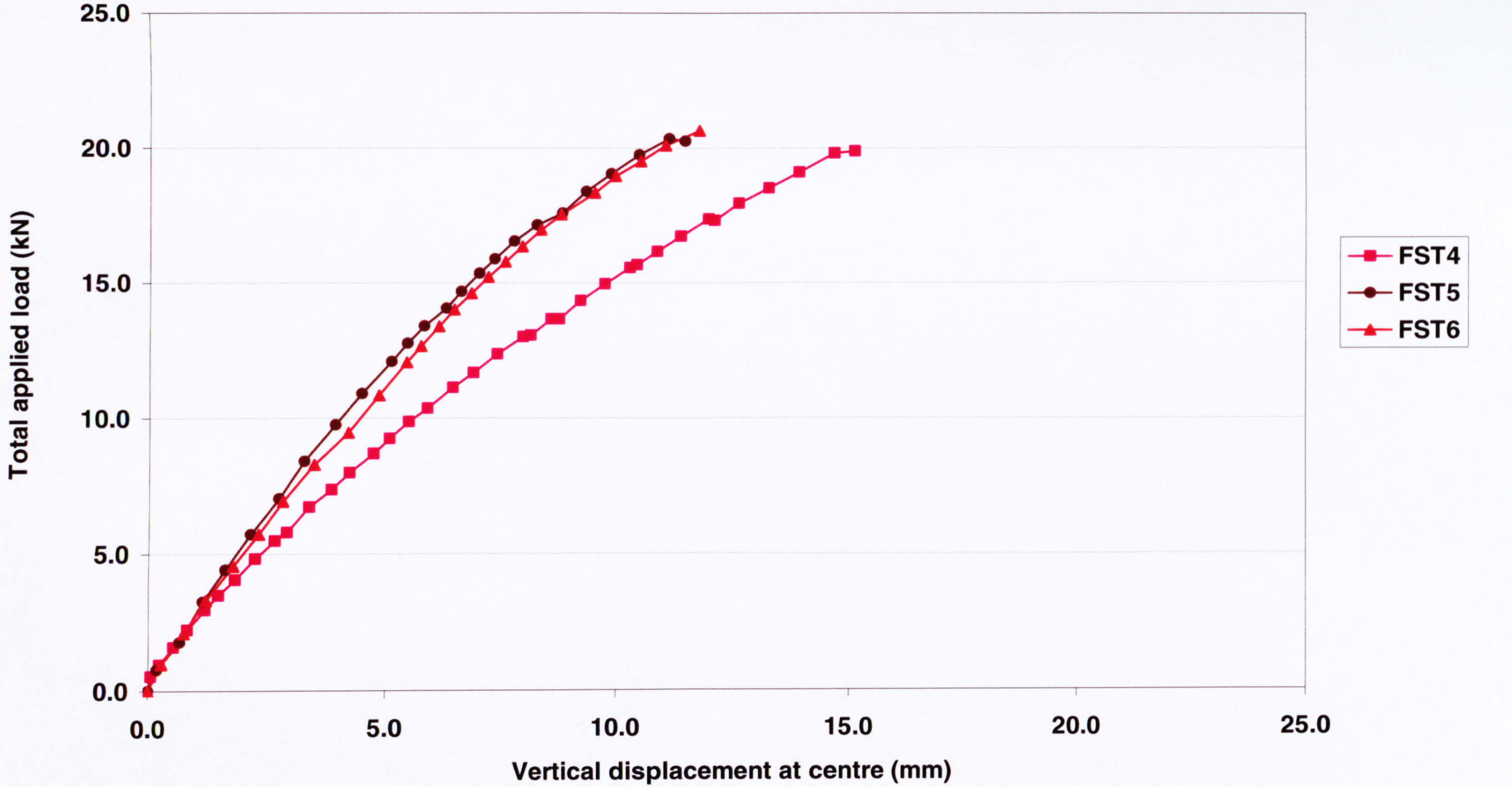

Fig. 6.7.5 – Results of the Unsymmetrical full scale truss test

The unsymmetrical load test was conducted three times. In all tests the heel joint failed first with the principal mode of failure being pull out of the nails at the top chord of the connection, similar to FST1 and FST2. Test results in Fig. 6.7.5 indicate slight variations in the load deflection curve in test FST4 compared to all the others

In all truss tests, the splitting of timber fibres could be heard just before failure. Although there was some warning of failure, it was still quite abrupt. Comparison of all the truss tests is shown below. The truss stiffness is consistent regardless of symmetry of the loads with the exception of test FST4. The truss capacity is reduced for the unsymmetrical tests as the loads are concentrated on one side of the truss.

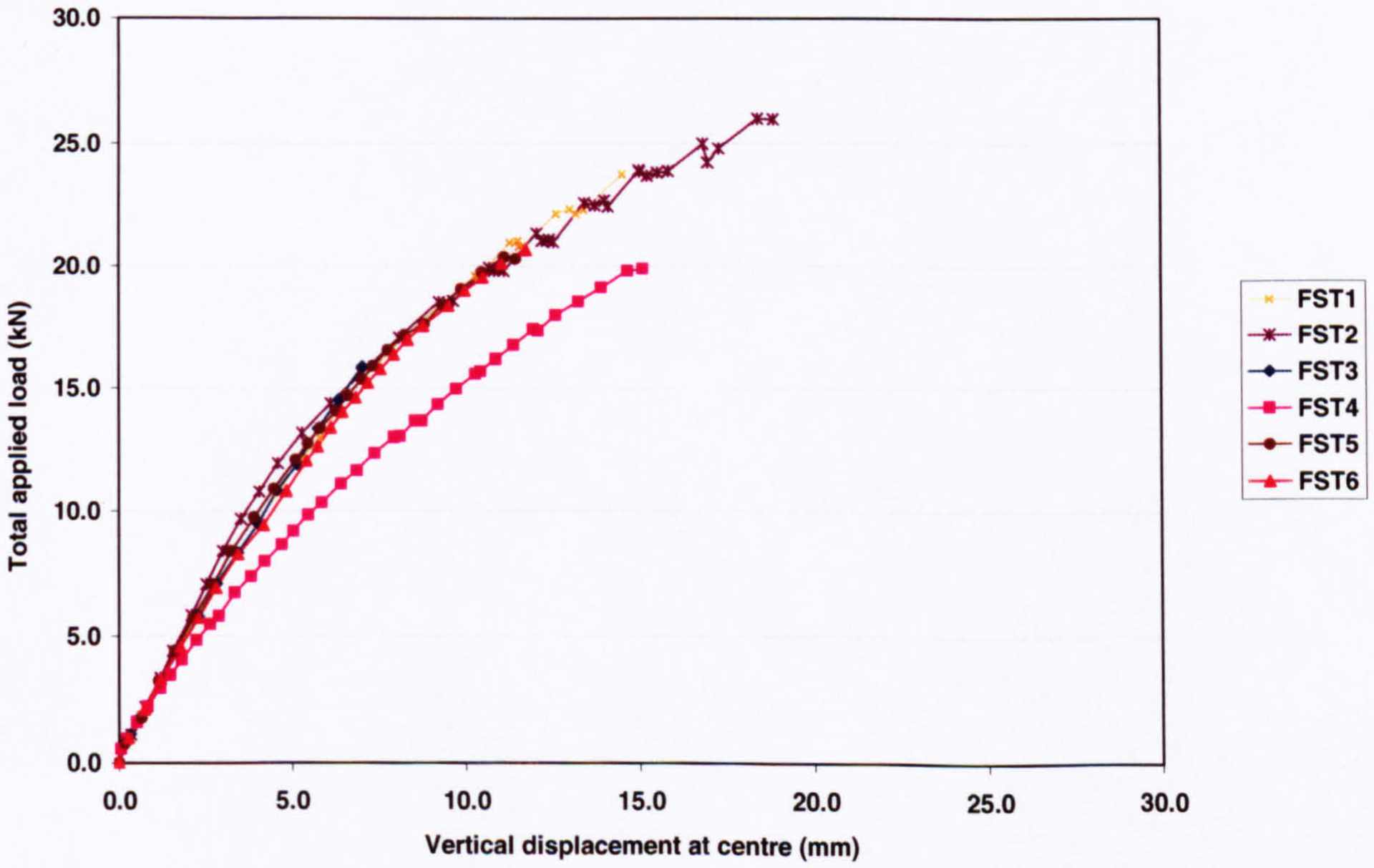

Fig. 6.7.6 – Overall truss results

6.8 Semi-rigid plane frame analysis

As explained in section 4.8 power functions are used to fit a curve to the joint test data, which is programmed into STRUSS giving the truss program non-linear semi-rigid connection capability. Both the symmetrical and unsymmetrical load cases were simulated. Fig. 6.8.1 below shows the conditions at which these simulations were ran under for both load cases.

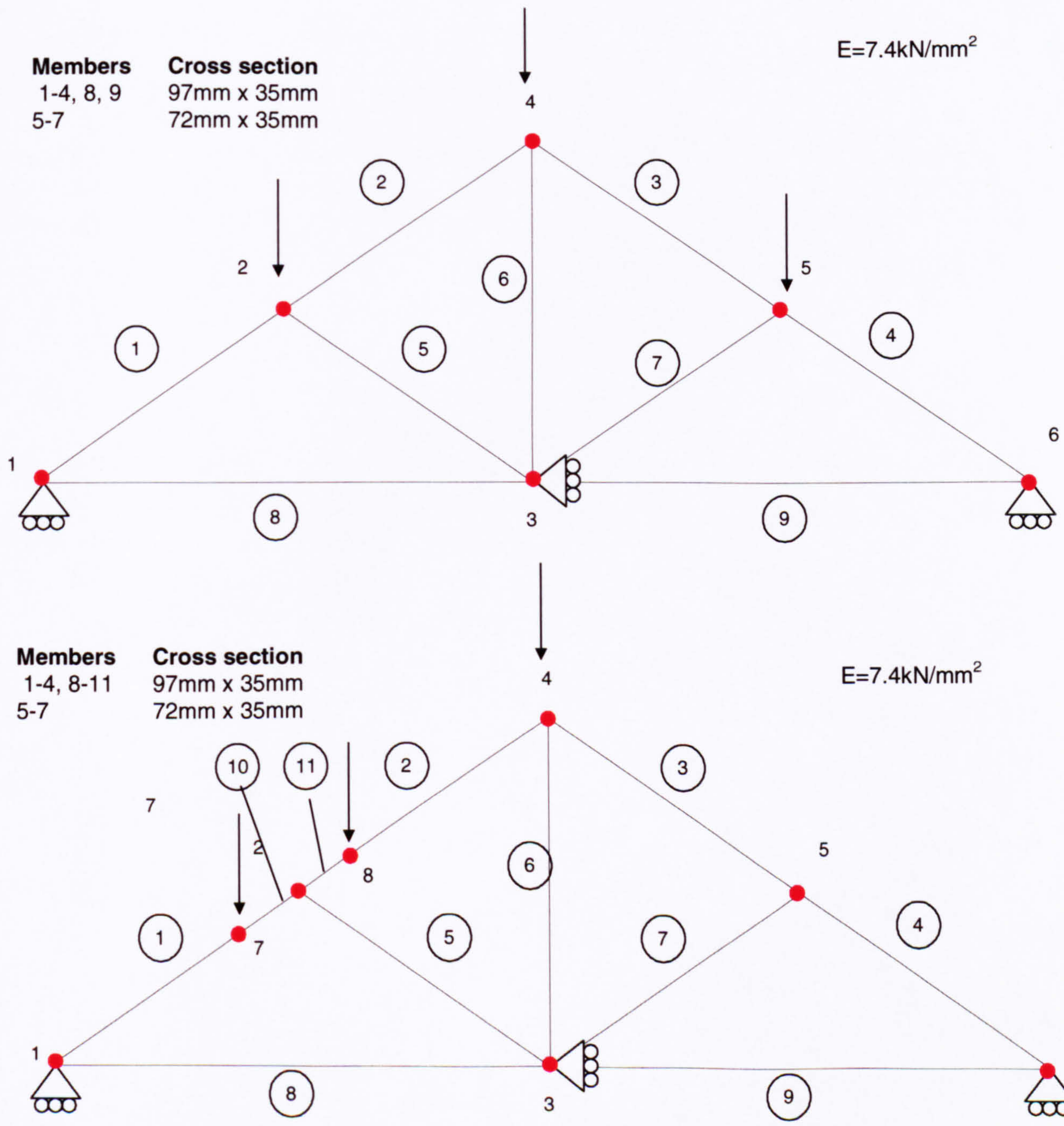

Fig. 6.8.1 – Load and Boundary conditions

As illustrated, nodes 1 and 6 are fixed vertically and node 3 is fixed horizontally to prevent the truss from sliding. In the laboratory tests, 2 rollers supported the

truss at either side of the bottom chord. The truss was free to move horizontally but did not. The boundary conditions prescribed closely resembles this behaviour. This is because the more load that was applied to the truss the more horizontally stable it became. Large rotational, axial and shear stiffness were prescribed where members are continuous at the joints, namely the top and bottom chords. Where loads were applied at the members, intermediate nodes 7 and 8 were placed where again large stiffness was prescribed. The Foschi parameters used to simulate non-linear semi-rigid joint stiffness in the analysis are presented in Table 6.8.1. An average was chosen for the heel joint axial stiffness. Other Foschi parameters for the combined loading tests are given in Appendix C1 along with individual joint test results.

Stiffnesses	**Joint Type**			
Rotational (kNmm)	**Crown**	**Heel**	**Topchord**	**Bottom chord**
KR	30000.0	70000.0	7300.0	27000.0
KR0	500.0	1350.0	220.0	550.0
KR1	0.0	0.1	350.0	0.0
Axial (kN)				
KA	2.3	8.0	2.3	4.5
KA0	8.5	11.0	10000.0	20000.0
KA1	4.0	0.8	0.0	0.0

Table 6.8.1 – Foschi parameters for truss joints

Where,

KR =Initial rotational stiffness

KR0 =Asymptotic to tangent rotational stiffness

KR1 =Tangent rotational stiffness

KA =Initial axial stiffness

KA0 =Asymptotic to tangent axial stiffness

KA1 =Tangent axial stiffness

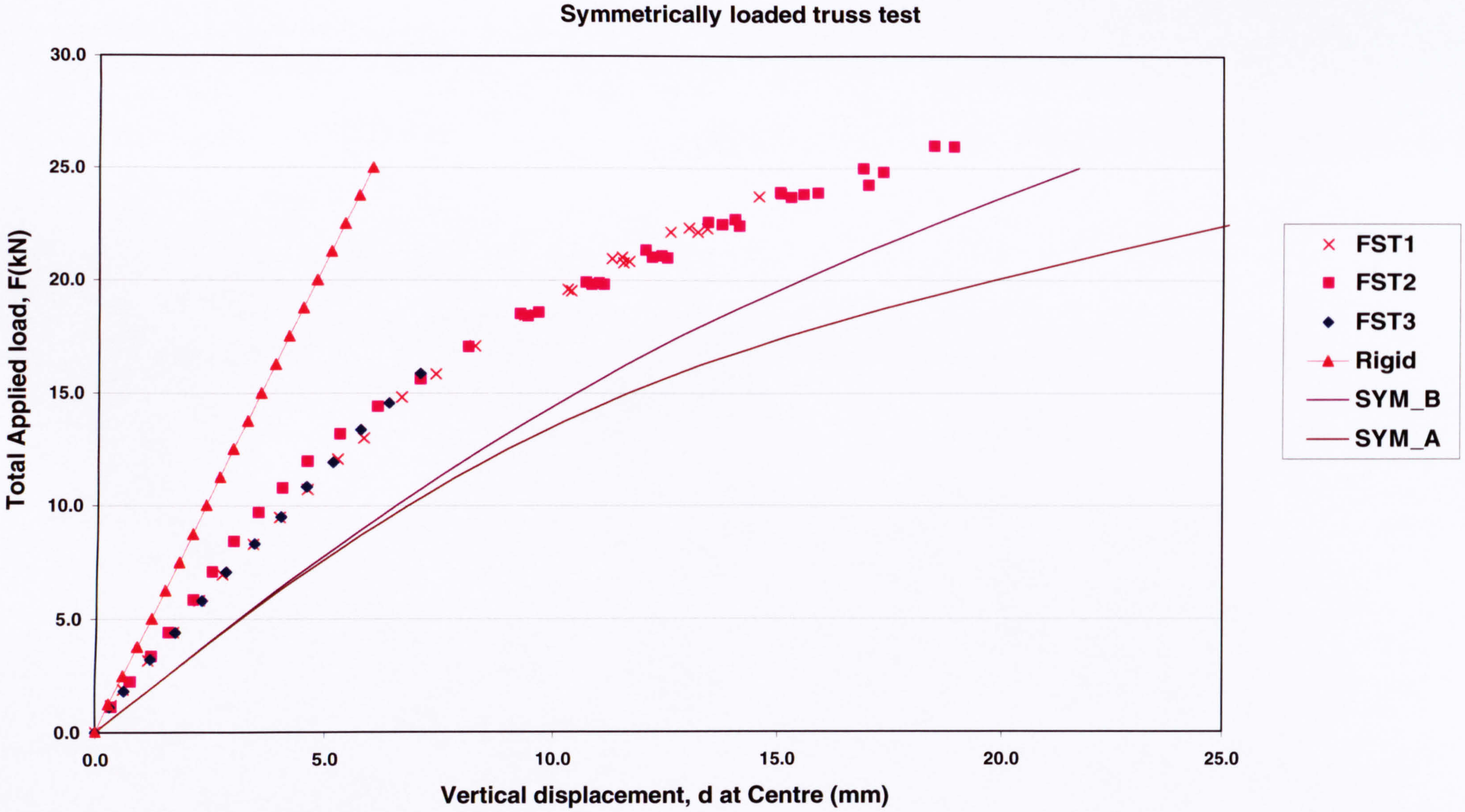

Fig. 6.8.2 – STRUSS compared to symmetrical test results

As explained in section 4.8, the Foschi parameters are determined by trial and error. Parameters are varied until a reasonable fit to the experimental data is achieved. Good fit is judged by the eye. As presented in Fig. 6.8.2, initially STRUSS results of the symmetrically loaded truss SYM_A do not compare well with test results. It appears that there is a lack of stiffness in the truss. From the experimental truss test results, it is postulated that the lack of stiffness is due to the heel joint. A sensitivity study as presented in curve SYM_B in the same graph, demonstrates improvement in the result due to an arbitrary increase of the axial tangent stiffness value KA1 to 1.5 for the heel joint.

As shown in Fig. D1.1 in Appendix D1 a sensitivity study revealed that the central deflection of the truss is sensitive to the axial stiffness of the heel joint. An explanation for the difference between the experimental results and the computed results (curve SYM_A) may lie in eccentric behaviour of the heel joint in the truss. Fig. 6.8.3 shows how eccentricity can affect the response of the truss.

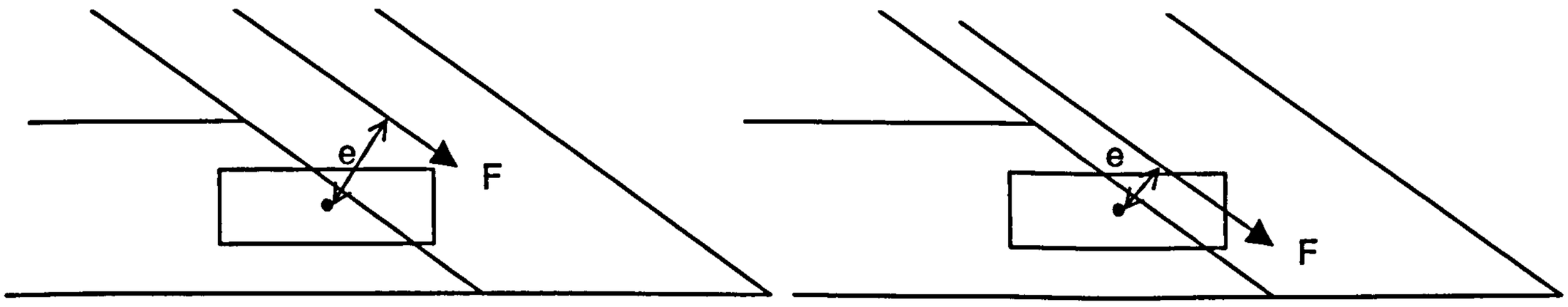

Case 1 - Eccentricity under joint tests

Case 2 - Eccentricity under connection tests

Fig. 6.8.3 – Load conditions in joint and truss tests

It demonstrates that the connection can actually behave differently depending on where the axial force is applied. It would be reasonable to assume that axial forces would not travel through the centre of the member under truss loading

conditions. The following sketch illustrates how the model can be improved to account for eccentric loads in STRUSS.

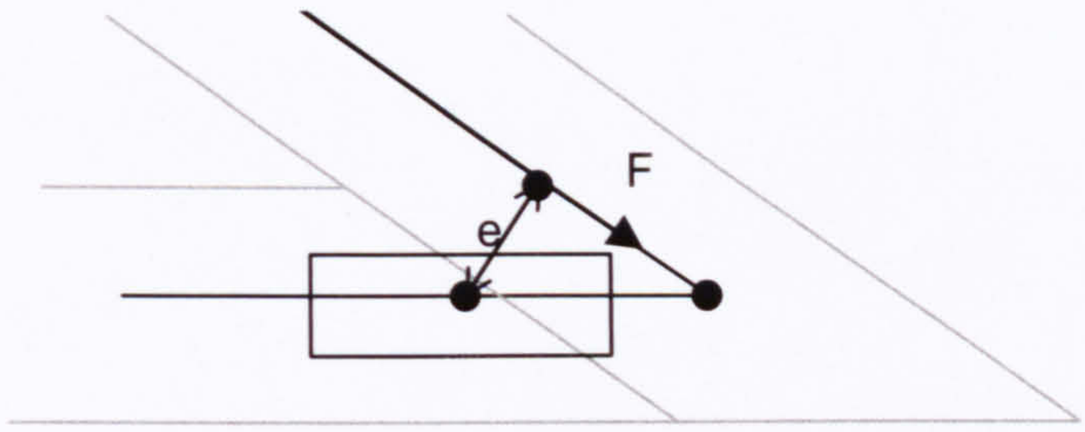

Fig. 6.8.4 – Modelling eccentricity in STRUSS

Although connection parameters are derived from actual connection tests where eccentricity within the joint is present, in STRUSS, eccentricity is not accounted for. It is assumed that the centre of the members meet at a common point with the connection and that the force only travels through the centre of the members. The difference in failure modes under connection and truss test conditions can also be observed. Recalling the mode of failure for the heel joint for the connection test and the truss test as shown below.

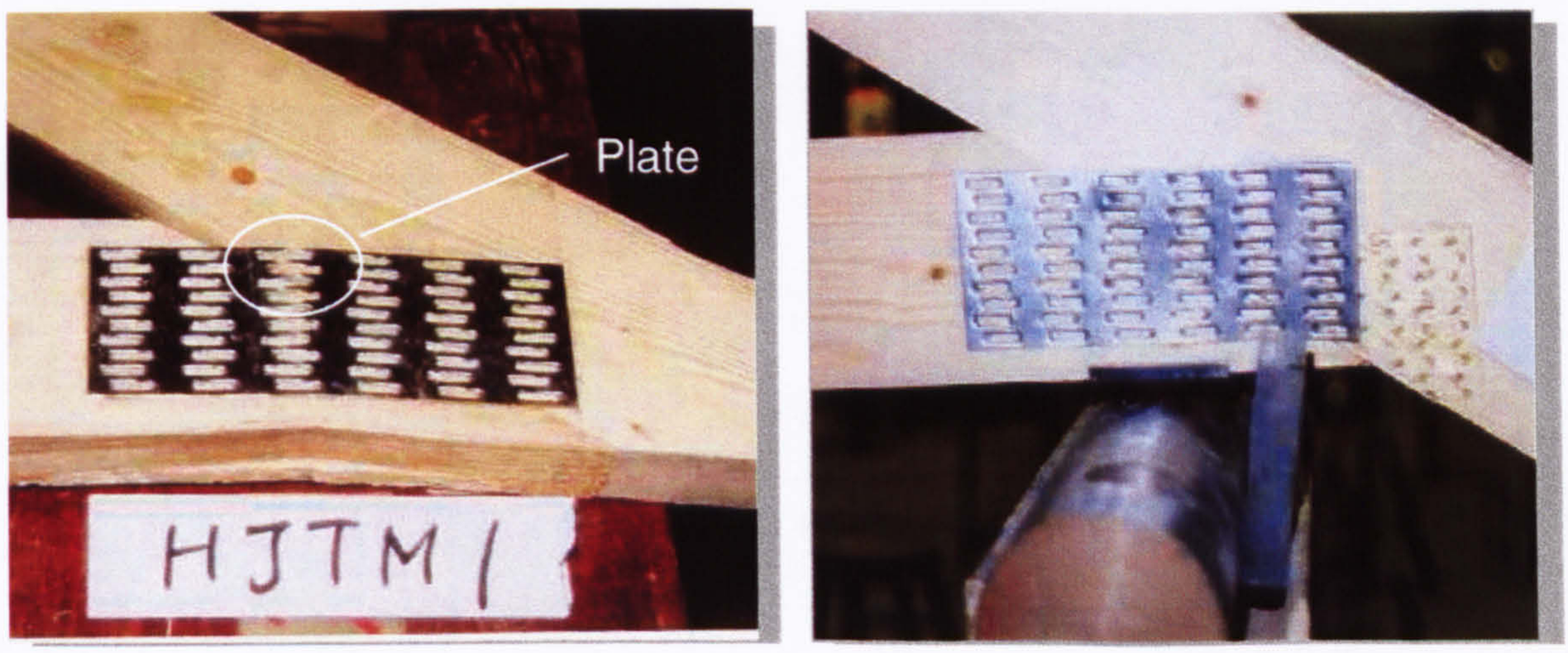

Fig. 6.8.5 – Joint and Truss test

In the joint test the connection failed at the plate whereas in the truss test, the failure is due to nail pullout. There are clearly two different modes of failure which is an indication of different heel joint behaviour for isolated single joint tests and truss tests.

A rigid analysis plotted in Fig. 6.8.2, diverges away due to non-linear nature of the truss. As specified in BS5268 Part 2 for strength class TR26 grade material, the average mean Young's Modulus of 11.0kN/mm^2 is adopted in the analysis. Fig. D1.2, in Appendix D illustrates demonstrates the how the Young's Modulus affects truss response.

The shear and bending effects at the Heel joint/ Top chord were found to be small. Due to the symmetrical loading of the truss, there are no shear forces and bending moments at the centre web member of the bottom chord joint, as shown in Table C1.3. The table shows that only the load for the top chord member (Member 1) at the heel joint (Node 1) exceeds axial capacity. An examination of the stiffness for the heel joint, presented in Table C1.3 shows that the bending moments are never exceeded for both the connections and the members.

Having discussed the results of the symmetrical load case, a similar comparison is presented for the unsymmetrical load case, Fig. 6.8.1. As demonstrated in Table C1.4 in Appendix C1, the unsymmetrical load case gave larger bending moments than the symmetrical case, but STRUSS shows that bending moment capacity of the connections are not breached. The largest bending moments were found at the load points.

Tables C1.3 and C1.4 also show that the shear forces are negligible compared to axial forces for the symmetrical tests. Shear forces are slightly larger for the unsymmetrical load case but do not exceed the shear capacity of the timber.

STRUSS indicates that the heel joint is the most critical part of the truss which agrees with the test results. The results of the sensitivity tests for the symmetrical load case used to validate STRUSS are presented in Fig. C1.45.

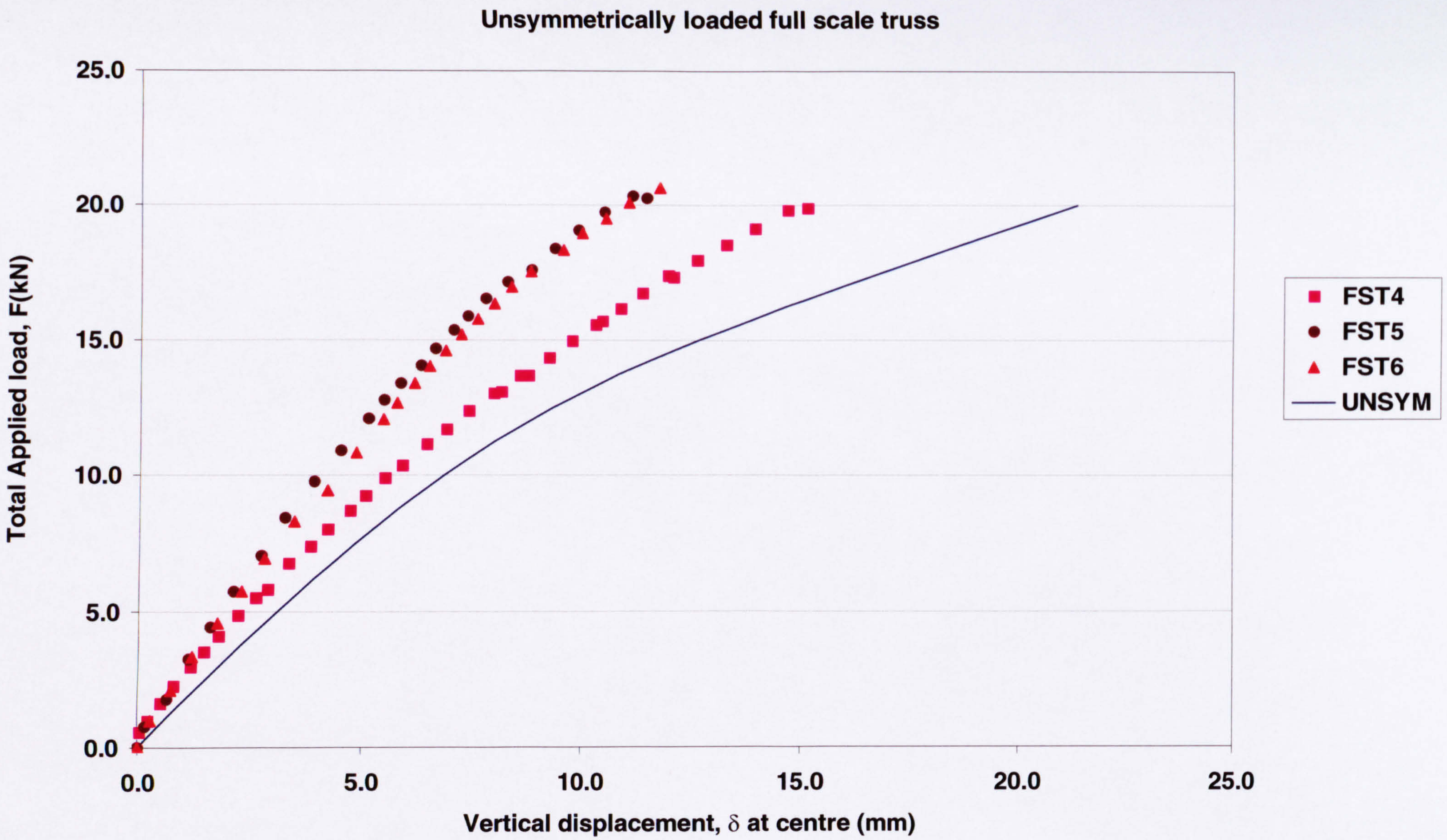

Fig. 6.8.6 - STRUSS compared to unsymmetrical test results

6.9 Finite element

Using the method mentioned in section 4.8 to determine the strength parameters the following strength values can be presented. The derivation of these values can be found in Appendix B2 and the results of the calculations are tabulated as follows

	Joint Type			
	Crown	Heel	Top chord	Bottom chord
Axial strength	CJTM1a	HJTM5	TCJTM1	BCJTM1
Load (N)	13000.000	10000.000	14000.000	11000.000
Anch. Width (mm)	72.000	70.257	44.219	72.000
Axial length(mm)	32.311	97.846	104.618	32.753
Elongation(mm)	3.250	3.500	7.807	3.000
Strain, ε	0.101	0.036	0.075	0.092
E (Nmm^{-2})	99.724	221.060	235.704	92.664
σ_y (Nmm^{-2})	10.031	7.907	17.589	8.488
E_T (Nmm^{-2})	0.000	44.212	0.000	0.000

Table 6.9.1 – Finite element joint strengths

The values are obtained from the pure axial load tests as indicated in the table and show that, the heel joint is the only connection that behaves non-linearly. Generally, axial loading of these connections produces a relatively linear and brittle response except for the heel joint. It is noted that the values represent the interaction between the nails and the timber and not the strength of the timber or the plate. The Young's Modulus of timber used for the analysis was $7.4kN/mm^2$.

Results in Fig. 6.9.1 and Fig. 6.9.2 show that there is generally good agreement between the FE model and test results for both symmetrical and unsymmetrical load systems respectively. Fig. 6.9.5 and Fig. 6.9.6 show a graphic plot from ANSYS which illustrates how the truss deflects.

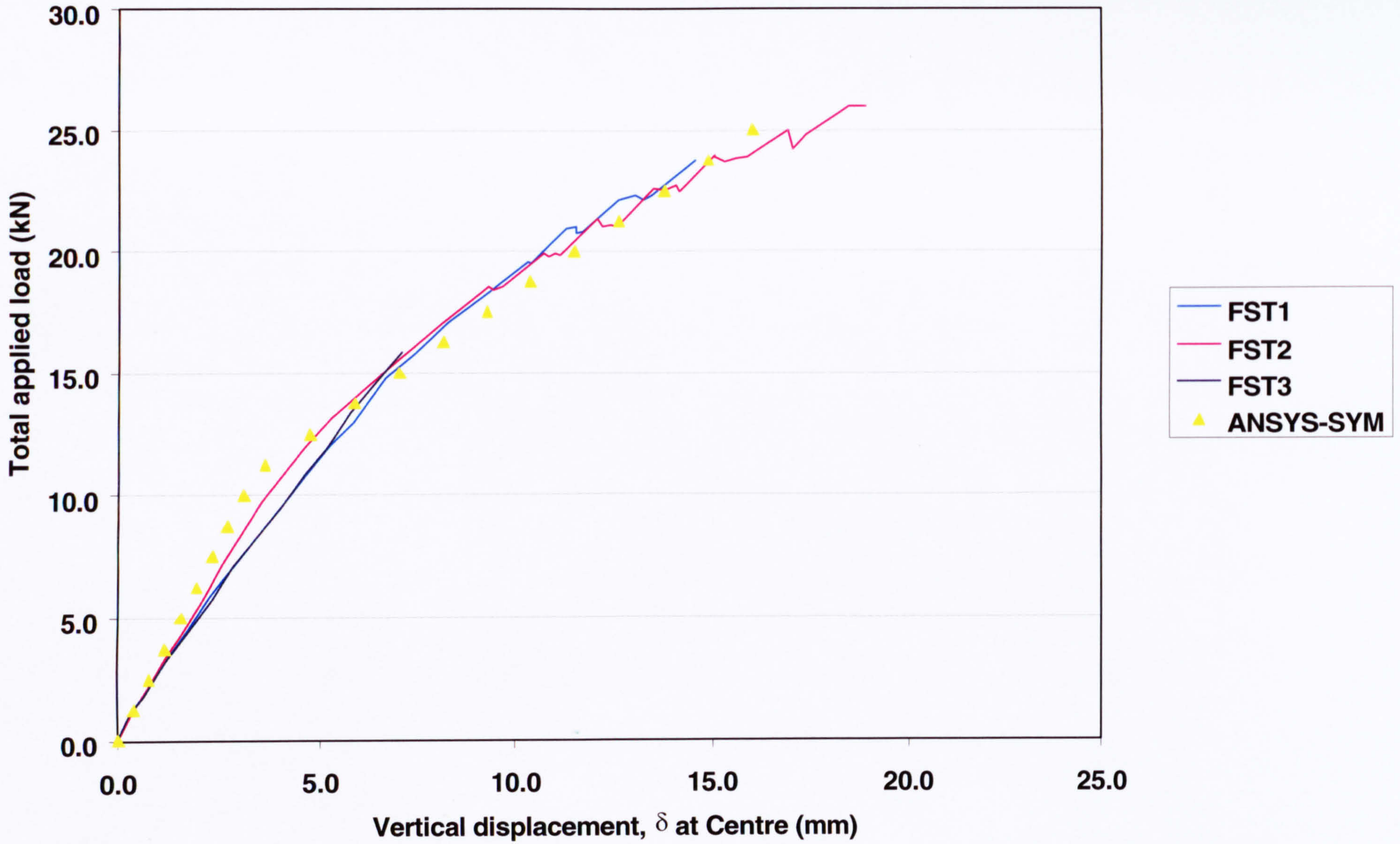

Fig. 6.9.1 – FE model compared to symmetrical truss load experimental results

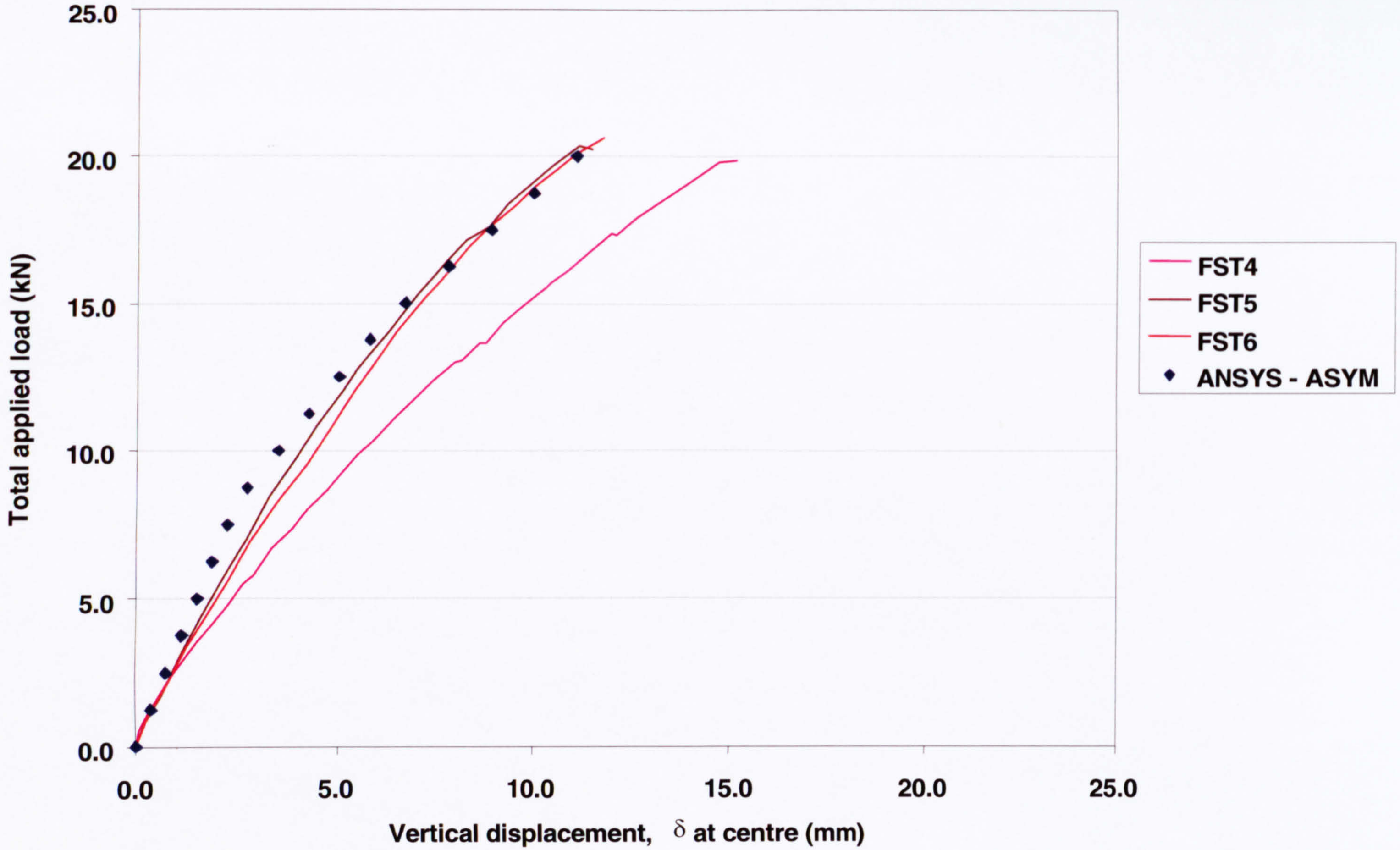

Fig. 6.9.2 – FE model compared to unsymmetrical truss load experimental results

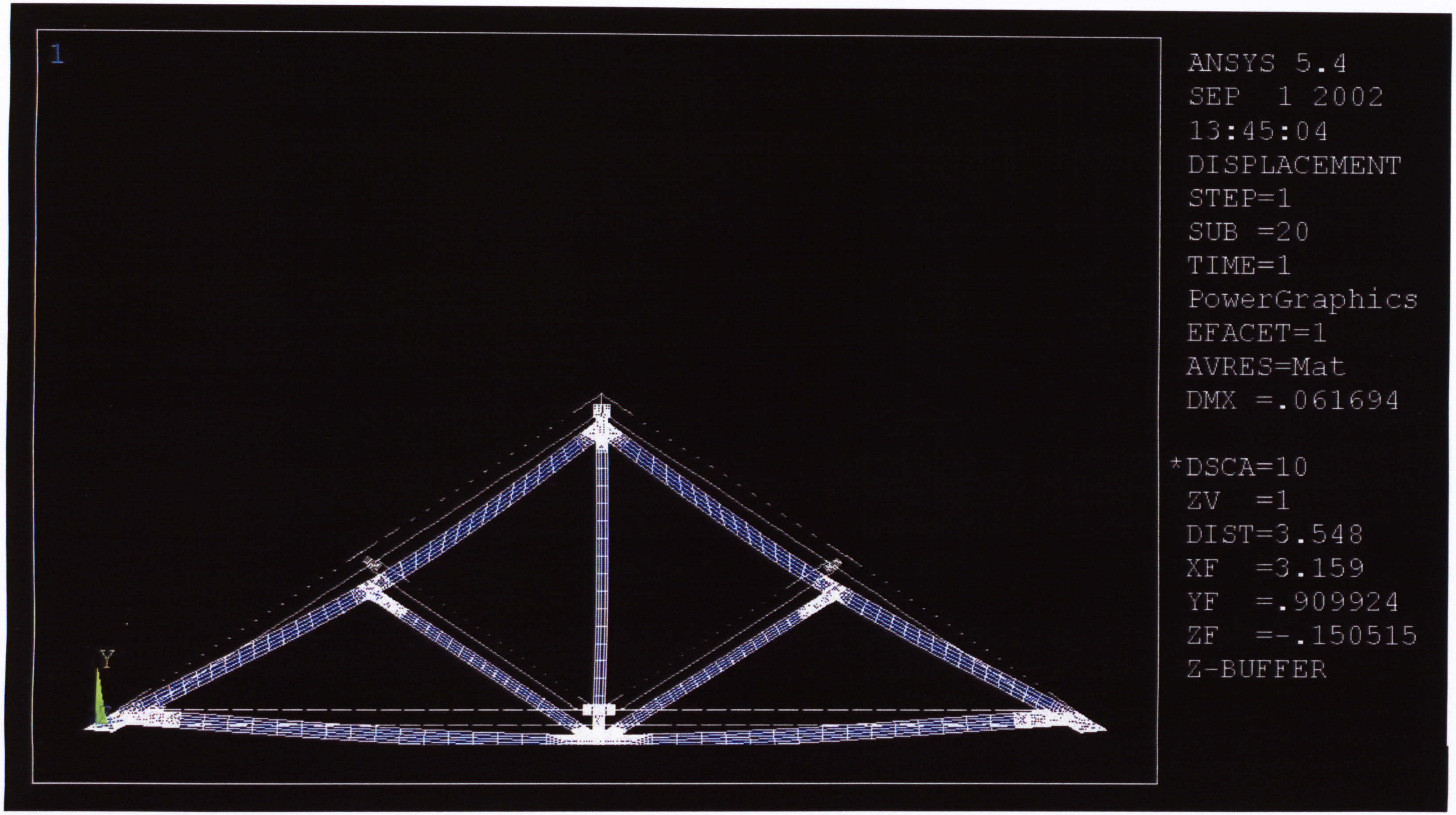

Fig. 6.9.3 – Deflection for symmetrical finite element analysis

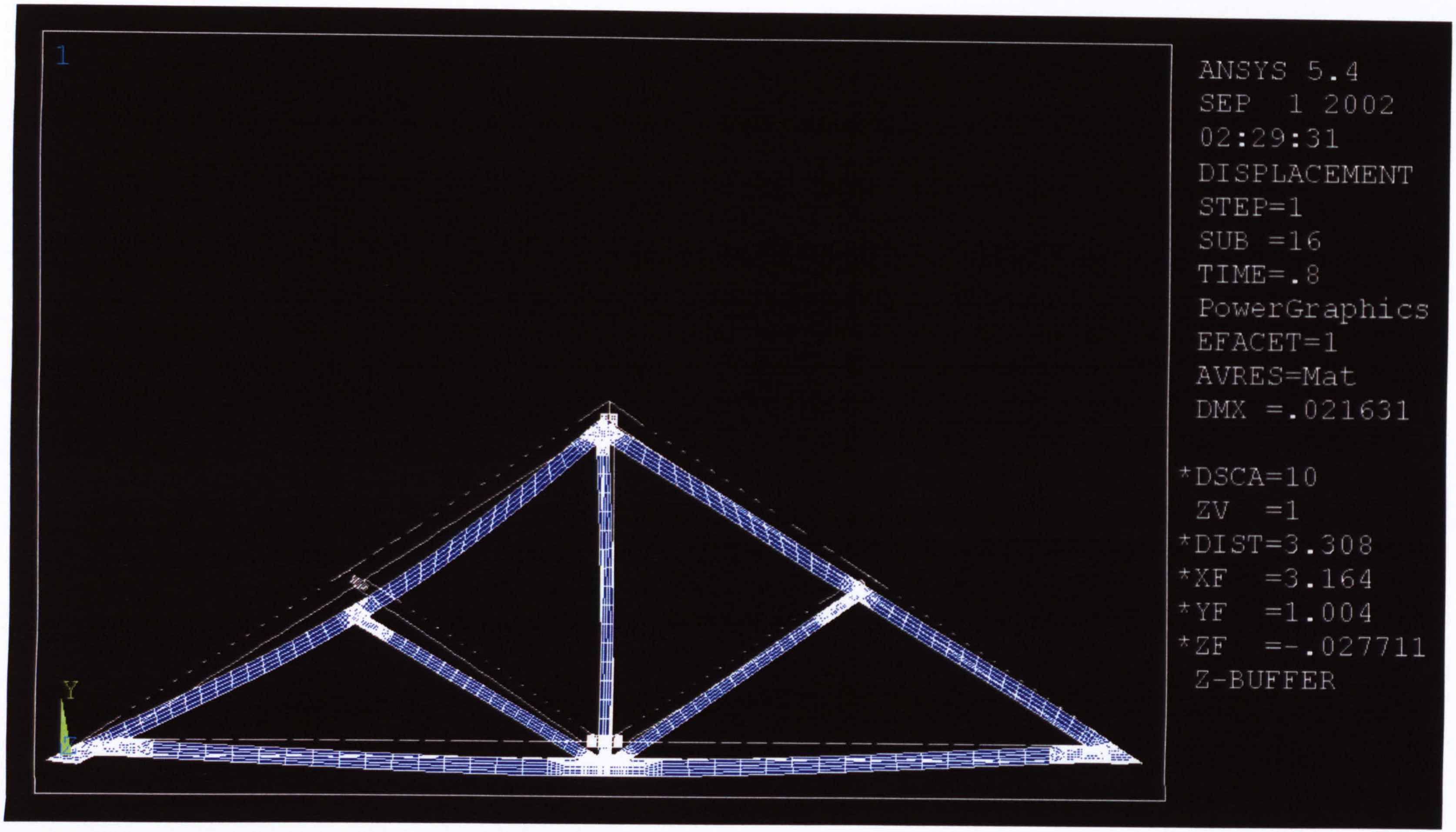

Fig. 6.9.4 – Deflection for unsymmetrical finite element analysis

The truss displacements in Fig 6.9.3 describe an accurate account of the actual behaviour of the truss near ultimate capacity. As observed in the test, maximum displacement is located at the centre of the truss. The load displacement plots in Fig. 6.9.1 confirm that the model closely represents the actual truss test results. The slight kink in the model results is due to the assumed bi-linear behaviour of the heel joint. Referring back to Fig. 6.9.3, the plot of the top chord slipping at the heel joint closely reflects the behaviour of the truss as observed in the symmetrically loaded truss tests. The result of the unsymmetrical case as plotted in Fig. 6.9.2 shows of similar accuracy. Model results closely follow the truss test data plots. In Fig. 6.9.4, the maximum displacement is located at the centre of the truss. This was also observed in the unsymmetrically loaded truss test. The unsymmetrical load is highlighted by biased displacement on the left side of the truss at the top chord joint where the load was applied. In addition, the plot shows slippage of the top chord at the heel joint is far greater on the left side of the truss than the right. This closely represents actual unsymmetrically loaded truss test observations. The displacement for both truss plots is scaled up 10 times the original to emphasise the response. As far as central truss deflection is concerned, the response for the symmetrical and unsymmetrical load cases are similar and is in close agreement with the test results.

From the failed test specimens it is postulated that failure of the heel joint was due to the pullout of the nail plate. This was located at the edge of the plate represented by the profound difference in behaviour between neasr the edge and away from the edge. This may be simply caused by weakness of the joint at the edge of the plate or an uneven distribution of stresses in the plate.

Indeed nail plate stress distribution ha been studied in articles as cited in the literature review.

A snapshot of the X and Y stresses in the heel joint at 25KN load is presented in Fig. 6.9.5 and Fig. 6.9.6. The ANSYS stress output shows there are great stress variations in the connection. The stresses peak in the area where the top and bottom chords meet whilst a gradual reduction of stress is exhibited away from this area. Plot of stresses in the X direction in Fig. 6.9.5 shows the plate is mainly in tension as the bottom chord is also in tension. The maximum tensile stresses are located parallel to the where the bottom and top chords meet at the joint. This is reasonable as in these areas, there is no timber to support tensile loads, thus the load is completely supported by the plate at these areas, hence a high concentration of stress Elsewhere on the plate, stresses are far lower as tensile stresses are distributed among the plate and timber. The same explanation can be given to stresses in the Y direction. As plotted in Fig. 6.9.4, the plate is in compression. Compression stresses are due to the top chord sliding. The maximum stresses are again at the interface between the top and bottom chord, the explanation is similar as the steel plate supports the load where there is no timber and shared among the timber and plate where the plate is connected to the timber. The stress plots show that stresses are low at the top corner of the plate, at the top chord. This is also the area where failure initiates. It is an indication of how weak the joint is at the edge and corners of the plate. In the truss tests, the largest deformation is at the corner of the plate at the top chord.

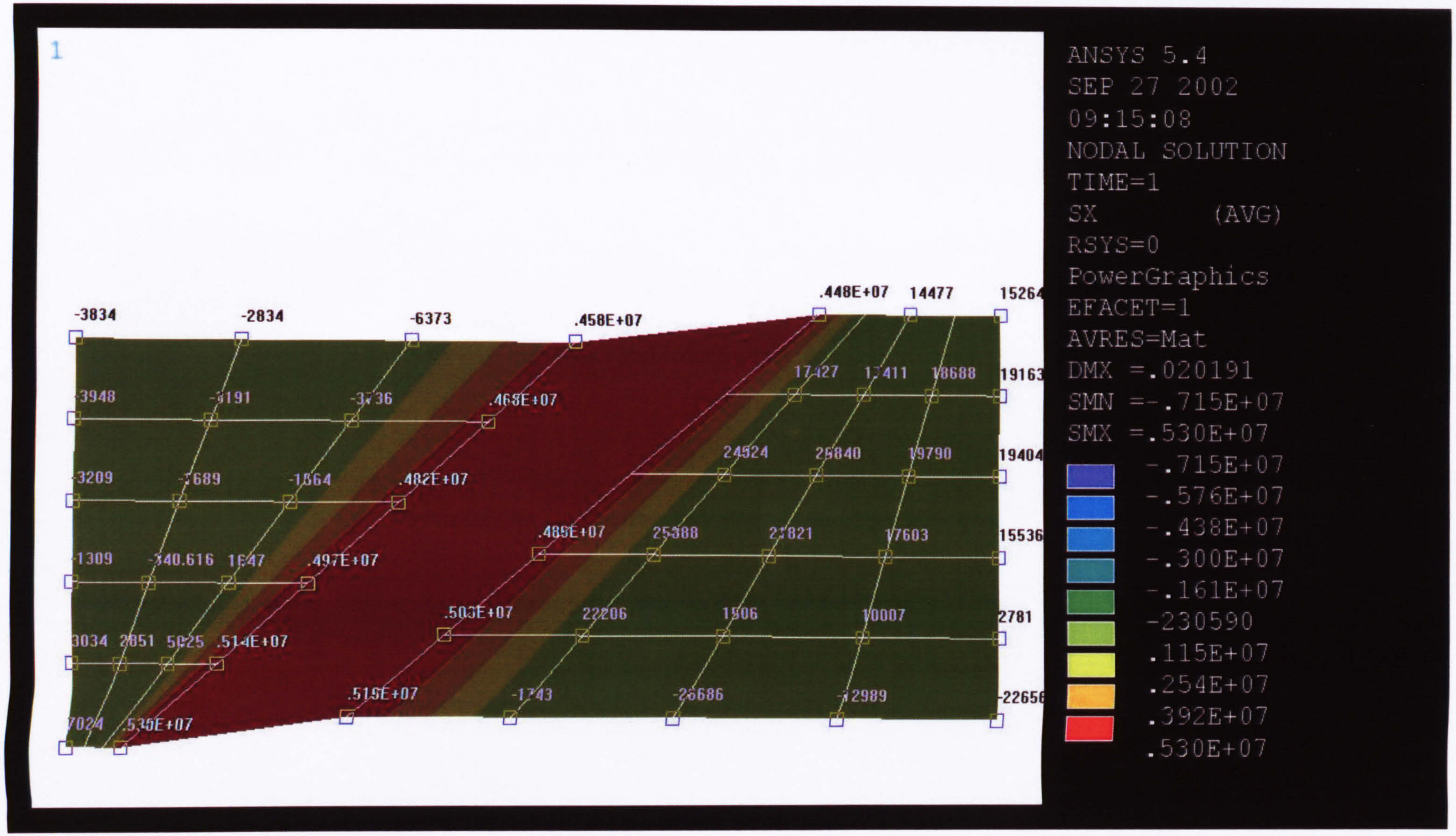

Fig. 6.9.5– Stress analysis of heel joint in X direction

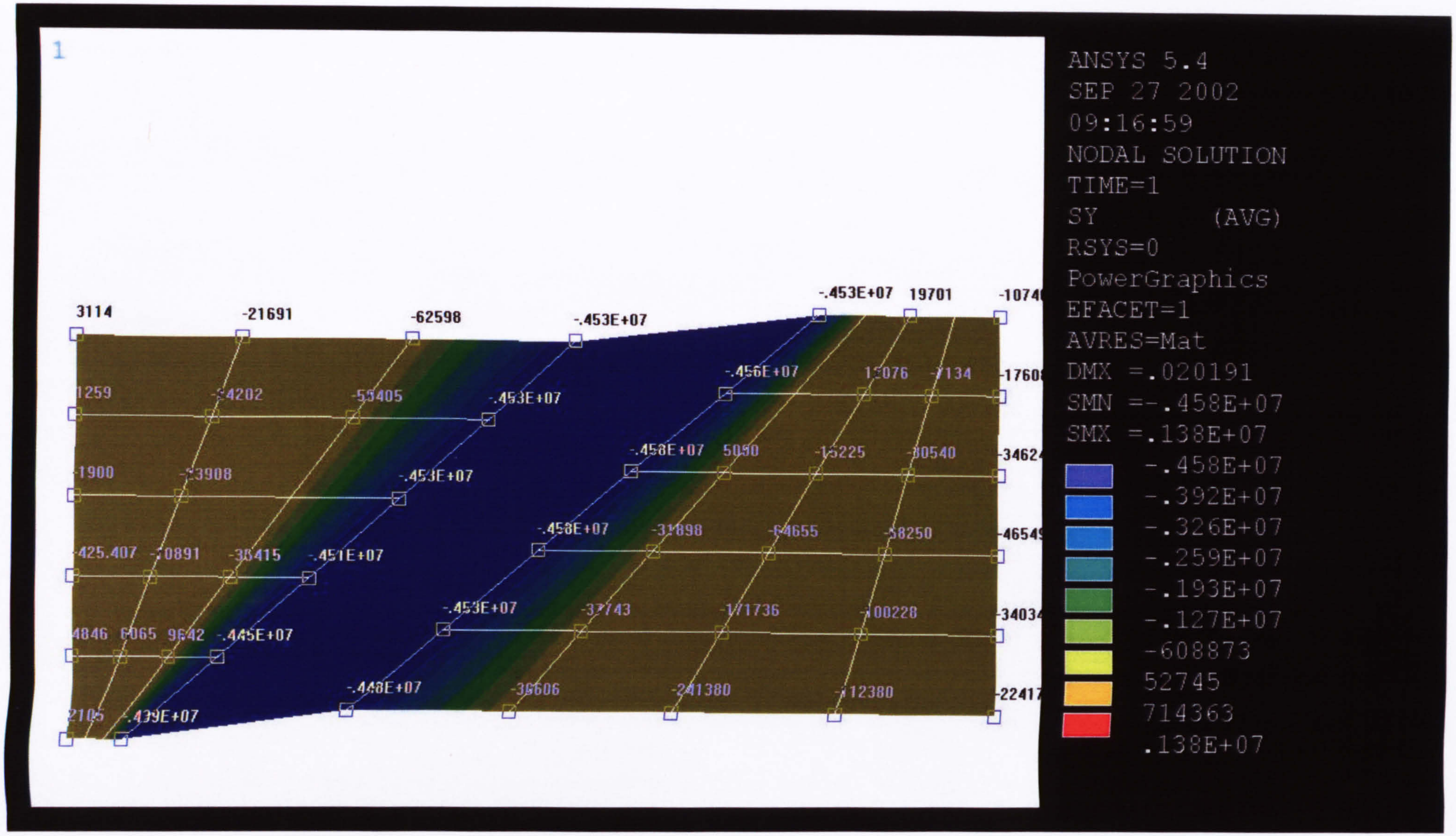

Fig. 6.9.6– Stress analysis of heel joint in Y direction

Chapter 7

Conclusion

7.1 General

An extensive test programme has been carried out in this thesis where all the connections comprising the Queen truss have been tested to determine connection properties. The effects of combined axial and flexural loads were also investigated. In this project, a new technique of measuring displacements using photogrammetry is used and shows a huge potential in delivering detailed results for member and plate distortion. Data that previously have not been retrieved can now be made available. In this project the deformations of the plates have been measured in detail. In the future data of this kind would be useful to plate manufacturers. The stress distribution in the plate can also be measured experimentally. However, the amount of work required for the measurements compared to conventional measuring methods also increased.

7.2 Joint tests

The results of the joint tests suggest that the connections respond differently under combined loads compared with flexural loading. In fact some connections showed higher stiffness under combined loads. A typical example is the HJTM series test where larger bending moments allowed the heel joint to show higher axial capacity. The initial stiffness in these tests were similar but the difference was in the axial load capacity. Generally, it has been observed that the combined loading has less effect on the stiffness of the connection, but more on its strength capacity. Results of repeated tests are close which suggests that the timber strength had varied little. However, variations in timber strengths were found in tests TCJTA4 and TCJTA5. Nevertheless, the general

quality of the timber was good. Closer observation of the failed specimens showed that pull out was the common failure mechanism. This also indicated that there existed either an uneven stress distribution in the plate or a profound weakness at the edge of the plate in the form of nail pulling out of the timber. Pullout is essentially caused by failure between the tooth plate and the timber. A tight fit of the tooth plate nail in the timber and ultimately the friction between the tooth and timber governs the pull out strength of the joint.

In the case of plate failure, usually between the slots where material is minimal, the failure mechanism here is simply shear in the steel.

7.3 Truss tests

Large bending moments were not achieved in the truss test due to the small dimensions of the truss members. As discussed, one way of achieving larger bending moments is to load the truss on the members away from the connections as adopted in tests FST4-6. The distance of the point of application of the force had to be limited as loading further away could possibly lead to premature failure of the member and would not have tested the joints under truss load conditions. Should the member be deeper, loading at the member further away from the joint would be feasible.

Failure of the Queen truss for the symmetrical and unsymmetrical load tests were located at the heel joint. This was due to loading at the top chord which was subjected to significant axial compression loads. The heel joint provided the main reaction to this load, making it the most heavily loaded joint in the truss which lead to the heel joint failing first. The mode of failure was pull out at the

corners of the plate at the top chord. This was with the exception of test FST2, where the truss was supported at the top chord instead of the bottom chord. The reaction to this was excessive tensile loading perpendicular to the grain at the top chord. In general, timber is weak perpendicular to the grain. In this test, the truss failed earlier as the strength of timber perpendicular to the grain appears to have dictated the truss capacity.

In all tests no signs of failure were observed at the other connections which means capacity was not reached in those regions.

7.4 STRUSS and Finite element model

Two approaches of predicting truss response through using test data have been reported. Initially, STRUSS results were compared to test results where discrepancies were found, most notably when load was approaching truss capacity. Sensitivity analysis showed that the truss is sensitive to the axial stiffness of the heel joint. An arbitrarily chosen tangent axial stiffness value was investigated, namely KA1 of the heel joint where improvement of the results were found.

STRUSS indicates that the heel joint is under substantial axial compression load where as the bending moment and axial capacity in the other joints were never reached. The analysis also revealed that rotational stiffness has little effect on truss response due to nodal loads and symmetrical loads which cause low bending moments in the truss and high axial loads. However, if the new proposed model in Fig. 6.8.4 is adopted substantial bending moments due to eccentricity, at the heel joint and other joints maybe detected. The sensitivity of the truss due to rotational stiffness and shear is difficult to determine with the current model. Nevertheless there is general agreement between STRUSS and tests that the capacity of the other connections have not been breached. To examine this issue, a pinned assumption in STRUSS was tried and this showed little difference in truss response compared to the rigid assumption, a sign of low bending moment in the truss. STRUSS had been validated with examples with pin and rigid jointed assumptions by Brebbia[47,48] as detailed in Appendix C3. Although non-linear timber behaviour was not accounted for in the analysis and observed in the tests, in other structures they could be significant.

The finite element connection model focuses on the load slip behaviour of the connection. The modulus, yield stress, and tangent modulus of each connection are derived from the joint test results and implemented into the model. Good agreement was obtained between the model and the test data for both symmetrical and asymmetrical load cases. The model has given good results as eccentricity in the connection is already accounted for due to the 2-D nature of the mesh. The deduced values of the heel joint are derived from pure axial load tests from HJT1. This indicates that in fact the values prescribed for the connection are accurate and leaves the eccentricity factor the cause of difference in the results in STRUSS model.

Generally STRUSS, ANSYS and the test results all agree that the heel joint is the most critical part of the truss. These also agree that the effects of symmetrical and unsymmetrical load systems are similar in terms of the central deflection of the truss.

The study shows that the heel joint is the most critical in the truss. As demonstrated in the truss tests, the mode of failure is nail pulling out of the timber. This behaviour is local to the heel joint and no other signs of failure or plastic behaviour were observed in the other joints. Although all joints should be treated equally, it seems obvious that the capacity of the truss can be increased if the strength of the heel joint is increased. This would allow more of the forces to be distributed to the other joints, thus achieving a more balanced truss in terms of force distribution. The truss is designed to BS 5268, but it is clear that a single weak joint results in an inefficient truss as demonstrated.

7.5 Summary

The objectives set out in Section 1.6 have been achieved. The axial and rotational stiffness for all the joints have been determined through extensive joint tests. In the presence of bending moment, an attempt has been made to measure the shear stiffness of the connections. Load deflection plots of the joint test results indicate that there is interaction between axial loading and rotational stiffness, and bending moments on axial stiffness. Full scale truss tests have been successfully conducted and have produced load displacement results for the overall comparison between the 2-D beam element and finite element model. The experimental results from joint tests have been implemented into a program STRUSS developed here and a finite element model. STRUSS has produced satisfactory results compared to the full scale truss test. Where the comparison was not so good an attempt has been made to explain the difference. The answer may lie in connection eccentricity. A good comparison is achieved between the 2-D finite element model and the truss test results. As discussed in Section 6.9, fundamental truss behaviour such as the top chord slipping at the heel joint have been successfully represented in the model. Both models compare well when defining fundamental characteristics of the Queen truss behaviour under nodal loads where truss response is sensitive to heel joint axial stiffness.

7.6 Future Work

This study has demonstrated the application of experimental data to theoretical analysis techniques. The use of photogrammetry have contributed to experimental data acquisition and proved a useful tool in measuring structural movement to a high degree of accuracy and also provide comprehensive data.

Although the model of the plate in the FE analysis has provided details of the stress distribution, its applicability and accuracy can only be measured through further tests. These tests would include obtaining displacement measurements on the surface of the plate. The photogrammetry method mentioned in this report can be employed to obtain these displacements. The strains can be determined from these tests thus deducing the stresses as the Young's modulus of the plate is known. Measured stresses can then be compared to the FE model.

In this study, the Foschi function proved to be a useful equation to implement into the stiffness matrix. The parameters K, K_0, and K_1 were determined by fitting the curve to the load displacement results of the joint experiments. The parameters were varied until a good fit, judged by eye, was achieved. Although it appears to be a reasonable fit it can be, however, a biased way to treat the data. A less biased way would be by using the least squares method to fit a regression curve to the data. Nevertheless results are not expected to change significantly.

The experimental tests reported herein lack repeatability. Although the quality of the timber supplied was generally of a high standard and there was consistency in repeated tests, each timber test should be repeated a few times before full confidence is achieved in there reliability.

References

[1] **Monforton,G.R; Wu,T.S**,(1963), Matrix analysis of SC steel frames, J Struct Eng, Vol. 8, pp. 13-42

[2] **Lei Xu; Grierson, D.E,** (1993), Computer automated design of semi-rigid steel frameworks, Vol 119, No. 6, June 1993, pp 1740-1760

[3] **Sasaki and Takemura**, (1990), Non-linear analysis of metal-plate wood trusses, 1990 International Timber Engineering Conference, Tokyo, pp 701-708

[4] **Gupta, R; Gebremedhin, K.G; Cooke, J. R**; (1992), Analysis of Metal-plate-connected wood trusses with semi-rigid joints, ASAE, Vol 35(3), pp 1011-1018

[5] **Vatovec, M; T.H, Miller; Gupta,R** (1996), Modeling of Metal-plate-connected wood truss joints, Transaction of the ASAE, Vol 39(3), pp 1101-1111

[6] **Vatovec, M; T.H, Miller; Gupta,R; Lewis, S** (1997), Modeling of Metal-plate-connected wood truss joints, Application to overall truss model, Transaction of the ASAE, Vol 40(6), pp 1667-1675

[7] **Crovella and Gebremedhin** (1990), Analyses of light frame wood truss tension joint stiffness, Forest Product Journal, Forest Products research society 40(4), pp 41-47

[8] **Gebremedhin and Crovella** (1990), Analysis of light frame wood truss joint using an elastic foundation model, 1990 International Timber Engineering Conference, Tokyo, pp709-715

[9] **Groom,L and Polensek,A** (1992), Nonlinear modeling of truss plate joints, Journal of Structural Engineering, Vol. 118, No. 9, pp2514-2531

[10] **Cramer, S.M; Shrestha, D; Fohrell, W.B** (1990), Theoretical consideration of Metal plate connected wood splice joints, Journal of Structural Engineering, Vol. 116, No. 2, pp3458-3474

[11] **Cramer, S.M; Shrestha, D; Mtenga, P.V**, (1993), Computation of member forces in metal plate connected trusses, Structural Engineering Review, Vol. 5, No. 3, pp209-217

[12] **Foschi, R.O** (1974), Load slip characteristics of nails, Wood Science, Vol 7, No. 1, pp69-76

[13] **Beineke, L.A; Suddarth, S.K,** (1977), Modeling joints made with light gauge metal connector plates, Forest Products Journal, Vol. 29, No. 8, pp39-45

[14] **Demarkles, L.R,** (1955), Investigation of the use of a rubber anolog in the study of stress distribution in riveted and cemented joints, National Advisory Committee for Aeronautics Tech. Note No. 3413

[15] **Kuenzi, E.W** (1953), Theoretical design of a nailed or bolted joint under lateral load, Forest products Lab. Report No.1951, USDA Forest Service, Forest Products laboratory, Madison, Wis.

[16] **Lau** (1987), Factors affecting the behaviour and modelling of toothed metal-plate joints, Canadian Journal of Civil Engineering, Vol(14), pp183-195

[17] **PPSA 2**, Purdue Plane Structural analyser, United states Forest Products Laboratory, Madison, WI
Suddarth, S.K and Wolfe,R.W (1984), Purdue Plane structures analyser 2, A computerised wood Engineering System. General technical report FPL-40, United states Department of Agriculture, Forest Service, Forest Products Laboratory, Madison, WI

[18] **SAT**, Forintek Western Laboratory, Vancouver, British Columbia.
Foschi, R.O (1977a) Analysis of wood diaphragms and trusses, Part 1; diaphragms. Canadian Journal of Civil Engineering, 4, pp345-352

Foschi, R.O (1977b) Analysis of wood diaphragms and trusses , Part 2, Truss-plate connections. Canadian Journal of Civil Engineering, 4, pp353-362

[19] **Poutanen,T.T** (1988) Proceedings of the 1988 International conference on timber engineering, Forest Prod. Res. Soc., p266-273

[20] **King and Wheat** (1998), Deflection and member behaviour of MPC parallel chord wood trusses, Proceedings of the 1998 International conference on timber engineering, Vol 1, pp482-500

[21] **Riley, G; Gebremedhin,K.G; White, R.N** (1993), Semi-rigid analysis of Metal Plate-Connected wood trusses using fictitious members, American Society of Agricultural Engineers, Vol 36(3), pp 887-894

[22] **Gupta,R ; Gebremedhin**,(1990), Destructive testing of Metal plate connected wood truss joints, Journal of Structural engineering, Vol 116, No. 7, pp 1971-1982

[23] **Vatovec, Gupta, Miller** (1996), Testing and Evaluation of Metal Plate Connected Wood Truss Joints, Journal of Testing and Evaluation, Vol. 24, No. 2, March 1996, pp63-72

[24] **Wolfe, W** (1989), Metal plate connections loaded in combined bending and tension, Forest Products Journal, Vol. 40(9), pp 17-23

[25] **Gupta,R**; Metal plate connected tension joints under different loading conditions, Wood and fiber science, Vol 26(2), pp 212-222

[26] **Massé, D.I; Salinas, J.J**; (1986), Analysis of timber trusses using semi-rigid joints, Canadian Agricultural Engineering, Vol 30, pp 111-124

[27] **O'Regan,P; Woeste, F.E; Lewis,S.L** (1998), Design procedure for the steel net-section of tension splice joints in MPC wood trusses, Forest Product Journal, 48(5), pp 35-42

[28] **Noguchi, M** (1980), Ultimate resisting moment joint of butt joints with plate connectors stressed in bending, Wood Science, 12(3), pp168-175

[29] **Tsai and Wu** (1971), A General Theory of strength for Anisotropic Materials, Journal of Composite Materials, Vol. 5, pp58-80

[30] **Hasbe and Usuki**, (1989), Application or Orthotropic failure Criterion to Wood, Journal of Engineering Mechanics, Vol.115, No. 4, pp867-872

[31] **Bouchair, A; Vergne** (1995), An application of the Tsai criterion as a plastic flow law for timber bolted joint modelling, Wood Science and Technology 30, pp3-19

[32] **Goodman, J.R ; Bodig,J** (1970), Orthotropic strength of wood in compression, Wood Science, Vol.4, No.2, pp83-94

[33] **Hankinson, R.L** (1921), Investigation of crushing strength of spruce at varying angles of grain, Air service information circular Vol 3, No. 259, (Materials Section paper No. 130)

[34] **Bodig,J ; Goodman, J.R** (1973), Prediction of elastic parameters for wood, Wood Science, Vol. 5, No.4, pp249-264

[35] **Pellicane, P.J; Bodig, J; Mrema, A.L** (1994), Behaviour of Wood in Transverse Compression, Vol. 22, No.4, pp383-387

[36] **Tabiei, A; Wu, J** (2000), Three dimensional non-linear orthotropic finite element material model for wood, Composite structures, vol. 50, No. 2, pp143-149

[37] **Mallory, M.P; Cramer, S.M; Smith, F.W; Pellicane, P.J** (1997), Non-linear material models for analysis of bolted wood connections, Journal of structural Engineering, Vol. 123, No. 8, pp1063-1070

[38] **BS5268**, Structural use of timber Part 2 (1996), Code of practice for permissible stress design, materials and workmanship & Part 3 (1997), Code of practice for trussed rafter roofs, BSI

[39) **Smith,T.R.G** (1983) Linear analysis of frameworks, Ellis Horwood Limited, pp316

[40] **Hall. A.S and Woodhead, R.W** (1967), Frame analysis, 2nd Edition, John Wiley and Sons, pp186

[41] **Coates, R.C; Coutie, M.G and Kong, F.K** (1988), Structural analysis, 3rd Edition, Chapman and Hall, pp253

[42] **Kirby, P.A and Nethercot, D.A** (1978), Design for structural stability, Granada publishing, pp40-44

[43] **Brebbia, C.A & Ferrante,** (1979) A.J, Computational methods for the solution of engineering problems, pp 179-187, Pentech press Ltd

[44] **Kermani, A** (1999), Structural timber design, Blackwell Science, pp18

[45] **Kermani, A** (1999), Structural timber design, Blackwell Science, pp7

[46] **ANSYS 5.4**, Theory Manual

[47] **Brebbia, C.A & Ferrante,** (1979) A.J, Computational methods for the solution of engineering problems, pp 147-148, Pentech press Ltd

[48] **Brebbia, C.A & Ferrante,** (1979) A.J, Computational methods for the solution of engineering problems, pp 188-189, Pentech press Ltd

[49] **ASCE** (1975), A design guide and commentary – Wood structures, American society of Civil engineers.

[50] **STEP** (1995), Timber Engineering Step 1, 1st Edition

[51] **American Society for photogrammetry and remote sensing** (1989), Science and Engineering series, Non-topographic photogrammetry, 2nd Edition, Edwards Brothers Incorporated, pp37-69

[52] **Atkinson, K.B** (1996), Close range photogrammetry and machine vision, Whittles publishing, pp9-51

Bibliography

[1] **Cook, R.D** (1981), Concepts and Applications of Finite element analysis, 2nd Ed., John Wiley and Sons

[2] **Desai, C.S & Abel, J.F** (1972), Introduction to the finite element method, Van Nostrand Reinhold Company.

[3] **Zienkiewicz, O.C** (1997), The Finite Element method, 3rd Ed., McGraw-Hill Book Company (UK) Limited

[4] **James, A.D Balfour,** (1992), Computer analysis of structural frameworks, 2nd Ed., Blackwell Scientific Publications.

[5] **Hill, R** (1971), The Mathematical theory of Plasticity, Oxford Engineering Science series, Oxford University Press

[6] **John, L. Meek,** (1971), Matrix structural analysis, McGraw-Hill Book Company

[7] **Smith, I.M & Griffiths, D.V** (1988), Programming the finite element method, 2nd Ed, John Wiley & Sons

[8] **Megson, T.H.G** (1987), Strength of materials for civil engineers, 2nd Edition, Edward Arnold (Publishers) Ltd.

[9] **Breyer, D.E** (1993), Design of wood structures, 3rd Edition, McGraw Hill

[10] **Baird, J.A. & Ozelton, E.C.** (1984) Timber designers manual, 2nd Edition, Granada publishing.

[11] **W. M. C. Mckenzie** (2000), Design of structural timber, Macmillan press Ltd

[12] **Gurewich, N & Gurewich, O** (1993), Visual basic 4.0 in 21 days, Sams publishing, 3rd Edition.

[13] **John Cowell** (1997), Essential visual basic 5.0, Springer

Appendix A1 Truss design

City University London	Subject: Design of Queen truss		Date: 17-02-04
Project: Analysis of Semi-rigid Metal Plate Connected Truss	Design code: BS5268 Part 2 & 3	Designed by: SKM Checked by: KSV	Sheet No.255

Trussed rafter design

Truss data

Top and Bottom members	35x97 1,2,4,5,7,8
Web members	35x72 3,9,6

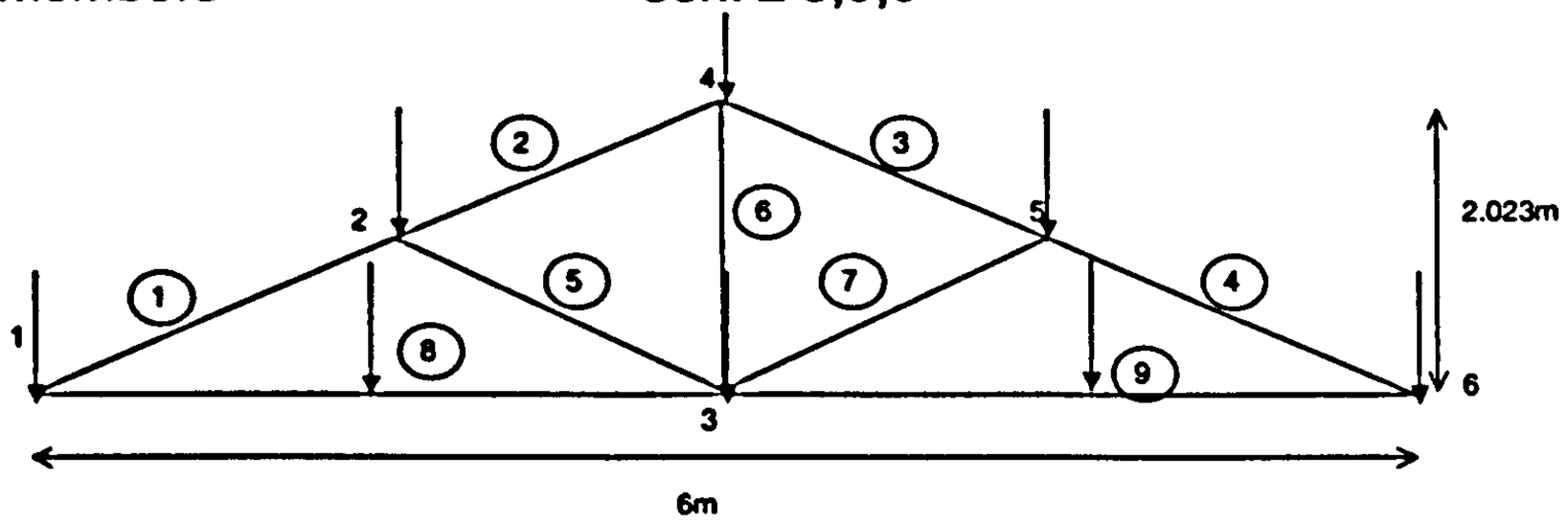

Forces in members as a result of BS5268-3, 6.4. Loads converted to point loads as detailed above.

Timber Specification

Strength class	:TR26
Bending // to grain	:10.0N/mm^2
Tension // to grain	:6.0N/mm^2
Compression // to grain	:8.2N/mm^2
Compression - to grain	:2.5N/mm^2
Shear // to grain	:1.10N/mm^2
Modulus of elasticity (mean)	:11000N/mm^2
Modulus of elasticity (min)	:7400N/mm^2
Characteristic density	:370kg/m^3
Average density	:450kg/m^3

Loads

Dead loads and live/imposed loads

loads on top chord

Dead loads

Weight of tiles	$0.575 KN/m^2$
Weight of felt battens and rafter	$0.110 KN/m^2$
Total	$0.685 KN/m^2$

Live/imposed

Snow loading	$0.683 KN/m^2$

CITY City University London	Subject: Design of Queen truss		Date: 17-02-04
Project: Analysis of Semi-rigid Metal Plate Connected Truss	Design code: BS5268 Part 2 & 3	Designed by: SKM Checked by: KSV	Sheet No.256

Loads on Bottom chord

Dead loads

Weight of whole ceiling area $0.25KN/m^2$

Live/imposed

Concentrated load (Man) $0.9KN$

Type 3,

Load duration

Modification factor K_3 for duration of loading Table 14, $K_3 = 1.25$

Applicable for stress values only, not E

Depth factor

For members with a depth of 72 mm or more, apply depth factor for bending stresses

$K_7 = (300/h)^{0.11} = (300/97)^{0.11} = 1.132$

For members with a depth of 72 mm or less, apply depth factor of $K_7 = 1.17$ for bending stresses.

Method of design

Generalised method of analysis

The analysis assumes the joint is rotationally pinned. Centre lines of the joints do not meet at a common point. However, they can be ignored according to fig. 2

The height of the rafter measured at the centre of the span exceeds 0.15 times the span of the truss.

Member design

Members are designed in accordance with the recommendations of BS5268-2

Lateral support

It is assumed that lateral restraints for the members will be provided by purlins and will therefore satisfy BS5268-3, cl. 2.10.8, table 16. In any case, the calculation is carried out. Checks are also carried out for buckling.

Depth to breadth ratio $= \frac{97}{35} = 2.771$, therefore ok as ends are held in position.

City University London	Subject: Design of Queen truss		Date: 17-02-04
Project: Analysis of Semi-rigid Metal Plate Connected Truss	Design code: BS5268 Part 2 & 3	Designed by: SKM Checked by: KSV	Sheet No.257

Design for compression members 5, and 7

a) Internal compression members 5 and 7

$k_l = 0.9$

Depth factor

Depth factor not applicable as member is subjected to axial loading only.

Slenderness ratio

The slendemess ratio of compression member 5 & 7 is the effective length divided by the radius of gyration

The radius of gyration is $i = \sqrt{\frac{I_z}{A}} = \sqrt{\frac{1088640}{2520}} = 20.785$

$\therefore \quad L_e = 0.9 \times 1809 = 1628.1mm$

Hence, the slendemess ratio is $\lambda = \frac{L_e}{i} = \frac{1628.1}{20.785} \approx 79$ ∴ O.K

Members subject to axial compression (without bending)

Axial loading for members 5 & 7 $= 947.4N$

compression stress // to grain $\sigma_{c,//} = \frac{947.4}{2520} = 0.376Nmm^{-2}$

$\sigma_{c,adm,//} = 8.2K_3 = 8.2 \times 1.25 = 10.25Nmm^{-2}$ ∴ O.K

Lateral buckling

Refer to note BS5268-2, 2.10.8.

Shear

N/A

Deflection

See end for global deflection of truss

Bearing perpendicular to the grain

N/A

Design for compression members 1,2, 3 and 4

b) Chord compression members 1, 2, 3 and 4

$k_l = 0.8$

Depth factor

$K_7 = 1.132$

City University London	Subject: Design of Queen truss		Date: 17-02-04
Project: Analysis of Semi-rigid Metal Plate Connected Truss	Design code: BS5268 Part 2 & 3	Designed by: SKM Checked by: KSV	Sheet No.258

Slenderness ratio

Radius of gyration $i = \sqrt{\frac{I_z}{A}} = \sqrt{\frac{2661962.927}{3395}} = 28.001$

$\therefore \quad L_e = 0.8 \times 1809 = 1447.2mm$

Hence, the slenderness ratio, $\lambda = \frac{L_e}{i} = \frac{1447.2}{28.001} = 51.684$ ∴O.K

Check for buckling

Member 1 and 4

Axial loading for both members $= 5244.3N$

External loading $=$

compression stress // to grain $\sigma_{c,//} = \frac{5244.3}{3395} = 1.545 Nmm^{-2}$ ∴ O.K

Member 2 and 3

Axial loading for both members $= 4280.5N$

Compression stress // to grain $\sigma_{c,//} = \frac{4280.5}{3395} = 1.261 Nmm^{-2}$

For members 1, 2, 3 and 4

Members subject to axial compression and bending

$$\frac{\sigma_{m,a//}}{\sigma_{m,adm//} K_7 \left(1 - \frac{1.5\sigma_{c,a//} K_3}{\sigma_e} \times K_{12}\right)} + \frac{\sigma_{c,a//}}{\sigma_{c,adm//}} \leq 1$$

$\sigma_{m,a//}$ is the maximum applied moment in the member, which is at the fixed end in this case as the other end is pinned.

Modification factor for compression member 1, 2, 3, and 4

$$K_{12} = \left\{\frac{1}{2} + \frac{(1+\eta)\pi^2 E}{2N\lambda^2 \sigma_c K_3}\right\} - \left[\left\{\frac{1}{2} + \frac{(1+\eta)\pi^2 E}{2N\lambda^2 \sigma_c K_3}\right\}^2 - \frac{\pi^2 E}{N\lambda^2 \sigma_c K_3}\right]^{\frac{1}{2}}$$

detailed in **6.4.3** $K_3 = 1.25$

$$\left\{\frac{1}{2} + \frac{(1+\eta)\pi^2 E}{2N\lambda^2 \sigma_c K_3}\right\} = \left\{\frac{1}{2} + \frac{(1+0.258)\pi^2 \times 7400}{2 \times 1.5 \times 51.684^2 \times 10 \times 1.25}\right\} = 1.417$$

$$\frac{\pi^2 E}{N\lambda^2 \sigma_c} = \frac{\pi^2 \times 7400}{1.5 \times 78.331^2 \times 10 \times 1.25} = 1.458$$

$\therefore \quad K_{12} = 0.675$

$\sigma_{c,adm//} = 8.2 K_3 K_{12} = 8.2 \times 1.25 \times 0.675 = 6.919 Nmm^{-2}$

Maximum moments at joint 2 and 5, ie.

City University London	Subject: Design of Queen truss		Date: 17-02-04
Project: Analysis of Semi-rigid Metal Plate Connected Truss	Design code: BS5268 Part 2 & 3	Designed by: SKM Checked by: KSV	Sheet No.259

$$\sigma_{m,all} = \frac{My}{I} = \frac{0.0201\times10^{6}\times48.5}{2.662\times10^{6}} = 0.366 Nmm^{-2}$$

$$\sigma_{c,all} = \frac{5244.3}{3395} = 1.545 Nmm^{-2}$$

$$\sigma_{e} = \frac{\pi^2 E}{(L_e/i)^2} = \frac{\pi^2(7400)}{(1447.2/28.001)^2} = 27.341 Nmm^{-2}$$

$$\frac{0.366}{10\times1.132\left(1-\frac{1.5(1.545)\times1.25}{27.341}\times0.675\right)} + \frac{1.545}{8.2(1.25)} = 0.1856 \therefore \text{O.K}$$

Lateral buckling
Refer to note BS5268-2, 2.10.8.

Shear stress at member

$\tau_{adm} = 1.10 Nmm^{-2}$

$\tau_{a} = \frac{3F_v}{2A} = \frac{3(11.1)}{2(3395)} = 4.904\times10^{-3} Nmm^{-2}$ ∴ O.K

Bearing
N/A

Deflection
Local deflection of nodes

Member	X_i(mm)	Y_i(mm)	θ_i(Rad)	X_j(mm)	Y_j(mm)	θ_j(Rad)
1	0.000	0.000	0.006	0.378	2.087	0.001
2	0.377	2.088	0.001	0.685	1.944	0.000
3	-1.545	1.364	0.000	-1.236	1.508	-0.001
4	-1.237	1.508	-0.001	-0.859	-0.580	-0.007

Local mid span deflection of rafters

Member	X(mm)	Y(mm)	θ(Rad)
1	0.189	1.260	0.001233
2	0.532	2.206	-0.000159
3	-1.390	1.628	-0.000159
4	-1.048	0.680	-0.001233

a) Local deflection of rafters must not exceed
$0.004\times1809 = 7.236mm$ ∴ O.K

Bearing
N/A
Design for Tension member 6

Depth factor
$K_7 = 1.17$

Tension members

Width factor

$K_{14} = 1.17$

Member subjected to just tension
$\sigma_{t,adm,ll} K_3 K_7 K_{14} = 6.0 \times 1.25 \times 1.17^2 = 10.267 Nmm^{-2}$
$\sigma_{t,a,ll} = \frac{2587.3}{2520} = 1.027 Nmm^{-2}$ ∴ O.K

Lateral buckling

Refer to note BS5268-2, 2.10.8.

Shear
N/A

Deflection

Member	X_i(mm)	Y_i(mm)	θ_i(Rad)	X_j(mm)	Y_j(mm)	θ_j(Rad)
6	-1.995	-0.158	0.000	-2.275	-0.518	0.000

No checks.
Design for Tension member 8, and 9

Simplified analysis
Along with the conditions as mentioned previously the following must also be complied to

Depth factor
$K_7 = (300/h)^{0.11} = (300/97)^{0.11} = 1.132$
Tension members

Width factor
$K_{14} = (300/h)^{0.11} = (300/97)^{0.11} = 1.132$

City University London	Subject: Design of Queen truss		Date: 17-02-04
Project: Analysis of Semi-rigid Metal Plate Connected Truss	Design code: BS5268 Part 2 & 3	Designed by: SKM Checked by: KSV	Sheet No.261

Member subjected to axial tension and bending

$\sigma_{t,adm,//} K_3 K_{14} = 6.0 \times 1.25 \times 1.132 = 8.49 Nmm^{-2}$

$\sigma_{m,adm,//} K_3 K_7 K_{14} = 10.0 \times 1.25 \times 1.132^2 = 16.018 Nmm^{-2}$

Bending moment will be at peak at the centre of the truss.

$= 0.9(1.5) - 0.491 = 0.859 KNm$

$$\sigma_{m,a,//} = \frac{My}{I} = \frac{0.859 \times 10^6 \times 48.5}{2.662 \times 10^6} = 15.650 Nmm^{-2}$$

$$\sigma_{t,a,//} = \frac{4341.2}{3395} = 1.279 Nmm^{-2}$$

$$\frac{\sigma_{m,a,//}}{\sigma_{m,adm,//}} + \frac{\sigma_{t,a,//}}{\sigma_{t,adm,//}} = \frac{8.952}{14.15} + \frac{1.279}{8.49} = 0.783 \qquad \therefore \text{O.K}$$

Lateral buckling

Refer to note BS5268-2, 2.10.8.

Shear

Maximum shear at node 3

Shear force in the member $= 613.8N$

$$\tau_a = \frac{3F_v}{2A} = \frac{3(613.8)}{2(3395)} = 0.271 Nmm^{-2}$$

Deflection

Local nodal deflections

Node	X_i(mm)	Y_i(mm)	θ_i(Rad)	X_j(mm)	Y_j(mm)	θ_j(Rad)
8	0.000	0.000	0.006	-0.518	2.275	0.000
9	-0.518	2.275	0.000	-1.037	0.000	-0.007

Local ceiling tie centre deflections

Member	X(mm)	Y(mm)
8	-0.259	12.808
9	-0.777	12.808

Local deflection of ceiling ties must not exceed the following

b) $0.006 L_{bay} = 0.006(3000) = 18mm$ $\therefore$ O.K

Wall plates

Bearing at nodes 1 and 6

Total loads is 9235N, distributed equally among the bearings

The vertical bearing load is the sum of the loads equally distributed to the supports 1 and 6.

$$= \frac{9235}{2} = 4.6175N$$

The position and size of the wall plate is specified in the sketch below and is designed in accordance to BS 5268-3.

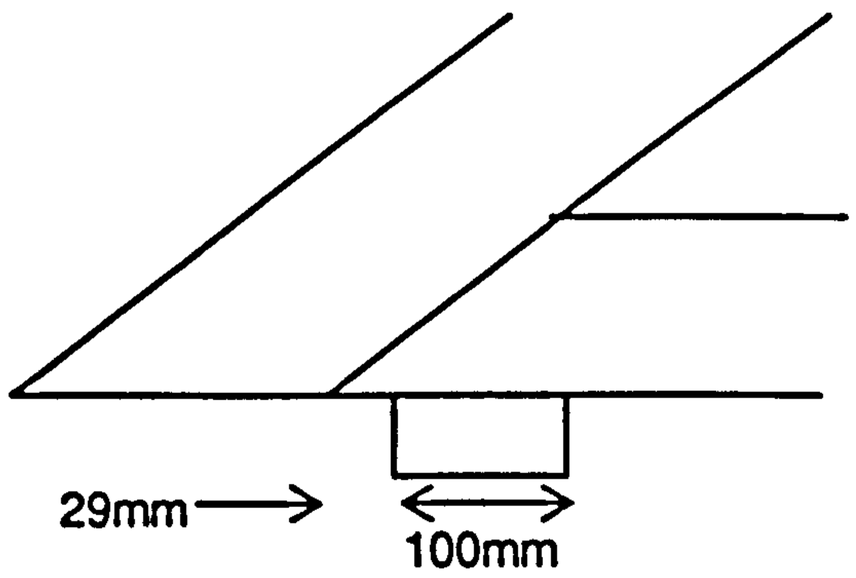

Area of bearing $= 35 \times 100 = 3500mm^2$

Hence, bearing force $= \frac{4617.5}{3500} = 1.319Nmm^{-2}$

Permissible compression stress perpendicular to the grain $= 2.5Nmm^{-2}$

∴O.K

Deflection of truss

Overall member displacements

Member	X(mm)	Y(mm)
1	-0.55	1.15
2	-0.79	2.13
3	-0.24	2.13
4	0.49	1.15
8	0.26	12.81
9	0.78	12.81

City University London	Subject: Design of Queen truss		Date: 17-02-04
Project: Analysis of Semi-rigid Metal Plate Connected Truss	Design code: BS5268 Part 2 & 3	Designed by: SKM Checked by: KSV	Sheet No.263

Deflections must not exceed the following.

O.K $0.003 \times 6000 = 18mm$ ∴ O.K

For Horizontal displacement
N/A

Global displacement

Node	X(mm)	Y(mm)	θ(mm)
1	0.00	0.00	6.25
2	-0.85	1.94	0.54
3	-0.52	2.28	0.00
4	-0.52	1.99	-0.35
5	-0.18	1.94	-0.54
6	-1.4	0.00	-6.51

d) **For vertical node displacement**
Any node must not exceed $12mm$ ∴ O.K

City University London	Subject: Design of Queen truss		Date: 17-02-04
Project: Analysis of Semi-rigid Metal Plate Connected Truss	Design code: BS5268 Part 2 & 3	Designed by: SKM Checked by: KSV	Sheet No.264

Design for joint 1 Heel joint

Structural performance

Lateral resistance of fastener

Edge distance of plate at bottom chord is

$\frac{97-93}{2} = 2mm$ $\therefore$ ignore 5mm at each side, hence plate width is 83mm.

Refer to drawing for dimensions

Nails required

Top chord member 1

Resultant of 2 forces

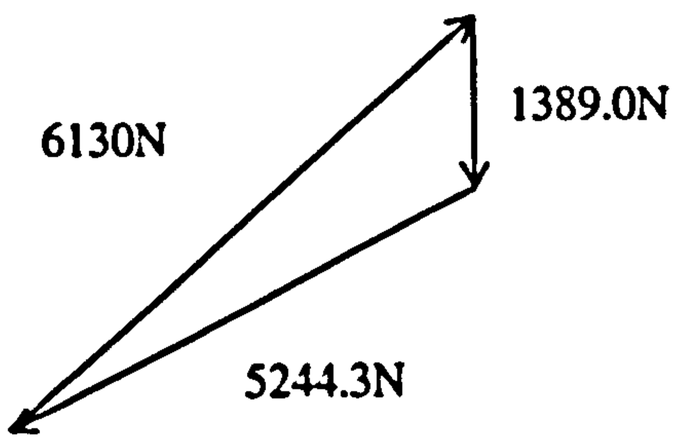

$A^2 = B^2 + C^2 - 2BC\cos 114$

$A^2 = 1.389^2 + 5.2443^2 - 2\times 1.389\times 5.2443\times\cos 124$

Solving the equation, $\therefore A = 6.130$ i.e. $6130.147N$

Use sine rule to determine angle between load and chord grain

$\frac{\sin 124}{6130.147} = \frac{\sin\vartheta}{1389}$ $\therefore$ $\vartheta = 10.827^\circ$

Angle of load to fastener length direction is 44.827°

Angle of load to grain member 10.827°

Hence, permissible load is $80K_3 = 80\times 1.25 = 100N$

Nails required in top chord $= \frac{6130.147}{2\times 100} = 30.651$, say 31

Bottom chord member 8

For equilibrium nails at bottom chord must oppose the force

Angle of load to fastener length direction is 44.827°

Angle of load to grain member 44.827°

Hence, permissible load is $51K_3 = 51 \times 1.25 = 63.75N$

Nails required in bottom chord $\frac{6130.147}{2 \times 63.75} = 48.080$, say 49

Tensile strength

Force acting in the direction of the fastener length = 4341.2

Minimal width required for tensile strength

$w = \left(\frac{4341.2}{2 \times 58}\right) \sin 34 = 20.927mm$, say 21mm

Compression strength

Force acting in the direction of the width at member 1 $= 1389N$

$l = \frac{1389}{2 \times 39} = 17.81mm$, say 18

same applies for member 8

Shear strength

Angle of shear to the plate is $34°$, permissible shear line $= 28Nmm^{-1}$

Required width of the plate for shear $w = \frac{5244.3}{2 \times 28} \sin 34 = 52.367mm$,

say 53mm

Required dimensions of plate

Length $= 2(18) = 36mm$

Width $= 53mm$

Joint design

Minimum fastener bite

Minimum fastener bite on chord members must not be less than the following

- $(0.2l + 15) = (0.2(\ ) + 15) = 28.4mm$
- $30mm$

$0.25(97) = 24.25mm$

Deflection

See deflection of truss for nodal deflection

Recommended plate size F67 150x67

Joint specification

City University London	Subject: Design of Queen truss		Date: 17-02-04
Project: Analysis of Semi-rigid Metal Plate Connected Truss	Design code: BS5268 Part 2 & 3	Designed by: SKM Checked by: KSV	Sheet No.266

Nails provided for top chord member 1: = 38

New strength $= 2 \times 100 \times 38 = 7.6KN$

Axial loading $= 6.5018KN$

Vertical load $= 1.722KN$

Nails provided for bottom chord member 8: = 58

New strength

$= 2 \times 63.75 \times 58 = 7.395KN$

Design for joint 2 Top Chord

Lateral resistance of fastener

Edge distance of plate is member depth minus plate width divided by 2

i.e. $\frac{72-41}{2}=15.5mm$ ∴ O.K

Nails required

For web member 5

Angle of load to fastener length direction is 0°

Angle of load to grain member 0°

Hence, permissible load is $100K_3=100\times1.25=125N$

Nails required $=\frac{947.4}{2\times125}=3.790$, say 4

For member 1 / 2

Force must be equal and opposite

Angle of load to fastener length direction is 0°

Angle of load to grain member 68°

Hence, permissible load is $38K_3=38\times1.25=47.5N$

Nails required $=\frac{947.4}{2\times47.5}=9.973$, say 10

Tensile strength

N/A

Compression strength

Minimal width of the plate

$=\frac{947.4}{2\times37}=12.803mm$, say 13mm

Shear strength

Force acting at 68° to the length of the fastener is $947.4N$

The permissible shear line at 68° by interpolation of table 3 $=46.4Nmm^{-1}$

Calculated shear line

Force shearing plate at angle $68^{\circ}=947.4\cos68^{\circ}=354.902N$

Therefore required plate width $=\frac{354.902}{2\times46.4}\cos22=3.560mm$, say 4mm

City University London	Subject: Design of Queen truss		Date: 17-02-04
Project: Analysis of Semi-rigid Metal Plate Connected Truss	Design code: BS5268 Part 2 & 3	Designed by: SKM Checked by: KSV	Sheet No.268

Joint design

Timber shear stress condition

$$\sigma_{v,adm} K_3 \geq \frac{3V}{2bh_e}$$

Compression force at member 5/7 exerts shear on top chord, hence,

$V = 947.4N$, hence minimal bite $h_e = \frac{3V}{2b\sigma_{v,adm}K_3} = \frac{3(947.4)}{2\times35\times1.1\times1.25} = 29.530mm$

say 37mm

Minimum fastener bite

Minimum fastener bite on chord members must not be less than the following

- $(0.2l+15) = (0.2(75)+15) = 30mm$
- $30mm$
- $0.25(97) = 24.25mm$, O.K

Deflection

See deflection of truss for nodal deflection

Recommended plate size D41, 100x41

Joint specification

Nails provided for top chord member 1 / 2 = 18
New strength $= 2 \times 47.5 \times 18 = 1.71KN$
Web member 5

Nails provided for web member 5 = 4
New strength

Design for joint 3 - Bottom chord

Structural performance

Refer to drawing for dimensions

Nails required

Web members(5, and 7)

Angle of load to fastener length direction is 34°
Angle of load to grain member 0°
Hence, permissible load is $88K_3 = 88 \times 1.25 = 110N$

Nails required in web 5 and $7 = \frac{947.4}{2 \times 110} = 4.306$, say 5

Member 6
Angle of load to fastener length direction is 90°
Angle of load to grain member 0°
Hence, permissible load is $85K_3 = 85 \times 1.25 = 106.25N$

Nails required in web $6 = \frac{2587.3}{2 \times 106.25} = 12.176$, say 13

Member 8 and 9 (continuous)
The resultant of the web is $= 2587.3 - 2(947.4 \sin 34) = 1528.0N$ acting vertically.
Joint must be equal and opposite, hence total vertical force at bottom chord $= 1528.0 + 300 = 1828.0N$

Angle of load to fastener length direction is 90°
Angle of load to grain member 90°
Hence, permissible load is $54K_3 = 54 \times 1.25 = 67.5N$

Nails required in member 8 and 9 $= \frac{1828.0}{2 \times 67.5} = 13.54$, say 14

Strength of the plate is calculated where the members are discontinuous

Plate Tensile strength
Minimal length dimension to support tension web
$= \frac{2587.3}{2 \times 65} = 19.902mm$, say 20mm

Minimal length dimension to support bottom chord vertical tensile force

$= \frac{1828}{2\times 65} = 14.06mm$, say 15mm

Plate compressive strength

Minimal width dimension to support web

Force acting in fastener length direction due to web $= 947.4\cos 34^\circ = 785.43N$

Width required $= \frac{785.43}{2\times 37} = 10.614mm$, say 11mm

Minimal length dimension to support web

Force acting in fastener width direction due to web $= 947.4\sin 34^\circ = 529.78N$

length required $= \frac{529.78}{2\times 39} = 6.792mm$, say 7mm

Plate Shear

Member 8/9

No plate shear as member forces cancel each other out

Width $= 38+11 = 49mm$

For tolerance

Recommended plate size 75x54

Joint design

Timber shear stress condition

$$\sigma_{v,adm} K_3 \geq \frac{3V}{2bh_e}$$

Net tension force in member 6 $= 1528.0N$
Vertical load at joint 3 $= 300N$

$V = 1228.0N$, hence minimal bite $h_e = \frac{3V}{2b\sigma_{v,adm}K_3} = \frac{3(1228)}{2\times 35\times 1.1\times 1.25} = 38.275mm$

say 37mm

Tension stress

$$\sigma_{t,90,adm} \geq K_e\left(\frac{0.06T}{w+16d}\right)$$

For tension perpendicular to the grain, refer to **BS 5268-2, cl. 2.7**
Permissible tension load perpendicular to the grain.

$\sigma_{t,90,adm} K_3 = \frac{1.10}{3}\times 1.25 = 0.458 Nmm^{-2}$

Hence, the minimal fastener bite for tension load perpendicular to the grain

$$d = \left(\frac{0.06K_eT}{\sigma_{t.90.adm}} - w\right) \Big/ 16$$

$$= \left(\frac{0.06\times1.0\times1827.741}{0.458} - 75\right) \Big/ 16$$

$= 10.278mm$, say 11mm

Minimum fastener bite

Minimum fastener bite on chord members must not be less than the following

- $(0.2l + 15) = (0.2(67) + 15) = 28.4mm$
- $30mm$

$0.25(97) = 24.25mm$

Deflection

See deflection of truss for nodal deflection

Recommended plate size H67 200x67

Joint specification

Nails provided for web member 5 & 7	= 19
New strength	$= 2 \times 110 \times 19 = 4.18KN$
Nails provided for web member 6	= 16
New strength	$= 2 \times 106.25 \times 16 = 3.4KN$
Nails provided for bottom chord	= 64
New strength	$= 2 \times 67.5 \times 64 = 8.64KN$

City University London	Subject: Design of Queen truss		Date: 17-02-04
Project: Analysis of Semi-rigid Metal Plate Connected Truss	Design code: BS5268 Part 2 & 3	Designed by: SKM Checked by: KSV	Sheet No.272

Design for joint 4

Structural performance

Lateral resistance of fastener

$\frac{97-93}{2} = 2mm$ ∴ ignore 5mm at each side, hence plate width is 83mm.
Refer to drawing for dimensions

Nails required
Top chord members 2 and 3

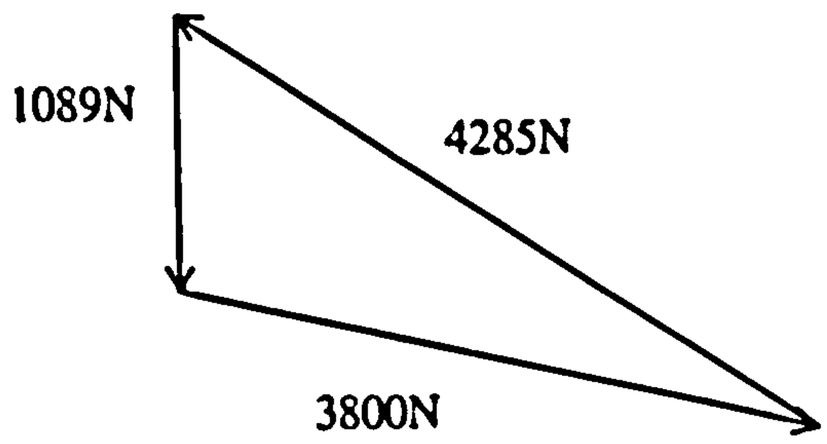

Angle of load to fastener length direction is 20°
Angle of load to grain member 14°
Hence, permissible load is $83K_3 = 83 \times 1.25 = 103.75N$

Nails required in top chord, members 2 and 3 $= \frac{3800}{2 \times 103.75} = 18.314$,

say 19

Web member 6
Resultant load of upper chord cancels out due to symmetry
Angle of load to fastener length direction is 90°
Angle of load to grain member 0°
Hence, permissible load is $85K_3 = 85 \times 1.25 = 106.25N$

Nails required in web, member 6 $= \frac{2587.3}{2 \times 106.25} = 12.18$, say 13

Tensile strength
Force acting in the direction of the fastener width $= 2587.3N$

Minimal length required for web tension member
$l = \frac{2587.3}{2 \times 65} = 19.902mm$, say 20mm

City University London	Subject: Design of Queen truss		Date: 17-02-04
Project: Analysis of Semi-rigid Metal Plate Connected Truss	Design code: BS5268 Part 2 & 3	Designed by: SKM Checked by: KSV	Sheet No.273

Compression member

Resultant Compression force acting at member $= 3800N$

Minimal plate width required $w = \frac{3800\cos 20}{2\times 37} = 48.254mm$, say 49mm

sssMinimal plate length required $l = \frac{3800\sin 20}{2\times 39} = 16.663mm$, say 17mm

Joint design

Minimum fastener bite

Minimum fastener bite on chord members must not be less than the following

- $(0.2l + 15) = (0.2(112.178) + 15) = 37.436mm$
- $30mm$

  $0.25(97) = 24.25mm$

Deflection

See deflection of truss for nodal deflection

Recommended plate size D93, 100x93

Joint specification

Nails provided for both top chord members 2 & 3 $= 28$
New strength $= 2 \times 103.75 \times 28 = 5.81KN$

Nails provided for web member 6 $= 18$
New strength $= 2 \times 106.25 \times 18 = 3.825KN$

City University London	Subject: Design of Queen truss		Date: 17-02-04
Project: Analysis of Semi-rigid Metal Plate Connected Truss	Design code: BS5268 Part 2 & 3	Designed by: SKM Checked by: KSV	Sheet No.274

Glue Line

cl. 6.10.1.3 Timber to timber joints

Permissible

$$\tau_\alpha = \tau_{adm} // (1 - 0.67 \sin \alpha)$$

$$\tau_\alpha = 1.0 \times (1 - 0.67 \sin 0) = 1.0 N/mm^2$$

Assume 1 ton load at each load point

$$10000 \times \cos 56 = 5591.93 N$$

Required glue area

$$A = \frac{5591.93}{1.0} = 5591.3 mm^2$$

therefore, length required $= \frac{5591.93}{35} = 159.77 mm$

Provide $200 mm$

New permissible force

$$\frac{200 \times 35 \times 1.0}{\cos 56} = 12518 N \approx 1.25 Tons$$

Appendix A2 Punched metal plate certificate

BBA BRITISH BOARD OF AGRÉMENT
ASSESSMENT OF PRODUCTS FOR CONSTRUCTION

Twinaplate Ltd

Certificate No 90/2383

DETAIL SHEET 3

TWINAPLATE TWISTNAIL PUNCHED METAL PLATE TIMBER FASTENERS

Product

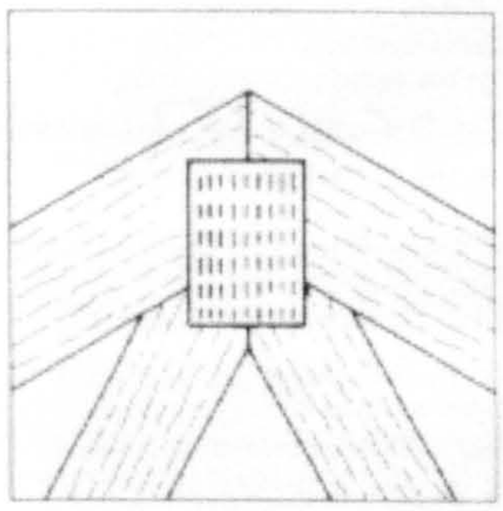

• *THIS DETAIL SHEET REPLACES CERTIFICATE No 84/1426 AND RELATES TO TWINAPLATE TWISTNAIL PUNCHED METAL PLATE TIMBER FASTENERS.*

This Detail Sheet must be read in conjunction with the Front Sheet and Detail Sheet 1, which give Conditions of Certification, details common to all Twinaplate certificated fasteners and the product's position regarding the Building Regulations respectively.

Technical Specification

1 Description

1.1 Twinaplate Twistnail Punched Metal Plate Timber Fasteners are galvanized mild steel plates having rows of integral nails pressed out to project at approximately right-angles to one face of the plates (see Figure 1). The slots so formed define the length direction of the fastener. Two nails are formed from each slot. From a distance of 4 mm from the face of the plates, each nail is twisted through 40°. Across the width of the fastener three pairs of nails of equal length are followed by one pair of nails of unequal length. Alternate rows of nails are staggered.

1.2 The fasteners are manufactured from material designation Z2 G275 to BS 2989 : 1982 *Specification for continuously hot-dip zinc coated and iron-zinc alloy coated steel : wide strip, sheet/plate and slit wide strip.* An upper limit on ultimate tensile strength is additionally imposed to ensure suitability for pressing. Reference should be made to BBA Information No 9 *Punched Metal Plate Timber Fasteners : Specification for Hot-Dip Zinc Coated Steel and Quality Control Guidance Notes.*

1.3 The dimensions and spacing of the nails are shown in Figure 2. The thickness of the plate including zinc coating is nominally 0.91 mm.

2 Sizes

The standard sizes of fastener are given in Table 1.

Figure 1 A typical Twinaplate Twistnail Punched Metal Plate Timber Fastener

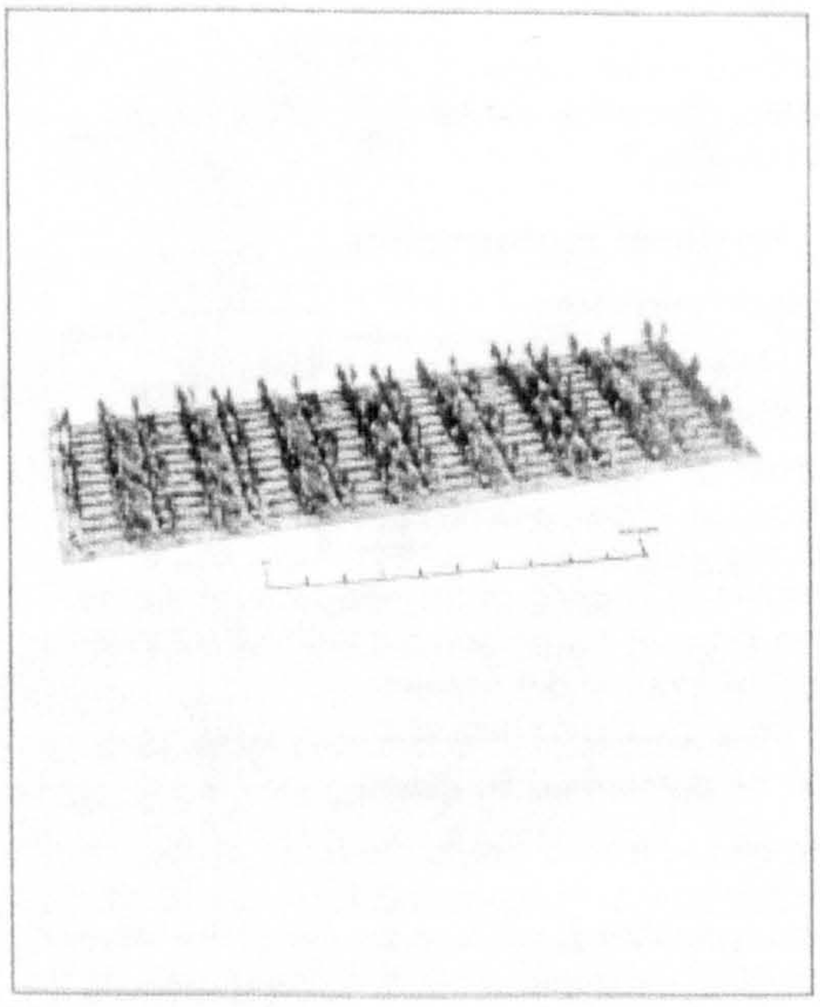

3 Identification

The fasteners are stamped with the manufacturer's identification mark *TNP*, and are packed in boxes bearing the BBA identification mark incorporating the number of this Certificate.

Certificate No 90/2383

DETAIL SHEET 3

Twinaplate Ltd

TWINAPLATE TWISTNAIL PUNCHED METAL PLATE TIMBER FASTENERS

Product

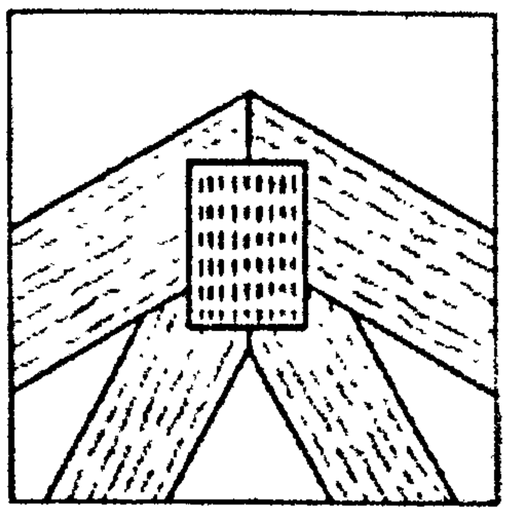

• *THIS DETAIL SHEET REPLACES CERTIFICATE No 84/1426 AND RELATES TO TWINAPLATE TWISTNAIL PUNCHED METAL PLATE TIMBER FASTENERS.*

This Detail Sheet must be read in conjunction with the Front Sheet and Detail Sheet 1, which give Conditions of Certification, details common to all Twinaplate certificated fasteners and the product's position regarding the Building Regulations respectively.

1 Description

1.1 Twinaplate Twistnail Punched Metal Plate Timber Fasteners are galvanized mild steel plates having rows of integral nails pressed out to project at approximately right-angles to one face of the plates (see Figure 1). The slots so formed define the length direction of the fastener. Two nails are formed from each slot. From a distance of 4 mm from the face of the plates, each nail is twisted through 40°. Across the width of the fastener three pairs of nails of equal length are followed by one pair of nails of unequal length. Alternate rows of nails are staggered.

1.2 The fasteners are manufactured from material designation Z2 G275 to BS 2989 : 1982 *Specification for continuously hot-dip zinc coated and iron-zinc alloy coated steel : wide strip, sheet/plate and slit wide strip.* An upper limit on ultimate tensile strength is additionally imposed to ensure suitability for pressing. Reference should be made to BBA Information No 9 *Punched Metal Plate Timber Fasteners : Specification for Hot-Dip Zinc Coated Steel and Quality Control Guidance Notes.*

1.3 The dimensions and spacing of the nails are shown in Figure 2. The thickness of the plate including zinc coating is nominally 0.91 mm.

2 Sizes

The standard sizes of fastener are given in Table 1.

Figure 1 A typical Twinaplate Twistnail Punched Metal Plate Timber Fastener

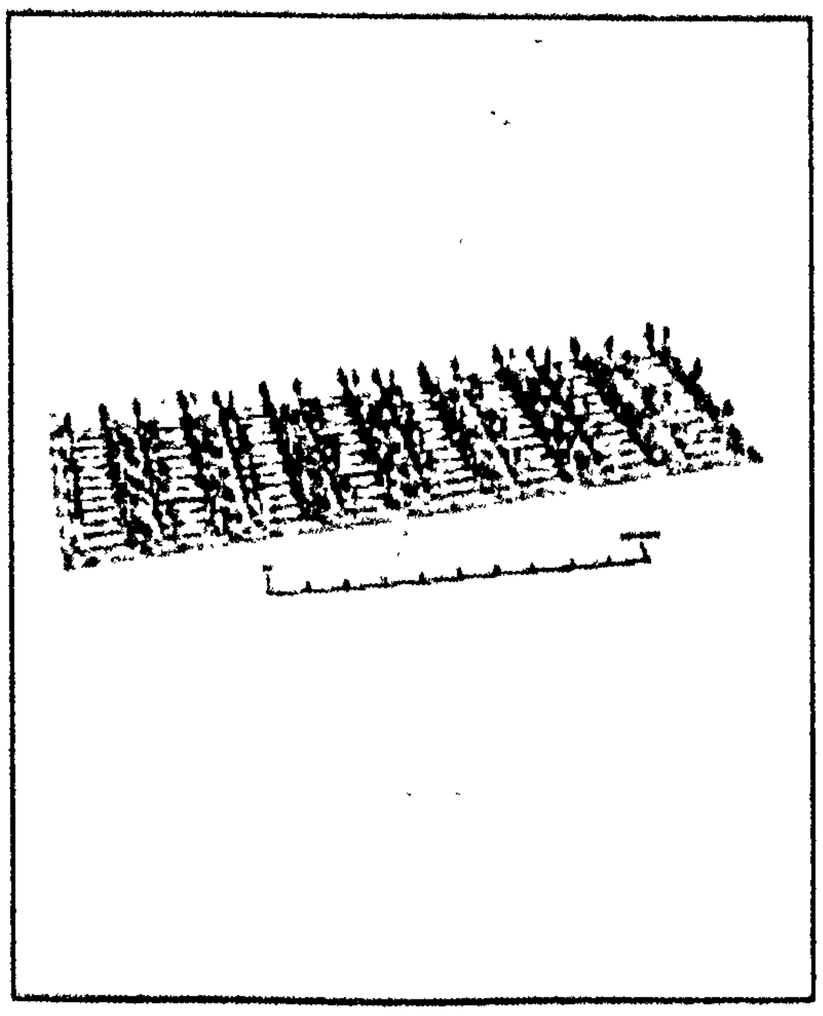

3 Identification

The fasteners are stamped with the manufacturer's identification mark *TNP*, and are packed in boxes bearing the BBA identification mark incorporating the number of this Certificate.

Figure 2 Details of a typical fastener

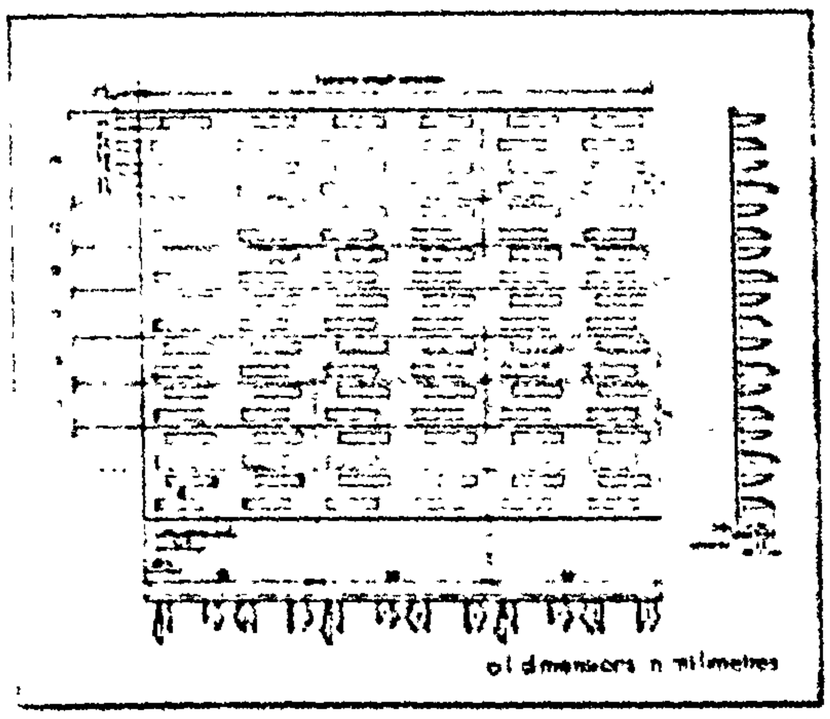

of dimensions in millimetres

Table 1 Range of standard fastener sizes and code reference*

Length (mm)	Width (mm) 28	41	54	67	80	93	106	119	132	145	158
40	[illegible]	[illegible]	[illegible]	[illegible]	[illegible]	[illegible]	[illegible]	[illegible]	[illegible]	[illegible]	[illegible]
100	[illegible]	[illegible]	[illegible]	[illegible]	[illegible]	[illegible]	[illegible]	[illegible]	[illegible]	[illegible]	[illegible]
150	[illegible]	[illegible]	[illegible]	[illegible]	[illegible]	[illegible]	[illegible]	[illegible]	[illegible]	[illegible]	[illegible]
200	[illegible]	[illegible]	[illegible]	[illegible]	[illegible]	[illegible]	[illegible]	[illegible]	[illegible]	[illegible]	[illegible]
250	[illegible]	[illegible]	[illegible]	[illegible]	[illegible]	[illegible]	[illegible]	[illegible]	[illegible]	[illegible]	[illegible]
300	[illegible]	[illegible]	[illegible]	[illegible]	[illegible]	[illegible]	[illegible]	[illegible]	[illegible]	[illegible]	[illegible]
350	[illegible]	[illegible]	[illegible]	[illegible]	[illegible]	[illegible]	[illegible]	[illegible]	[illegible]	[illegible]	[illegible]
400	[illegible]	[illegible]	[illegible]	[illegible]	[illegible]	[illegible]	[illegible]	[illegible]	[illegible]	[illegible]	[illegible]

*Number denotes fastener size covered by the Certificate

D = fastener size not covered by the Certificate

4 Timber species

This Detail Sheet covers the use of Twinaplate Twistrail fasteners in sawn or planed, treated or untreated, stress graded timber of minimum specified thickness of at least 35 mm, −0 −1 mm divergence throughout a member (when measured at 20% moisture content) of the following species:

European whitewood
European redwood
Hem-fir
Western white spruce
Eastern Canadian spruce (princess spruce)
spruce-pine-fir.

Table 2 Permissible loads (Newtons) per nail for Twinaplate Twistrail fasteners*

Angle of load to fastener length direction (°)	Angle of load to grain of member 0°	15°	30°	45°	60°	75°	90°
Long-term loading							
0	100	89	71	53	43	38	36
15	96	86	68	52	43	38	36
30	92	83	66	52	42	37	36
45	88	80	65	51	42	37	36
60	85	78	63	51	42	37	36
75	85	78	63	51	42	37	36
90	85	82	74	66	59	55	54

*The tabulated values are for fasteners in planed timber. For sawn timber the permissible load values must be modified by multiplying by 0.9.

5 Structural performance

Lateral resistance

5.1 The lateral resistance of a fastener depends upon:

number of effective nails in the joint
species of timber and its moisture content
duration of load
direction of bearing of the nail with respect to the grain of the timber
angle of load to the fastener.

5.2 The number of effective nails in the joint shall be determined by omitting:

nails nearer than 6 mm to the edge of the timber
nails nearer than 6 mm from the end of the timber member measured parallel to the grain.

5.3 The permissible lateral load per effective nail for the fasteners under long-term loading for the softwood species included in this assessment is given in Table 2. The permissible loads are specified for 15° increments of angle of load to the grain and nail orientation, as indicated in Figure 3.

5.4 The permissible lateral load for medium-, short- and very short-term duration of load should be obtained in accordance with BS 5268 : Part 2 : 1989 *Structural use of timber — Code of practice for permissible stress design, materials and workmanship* by modifying the long-term permissible loads given in Table 2 by the following factors:

Medium term (eg dead + snow, dead + temporary imposed)	1.12
Short term (eg dead + imposed + wind*, dead + imposed + snow + wind*)	1.25
Very short term (eg dead + imposed + wind†)	1.25

*For wind, short-term category applies to class C (15 s gust) as defined in CP3 : Chapter V : Part 2.

†For wind, very short-term category applies to classes A and B (3 s or 5 s gust) as defined in CP3 : Chapter V : Part 2.

Figure 2 *Details of a typical fastener*

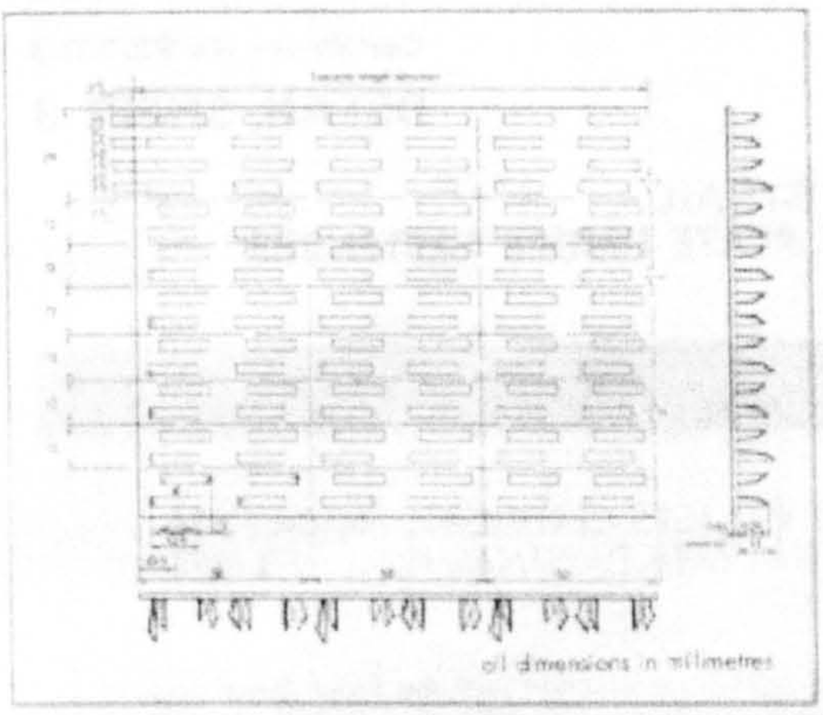

Table 1 *Range of standard fastener sizes and code reference***

Length (mm)	Width (mm)										
	28	41	54	67	80	93	106	119	132	145	158
50	B28	D	D	D	D	D	D	D	D	D	D
100	D28	D41	D54	D67	D80	D93	D106	D119	D	D	D
150	F28	F	F54	F67	F80	F93	F106	F119	F132	F145	F158
200	H28	H	H	H67	H80	H93	H106	H119	H132	H145	H158
250	K	K	K	K67	K80	K93	K106	K119	K132	K145	K158
300	M	M	M	M67	M80	M93	M106	M119	M132	M145	M158
350	P	P	P	P	P80	P93	P106	P119	P	P	P
400	R	R	R	R	R80	R93	R106	R119	R	R	R

*Number denotes fastener size covered by the Certificate.
D = fastener size not covered by the Certificate.

4 Timber species

This Detail Sheet covers the use of Twinaplate Twistnail fasteners in sawn or planed, treated or untreated, stress graded timber of minimum specified thickness of at least 35 mm, −0 −1 mm divergence throughout a member (when measured at 20% moisture content) of the following species:

European whitewood
European redwood
hem-fir
Western white spruce
Eastern Canadian spruce (princess spruce)
spruce-pine-fir.

5 Structural performance

Lateral resistance

5.1 The lateral resistance of a fastener depends upon:

number of effective nails in the joint
species of timber and its moisture content
duration of load
direction of bearing of the nail with respect to the grain of the timber
angle of load to the fastener.

5.2 The number of effective nails in the joint shall be determined by omitting:

nails nearer than 6 mm to the edge of the timber
nails nearer than 6 mm from the end of the timber member measured parallel to the grain.

5.3 The permissible lateral load per effective nail for the fasteners under long-term loading for the softwood species included in this assessment is given in Table 2. The permissible loads are specified for 15° increments of angle of load to the grain and nail orientation, as indicated in Figure 3.

Table 2 *Permissible loads (Newtons) per nail for Twinaplate Twistnail fasteners**

Angle of load to fastener length direction (°)	Angle of load to grain of member						
	0°	15°	30°	45°	60°	75°	90°
Long-term loading							
0	100	89	71	53	43	38	36
15	96	86	68	52	43	38	36
30	92	83	66	52	42	37	36
45	88	80	65	51	42	37	36
60	85	78	63	51	42	37	36
75	85	78	63	51	42	37	36
90	85	82	76	66	59	55	54

*The tabulated values are for fasteners in planed timber. For sawn timber the permissible load values must be modified by multiplying by 0.9.

5.4 The permissible lateral load for medium-, short- and very short-term duration of load should be obtained in accordance with BS 5268 : Part 2 : 1989 *Structural use of timber — Code of practice for permissible stress design, materials and workmanship* by modifying the long-term permissible loads given in Table 2 by the following factors:

Medium term (eg dead + snow, dead + temporary imposed)	1.12
Short term (eg dead + imposed + wind*, dead + imposed + snow + wind*)	1.25
Very short term (eg dead + imposed + wind†)	1.25

*For wind, short-term category applies to class C (15 s gust) as defined in CP3 : Chapter V : Part 2.

†For wind, very short-term category applies to classes A and B (3 s or 5 s gust) as defined in CP3 : Chapter V : Part 2.

Tensile strength

5.5 The maximum tensile force acting on the fasteners, for all four categories of load duration, must not exceed the following:

force acting in direction of fastener length — 58 Nmm^{-1} of fastener width

force acting in direction of fastener width — 65 Nmm^{-1} of fastener length.

Compressive strength

5.6 The maximum compressive force acting on the fasteners, for all four categories of load duration, must not exceed the following:

force acting in direction of fastener length — 37 Nmm^{-1} of fastener width

force acting in direction of fastener widths — 39 Nmm^{-1} of fastener length.

5.7 The loads given in section 5.6 were derived from tests and are based on a typical factor of safety for general use. Where failure of the fastener will result in forces being taken in end bearing, and the joint will not be subject to stress reversal, the permissible values for compressive force may be modified by multiplying by 1.5. A suitably qualified engineer shall be responsible for considering the merits of each application and deciding upon the appropriate permissible value.

Shear strength

5.8 The maximum shear force acting on a fastener, for all four categories of load duration, must not exceed the value given in Table 3 for the angle α, the angle between the fastener length direction and the direction in which the load is acting.

Table 3 Maximum shear forces*

Angle α	Nmm^{-1} of shear line
0	31
10	28
20	28
30	28
40	28
50	42
60	56
70	44
80	32
90	21

*Values for intermediate angles can be interpolated.

5.9 The values are limited to angle α up to and including 90°, as required by conventional UK practice. The requirements relating to shear given in MOAT No 16 : 1979 include values for angle α from 0° to 180°. An assessment will therefore be necessary in each particular case where values for shear angle α greater than 90° are required.

6 Practicability of installation

The fasteners are easy to embed using the commercial platen or roller press equipment normally employed for truss fabrication.

Figure 3 Angle of load to grain and nail orientation

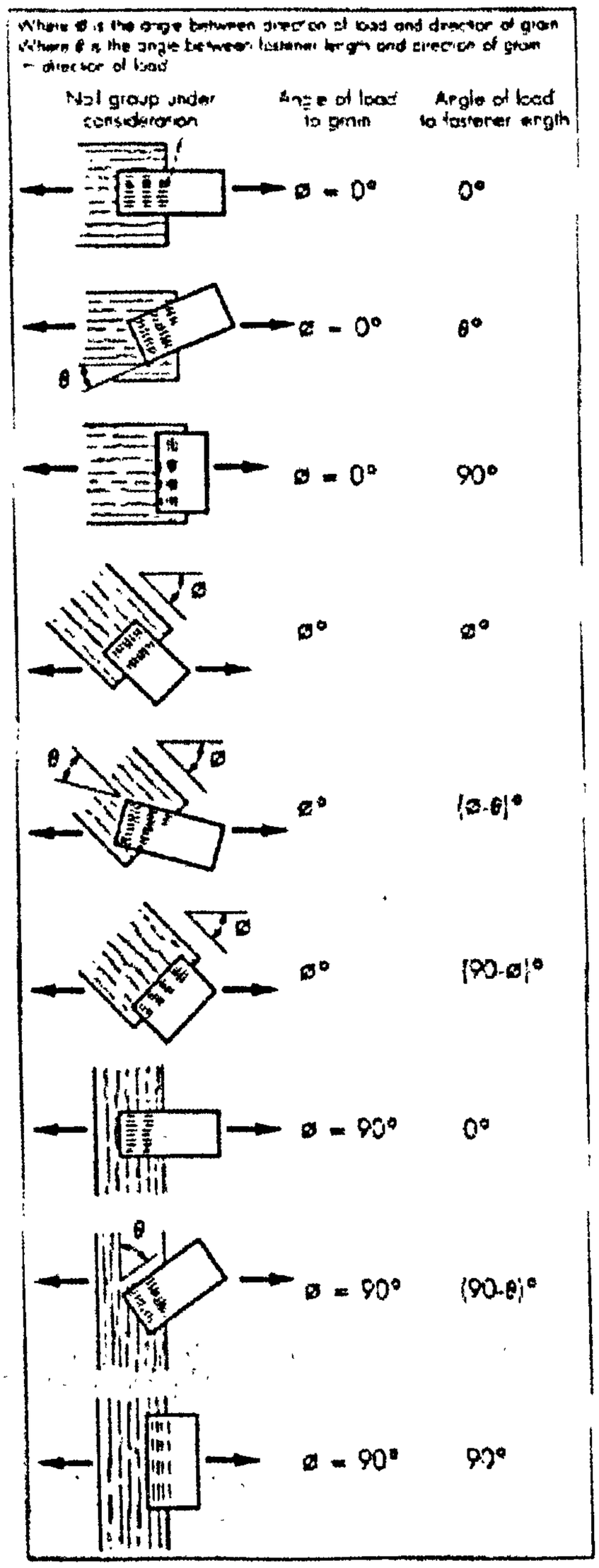

7 Durability

The fasteners have a zinc coating (see section 1.2 of this Detail Sheet), which will give adequate protection against corrosion in normal internal domestic situations, where the moisture content of the timber does not exceed 18% for any significant period and does not exceed 22% at any time.

Tensile strength

5.5 The maximum tensile force acting on the fasteners, for all four categories of load duration, must not exceed the following:

force acting in direction of fastener length — 58 Nmm^{-1} of fastener width

force acting in direction of fastener width — 65 Nmm^{-1} of fastener length.

Compressive strength

5.6 The maximum compressive force acting on the fasteners, for all four categories of load duration, must not exceed the following:

force acting in direction of fastener length — 37 Nmm^{-1} of fastener width

force acting in direction of fastener widths — 39 Nmm^{-1} of fastener length.

5.7 The loads given in section 5.6 were derived from tests and are based on a typical factor of safety for general use. Where failure of the fastener will result in forces being taken in end bearing, and the joint will not be subject to stress reversal, the permissible values for compressive force may be modified by multiplying by 1.5. A suitably qualified engineer shall be responsible for considering the merits of each application and deciding upon the appropriate permissible value.

Shear strength

5.8 The maximum shear force acting on a fastener, for all four categories of load duration, must not exceed the value given in Table 3 for the angle α, the angle between the fastener length direction and the direction in which the load is acting.

*Table 3 Maximum shear forces**

Angle α	Nmm^{-1} of shear line
0	31
10	28
20	28
30	28
40	28
50	42
60	56
70	44
80	32
90	21

*Values for intermediate angles can be interpolated.

5.9 The values are limited to angle α up to and including 90°, as required by conventional UK practice. The requirements relating to shear given in MOAT No 16 : 1979 include values for angle α from 0° to 180°. An assessment will therefore be necessary in each particular case where values for shear angle α greater than 90° are required.

6 Practicability of installation

The fasteners are easy to embed using the commercial platen or roller press equipment normally employed for truss fabrication.

Figure 3 Angle of load to grain and nail orientation

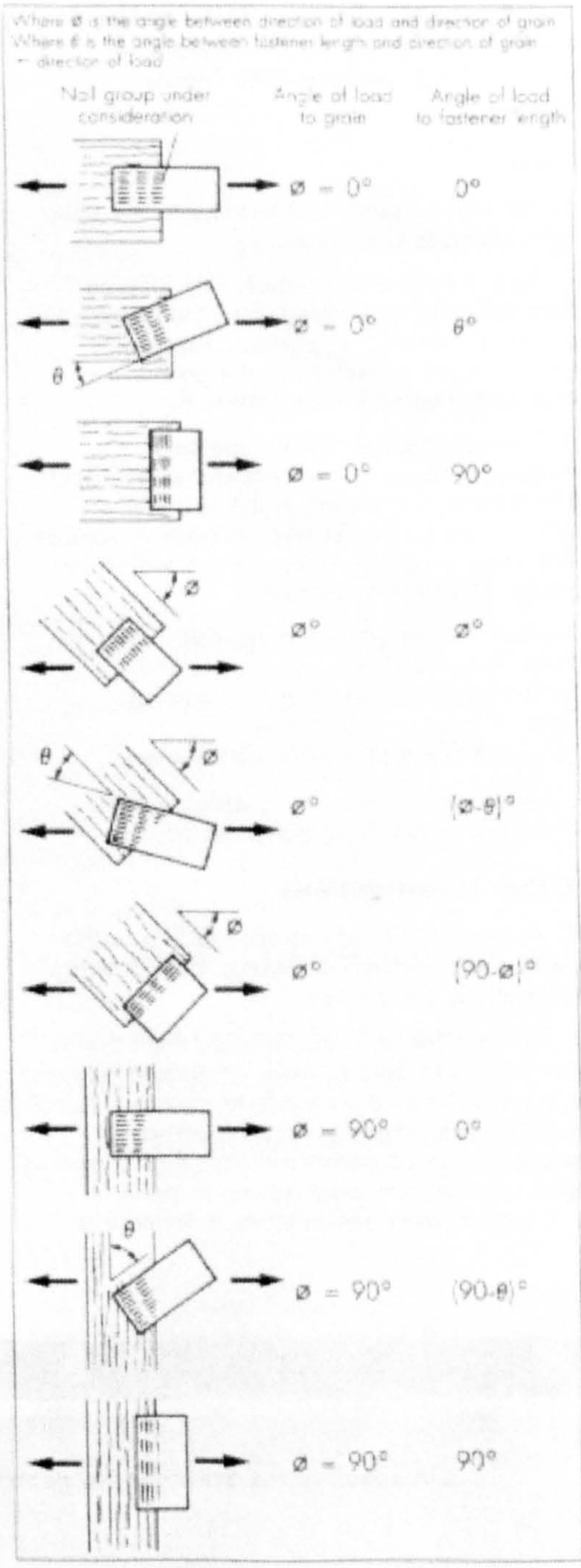

7 Durability

The fasteners have a zinc coating (see section 1.2 of this Detail Sheet), which will give adequate protection against corrosion in normal internal domestic situations, where the moisture content of the timber does not exceed 18% for any significant period and does not exceed 22% at any time.

The following is a summary of the technical investigations carried out on Twinraplate Twistrail Punched Metal Plate Timber Fasteners.

8 Tests

As part of the assessment leading to the issue of the previous Certificate:

(1) Tests were carried out on 126 full-size structural joints, assembled using the commercial equipment normally employed. The results were assessed to determine the permissible loads and stresses for the fasterers.

(2) Three species of timber, European whitewood, European redwood and Western white spruce, were used in the test joints. Existing data on the relative strength of species were used to derive values for use with other species. The tests examined:

variations in strength within species
effects of surface finish
effects of direction and type of loading
effects of fastener orientation
tensile and shear properties of fasterers.

(3) Tests were conducted to determine the thickness and quality of galvanizing.

9 Other investigations

9.1 As part of the assessment leading to the issue of the previous Certificate, the following investigations were made:

(1) The permissible loads, derived from the tests referred to above, were compared with the estimated maximum loads to cause a joint slip of 0.8 mm. These latter load values, however, were consistently higher than those based on maximum load values. In general, the maximum initial slip in joints in tension, at the permissible long-term loads, will not be greater than 0.25 mm and the average initial slip not greater than 0.1 mm.

(2) Existing data on the durability of punched metal plate timber fasteners were examined.

(3) Existing data relating to cyclic loading on fasteners in dwellings and similar structures were examined and the effects found to be insignificant.

(4) An assessment was made on the practicability of joint assembly.

(5) The test data on which the previous Certificate was based were re-examined and analysed in accordance with BBA MOAT 16 : 1979, and compared with related comparative research data. The analysis established that the design data previously derived remain valid.

(6) The manufacturing process was examined, including the methods adopted for quality control, and details were obtained of the quality and composition of the materials used.

9.2 As part of the assessment leading to the issue of this Certificate, the following investigations were made:

(1) A re-examination was made of the data and investigations on which the previous Certificate was based.

(2) The strength of joints in compression was investigated.

9.3 Regular factory inspections have been carried out to ensure that quality is being maintained.

9.4 No failure of the product in use has been reported to the BBA.

BBA BRITISH BOARD OF AGREMENT

On behalf of the British Board of Agrément

Date of issue: 19th January 1990 P.C. Hewlett **Director**

British Board of Agrément
P O Box No 195, Bucknalls Lane
Garston, Watford, Herts WD2 7NG
Fax 0923 662733

Technical Investigations

The following is a summary of the technical investigations carried out on Twinaplate Twistnail Punched Metal Plate Timber Fasteners.

8 Tests

As part of the assessment leading to the issue of the previous Certificate:

(1) Tests were carried out on 126 full-size structural joints, assembled using the commercial equipment normally employed. The results were assessed to determine the permissible loads and stresses for the fasteners.

(2) Three species of timber, European whitewood, European redwood and Western white spruce, were used in the test joints. Existing data on the relative strength of species were used to derive values for use with other species. The tests examined:

variations in strength within species
effects of surface finish
effects of direction and type of loading
effects of fastener orientation
tensile and shear properties of fasteners.

(3) Tests were conducted to determine the thickness and quality of galvanizing.

9 Other investigations

9.1 As part of the assessment leading to the issue of the previous Certificate, the following investigations were made:

(1) The permissible loads, derived from the tests referred to above, were compared with the estimated maximum loads to cause a joint slip of 0.8 mm. These latter load values, however, were consistently higher than those based on maximum load values. In general, the maximum initial slip in joints in tension, at the permissible long-term loads, will not be greater than 0.25 mm and the average initial slip not greater than 0.1 mm.

(2) Existing data on the durability of punched metal plate timber fasteners were examined.

(3) Existing data relating to cyclic loading on fasteners in dwellings and similar structures were examined and the effects found to be insignificant.

(4) An assessment was made on the practicability of joint assembly.

(5) The test data on which the previous Certificate was based were re-examined and analysed in accordance with BBA MOAT 16 : 1979, and compared with related comparative research data. The analysis established that the design data previously derived remain valid.

(6) The manufacturing process was examined, including the methods adopted for quality control, and details were obtained of the quality and composition of the materials used.

9.2 As part of the assessment leading to the issue of this Certificate, the following investigations were made:

(1) A re-examination was made of the data and investigations on which the previous Certificate was based.

(2) The strength of joints in compression was investigated.

9.3 Regular factory inspections have been carried out to ensure that quality is being maintained.

9.4 No failure of the product in use has been reported to the BBA.

BBA BRITISH BOARD OF AGRÉMENT

On behalf of the British Board of Agrément

P.C. Hewlett

Date of issue: 19th January 1990 Director

British Board of Agrément
P O Box No 195, Bucknalls Lane
Garston, Watford, Herts WD2 7NG
Fax: 0923 662133

Appendix A3 Loading arrangement

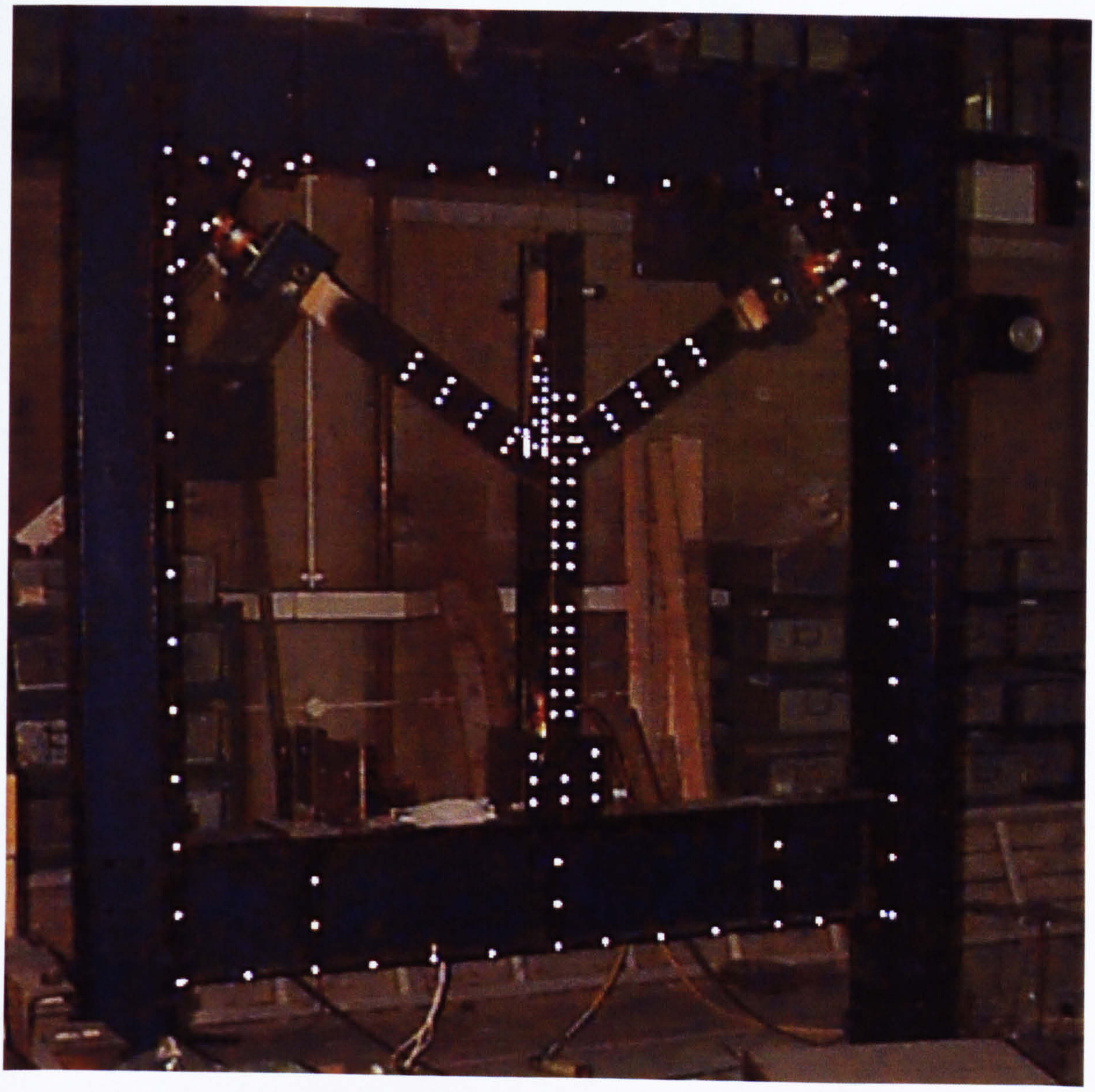

Fig. A3.1 – Crown Joint test

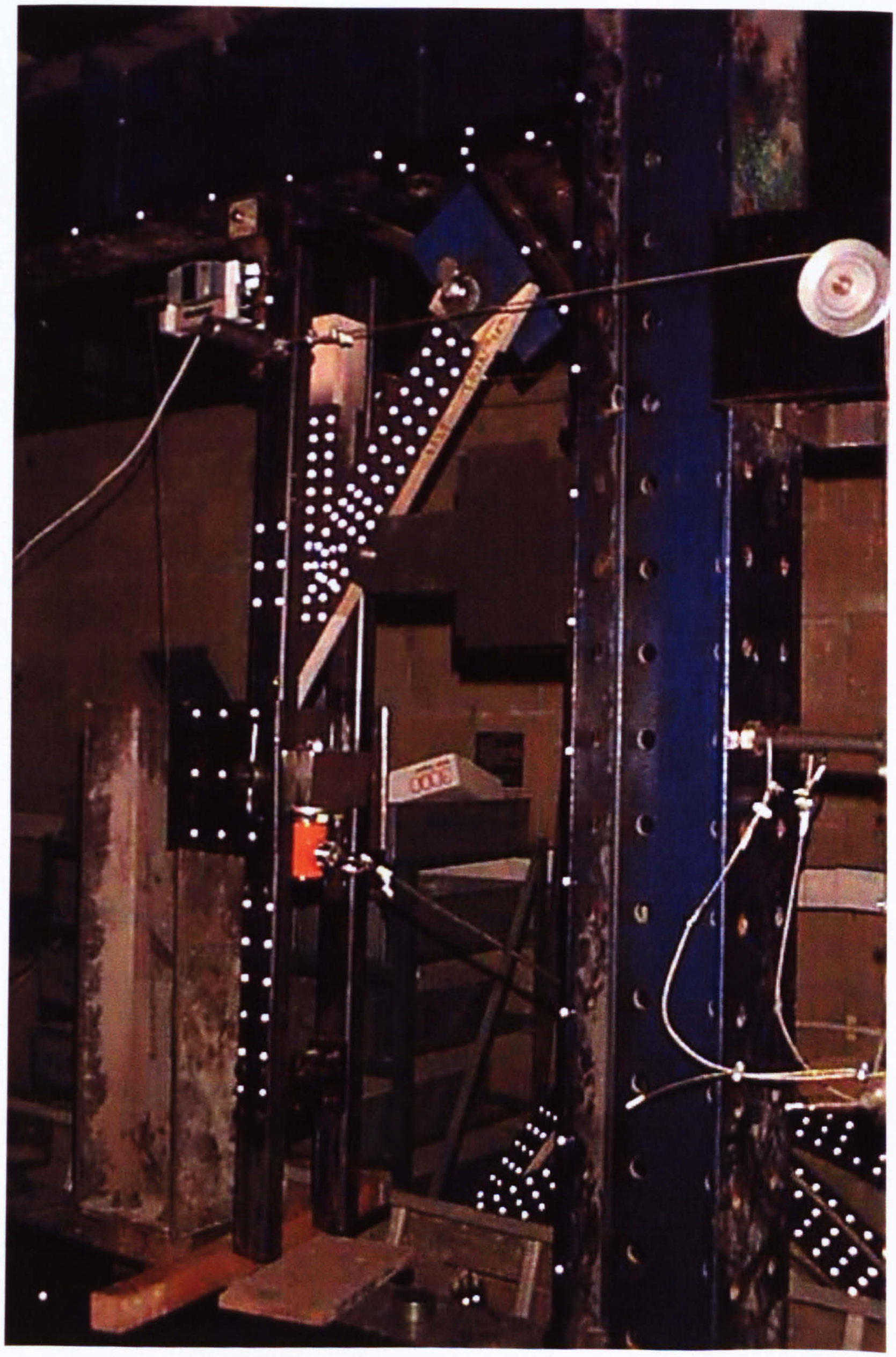

Fig. A3.2 – Heel Joint test

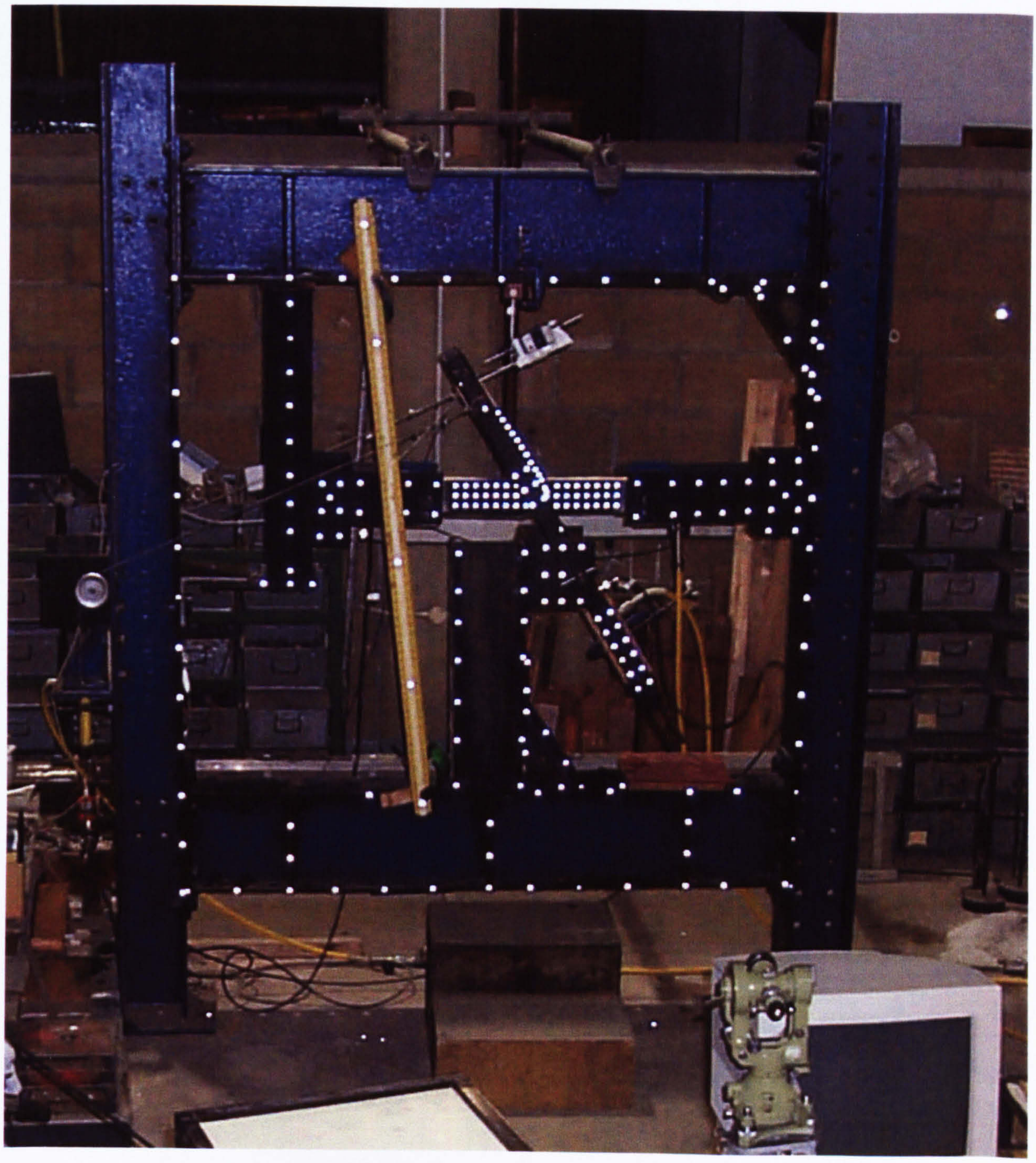

Fig. A3.3 – Top chord joint test

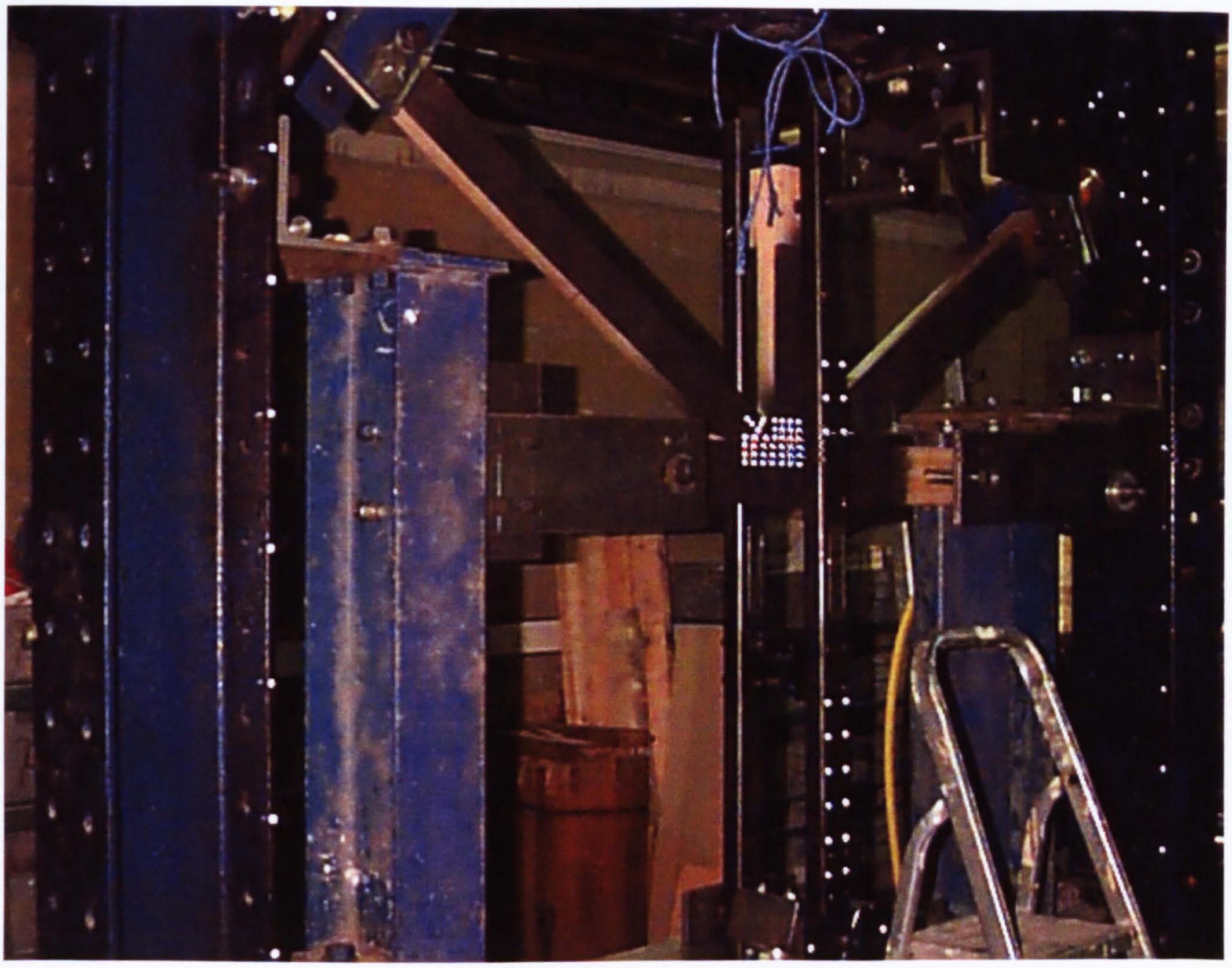

Fig. A3.4 – Bottom Chord Joint test

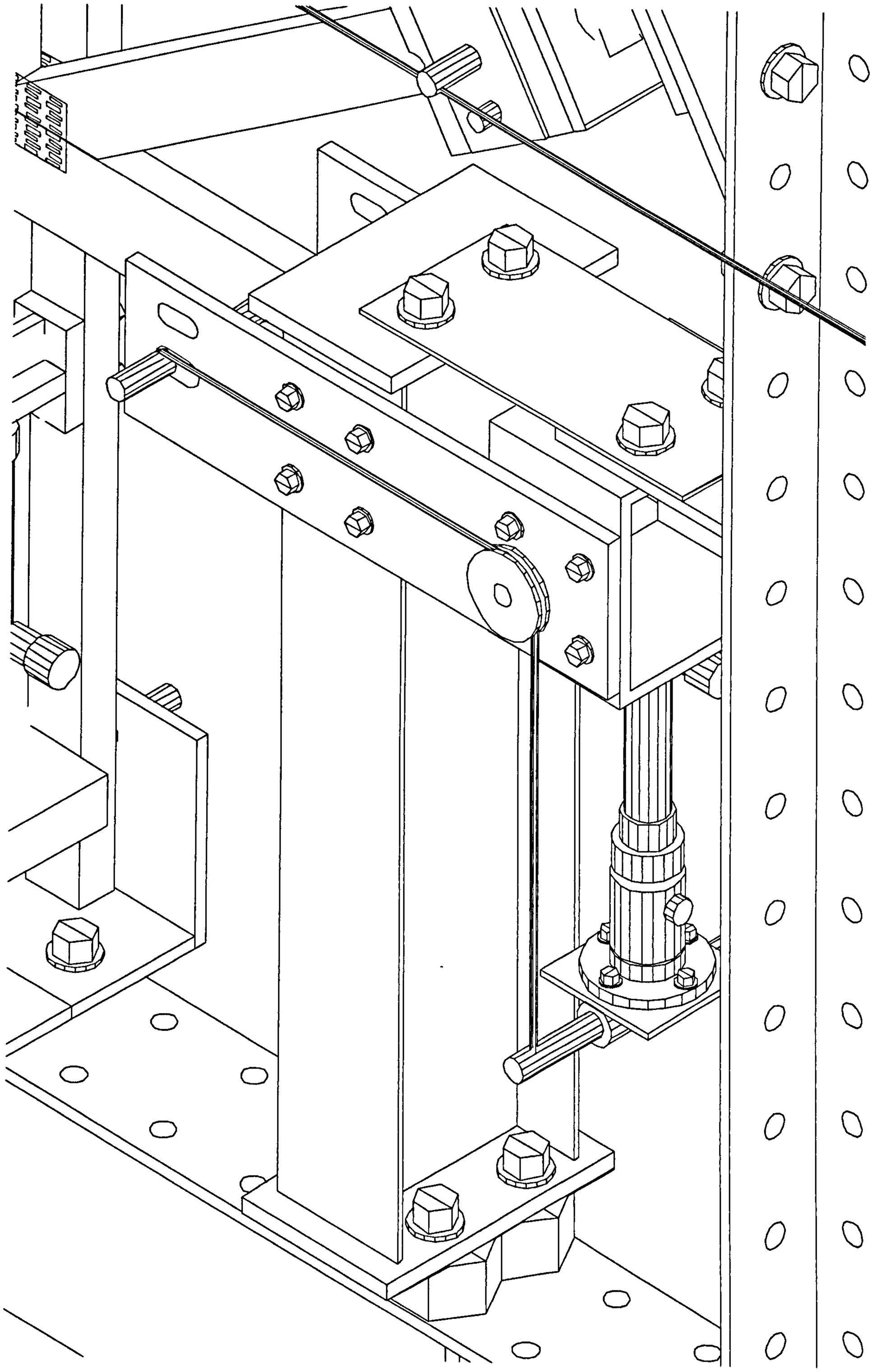

Fig. A3.5 – Tensile loading of Bottom chord test

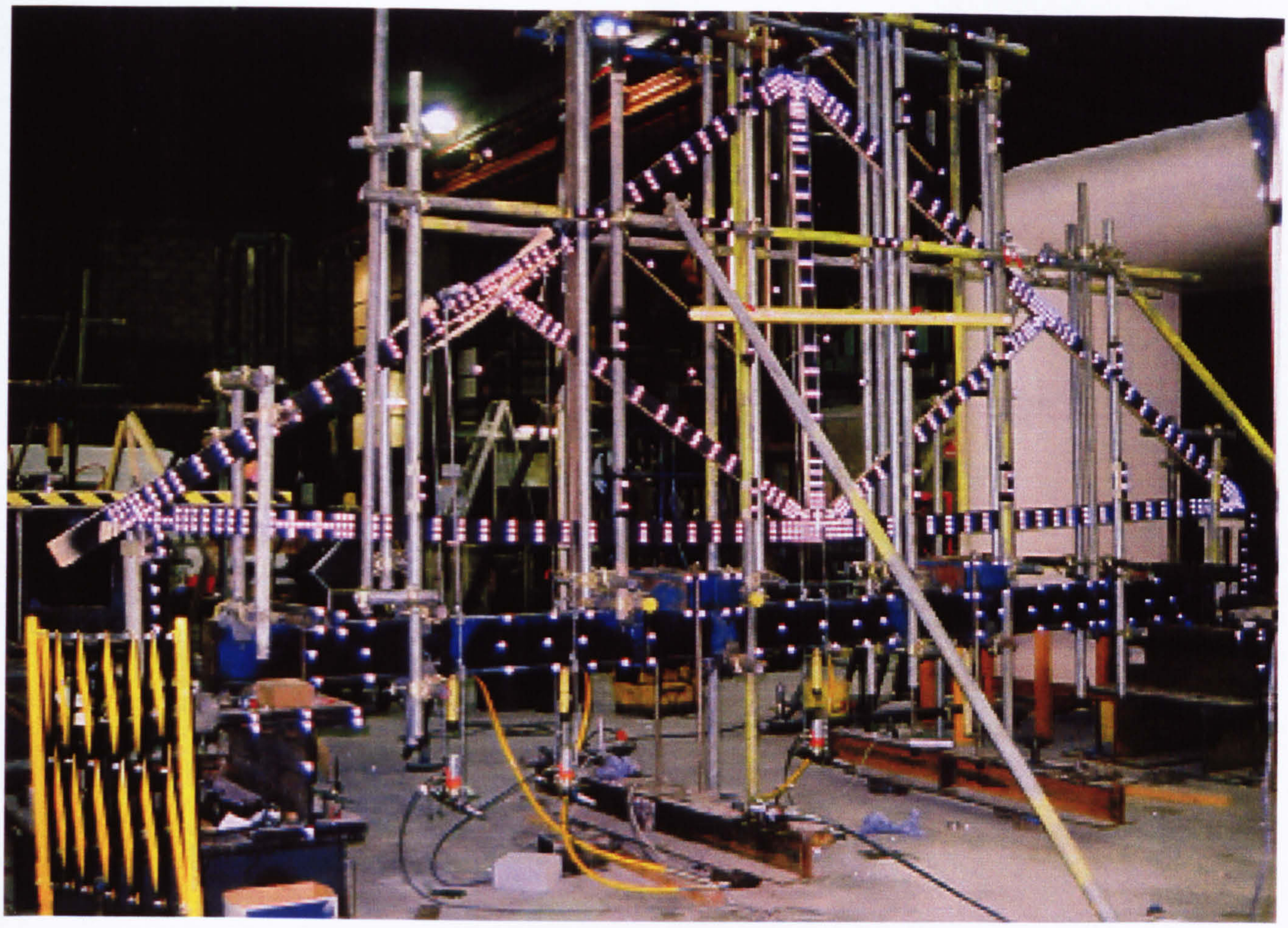

Fig. A3.6 – Full scale truss set-up

Appendix B1 2-D non-linear semi-rigid analysis

Semi-rigid joint rotational stiffness

$$M_i = \frac{4EI}{l}\vartheta_{mi} + \frac{2EI}{l}\vartheta_{mj} - \frac{6EI}{l}R + M_i^F \qquad (4.4.1a)$$

$$M_j = \frac{4EI}{l}\vartheta_{mj} + \frac{2EI}{l}\vartheta_{mi} - \frac{6EI}{l}R + M_j^F \qquad (4.4.1b)$$

$$R = \frac{(v_{mj} - v_{mi})}{l} \qquad (4.4.2)$$

Referring to Fig. 4.32 let ϑ_r be the rotational displacement due to the spring, and total rotational displacement

$$\vartheta_i = \vartheta_{mi} + \vartheta_{ri} \qquad (4.4.3a)$$

$$\vartheta_j = \vartheta_{mj} + \vartheta_{rj} \qquad (4.4.3b)$$

Hence, rearranging the two equations and substituting for ϑ_{mi} and ϑ_{mj}

$$M_i = \frac{4EI}{l}(\vartheta_i - \vartheta_{ri}) + \frac{2EI}{l}(\vartheta_j - \vartheta_{rj}) - \frac{6EI}{l}R + M_i^F \qquad (4.4.4a)$$

$$M_j = \frac{4EI}{l}(\vartheta_j - \vartheta_{rj}) + \frac{2EI}{l}(\vartheta_i - \vartheta_{ri}) - \frac{6EI}{l}R + M_j^F \qquad (4.4.4b)$$

Expanding the two equations

$$\frac{M_i l}{EI} = 4\vartheta_i - 4\vartheta_{ri} + 2\vartheta_j - 2\vartheta_{rj} - 6R + \frac{M_i^F l}{EI} \qquad (4.4.5a)$$

$$\frac{M_j l}{EI} = 4\vartheta_j - 4\vartheta_{rj} + 2\vartheta_i - 2\vartheta_{ri} - 6R + \frac{M_j^F l}{EI} \qquad (4.4.5b)$$

Dividing equation (4.4.4a) by 2 and subtract from (4.4.4b)

$$\frac{M_i l}{2EI} = 2\vartheta_i - 2\vartheta_{ri} + \vartheta_j - \vartheta_{rj} - 3R + \frac{M_i^F l}{2EI}$$

$$\frac{M_i l}{2EI} - \frac{M_j l}{EI} = -3\vartheta_j + 3\vartheta_{rj} + 3R + \frac{M_i^F l}{2EI} - \frac{M_j^F l}{EI} \qquad (4.4.6a)$$

Now divide equation (4.4.4b) by 2 and subtracting from (4.4.4a)

$$\frac{M_j l}{2EI} - \frac{M_i l}{EI} = -3\vartheta_i + 3\vartheta_{ri} + 3R + \frac{M_j^F l}{2EI} - \frac{M_i^F l}{EI} \qquad (4.4.6b)$$

Rearranging (4.4.5b) and substitute the relationship for spring $M_i = \vartheta_{ri}\lambda_i$.

Where, M_i = Moment at joint i

λ_i = Rotational spring stiffness at joint i

$$\frac{M_j l}{2EI} - \frac{M_i l}{EI} = -3\vartheta_i + \frac{3M_i}{\lambda_i} + 3R + \frac{M_j^F l}{2EI} - \frac{M_i^F l}{EI}$$

$$-\frac{M_i l}{EI} - \frac{3M_i}{\lambda_i} = -3\vartheta_i + 3R - \frac{M_j l}{2EI} + \frac{M_j^F l}{2EI} - \frac{M_i^F l}{EI}$$

$$M_i + \frac{3M_i EI}{\lambda_i l} = \frac{3EI}{l}(\vartheta_i - R) + \frac{M_j}{2} - \frac{M_j^F}{2} + M_i^F$$

$$M_i\left(1 + \frac{3EI}{\lambda_i l}\right) = \frac{3EI}{l}(\vartheta_i - R) + \frac{M_j}{2} - \frac{M_j^F}{2} + M_i^F$$

$$M_i\left(\frac{\lambda_i l + 3EI}{\lambda_i l}\right) = \frac{3EI}{l}(\vartheta_i - R) + \frac{M_j}{2} - \frac{M_j^F}{2} + M_i^F$$

let $r_i = \left(\frac{\lambda_i l}{\lambda_i l + 3EI}\right)$, hence,

$$M_i = \frac{3EIr_i}{l}(\vartheta_i - R) + \frac{M_j r_i}{2} - r_i\left(\frac{M_j^F}{2} - M_i^F\right) \qquad (4.4.6a)$$

Repeating the same algebraic manipulations for equation (4.4.3a) and substituting $\lambda_j = \frac{M_j}{\vartheta_{rj}}$ gives

$$M_j = \frac{3EIr_j}{l}(\vartheta_j - R) + \frac{M_i r_j}{2} - r_j\left(\frac{M_i^F}{2} - M_j^F\right) \qquad (4.4.6b)$$

let $r_j = \left(\frac{\lambda_j l}{\lambda_j l + 3EI}\right)$

Substituting M_j into M_i

$$M_i = \frac{3EIr_i}{l}(\vartheta_i - R) + \left[\frac{3EIr_i r_j}{2l}(\vartheta_j - R) + \frac{M_i r_i r_j}{4} - \frac{r_i r_j}{2}\left(\frac{M_i^F}{2} - M_j^F\right)\right] - r_i\left(\frac{M_j^F}{2} - M_i^F\right)$$

re-arranging the equation

$$M_i - \frac{M_i r_i r_j}{4} = \frac{3EIr_i}{l}(\vartheta_i - R) + \frac{3EIr_i r_j}{2l}(\vartheta_j - R) - \frac{r_i r_j}{2}\left(\frac{M_i^F}{2} - M_j^F\right) - r_i\left(\frac{M_j^F}{2} - M_i^F\right)$$

$$M_i = \left[\frac{4r_i}{4 - r_i r_j}\right]\frac{3EI}{l}\left(\vartheta_i - R + \frac{r_j\vartheta_j}{2} - \frac{r_j R}{2}\right) + \left[\frac{4r_i}{4 - r_i r_j}\right]\left(-\frac{r_j}{2}\left(\frac{M_i^F}{2} - M_j^F\right) - \left(\frac{M_j^F}{2} - M_i^F\right)\right)$$

$$M_i = \left[\frac{r_i}{4 - r_i r_j}\right]\frac{6EI}{l}(2\vartheta_i - 2R + r_j\vartheta_j - r_j R) + \left[\frac{r_i}{4 - r_i r_j}\right]\left(-2r_j\left(\frac{M_i^F}{2} - M_j^F\right) - 4\left(\frac{M_j^F}{2} - M_i^F\right)\right)$$

$$M_i = \left[\frac{r_i}{4 - r_i r_j}\right]\frac{6EI}{l}(2\vartheta_i - 2R + r_j\vartheta_j - r_j R) + \left[\frac{r_i}{4 - r_i r_j}\right](-M_i^F r_j + 2M_j^F r_j - 2M_j^F + 4M_i^F)$$

$$M_i = \left[\frac{r_i}{4 - r_i r_j}\right]\frac{6EI}{l}(2\vartheta_i - 2R + r_j\vartheta_j - r_j R) + \left[\frac{r_i}{4 - r_i r_j}\right] - M_i^F(r_j - 4) + M_j^F(2r_j - 2)$$

Likewise

$$M_j = \left[\frac{r_j}{4 - r_i r_j}\right]\frac{6EI}{l}(2\vartheta_j - 2R + r_i\vartheta_i - r_i R) + \left[\frac{r_j}{4 - r_i r_j}\right] - M_j^F(r_i - 4) + M_i^F(2r_i - 2)$$

$$R = \frac{(v_{mj} - v_{mi})}{l}$$

$$M_i = \frac{4EI}{l}\left[\frac{3r_i}{4 - r_i r_j}\right]\vartheta_i + \frac{2EI}{l}\left[\frac{3r_i r_j}{4 - r_i r_j}\right]\vartheta_j - \frac{6EI}{l^2}\left[\frac{r_i(2 + r_j)}{4 - r_i r_j}\right]v_{mj}$$
$$+ \frac{6EI}{l^2}\left[\frac{r_i(2 + r_j)}{4 - r_i r_j}\right]v_{mi} + \left[\frac{r_i}{4 - r_i r_j}\right] - M_i^F(r_j - 4) + M_j^F(2r_j - 2) \qquad (4.4.7a)$$

$$M_j = \frac{4EI}{l}\left[\frac{3r_j}{4 - r_i r_j}\right]\vartheta_j + \frac{2EI}{l}\left[\frac{3r_i r_j}{4 - r_i r_j}\right]\vartheta_i - \frac{6EI}{l^2}\left[\frac{r_j(2 + r_i)}{4 - r_i r_j}\right]v_{mj}$$
$$+ \frac{6EI}{l^2}\left[\frac{r_j(2 + r_i)}{4 - r_i r_j}\right]v_{mi} + \left[\frac{r_j}{4 - r_i r_j}\right] - M_j^F(r_i - 4) + M_i^F(2r_i - 2) \qquad (4.4.7b)$$

Applying

$$S_i = \frac{M_j + M_i}{l} \qquad (4.4.8a) \qquad \text{and} \qquad -S_j = \frac{M_i + M_j}{l} \qquad (4.4.8b)$$

gives

$$S_i = \frac{6EI}{l^2}\left[\frac{r_i(2+r_j)}{4-r_ir_j}\right]\vartheta_i + \frac{6EI}{l^2}\left[\frac{r_j(2+r_i)}{4-r_ir_j}\right]\vartheta_j + \frac{12EI}{l^3}\left[\frac{r_i+r_ir_j+r_j}{4-r_ir_j}\right]v_{mi}$$
$$-\frac{12EI}{l^3}\left[\frac{r_i+r_ir_j+r_j}{4-r_ir_j}\right]v_{mj} + \left[\frac{r_ir_j}{4-r_ir_j}\right]\frac{M_i^F\left(1+\frac{4}{r_j}-\frac{2}{r_i}\right)+M_j^F\left(1-\frac{2}{r_j}+\frac{4}{r_i}\right)}{l} \quad (4.4.9a)$$

$$S_j = -\frac{6EI}{l^2}\left[\frac{r_i(2+r_j)}{4-r_ir_j}\right]\vartheta_i - \frac{6EI}{l^2}\left[\frac{r_j(2+r_i)}{4-r_ir_j}\right]\vartheta_j - \frac{12EI}{l^3}\left[\frac{r_i+r_ir_j+r_j}{4-r_ir_j}\right]v_{mi}$$
$$+\frac{12EI}{l^3}\left[\frac{r_i+r_ir_j+r_j}{4-r_ir_j}\right]v_{mj} - \left[\frac{r_ir_j}{4-r_ir_j}\right]\frac{M_i^F\left(1+\frac{4}{r_j}-\frac{2}{r_i}\right)+M_j^F\left(1-\frac{2}{r_j}+\frac{4}{r_i}\right)}{l} \quad (4.4.9b)$$

(4.4.9b)

Semi-rigid joint axial stiffness

Recall the axial force equation for a member,

$$P_i = \frac{EA}{L}(u_i - u_j) \tag{4.3.3a}$$

$$P_j = \frac{EA}{L}(u_j - u_i) \tag{4.3.3b}$$

for end i and j respectively.

The total displacement equations

$$u_i = u_{mi} + u_{ai} \qquad u_i - u_{ai} = u_{mi}$$

$$u_j = u_{mj} + \delta_{aj} \qquad u_j - u_{aj} = u_{mj}$$

re arranged and substituted into the force equation as follows,

Therefore,

$$P_i = \frac{EA}{l}(u_i - u_{ai} - u_j + u_{sj})$$

But, $u_{ai} = \frac{P_i}{r_{ai}}$ and $u_{aj} = \frac{P_j}{r_{aj}}$

Where r_{ai} =Axial spring stiffness at joint i

r_{aj} =Axial spring stiffness at joint j

Substituting into equation

$$P_i = \frac{EA}{l}\left(u_i - \frac{P_i}{r_{ai}} - u_j + \frac{P_j}{r_{aj}}\right) \tag{4.5.1}$$

Since only axial forces are considered, for equilibrium $P = P_i = -P_j$, hence we have the following:

Expanding equation (4.5.1)

$$P_i = \frac{EA}{l}u_i - \frac{EA}{l}\frac{P_i}{r_{ai}} - \frac{EA}{l}u_j - \frac{EA}{l}\frac{P_i}{r_{aj}}$$

Rearranging

$$P_i + \frac{EA}{l}\frac{P_i}{r_{ai}} + \frac{EA}{l}\frac{P_i}{r_{aj}} = \frac{EA}{l}u_i - \frac{EA}{l}u_j$$

$$P_i\left(1 + \frac{EA}{lr_{ai}} + \frac{EA}{lr_{aj}}\right) = \frac{EA}{l}(u_i - u_j)$$

Letting $\rho_i = \left(1 + \frac{EA}{lr_{ai}} + \frac{EA}{lr_{aj}}\right)$, hence

$$P_i = \frac{EA}{l\rho_i}(u_i - u_j) \qquad (4.5.2a)$$

Likewise for P_j,

$$\rho_j = \left(1 + \frac{EA}{lr_{aj}} + \frac{EA}{lr_{ai}}\right) \quad \therefore \rho_i = \rho_j = \rho$$

$$P_i = -P_j = \frac{EA}{l\rho}(u_i - u_j) \qquad (4.5.2b)$$

Semi-Rigid Shear stiffness

$$R = \frac{\Delta_m}{l} = \frac{v_{mj} - v_{mi}}{l}$$

Denoting the following

$$\Delta_t = v_j - v_i$$

$$\Delta_s = v_{sj} - v_{si}$$

$$\Delta_m = v_{mj} - v_{mi}$$

where, $\Delta_t =$ Total vertical relative displacement

$\Delta_s =$ Spring relative displacement

$\Delta_m =$ Member relative displacement

Also,

$\Delta_t = \Delta_s + \Delta_m \ \therefore \quad \Delta_m = \Delta_t - \Delta_s$

Hence, $v_{mj} = v_j - v_{sj}$ $\qquad$ $v_{mi} = v_i - v_{si}$

Therefore,

$$R = \frac{v_{mj} - v_{mi}}{l} = \frac{(v_j - v_{sj}) - (v_i - v_{si})}{l}$$

But $v_{si} = \frac{S_i}{r_{si}}$ & $\qquad v_{sj} = \frac{S_j}{r_{sj}}$

Substituting into the equation above

$$R = \frac{(v_j - v_{sj}) - (v_i - v_{si})}{l} = \frac{\left(v_j - \frac{S_j}{r_{sj}}\right) - \left(v_i - \frac{S_i}{r_{si}}\right)}{l}$$

Recalling shear force equation (4.4.8a) and (4.4.8b) respectively

$$S_i = \frac{M_j + M_i}{l}, \qquad S_j = -\left(\frac{M_i + M_j}{l}\right)$$

Hence, substituting into R

$$R=\frac{\left(v_j-\frac{S_j}{r_{sj}}\right)-\left(v_i-\frac{S_i}{r_{si}}\right)}{l}=\frac{\left(v_j+\frac{\left(M_i+M_j\right)}{lr_{sj}}\right)-\left(v_i-\frac{\left(M_j+M_i\right)}{lr_{si}}\right)}{l}$$

$$=\frac{v_j}{l}+\frac{M_i}{l^2r_{sj}}+\frac{M_j}{l^2r_{sj}}-\frac{v_j}{l}+\frac{M_i}{l^2r_{si}}+\frac{M_j}{l^2r_{si}}$$

$$=\frac{1}{l}\left(v_j-v_i\right)+M_i\left(\frac{1}{l^2r_{sj}}+\frac{1}{l^2r_{si}}\right)+M_j\left(\frac{1}{l^2r_{sj}}+\frac{1}{l^2r_{si}}\right)$$

Letting $\beta=\left(\frac{1}{l^2r_{sj}}+\frac{1}{l^2r_{si}}\right)$

Therefore,

$$R=\frac{1}{l}\left(v_j-v_i\right)+M_i\beta+M_j\beta$$

Before proceeding any further the equation β can be tested. It is assumed that the spring is very stiff this will be the rigid condition. Just by inspection if r_{si} and r_{sj} are infinitely large then β tends to zero. Therefore, R is equal to $\frac{1}{l}\left(v_j-v_i\right)$ which is equal to $\frac{1}{l}\left(v_{mj}-v_{mi}\right)$ and reduces to the slope deflection equation.

We recall the equations (4.4.6a) and (4.4.6b).

$$M_i=\frac{3EIr_i}{l}\left(\vartheta_i-R\right)+\frac{M_jr_i}{2}-r_i\left(\frac{M_j^F}{2}-M_i^F\right)$$

$$M_j=\frac{3EIr_j}{l}\left(\vartheta_j-R\right)+\frac{M_ir_j}{2}-r_j\left(\frac{M_i^F}{2}-M_j^F\right)$$

By substituting for R in the equation the shear spring has been introduced to the system.

$$M_i=\frac{3EIr_i}{l}\left[\vartheta_i-\left(\frac{1}{l}\left(v_j-v_i\right)+M_i\beta+M_j\beta\right)\right]+\frac{M_jr_i}{2}-r_i\left(\frac{M_j^F}{2}-M_i^F\right)\quad(4.6.1a)$$

$$M_j=\frac{3EIr_j}{l}\left[\vartheta_j-\left(\frac{1}{l}\left(v_j-v_i\right)+M_i\beta+M_j\beta\right)\right]+\frac{M_ir_j}{2}-r_j\left(\frac{M_i^F}{2}-M_j^F\right)\quad(4.6.1b)$$

Expanding

$$M_i\left(1+\frac{3EIr_i\beta}{l}\right)=\frac{3EIr_i}{l}\left[\vartheta_i-\left(\frac{1}{l}(v_j-v_i)+M_j\beta\right)\right]+\frac{M_jr_i}{2}-r_i\left(\frac{M_j^F}{2}-M_i^F\right)$$

(4.6.1a)

$$M_j\left(1+\frac{3EIr_j\beta}{l}\right)=\frac{3EIr_j}{l}\left[\vartheta_j-\left(\frac{1}{l}(v_j-v_i)+M_i\beta\right)\right]+\frac{M_ir_j}{2}-r_j\left(\frac{M_i^F}{2}-M_j^F\right)$$

(4.6.1b)

Letting $\alpha_i=1+\frac{3EIr_i\beta}{l}$ and $\alpha_j=1+\frac{3EIr_j\beta}{l}$

Therefore

$$M_i=\frac{3EIr_i}{\alpha_il}\left[\vartheta_i-\left(\frac{1}{l}(v_j-v_i)+M_j\beta\right)\right]+\frac{M_jr_i}{2\alpha_i}-\frac{r_i}{\alpha_i}\left(\frac{M_j^F}{2}-M_i^F\right)$$

(4.6.2a)

$$M_j=\frac{3EIr_j}{\alpha_jl}\left[\vartheta_j-\left(\frac{1}{l}(v_j-v_i)+M_i\beta\right)\right]+\frac{M_ir_j}{2\alpha_j}-\frac{r_j}{\alpha_j}\left(\frac{M_i^F}{2}-M_j^F\right)$$

(4.6.2b)

Letting $R'=\frac{1}{l}(v_j-v_i)$ to simplify solution

Therefore,

$$M_i=\frac{3EIr_i}{\alpha_il}\left[\vartheta_i-\left(R'+M_j\beta\right)\right]+\frac{M_jr_i}{2\alpha_i}-\frac{r_i}{\alpha_i}\left(\frac{M_j^F}{2}-M_i^F\right)$$

(4.6.3a)

$$M_j=\frac{3EIr_j}{\alpha_jl}\left[\vartheta_j-\left(R'-M_i\beta\right)\right]+\frac{M_ir_j}{2\alpha_j}-\frac{r_j}{\alpha_j}\left(\frac{M_i^F}{2}-M_j^F\right)$$

(4.6.3b)

Letting $\gamma_j=\frac{3EIr_j}{\alpha_jl}$ and $\gamma_i=\frac{3EIr_i}{\alpha_il}$

Therefore,

$$M_i=\gamma_i\left[\vartheta_i-\left(R'+M_j\beta\right)\right]+\frac{M_jr_i}{2\alpha_i}-\frac{r_i}{\alpha_i}\left(\frac{M_j^F}{2}-M_i^F\right)$$

(4.6.4a)

$$M_j=\gamma_j\left[\vartheta_j-\left(R'+M_i\beta\right)\right]+\frac{M_ir_j}{2\alpha_j}-\frac{r_j}{\alpha_j}\left(\frac{M_i^F}{2}-M_j^F\right)$$

(4.6.4b)

$$M_i = \gamma_i(\vartheta_i - R') - M_j\left(\gamma_i\beta - \frac{r_i}{2\alpha_i}\right) - \frac{r_i}{\alpha_i}\left(\frac{M_j^F}{2} - M_i^F\right) \qquad (4.6.5a)$$

$$M_j = \gamma_j(\vartheta_j - R') - M_i\left(\gamma_j\beta + \frac{r_j}{2\alpha_j}\right) - \frac{r_j}{\alpha_j}\left(\frac{M_i^F}{2} - M_j^F\right) \qquad (4.6.5b)$$

Substituting M_j into M_i

Therefore,

$$M_i = \gamma_i(\vartheta_i - R') - \left[\gamma_j(\vartheta_j - R') - M_i\left(\gamma_j\beta - \frac{r_j}{2\alpha_j}\right) - \frac{r_j}{\alpha_j}\left(\frac{M_i^F}{2} - M_j^F\right)\right]\left(\gamma_i\beta - \frac{r_i}{2\alpha_i}\right) - \frac{r_i}{\alpha_i}\left(\frac{M_j^F}{2} - M_i^F\right)$$

(4.6.6a)

If we assume that the system is rigid we should end up with the original semi-rigid matrix as derived in the slope deflection equation for semi-rigid joints. The test can be found in Appendix 3

We can now continue evaluating Equation (4.6.6a). For programming purposes we shall separate the new terms from the old terms, thereby high-lighting changes required in the program.

$$M_i = \gamma_i\vartheta_i - \gamma_i R' - \left[\gamma_j\vartheta_j - \gamma_j R' - \gamma_j\beta M_i + \frac{r_j}{2\alpha_j}M_i - \frac{r_j}{2\alpha_j}M_i^F + \frac{r_j}{\alpha_j}M_j^F\right]\left(\gamma_i\beta - \frac{r_i}{2\alpha_i}\right) - \frac{r_i}{\alpha_i}\frac{M_j^F}{2} + \frac{r_i}{\alpha_i}M_i^F$$

Expanding the brackets

$$M_i = \gamma_i\vartheta_i - \gamma_i R' - \left[\begin{array}{l}\gamma_i\gamma_j\beta\vartheta_j - \frac{\gamma_j r_i}{2\alpha_i}\vartheta_j - \gamma_i\gamma_j\beta R' + \frac{\gamma_j r_i}{2\alpha_i}R' - \gamma_i\gamma_j\beta^2 M_i + \frac{\gamma_j r_i\beta}{2\alpha_i}M_i + \frac{\gamma_i r_j\beta}{2\alpha_j}M_i \\ -\frac{r_i r_j}{4\alpha_i\alpha_j}M_i - \frac{\gamma_i r_j\beta}{2\alpha_j}M_i^F + \frac{r_i r_j}{4\alpha_i\alpha_j}M_i^F + \frac{\gamma_i r_j\beta}{\alpha_j}M_j^F - \frac{r_i r_j}{2\alpha_i\alpha_j}M_j^F\end{array}\right] - \frac{r_i}{2\alpha_i}M_j^F + \frac{r_i}{\alpha_i}M_i^F$$

$$M_i = \gamma_i \vartheta_i - \gamma_i R' - \gamma_i \gamma_j \beta \vartheta_j + \frac{\gamma_j r_i}{2\alpha_i}\vartheta_j + \gamma_i \gamma_j \beta R' - \frac{\gamma_j r_i}{2\alpha_i}R' + \gamma_i \gamma_j \beta^2 M_i - \frac{\gamma_j r_i \beta}{2\alpha_i}M_i - \frac{\gamma_i r_j \beta}{2\alpha_j}M_i$$

$$+\frac{r_i r_j}{4\alpha_i \alpha_j}M_i + \frac{\gamma_i r_j \beta}{2\alpha_j}M_i^F - \frac{r_i r_j}{4\alpha_i \alpha_j}M_i^F - \frac{\gamma_i r_j \beta}{\alpha_j}M_j^F + \frac{r_i r_j}{2\alpha_i \alpha_j}M_j^F - \frac{r_i}{2\alpha_i}M_j^F + \frac{r_i}{\alpha_i}M_i^F$$

$$\left(1 - \gamma_i \gamma_j \beta^2 + \frac{r_i \gamma_j \beta}{2\alpha_i} + \frac{\gamma_i r_j \beta}{2\alpha_j} - \frac{r_i r_j}{4\alpha_i \alpha_j}\right)M_i = \gamma_i \vartheta_i - \gamma_i R' - \gamma_i \gamma_j \beta \vartheta_j + \frac{\gamma_j r_i}{2\alpha_i}\vartheta_j + \gamma_i \gamma_j \beta R' - \frac{\gamma_j r_i}{2\alpha_i}R'$$

$$+\frac{\gamma_i r_j \beta}{2\alpha_j}M_i^F - \frac{r_i r_j}{4\alpha_i \alpha_j}M_i^F - \frac{\gamma_i r_j \beta}{\alpha_j}M_j^F + \frac{r_i r_j}{2\alpha_i \alpha_j}M_j^F - \frac{r_i}{2\alpha_i}M_j^F + \frac{r_i}{\alpha_i}M_i^F$$

Separating the coefficients

$$\left(1 - \gamma_i \gamma_j \beta^2 + \frac{\gamma_j r_i \beta}{2\alpha_i} + \frac{\gamma_i r_j \beta}{2\alpha_j} - \frac{r_i r_j}{4\alpha_i \alpha_j}\right)M_i = \gamma_i \vartheta_i - \left(\gamma_i \gamma_j \beta - \frac{\gamma_j r_i}{2\alpha_i}\right)\vartheta_j - \left(\gamma_i - \gamma_i \gamma_j \beta + \frac{\gamma_j r_i}{2\alpha_i}\right)R'$$

$$+\left(\frac{\gamma_i r_j \beta}{2\alpha_j} - \frac{r_i r_j}{4\alpha_i \alpha_j} + \frac{r_i}{\alpha_i}\right)M_i^F - \left(\frac{\gamma_i r_j \beta}{\alpha_j} - \frac{r_i r_j}{2\alpha_i \alpha_j} + \frac{r_i}{2\alpha_i}\right)M_j^F$$

We have now deduced the full equation. The equation will now be re-written so that we can distinguish the new terms from the old terms. This allows the preservation of the original equation thus allowing easier implementation of the equation in the existing program.

Letting $\varepsilon_i = -\left(\gamma_i \gamma_j \beta^2 - \frac{\gamma_j r_i \beta}{2\alpha_i} - \frac{\gamma_i r_j \beta}{2\alpha_j}\right)$

Hence

$$\left(\varepsilon_i + 1 - \frac{r_i r_j}{4\alpha_i \alpha_j}\right)M_i = \gamma_i \vartheta_i - \left(\gamma_i \gamma_j \beta - \frac{\gamma_j r_i}{2\alpha_i}\right)\vartheta_j - \left(\gamma_i - \gamma_i \gamma_j \beta + \frac{\gamma_j r_i}{2\alpha_i}\right)R'$$

$$+\left(\frac{\gamma_i r_j \beta}{2\alpha_j} - \frac{r_i r_j}{4\alpha_i \alpha_j} + \frac{r_i}{\alpha_i}\right)M_i^F - \left(\frac{\gamma_i r_j \beta}{\alpha_j} - \frac{r_i r_j}{2\alpha_i \alpha_j} + \frac{r_i}{2\alpha_i}\right)M_j^F$$

substituting

$\gamma_i = \frac{3EIr_i}{l}$ and $\gamma_j = \frac{3EIr_j}{l}$ back into the equation.

$$\left(\varepsilon_i+\left(\frac{4\alpha_i\alpha_j-r_ir_j}{4\alpha_i\alpha_j}\right)\right)M_i=\frac{3EIr_i}{l}\vartheta_i-\left(\frac{3EIr_i}{l}\frac{3EIr_j}{l}\beta-\frac{3EIr_j}{l}\frac{r_i}{2\alpha_i}\right)\vartheta_j$$

$$\Rightarrow -\left(\frac{3EIr_i}{l}-\frac{3EIr_i}{l}\frac{3EIr_j}{l}\beta+\frac{3EIr_j}{l}\frac{r_i}{2\alpha_i}\right)R'$$

$$+\left(\frac{3EIr_i}{l}\frac{r_j\beta}{2\alpha_j}-\frac{r_ir_j}{4\alpha_i\alpha_j}+\frac{r_i}{\alpha_i}\right)M_i^F-\left(\frac{3EIr_i}{l}\frac{r_j\beta}{\alpha_j}-\frac{r_ir_j}{2\alpha_i\alpha_j}+\frac{r_i}{2\alpha_i}\right)M_j^F$$

$$M_i=\left[\frac{3\alpha_i\alpha_jr_i}{4\varepsilon_i\alpha_i\alpha_j+4\alpha_i\alpha_j-r_ir_j}\right]\frac{4EI}{l}\vartheta_i-\left[\frac{3\alpha_i\alpha_jr_ir_j}{4\varepsilon_i\alpha_i\alpha_j+4\alpha_i\alpha_j-r_ir_j}\right]\left(\frac{12(EI)^2}{l^2}\beta-\frac{2EI}{\alpha_il}\right)\vartheta_j$$

$$-\left[\frac{\alpha_i\alpha_jr_i(2\alpha_i+r_j)}{4\varepsilon_i\alpha_i\alpha_j+4\alpha_i\alpha_j-r_ir_j}\right]\left(\frac{6EI}{\alpha_il}-\frac{36(EI)^2r_j}{(2\alpha_i+r_j)l^2}\beta\right)R'+\left[\frac{r_i}{4\varepsilon_i\alpha_i\alpha_j+4\alpha_i\alpha_j-r_ir_j}\right]\left(\frac{6EI\alpha_i\beta r_j}{l}-r_j+4\alpha_j\right)M_i^F$$

$$-\left[\frac{r_i}{4\varepsilon_i\alpha_i\alpha_j+4\alpha_i\alpha_j-r_ir_j}\right]\left(\frac{12EI\alpha_i\beta r_j}{l}-2r_j+2\alpha_j\right)M_j^F$$

Substituting $R'=\frac{(v_j-v_i)}{l}$ back in

It should be remembered that the vertical displacement is now in terms of total displacements V_i and V_j for nodes i and j respectively and not member displacements v_{mi} and v_{mj}.

$$M_i=\frac{4EI}{l}\left[\frac{3\alpha_i\alpha_jr_i}{4\varepsilon_i\alpha_i\alpha_j+4\alpha_i\alpha_j-r_ir_j}\right]\vartheta_i+\left(-\frac{12(EI)^2}{l^2}\beta+\frac{2EI}{\alpha_il}\right)\left[\frac{3\alpha_i\alpha_jr_ir_j}{4\varepsilon_i\alpha_i\alpha_j+4\alpha_i\alpha_j-r_ir_j}\right]\vartheta_j$$

$$-\left(\frac{6EI}{l^2}\right)\left[\frac{\alpha_i\alpha_jr_i\left(2+\frac{r_j}{\alpha_i}-\frac{6EIr_j\beta}{l}\right)}{4\varepsilon_i\alpha_i\alpha_j+4\alpha_i\alpha_j-r_ir_j}\right]v_j+\left(\frac{6EI}{l^2}\right)\left[\frac{\alpha_i\alpha_jr_i\left(2+\frac{r_j}{\alpha_i}-\frac{6EIr_j\beta}{l}\right)}{4\varepsilon_i\alpha_i\alpha_j+4\alpha_i\alpha_j-r_ir_j}\right]v_i$$

$$-\left(r_j-4\alpha_j-\frac{6EI\alpha_i\beta r_j}{l}\right)\left[\frac{r_i}{4\varepsilon_i\alpha_i\alpha_j+4\alpha_i\alpha_j-r_ir_j}\right]M_i^F+\left(2r_j-2\alpha_j-\frac{12EI\alpha_i\beta r_j}{l}\right)\left[\frac{r_i}{4\varepsilon_i\alpha_i\alpha_j+4\alpha_i\alpha_j-r_ir_j}\right]M_j^F$$

(4.6.7a)

Substituting M_i into M_j

$$\Rightarrow \quad M_j = \gamma_j(\vartheta_j - R') - \left[\gamma_i(\vartheta_i - R') - M_j\left(\gamma_i\beta - \frac{r_i}{2\alpha_i}\right) - \frac{r_i}{\alpha_i}\left(\frac{M_j^F}{2} - M_i^F\right)\right]\left(\gamma_j\beta - \frac{r_j}{2\alpha_j}\right)$$

$$- \frac{r_j}{\alpha_j}\left(\frac{M_i^F}{2} - M_j^F\right)$$

$$M_j = \gamma_j(\vartheta_j - R') - \left[\gamma_i\vartheta_i - \gamma_i R' - \gamma_i\beta M_j + \frac{r_i}{2\alpha_i}M_j - \frac{r_i}{2\alpha_i}M_j^F + \frac{r_i}{\alpha_i}M_i^F\right]\left(\gamma_j\beta - \frac{r_j}{2\alpha_j}\right)$$

$$- \frac{r_j}{\alpha_j}\frac{M_i^F}{2} + \frac{r_j}{\alpha_j}M_j^F$$

(4.6.6b)

$$M_j = \gamma_j\vartheta_j - \gamma_j R' - \left[\begin{array}{l}\gamma_i\gamma_j\beta\vartheta_i - \frac{\gamma_i r_j}{2\alpha_j}\vartheta_i - \gamma_i\gamma_j\beta R' + \frac{\gamma_i r_j}{2\alpha_j}R' - \gamma_i\gamma_j\beta^2 M_j + \frac{\gamma_i\beta r_j}{2\alpha_j}M_j + \frac{\gamma_j\beta r_i}{2\alpha_i}M_j \\ - \frac{r_i r_j}{4\alpha_i\alpha_j}M_j - \frac{\gamma_j\beta r_i}{2\alpha_i}M_j^F + \frac{r_i r_j}{4\alpha_i\alpha_j}M_j^F + \frac{\gamma_j\beta r_i}{\alpha_i}M_i^F - \frac{r_i r_j}{2\alpha_i\alpha_j}M_i^F\end{array}\right]$$

$$- \frac{r_j}{\alpha_j}\frac{M_i^F}{2} + \frac{r_j}{\alpha_j}M_j^F$$

$$\left(1 - \gamma_i\gamma_j\beta^2 + \frac{\gamma_i\beta r_j}{2\alpha_j} + \frac{\gamma_j\beta r_i}{2\alpha_i} - \frac{r_i r_j}{4\alpha_i\alpha_j}\right)M_j = \gamma_j\vartheta_j - \left(\gamma_i\gamma_j\beta - \frac{\gamma_i r_j}{2\alpha_j}\right)\vartheta_i - \left(\gamma_j - \gamma_i\gamma_j\beta + \frac{\gamma_i r_j}{2\alpha_j}\right)R'$$

$$- \left(\frac{\gamma_j\beta r_i}{\alpha_i} - \frac{r_i r_j}{2\alpha_i\alpha_j} + \frac{r_j}{2\alpha_j}\right)M_i^F + \left(\frac{r_j}{\alpha_j} + \frac{\gamma_j\beta r_i}{2\alpha_i} - \frac{r_i r_j}{4\alpha_i\alpha_j}\right)M_j^F$$

Letting $\varepsilon_j = -\left(\gamma_i\gamma_j\beta^2 - \frac{\gamma_i\beta r_j}{2\alpha_j} - \frac{\gamma_j\beta r_i}{2\alpha_i}\right)$

$$\left(\varepsilon_j + 1 - \frac{r_i r_j}{4\alpha_i\alpha_j}\right)M_j = \gamma_j\vartheta_j - \left(\gamma_i\gamma_j\beta - \frac{\gamma_i r_j}{2\alpha_j}\right)\vartheta_i - \left(\gamma_j - \gamma_i\gamma_j\beta + \frac{\gamma_i r_j}{2\alpha_j}\right)R'$$

$$- \left(\frac{\gamma_j\beta r_i}{\alpha_i} - \frac{r_i r_j}{2\alpha_i\alpha_j} + \frac{r_j}{2\alpha_j}\right)M_i^F + \left(\frac{r_j}{\alpha_j} + \frac{\gamma_j\beta r_i}{2\alpha_i} - \frac{r_i r_j}{4\alpha_i\alpha_j}\right)M_j^F$$

Substituting

$\gamma_i = \frac{3EIr_i}{l}$ and $\gamma_j = \frac{3EIr_j}{l}$ back into the equation and re-arranging.

$$M_j=\left[\frac{4\alpha_i\alpha_j r_j}{4\varepsilon_j\alpha_i\alpha_j+4\alpha_i\alpha_j-r_i r_j}\right]\frac{3EI}{l}\vartheta_j-\left[\frac{4\alpha_i\alpha_j r_j}{4\varepsilon_j\alpha_i\alpha_j+4\alpha_i\alpha_j-r_i r_j}\right]\left(\frac{3EIr_i}{l}\frac{3EI}{l}\beta-\frac{3EIr_i}{2\alpha_j l}\right)\vartheta_i$$

$$\Rightarrow\quad -\left[\frac{4\alpha_i\alpha_j r_j}{4\varepsilon_j\alpha_i\alpha_j+4\alpha_i\alpha_j-r_i r_j}\right]\left(\frac{3EI}{l}-\frac{3EIr_i}{l}\frac{3EI}{l}\beta+\frac{3EIr_i}{2\alpha_j l}\right)R'$$

$$-\left[\frac{4\alpha_i\alpha_j r_j}{4\varepsilon_j\alpha_i\alpha_j+4\alpha_i\alpha_j-r_i r_j}\right]\left(\frac{3EI}{l}\frac{\beta r_i}{\alpha_i}-\frac{r_i}{2\alpha_i\alpha_j}+\frac{1}{2\alpha_j}\right)M_i^F$$

$$+\left[\frac{4\alpha_i\alpha_j r_j}{4\varepsilon_j\alpha_i\alpha_j+4\alpha_i\alpha_j-r_i r_j}\right]\left(\frac{1}{\alpha_j}+\frac{3EI}{l}\frac{\beta r_i}{2\alpha_i}-\frac{r_i}{4\alpha_i\alpha_j}\right)M_j^F$$

$$M_j=\left[\frac{4\alpha_i\alpha_j r_j}{4\varepsilon_j\alpha_i\alpha_j+4\alpha_i\alpha_j-r_i r_j}\right]\frac{3EI}{l}\vartheta_j-\left[\frac{\alpha_i\alpha_j r_j}{4\varepsilon_j\alpha_i\alpha_j+4\alpha_i\alpha_j-r_i r_j}\right]\left(\frac{36(EI)^2 r_i}{l^2}\beta-\frac{6EIr_i}{\alpha_j l}\right)\vartheta_i$$

$$\Rightarrow\quad -\left[\frac{\alpha_i\alpha_j r_j}{4\varepsilon_j\alpha_i\alpha_j+4\alpha_i\alpha_j-r_i r_j}\right]\left(\frac{12EI}{l}-\frac{36(EI)^2 r_i}{l^2}\beta+\frac{6EIr_i}{\alpha_j l}\right)R'$$

$$-\left[\frac{\alpha_i\alpha_j r_j}{4\varepsilon_j\alpha_i\alpha_j+4\alpha_i\alpha_j-r_i r_j}\right]\left(\frac{12EI}{l}\frac{\beta r_i}{\alpha_i}-\frac{2r_i}{\alpha_i\alpha_j}+\frac{2}{\alpha_j}\right)M_i^F$$

$$+\left[\frac{\alpha_i\alpha_j r_j}{4\varepsilon_j\alpha_i\alpha_j+4\alpha_i\alpha_j-r_i r_j}\right]\left(\frac{4}{\alpha_j}+\frac{6EI}{l}\frac{\beta r_i}{\alpha_i}-\frac{r_i}{\alpha_i\alpha_j}\right)M_j^F$$

$$M_j=\frac{4EI}{l}\left[\frac{3\alpha_i\alpha_j r_j}{4\varepsilon_j\alpha_i\alpha_j+4\alpha_i\alpha_j-r_i r_j}\right]\vartheta_j+\left(\frac{2EI}{\alpha_j l}-\frac{12(EI)^2}{l^2}\beta\right)\left[\frac{3\alpha_i\alpha_j r_i r_j}{4\varepsilon_j\alpha_i\alpha_j+4\alpha_i\alpha_j-r_i r_j}\right]\vartheta_i$$

$$-\left(\frac{6EI}{l^2}\right)\left[\frac{\alpha_i\alpha_j r_j\left(2+\frac{r_i}{\alpha_j}-\frac{6EIr_i\beta}{l}\right)}{4\varepsilon_i\alpha_i\alpha_j+4\alpha_i\alpha_j-r_i r_j}\right]v_j+\left(\frac{6EI}{l^2}\right)\left[\frac{\alpha_i\alpha_j r_j\left(2+\frac{r_i}{\alpha_j}-\frac{6EIr_i\beta}{l}\right)}{4\varepsilon_i\alpha_i\alpha_j+4\alpha_i\alpha_j-r_i r_j}\right]v_i$$

$$+\left(2r_i-2\alpha_i-\frac{12EIr_i\alpha_j\beta}{l}\right)\left[\frac{r_j}{4\varepsilon_j\alpha_i\alpha_j+4\alpha_i\alpha_j-r_i r_j}\right]M_i^F$$

$$-\left(r_i-4\alpha_i-\frac{6EI\beta\alpha_j r_i}{l}\right)\left[\frac{r_j}{4\varepsilon_j\alpha_i\alpha_j+4\alpha_i\alpha_j-r_i r_j}\right]M_j^F$$

(4.6.7b)

We can deduce the internal shear equation for the system by recalling the following shear equations.

$$S_i = \frac{M_j + M_i}{l} \qquad \text{and} \qquad S_j = -\left(\frac{M_i + M_j}{l}\right)$$

Note that $\varepsilon = \varepsilon_i = \varepsilon_j$

The coefficients ϑ_i, ϑ_j, v_i, v_j, M_i^F and M_j^F can be evaluated separately.

Evaluating ϑ_i

$$= \frac{4EI}{l}\left[\frac{3\alpha_i\alpha_j r_i}{4\varepsilon_i\alpha_i\alpha_j + 4\alpha_i\alpha_j - r_i r_j}\right] - \left(\frac{12(EI)^2}{l^2}\beta - \frac{2EI}{\alpha_j l}\right)\left[\frac{3\alpha_i\alpha_j r_i r_j}{4\varepsilon_j\alpha_i\alpha_j + 4\alpha_i\alpha_j - r_i r_j}\right]$$

$$= \left(\frac{6EI}{l} - \frac{18(EI)^2\beta r_j}{l^2} + \frac{3EIr_j}{\alpha_j l}\right)\left[\frac{2\alpha_i\alpha_j r_i}{4\varepsilon_j\alpha_i\alpha_j + 4\alpha_i\alpha_j - r_i r_j}\right]$$

$$= \frac{6EI}{l}\left[\frac{\alpha_i\alpha_j r_i\left(2 - \frac{6EI\beta r_j}{l} + \frac{r_j}{\alpha_j}\right)}{4\varepsilon_j\alpha_i\alpha_j + 4\alpha_i\alpha_j - r_i r_j}\right]\vartheta_i$$

Evaluating ϑ_j

$$= \left(\frac{2EI}{\alpha_i l} - \frac{12(EI)^2}{l^2}\beta\right)\left[\frac{3\alpha_i\alpha_j r_i r_j}{4\varepsilon_i\alpha_i\alpha_j + 4\alpha_i\alpha_j - r_i r_j}\right] + \frac{4EI}{l}\left[\frac{3\alpha_i\alpha_j r_j}{4\varepsilon_j\alpha_i\alpha_j + 4\alpha_i\alpha_j - r_i r_j}\right]$$

$$= \left(\frac{6EIr_i}{\alpha_i l} - \frac{36(EI)^2\beta r_i}{l^2} + \frac{12EI}{l}\right)\left[\frac{\alpha_i\alpha_j r_j}{4\varepsilon_j\alpha_i\alpha_j + 4\alpha_i\alpha_j - r_i r_j}\right]$$

$$= \frac{6EI}{l}\left[\frac{\alpha_i\alpha_j r_j\left(2 + \frac{r_i}{\alpha_i} - \frac{6EI\beta r_i}{l}\right)}{4\varepsilon_j\alpha_i\alpha_j + 4\alpha_i\alpha_j - r_i r_j}\right]\vartheta_j$$

Evaluating v_i's and v_j's

The vertical displacement will be expressed via the coefficient R' to minimise the task

$$= -\left(\frac{6EI}{l^2}\right)\left[\frac{\alpha_i\alpha_j r_i\left(2-\frac{6EIr_j\beta}{l}+\frac{r_j}{\alpha_i}\right)}{4\varepsilon_i\alpha_i\alpha_j+4\alpha_i\alpha_j-r_ir_j}\right]-\left(\frac{6EI}{l^2}\right)\left[\frac{\alpha_i\alpha_j r_j\left(2-\frac{6EIr_i\beta}{l}+\frac{r_i}{\alpha_j}\right)}{4\varepsilon_i\alpha_i\alpha_j+4\alpha_i\alpha_j-r_ir_j}\right]$$

$$= -\left(\frac{12EI}{l^2}\right)\left[\frac{\alpha_i\alpha_j r_i\left(1-\frac{3EIr_j\beta}{l}+\frac{r_j}{2\alpha_i}\right)}{4\varepsilon_i\alpha_i\alpha_j+4\alpha_i\alpha_j-r_ir_j}\right]-\left(\frac{12EI}{l^2}\right)\left[\frac{\alpha_i\alpha_j r_j\left(1-\frac{3EIr_i\beta}{l}+\frac{r_i}{2\alpha_j}\right)}{4\varepsilon_i\alpha_i\alpha_j+4\alpha_i\alpha_j-r_ir_j}\right]$$

$$= -\left(\frac{12EI}{l^2}\right)\left[\frac{\alpha_i\alpha_j\left(r_i-\frac{3EIr_ir_j\beta}{l}+\frac{r_ir_j}{2\alpha_i}+r_j-\frac{3EIr_ir_j\beta}{l}+\frac{r_ir_j}{2\alpha_j}\right)}{4\varepsilon_i\alpha_i\alpha_j+4\alpha_i\alpha_j-r_ir_j}\right]$$

$$= -\left(\frac{12EI}{l^2}\right)\left[\frac{\alpha_i\alpha_j\left(r_i+\frac{r_ir_j}{2}\left(\frac{1}{\alpha_i}+\frac{1}{\alpha_j}\right)+r_j-\frac{6EIr_ir_j\beta}{l}\right)}{4\varepsilon_i\alpha_i\alpha_j+4\alpha_i\alpha_j-r_ir_j}\right]R'$$

Evaluating M_i^F's

$$= -\left(r_j - 4\alpha_j - \frac{6EI\alpha_i\beta r_j}{l}\right)\left[\frac{r_i}{4\varepsilon_i\alpha_i\alpha_j + 4\alpha_i\alpha_j - r_i r_j}\right]$$

$$+\left(2r_i - 2\alpha_i + \frac{12EIr_i\alpha_j\beta}{l}\right)\left[\frac{r_j}{4\varepsilon_j\alpha_i\alpha_j + 4\alpha_i\alpha_j - r_i r_j}\right]$$

$$= \left(-r_i r_j + 4\alpha_j r_i + \frac{6EI\alpha_i\beta r_i r_j}{l} + 2r_i r_j - 2\alpha_i r_j - \frac{12EIr_i r_j\alpha_j\beta}{l}\right)\left[\frac{1}{4\varepsilon_j\alpha_i\alpha_j + 4\alpha_i\alpha_j - r_i r_j}\right]$$

$$= \left(-1 + \frac{4\alpha_j}{r_j} + \frac{6EI\alpha_i\beta}{l} + 2 - \frac{2\alpha_i}{r_i} - \frac{12EI\alpha_j\beta}{l}\right)\left[\frac{r_i r_j}{4\varepsilon_j\alpha_i\alpha_j + 4\alpha_i\alpha_j - r_i r_j}\right]$$

$$= \left(\frac{1}{l}\right)\left(1 + \frac{4\alpha_j}{r_j} - \frac{2\alpha_i}{r_i} + \frac{6EI\beta(\alpha_i - 2\alpha_j)}{l}\right)\left[\frac{r_i r_j}{4\varepsilon_j\alpha_i\alpha_j + 4\alpha_i\alpha_j - r_i r_j}\right]$$

Evaluating M_j^F's

$$= \left(2r_j - 2\alpha_j - \frac{12EI\beta r_j\alpha_i}{l}\right)\left[\frac{r_i}{4\varepsilon_j\alpha_i\alpha_j + 4\alpha_i\alpha_j - r_i r_j}\right] - \left(r_i - 4\alpha_i - \frac{6EI\beta\alpha_j r_i}{l}\right)\left[\frac{r_j}{4\varepsilon_i\alpha_i\alpha_j + 4\alpha_i\alpha_j - r_i r_j}\right]$$

$$= \left(2r_i r_j - 2\alpha_j r_i - \frac{12EIr_i r_j\alpha_i\beta}{l} - r_i r_j + 4\alpha_i r_j + \frac{6EI\alpha_j\beta r_i r_j}{l}\right)\left[\frac{1}{4\varepsilon_j\alpha_i\alpha_j + 4\alpha_i\alpha_j - r_i r_j}\right]$$

$$= \left(2 - \frac{2\alpha_j}{r_j} - \frac{12EI\alpha_i\beta}{l} - 1 + \frac{4\alpha_i}{r_i} + \frac{6EI\alpha_j\beta}{l}\right)\left[\frac{r_i r_j}{4\varepsilon_j\alpha_i\alpha_j + 4\alpha_i\alpha_j - r_i r_j}\right]$$

$$= \left(\frac{6EI\beta(\alpha_j - 2\alpha_i)}{l} + 1 - \frac{2\alpha_j}{r_j} + \frac{4\alpha_i}{r_i}\right)\left[\frac{r_i r_j}{4\varepsilon_j\alpha_i\alpha_j + 4\alpha_i\alpha_j - r_i r_j}\right]$$

Evaluating the whole shear equation

$$S_i = \frac{6EI}{l^2}\left[\frac{\alpha_i\alpha_j r_i\left(2-\frac{6EI\beta r_j}{l}+\frac{r_j}{\alpha_j}\right)}{4\varepsilon_j\alpha_i\alpha_j+4\alpha_i\alpha_j-r_i r_j}\right]\vartheta_i+\frac{6EI}{l^2}\left[\frac{\alpha_i\alpha_j r_j\left(2+\frac{r_i}{\alpha_i}-\frac{6EI\beta r_i}{l}\right)}{4\varepsilon_j\alpha_i\alpha_j+4\alpha_i\alpha_j-r_i r_j}\right]\vartheta_j$$

$$-\left(\frac{12EI}{l^3}\right)\left[\frac{\alpha_i\alpha_j\left(r_i\frac{r_i r_j}{2}\left(\frac{1}{\alpha_i}+\frac{1}{\alpha_j}\right)+r_j-\frac{6EIr_i r_j\beta}{l}\right)}{4\varepsilon_i\alpha_i\alpha_j+4\alpha_i\alpha_j-r_i r_j}\right]R' \qquad (4.6.8a)$$

$$+\left[\frac{r_i r_j}{4\varepsilon_j\alpha_i\alpha_j+4\alpha_i\alpha_j-r_i r_j}\right]\left[\frac{1}{l}\right]$$

$$\left\{\left(1+\frac{4\alpha_j}{r_j}-\frac{2\alpha_i}{r_i}+\frac{6EI\beta(\alpha_i-2\alpha_j)}{l}\right)M_i^F+\left(1+\frac{4\alpha_i}{r_i}-\frac{2\alpha_j}{r_j}+\frac{6EI\beta(\alpha_j-2\alpha_i)}{l}\right)M_j^F\right\}$$

Hence, S_j will be just negative of S_i

$$S_j = -\frac{6EI}{l^2}\left[\frac{\alpha_i\alpha_j r_i\left(2-\frac{6EI\beta r_j}{l}+\frac{r_j}{\alpha_j}\right)}{4\varepsilon_j\alpha_i\alpha_j+4\alpha_i\alpha_j-r_i r_j}\right]\vartheta_i-\frac{6EI}{l^2}\left[\frac{\alpha_i\alpha_j r_j\left(2+\frac{r_i}{\alpha_i}-\frac{6EI\beta r_i}{l}\right)}{4\varepsilon_j\alpha_i\alpha_j+4\alpha_i\alpha_j-r_i r_j}\right]\vartheta_j$$

$$+\left(\frac{12EI}{l^3}\right)\left[\frac{\alpha_i\alpha_j\left(r_i+\frac{r_i r_j}{2}\left(\frac{1}{\alpha_i}+\frac{1}{\alpha_j}\right)+r_j-\frac{6EIr_i r_j\beta}{l}\right)}{4\varepsilon_i\alpha_i\alpha_j+4\alpha_i\alpha_j-r_i r_j}\right]R' \qquad (4.6.8b)$$

$$-\left[\frac{r_i r_j}{4\varepsilon_j\alpha_i\alpha_j+4\alpha_i\alpha_j-r_i r_j}\right]\left[\frac{1}{l}\right]$$

$$\left\{\left(1+\frac{4\alpha_j}{r_j}-\frac{2\alpha_i}{r_i}+\frac{6EI\beta(\alpha_i-2\alpha_j)}{l}\right)M_i^F+\left(\frac{6EI\beta(\alpha_j-2\alpha_i)}{l}+1-\frac{2\alpha_j}{r_j}+\frac{4\alpha_i}{r_i}\right)M_j^F\right\}$$

Appendix B2 Finite element

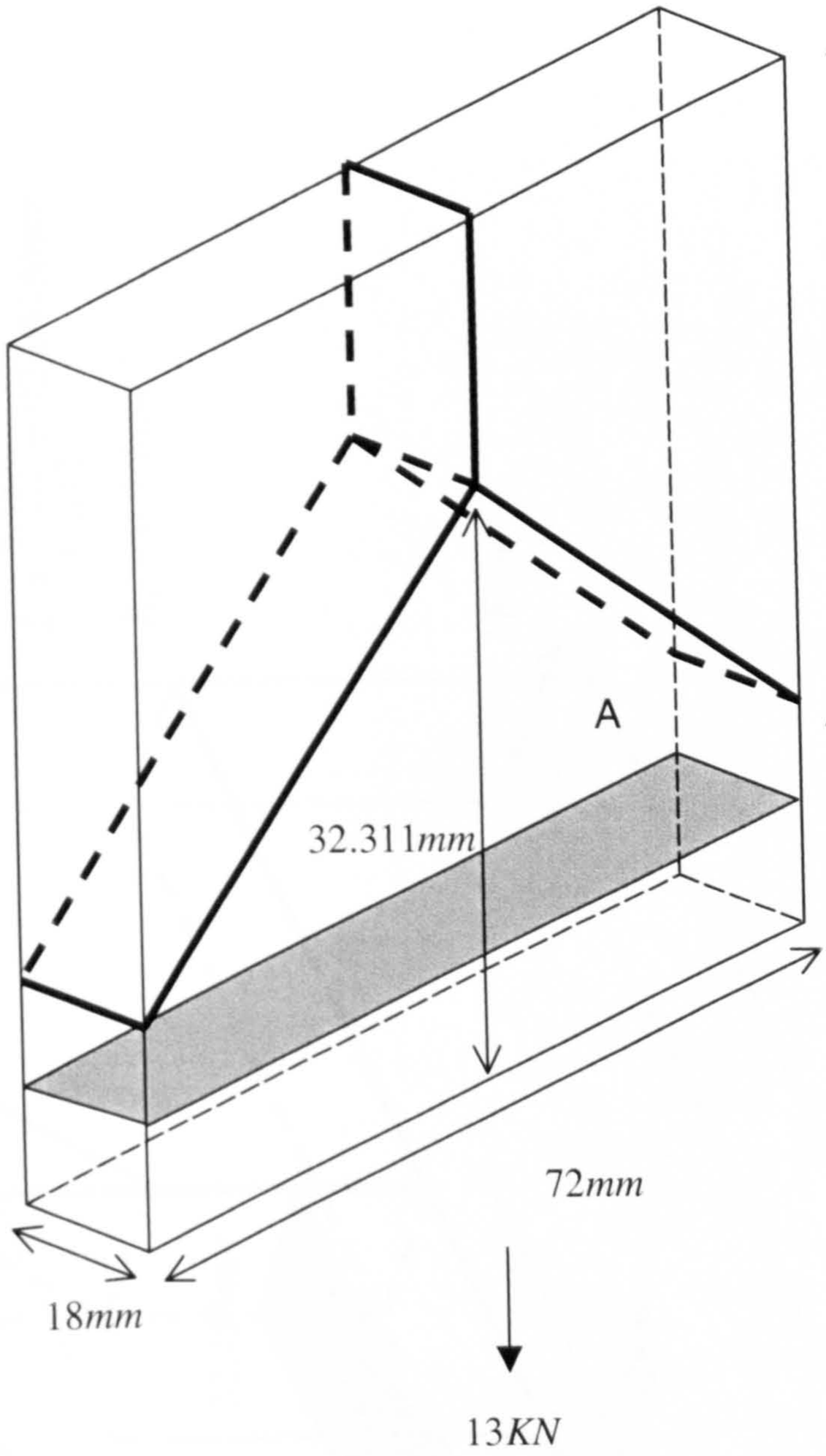

Axial length,

$$L_a = \frac{(2\times 24.217)+48.499}{3} = 32.311mm$$

$$\varepsilon = \frac{3.25}{32.311} = 0.101$$

$$\sigma_y = \frac{13\times 10^3}{18\times 72} = 10.03Nmm^{-2}$$

$$E = \frac{10.03}{0.101} = 99.315Nmm^{-2}$$

$$E_T = 0.0Nmm^{-2}$$

Fig. B2.1 – Crown Joint connection model

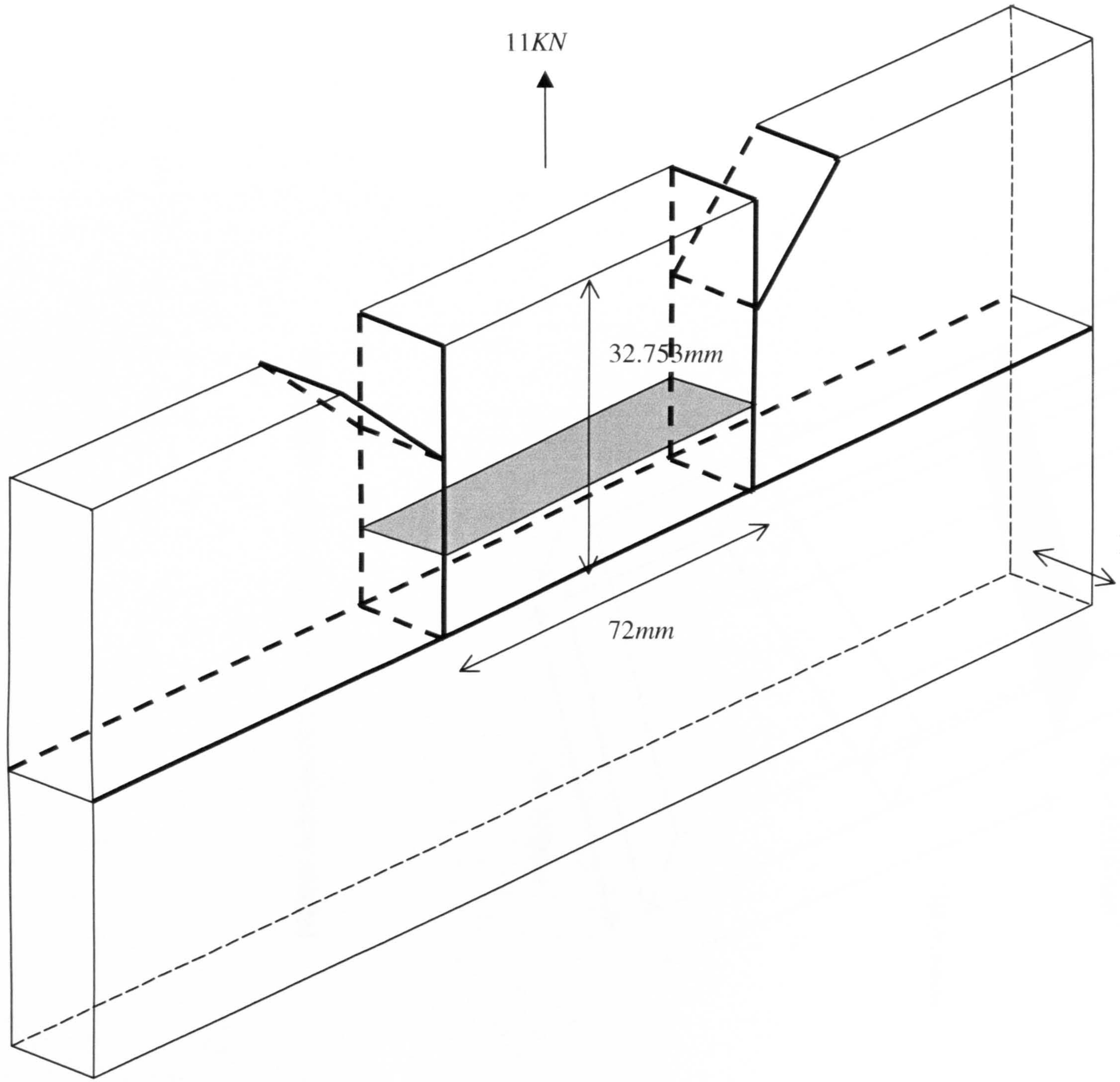

Axial length, $L_a = 32.753mm$

$$\varepsilon = \frac{3.0}{32.753} = 0.092$$

$$\sigma_y = \frac{11\times10^3}{18\times72} = 8.488Nmm^{-2}$$

$$E = \frac{8.488}{0.092} = 92.664Nmm^{-2}$$

$$E_T = 0.0Nmm^{-2}$$

Fig. B2.2 – Bottom Chord Joint connection model

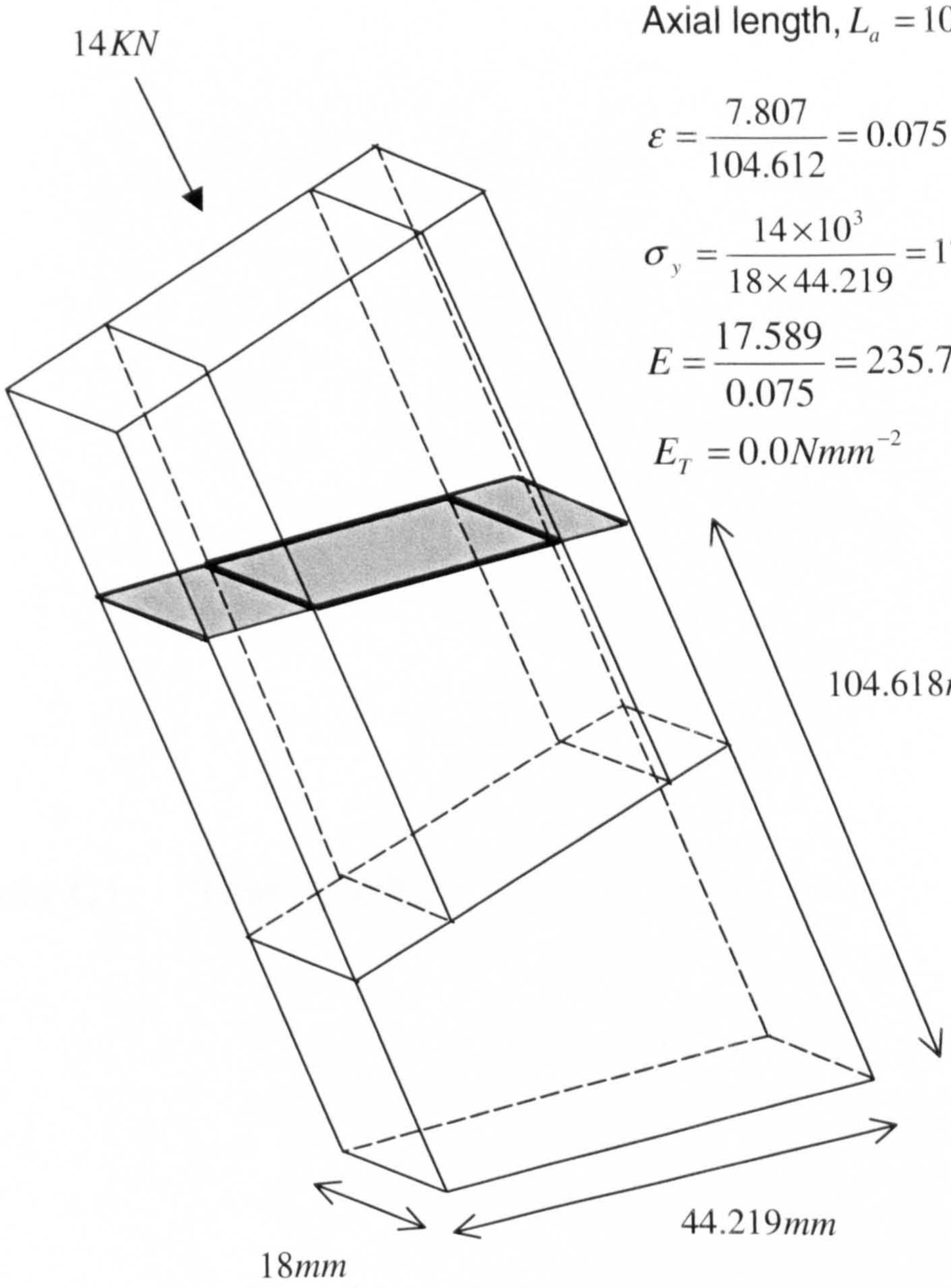

Axial length, $L_a = 104.612mm$

$$\varepsilon = \frac{7.807}{104.612} = 0.075$$

$$\sigma_y = \frac{14 \times 10^3}{18 \times 44.219} = 17.589 Nmm^{-2}$$

$$E = \frac{17.589}{0.075} = 235.704 Nmm^{-2}$$

$$E_T = 0.0 Nmm^{-2}$$

Fig. B2.3 – Top Chord joint connection model

Appendix C1 Test results

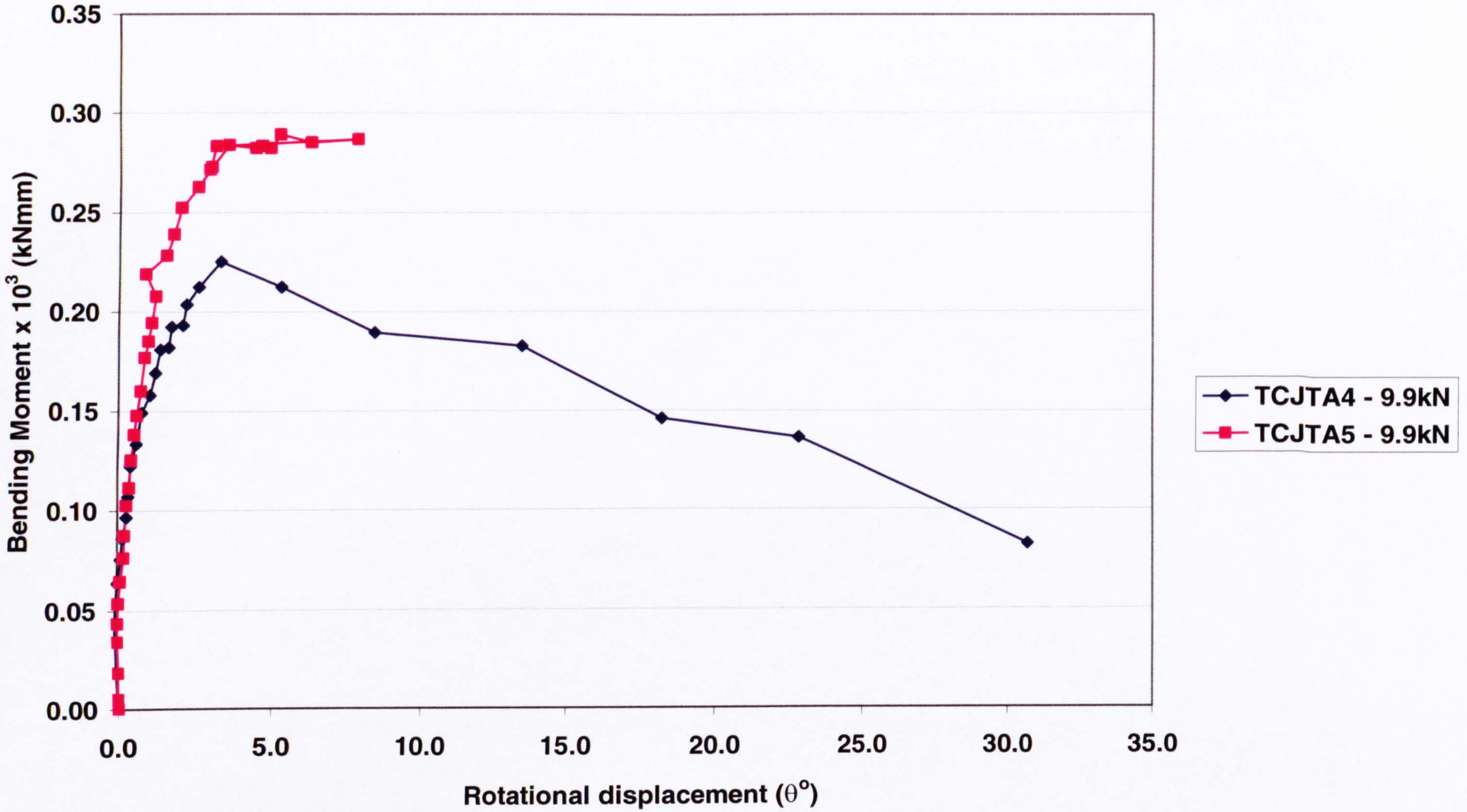

Fig. C1.1 – Variability of TCJTA series test results

Fig. C1.2 –Fig. C1.41 can be viewed in “test results.doc”, Word document on the disc attached

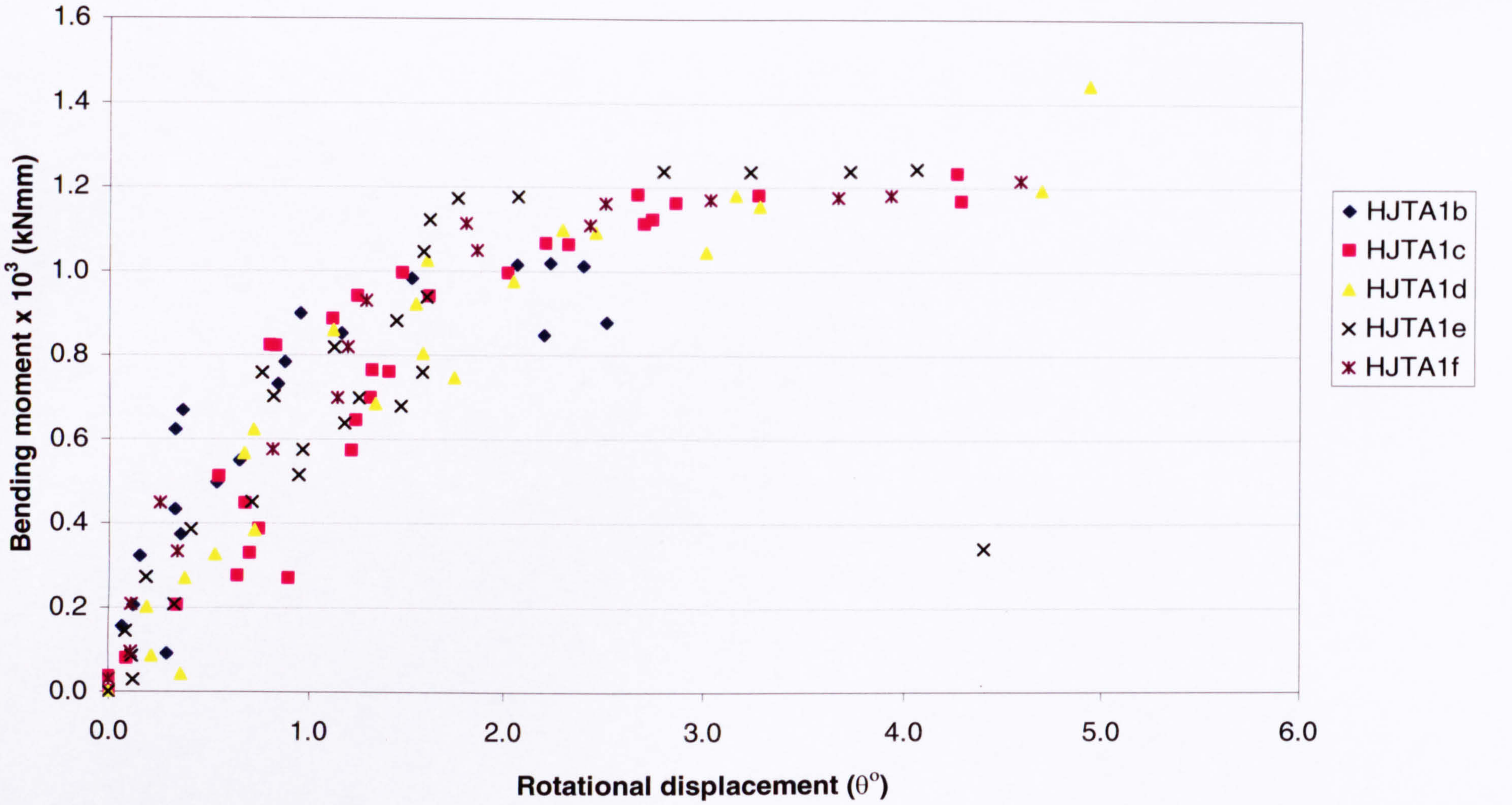

Fig. C1.42 – Pure bending moments / Rotational displacement test

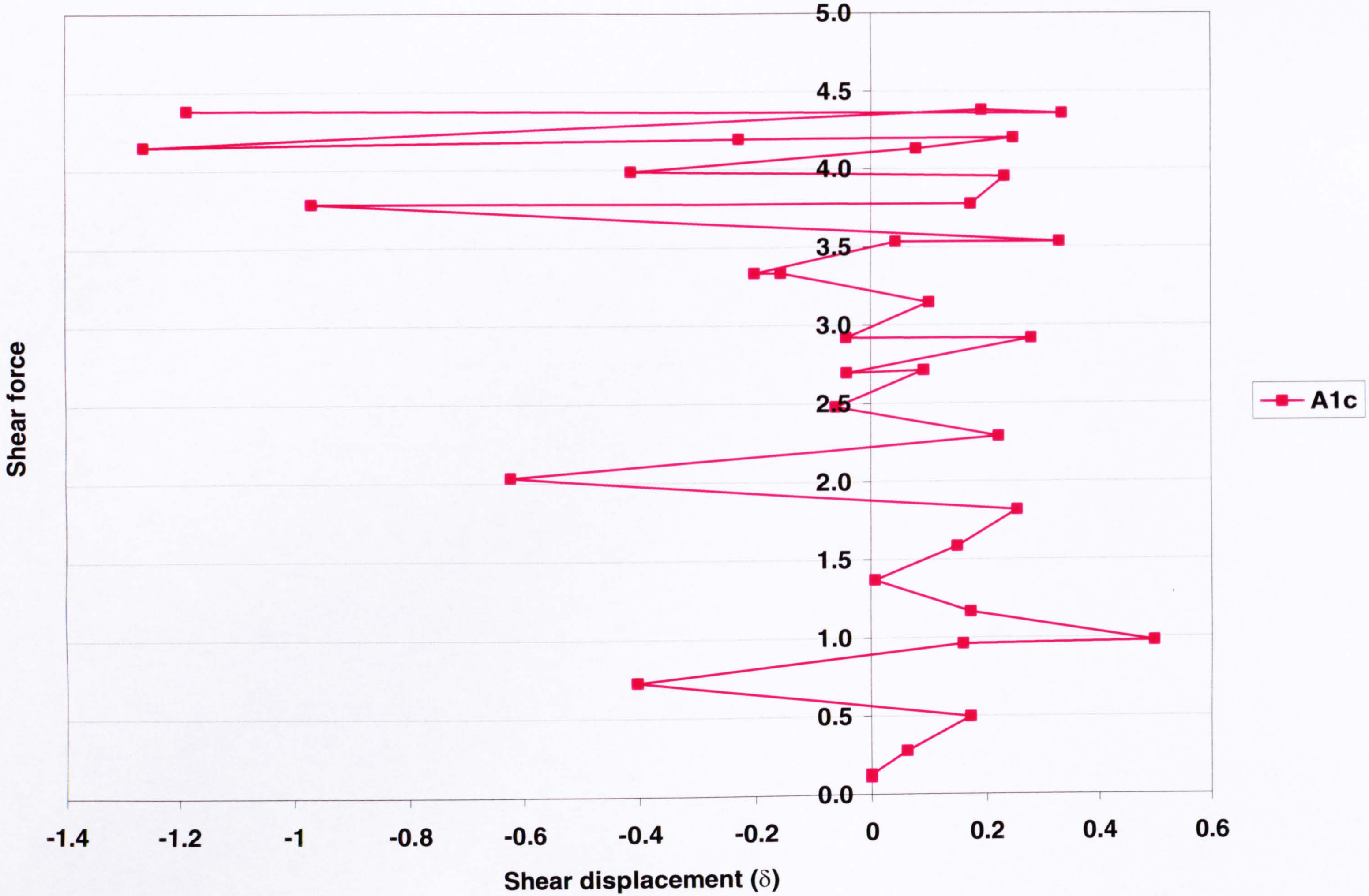

Fig. C1.43 – Heel Joint shear response

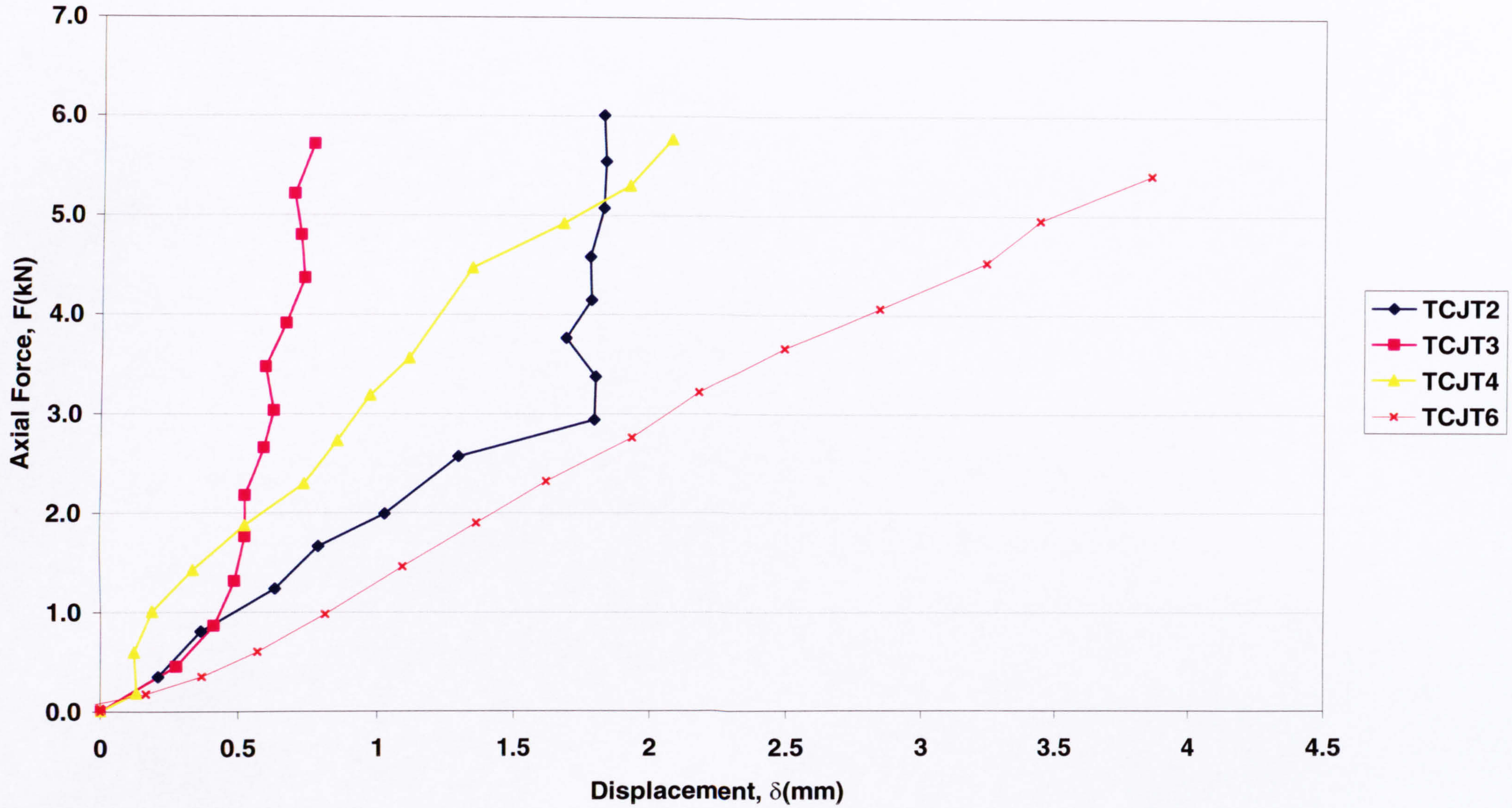

Fig. C1.44 – Affect of compression in the top chord on compression in the web

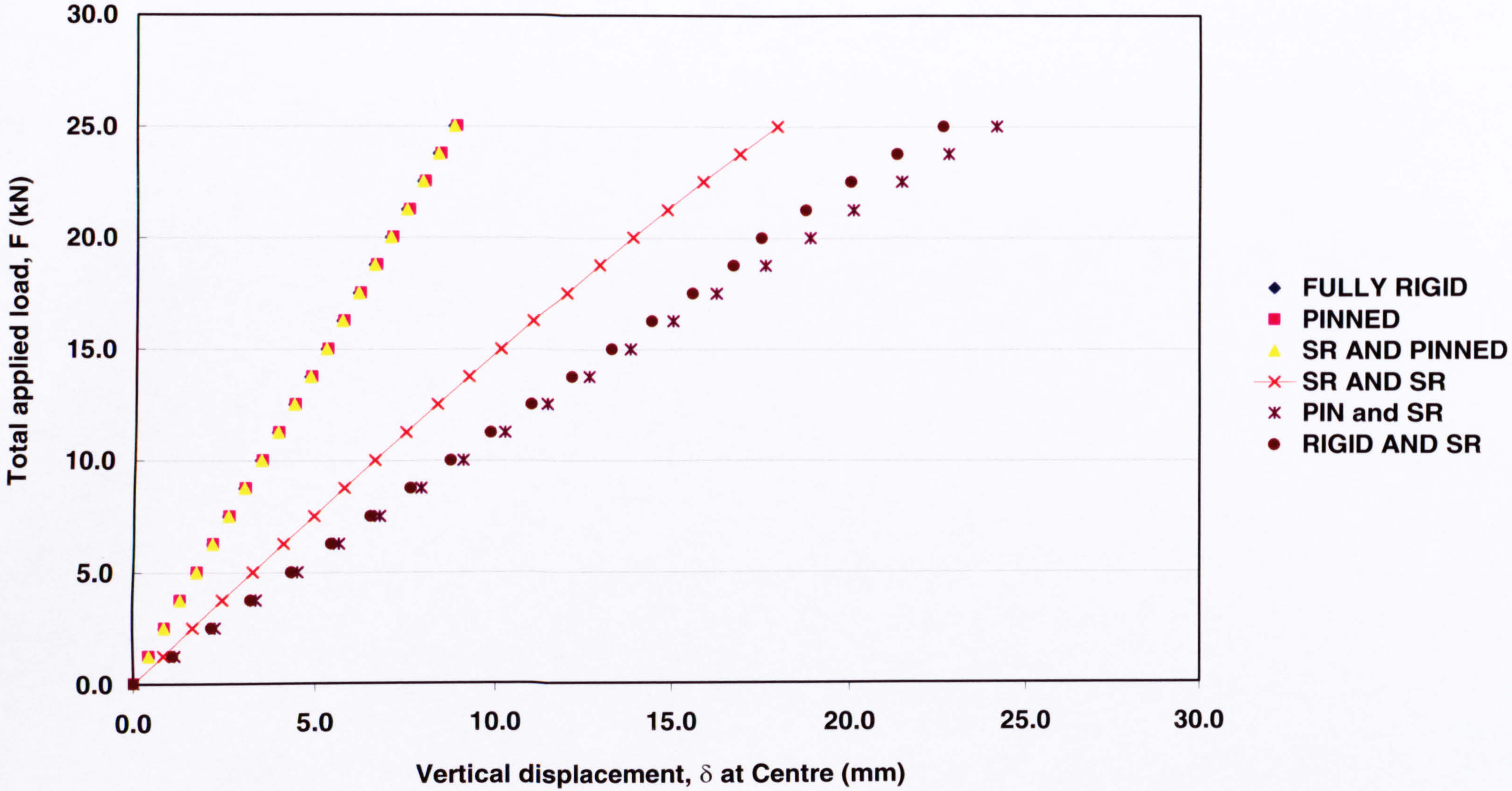

Fig. C1.45 – Symmetrically loaded full scale truss test

Test no.	Dimensions (mm)			Volume (mm^3)	Weight b4 oven (g)	Weight after oven (g)	Density (g/mm^3) $x10^{-3}$	moisture %
	B	W	D					
CJT								
A1	96	50	34	163200	68.96	62.75	0.42	9.01
A2	94	50	34	159800	67.84	61.59	0.42	9.21
A3	94	50	34	159800	67.54	61.33	0.42	9.19
A4	95	50	34	161500	77.85	70.58	0.48	9.34
A5	95	50	34	161500	76.35	69.27	0.47	9.27
M1	95	50	34	161500	67.24	61.25	0.42	8.91
M2	94	50	35	164500	74.24	67.58	0.45	8.97
M3	95	50	35	166250	74.26	67.53	0.45	9.06
M4	94	50	34	159800	73.32	66.75	0.46	8.96
M5	94	50	34	159800	68.97	62.67	0.43	9.13
MOCK	95	51	34	164730	71.63	65.27	0.43	8.88
HJT								
A1	95	50	35	166250	74.03	67.47	0.45	8.86
A1C	95	50	34	161500	76.07	69.22	0.47	9.00
A1D	95	50	34	161500	68.11	61.94	0.42	9.06
A1E	95	50	35	166250	68.05	61.89	0.41	9.05
A1F	95	50	35	166250	69.05	62.83	0.42	9.01
A2	95	50	35	166250	61.45	55.95	0.37	8.95
A3	96	50	35	168000	68.7	62.54	0.41	8.97
A4	95	50	34	161500	66.68	60.7	0.41	8.97
A5	95	50	35	166250	61.14	55.68	0.37	8.93
M1	95	50	34	161500	71.18	64.85	0.44	8.89
M2	95	50	35	166250	65.57	59.7	0.39	8.95
M3	94	50	34	159800	74.01	67.5	0.46	8.80
M4	95	50	34	161500	60.76	55.27	0.38	9.04
M5	95	50	35	166250	69.2	63.09	0.42	8.83
MOCK	95	51	35	169575	64.13	58.43	0.38	8.89

Table C1.1 – Timber density and moisture content

Test no.	Dimensions (mm)			Volume (mm^3)	Weight b4 oven (g)	Weight after oven (g)	Density (g/mm^3) $x10^{-3}$	moisture %
	B	W	D					
TCJT								
1	95.45	49.74	34.44	163510	66.57	59.91	0.41	10.00
2	95.8	49.47	34.57	163835	67.88	61.08	0.41	10.02
3	95.79	49.4	34.85	164911	72.22	64.89	0.44	10.15
4	96.17	49.58	34.42	164118	69.33	62.36	0.42	10.05
5	95.17	49.38	34.48	162039	70.78	63.72	0.44	9.97
6	95.5	49.52	35.06	165804	75.22	67.52	0.45	10.24
A1	94.87	49.87	35.18	166442	63.01	56.77	0.38	9.90
A2	95.6	49.59	35.05	166165	62.15	55.99	0.37	9.91
A3	95.45	49.73	34.85	165423	67.85	61.11	0.41	9.93
A4	95.26	49.52	35.2	166048	60.06	54.04	0.36	10.02
A5	95.95	48.73	34.61	161824	68.05	61.24	0.42	10.01
A6	95.14	49.47	34.79	163742	70	62.61	0.43	10.56
M1	95.03	49.53	34.99	164692	61.72	55.51	0.37	10.06
M2	95.57	49.79	35.04	166735	61.47	55.31	0.37	10.02
M3	95.85	49.59	34.8	165411	60.99	54.87	0.37	10.03
M4	95.79	49.67	34.61	164671	68.1	61.28	0.41	10.01
M5	95.99	49.65	34.85	166092	69.26	62.22	0.42	10.16
M6	95.64	49.78	34.88	166062	74.35	66.43	0.45	10.65
MOCK	94.57	49.67	34.51	162104	71.8	64.9	0.44	9.61
BCJT								
BCJT1	72.11	54.97	34.89	138300	56.83	51.01	0.41	10.24
BCJT2	71.46	49.98	35.45	126612	63.49	56.88	0.50	10.41
BCJT3	71.42	53.18	35.35	134263	58.15	51.92	0.43	10.71
BCJT3a	71.42	49.83	35.20	125272	60.85	54.52	0.49	10.40
BCJT4	72.09	52.57	34.80	131884	54.35	48.85	0.41	10.12
BCJTA1	72.10	52.27	34.71	130810	57.94	52.20	0.44	9.91
BCJTA2	71.35	53.39	35.22	134166	59.19	52.85	0.44	10.71
BCJTA3	71.18	53.66	35.13	134180	58.97	52.52	0.44	10.94
BCJTA4	71.50	53.87	35.09	135156	62.95	56.24	0.47	10.66
BCJTA5	71.19	49.93	35.45	126008	61.70	55.27	0.49	10.42
BCJTM1	71.43	49.82	35.29	125584	60.20	53.98	0.48	10.33
BCJTM2	71.59	49.67	35.23	125273	60.72	54.33	0.48	10.52
BCJTM3	71.10	49.71	35.19	124375	54.56	48.73	0.44	10.69
BCJTM4	72.12	49.38	34.76	123790	53.17	47.77	0.43	10.16
BCJTM5	72.02	53.94	34.58	134335	54.56	48.96	0.41	10.26
BCJTM6	71.40	49.91	35.12	125153	55.23	49.26	0.44	10.81
BCJTM7	72.19	49.88	34.68	124877	56.54	50.95	0.45	9.89
MOCK	72.06	49.89	34.68	124677	51.60	46.38	0.41	10.12

Table C1.2 – Timber density and moisture content

Mem	Node	Axial (KN)	Shear (KN)	Moment (KNmm)
1	1	21.8942	0.2277	62.2448
	2	-21.8942	-0.2277	350.3343
2	2	14.7382	-0.3634	-346.1648
	4	-14.7382	0.3634	-311.3821
3	4	14.7576	0.3728	313.453
	5	-14.7576	-0.3728	361.0633
4	5	21.8957	-0.2516	-371.266
	6	-21.8957	0.2516	-84.5866
5	2	6.6545	0.0001	-4.1695
	3	-6.6545	-0.0001	4.2796
6	4	-7.4909	-0.0024	-2.0709
	3	7.4909	0.0024	-2.7766
7	3	6.6171	0.0042	-2.5834
	5	-6.6171	-0.0042	10.2027
8	1	-17.9586	0.0177	-62.2448
	3	17.9586	-0.0177	115.3792
9	3	-17.9465	-0.0099	-114.2988
	6	17.9465	0.0099	84.5866

Table C1.3 – STRUSS Symmetrical load case

Mem	Node	Axial (KN)	Shear (KN)	Moment (KNmm)
1	1	22.9788	0.6677	206.2885
	7	-22.9788	-0.6677	801.7909
2	8	8.769	-0.8305	-775.3515
	4	-8.769	0.8305	-476.5396
3	4	20.5813	0.3556	394.5038
	5	-20.5813	-0.3556	249.0526
4	5	20.3508	-0.1519	-244.6189
	6	-20.3508	0.1519	-30.5095
5	2	13.0474	0.0042	-2.2658
	3	-13.0474	-0.0042	9.8578
6	4	-7.0434	0.0583	82.0358
	3	7.0434	-0.0583	35.7148
7	3	-0.6376	-0.0092	-12.1396
	5	0.6376	0.0092	-4.4337
8	1	-18.5723	-0.0436	-206.2885
	3	18.5723	0.0436	75.5232
9	3	-16.7457	-0.0262	-108.9562
	6	16.7457	0.0262	30.5095
10	7	18.3108	-6.068	-801.7909
	2	-18.3108	6.068	-1029.9558
11	2	13.4454	5.9885	1032.2216
	8	-13.4454	-5.9885	775.3515

Table C1.4 – STRUSS Unysmmetrical load case

Appendix C2 – Close range photogrammetry

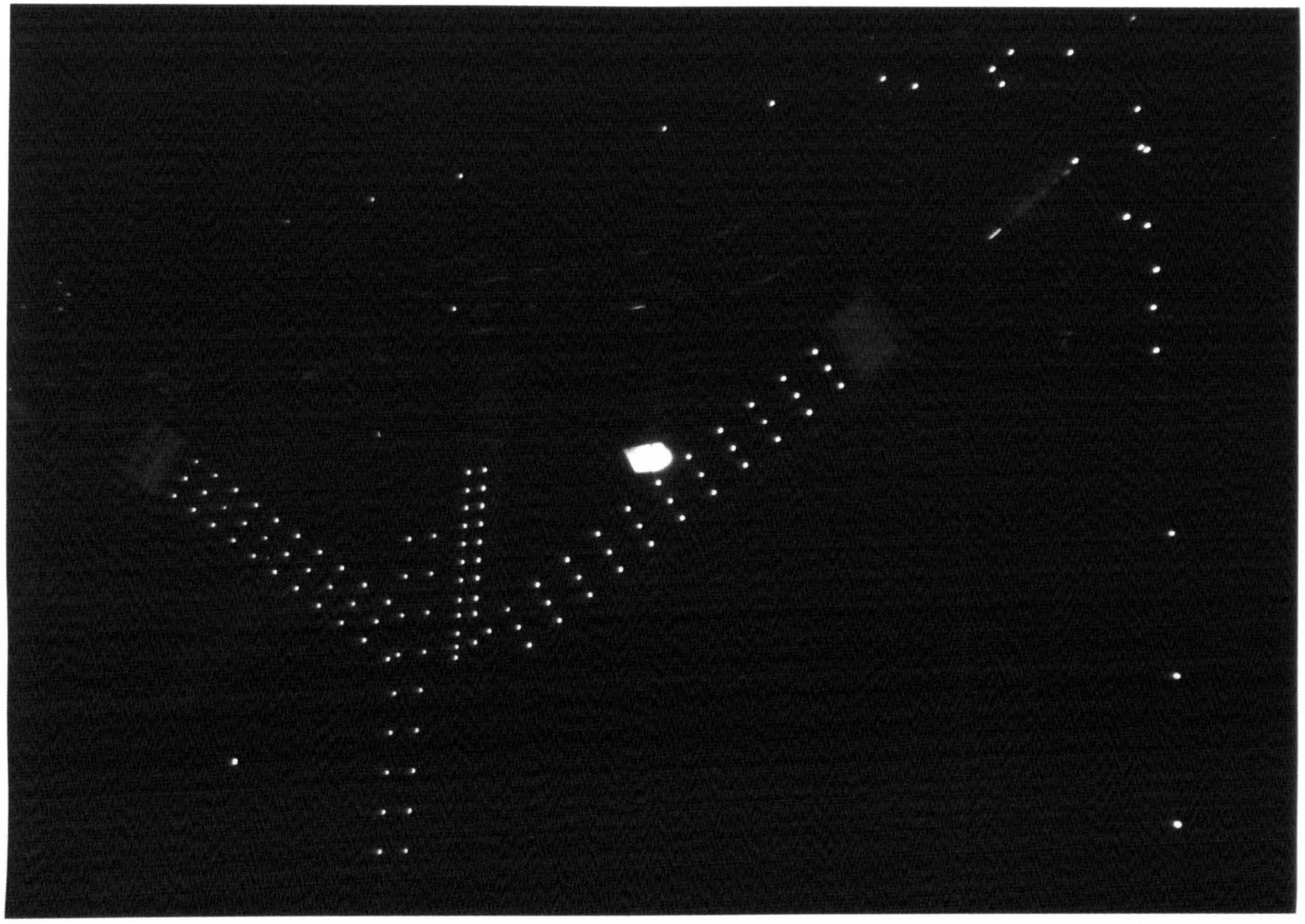

Fig. C2.1 – Captured image for processing

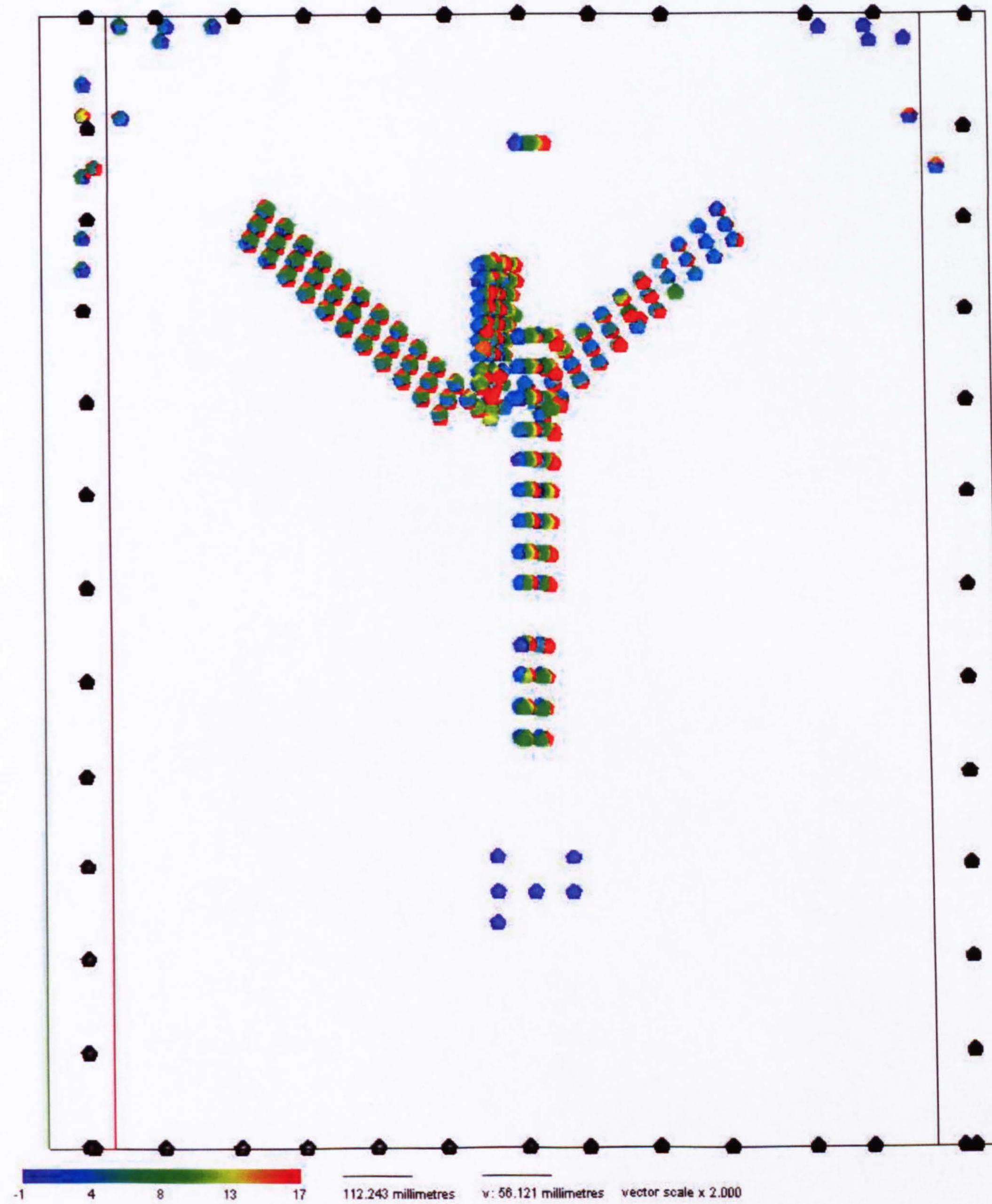

Fig. C2.2 – Deformation of CJTA1 test

Appendix C3 Pinned and rigid analysis

NUMBER OF NODES 6
NUMBER OF MEMBERS 10

[NODAL LOADS]

Node	X(N)	Y	
2	40000	0	0
3	0	-20000	0
5	0	-20000	0

[GLOBAL DISPLACEMENT]

NODE	X(m)	Y(m)	(rad)
1	0	0	0
2	0.08653	-0.07475	-0.00011
3	0.02399	-0.09193	-0.00012
4	0.05479	-0.04896	0.00004
5	0.05364	-0.08943	0.00007
6	0.06757	0	0

[MEMBER FORCES]

Mem	Node	Axial(N)	Shear(N)	Moment(Nm)
1	1	-44989.52	0.00	0.00
	3	44989.52	0.00	0.00
2	3	-31130.64	0.00	0.00
	5	31130.64	0.00	0.00
3	5	-26121.59	0.00	0.00
	6	26121.59	0.00	0.00
4	2	39980.47	0.00	0.00
	4	-39980.47	0.00	0.00
5	1	8127.04	0.00	0.00
	2	-8127.04	0.00	0.00
6	3	-10021.61	0.00	0.00
	2	10021.61	0.00	0.00
7	3	-17077.38	0.00	0.00
	4	17077.38	0.00	0.00
8	5	6172.31	0.00	0.00
	2	-6172.31	0.00	0.00
9	5	-23606.51	0.00	0.00
	4	23606.51	0.00	0.00
10	4	42547.43	0.00	0.00
	6	-42547.43	0.00	0.00

Pinned Analysis

NUMBER OF NODES 8
NUMBER OF MEMBERS 7

[NODAL LOADS]

Node	X(N)	Y(N)	M(Nmm)
2	30000	0	0
3	0	-40000	0
6	0	-40000	0

[GLOBAL DISPLACEMENT]

NODE	X(m)	Y(m)	(rad)
1	0.000	0.000	0.000
2	-0.804	-0.001	0.000
3	0.436	-5.012	0.001
4	1.676	-0.006	-0.003
5	0.000	0.000	0.000
6	3.059	-5.578	0.002
7	4.443	-0.002	-0.007
8	0.000	0.000	0.000

[MEMBER FORCES]

Mem	Node	Axial(N)	Shear(N)	Moment(Nm)
1	1	19431.64	-13511.56	-3953576.98
	2	-19431.64	13511.56	-4153357.09
2	5	38618.31	7015.79	2706715.44
	4	-38618.31	-7015.79	1502759.81
3	8	21950.05	36495.76	14210023.97
	7	-21950.05	-36495.76	7687434.85
4	2	46925.27	8298.35	4153357.09
	3	-46925.27	-8298.35	4400389.17
5	4	47200.97	-9401.14	-5290086.17
	3	-47200.97	9401.14	-4400389.17
6	4	39783.85	8659.50	3787326.36
	6	-39783.85	-8659.50	5138678.22
7	6	40729.76	-12443.16	-5138678.22
	7	-40729.76	12443.16	-7687434.85

Rigid Analysis

$E=21x10^{10}N/m^2$

Member 1,2 and 3
$A=2.5x10^{-3}m^2$
Member 4,5 and 10
$A=3.0x10^{-3}m^2$
Member 6,7, 8 and 9
$A=1.0x10^{-3}m^2$

Pinned analysis

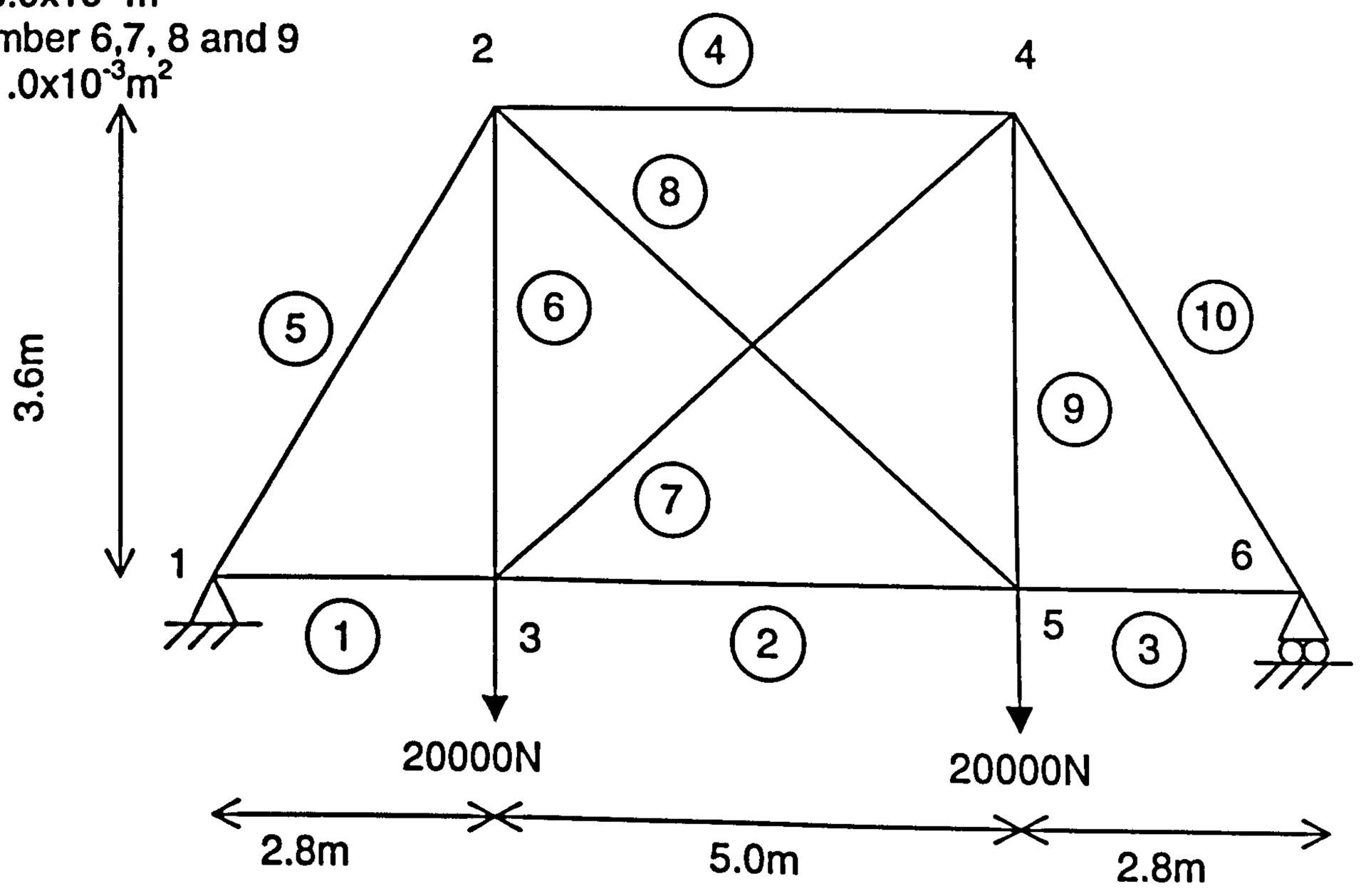

Members 2,4,5,6, and 7
$E=21x10^{10}N/m^2$
$A=0.02m^2$

Members 1 and 3
$I=6.666x10^{-5}m^4$
$A=0.04m^2$
$I=1.333x10^{-4}m^4$

Rigid analysis